SEISMIC UPGRADING OF REINFORCED CONCRETE FRAMES WITH STRUCTURAL STEEL ELEMENTS

A THESIS SUBMITTED TO
THE GRADUATE SCHOOL OF NATURAL APPLIED SCIENCES
OF
MIDDLE EAST TECHNICAL UNIVERSITY

BY

RAMAZAN ÖZÇELİK

IN PARTIAL FULFILLMENT OF THE REQUIREMENTS
FOR
THE DEGREE OF DOCTOR OF PHILOSOPHY
IN
CIVIL ENGINEERING

JUNE 2011

Approval of the thesis:

SEISMIC UPGRADING OF REINFORCED CONCRETE FRAMES WITH STRUCTURAL STEEL ELEMENTS

submitted by **RAMAZAN ÖZÇELİK** in partial fulfillment of the requirements for the degree of **Doctor of Philosophy in Civil Engineering Department, Middle East Technical University** by,

Prof. Dr. Canan Özgen ______________________
Dean, Graduate School of **Natural and Applied Sciences**

Prof. Dr. Güney Özcebe ______________________
Head of Department, **Civil Engineering**

Assoc. Prof. Dr. Barış Binici ______________________
Supervisor, **Civil Engineering Dept., METU**

Examining Committee Members:

Prof. Dr. Ahmet Yakut ______________________
Civil Engineering Dept., METU

Assoc. Prof. Dr. Barış Binici ______________________
Civil Engineering Dept., METU

Prof. Dr. Cem Topkaya ______________________
Civil Engineering Dept., METU

Assoc. Prof. Dr. Erdem Canbay ______________________
Civil Engineering Dept., METU

Assist. Prof. Dr. Kutay Orakçal ______________________
Civil Engineering Dept., Boğaziçi University

Date: 21.06.2011

I hereby declare that all information in this document has been obtained and resented in accordance with academic rules and ethical conduct. I also declare that, as required by these rules and conduct, I have fully cited and referenced all material and results that are not original to this work.

Name, Last name: Ramazan Özçelik

Signature:

ABSTRACT

SEISMIC UPGRADING OF REINFORCED CONCRETE FRAMES WITH STRUCTURAL STEEL ELEMENTS

Özçelik, Ramazan
Ph.D., Department of Civil Engineering
Supervisor: Assoc. Prof. Dr. Barış Binici
June 2011, 254 pages

This thesis examines the seismic internal retrofitting of existing deficient reinforced concrete (RC) structures by using structural steel members. Both experimental and numerical studies were performed. The strengthening methods utilized with the scope of this work are chevron braces, internal steel frames (ISFs), X-braces and column with shear plate. For this purpose, thirteen strengthened and two as built reference one bay one story portal frame specimens having 1/3 scales were tested under constant gravity load and increasing cyclic lateral displacement excursions. In addition, two ½ scaled three bay-two story frame specimens strengthened with chevron brace and ISF were tested by employing continuous pseudo dynamic testing methods. The test results indicated that the cyclic performance of the X-brace and column with shear plate assemblage technique were unsatisfactory. On the other hand, both chevron brace and ISF had acceptable cyclic performance and these two techniques were found to be candidate solutions for seismic retrofitting of deficient RC structures. The numerical simulations by conducting nonlinear static and dynamic analysis were used to estimate performance limits of the RC frame and steel members. Suggested strengthening approaches, chevron brace and ISF, were also employed to an existing five story case study RC building to demonstrate the performance efficiency. Finally, design approaches by using existing strengthening guidelines in Turkish Earthquake Code and ASCE/SEI 41 (2007) documents were suggested.

Keyword: Seismic retrofit, RC frames, chevron brace, internal steel frame, nonlinear static and dynamic analysis.

ÖZ

BETONARME ÇERÇEVELERİN ÇELİK YAPI ELEMANLARI İLE SİSMİK GÜÇLENDİRİLMESİ

Özçelik, Ramazan
Doktora, İnşaat Mühendisliği Bölümü
Tez Yöneticisi: Doç. Dr. Barış Binici
Haziran 2011, 254 sayfa

Bu tez, mevcut kusurlu betonarme yapıların çelik yapı elemanları ile deprem güçlendirilmesi uygulamalarını incelemektedir. Çalışma kapsamında hem deneysel hem de sayısal simulasyon çalışmaları yapılmıştır. İncelenen güçlendirme teknikleri iç ters V çelik çapraz (İTVÇÇ), iç çelik çerçeve (İÇÇ), X çelik çapraz ve kesme plakalı kolon uygulamalarından oluşmaktadır. Deneyler, 1/3 ölçekli tek katlı tek açıklıklı 13 adet güçlendirilmiş ve iki adet referans çerçevesi üzerinde sabit düşey yük ve artan tersinir çevrimli yatay yükleme altında gerçekleştirilmiştir. Buna ek olarak, İTVÇÇ ve İÇÇ ile güçlendirilen 2 adet ½ ölçekli üç açıklıklı iki katlı çerçeve Düzce deprem kaydı kullanılarak dinamik benzerli test yöntemi ile denenmiştir. Test sonuçları, X çapraz ve kesme plakalı kolon uygulamalarının yetersiz yapı performansı sunduğunu göstermiştir. İTVÇÇ ve İÇÇ ile güçlendirme yöntemleri ise kararlı bir performansa sahip olmakla beraber bu çalışma sonucunda güçlendirme için kullanılabilir bulunmuştur. Sayısal simulasyonlar, elastik ötesi statik ve dinamik analizler yapılarak çelik ve betonarme çerçeve elemanlarının performans sınırlarının tahmin edilebilmesi için gerçekleştirilmiştir. Bu çalışmada tavsiye edilen İTVÇÇ ve İÇÇ ile güçlendirme uygulamalarının etkili yöntemler olduğunu göstermek için 5 katlı mevcut kusurlu bir betonarme bina bu yöntemler ile güçlendirilmiştir. Sonuç olarak betonarme ve çelik yapı elemanları için mevcut olan Türk Deprem Yönetmeliği ve ASCE/SEI 41 (2007) dökümanları kullanılarak sismik güçlendirmenin nasıl gerçekleştirilebileceği konusunda öneriler getirilmiştir.

Anahtar Kelimeler: Sismik güçlendirme, betonarme yapılar, iç ters V çelik çaprazlar, iç çelik çerçeve, elastik ötesi statik ve dinamik analiz.

To my family

ACKNOWLEDGMENTS

I would like to express my deepest gratitude to my supervisor Assoc. Prof. Dr. Barış Binici for his guidance, advice, criticism, encouragements and insight throughout the research.

I would also like to thank to Prof. Dr. Güney Özcebe who is head of Department of Civil Engineering for his supports.

I would like to thank to Assoc. Prof. Dr. Erdem Canbay for his great support at the laboratory. I would like to thank to Prof. Dr. Cem Topkaya for his important suggestions throughout my research.

I would like to thank to my examining committee members, Prof. Dr. Ahmet Yakut, Prof. Dr. Cem Topkaya, Assoc. Dr. Erdem Canbay and Assist. Prof. Dr. Kutay Orakçal for their valuable suggestions and constructive comments.

I would like to thank to my office friends Barış Erdil and Dilek Okuyucu and Tuğba Özaktaş and Fadime Kara for their support.

The technical assistance of Hasan Metin, Salim Azak, Osman Keskin, Murat Demirel and Barış Esen are gratefully acknowledged.

The State Planning Organization (DPT) Grant No: BAP-08-11-DPT-2002K120510 and Technological Research Council of Turkey (TUBİTAK) project no 106M493 are gratefully acknowledged.

Finally, I would like to express my sincere gratitude to my parents Necibe Özçelik and Hüseyin Özçelik for their eternal love, encouragement and trust. I would like to thank to my daughter Kezban Ülker and my nieces Dilara and Buğlem Su Ülker for their endless love. I would like to express my special thanks and loves to my spouse Aysun Özçelik for her endless patience, encouragement, support and love.

TABLE OF CONTENTS

LIST OF TABLES

TABLES

LIST OF FIGURES

FIGURES

ABBREVIATIONS

AISC: American Institute of Steel Construction
ASCE: American Society of Civil Engineering
ASTM: American Society for Testing and Materials
BCJ: Japanese seismic code
CJP: Complete-joint-penetration
DBF: Ductile braced frame
DR: Drift ratio
EC: Euro Code 8
FE: Finite element
HDRD: High damping rubber pad
HSS: Hollow Structural Section
IDR: Inter-story drift ratio
ISF: Internal Steel Frame
LRFD: Load and Resistance Factor Design
LVDT: Linear Variable Differential Transducer
NDBF: Nominal ductility braced frame
OCBF: Concentric braced frame
PGA: Peak ground acceleration
PsD: Pseudo dynamic test
RC: Reinforced concrete
SCBF: Special concentric braced frame
SMAD: Shape memory alloy wire assemblage
SPSW: Steel plate shear walls
TEC: Turkish Earthquake Code
TS: Turk Standard

CHAPTER 1

1. INTRODUCTION

1.1 General

Poor performance of reinforced concrete (RC) buildings was demonstrated dramatically in recent earthquakes in Turkey, Taiwan, Sumatra, and Pakistan (Saatcioglu et al., 2001; Sezen et al., 2003; Yakut et al., 2005). In order to mitigate the seismic risk in these heavily populated yet seismically vulnerable regions, comprehensive programs including seismic risk assessment, urban city planning, building evaluation and strengthening/demolition feasibility studies need to be conducted. A key component of such programs is to develop and provide a wide variety of seismic upgrade methodologies that are suitable for developing countries with severe budgetary limitations.

Common deficiencies of RC buildings in many of the developing countries owe either to lack of knowledge about seismic risk or to malpractice and insufficient quality control during construction. Plan and elevation irregularities, short columns, weak and soft first stories (due to commercial places) are the system level deficiencies that adversely affect the seismic performance of the structures. The poor quality control usually results in low strength concrete (in the range of 7 to 15 MPa (Çağatay, 2005; Tezcan and İpek, 1995; Doğangün 2004)). Insufficient spacing of transverse confining reinforcement in beams, columns and joints, and insufficient splice length at column critical regions are member deficiencies commonly observed in RC members. While these deficiencies may be addressed by member-level seismic upgrade techniques, this study focuses on structural-level upgrade techniques, which imply installing new and much stronger structural systems such that the lateral strength, stiffness and perhaps deformability of the retrofitted structure are restored. The system strengthening methods provide global modification on the lateral resisting load path by strengthening the frame at selected bays.

There is a numbers of retrofitting techniques available to the use of engineers such as installation of structural shear wall, use of structural steel members (i.e. steel brace, internal steel frame), and application of FRP diagonal braces. Among these techniques, adding structural shear walls is the most commonly employed solution. It provides significant lateral stiffness and strength to the existing system and helps in relieving the demand on the deficient members under seismic attack. However, this method has disadvantages such as being time consuming and requiring the evacuation of the building during concrete casting. Therefore, the need to develop practical, rapid, safe and economical retrofitting techniques still remains to be an important task of structural and earthquake engineering.

Steel braces are known to be effective in providing lateral strength and stiffness for steel frames. High lateral stiffness of the braces controls lateral deflection of the structures. However, brace members experience severe strength degradation as a result of tension-compression cycles after buckling. This effect is reflected in the seismic codes through the use of relatively low response modification (or behavior) factors compared to those used for other structural systems (Marino and Nakashima, 2005). On the other hand, use of steel braces is very economical for low rise frame structures for seismic resistance (Tremblay and Robert, 2001). Noting the fact that most of the deficient RC frames lack deformation capacity, it seems to be an acceptable approach to use steel braces in controlling deformation demands within the range of moderate ductility demands. In other words, the objective of economical seismic retrofit for non-ductile buildings can be viewed as providing sufficient stiffness, strength and moderate ductility capacity. Furthermore, the use of steel braces for seismic retrofit is worth evaluating due to advantages such as addition of minimal mass to the structure, little disturbance on the functioning of the building, and its ability to accommodate openings for architectural purposes. In light of the literature review presented in next section, it was observed that there is limited number of comprehensive studies on the use of post installed structural steel members for seismic strengthening of deficient RC frames with low strength concrete, plain bars and insufficient confining steel. The objective of this study is to investigate the performance of structural steel members when they are used in the upgrade of such deficient RC frames. In this way, possible design methods and limitations of such systems in seismic retrofits of low to mid-rise frames can be established.

The internal steel frame (ISF) is a relatively new subject to retrofit the deficient RC building stocks in Turkey. The ISF is intended to easily accommodate wall openings for architectural requirements. Furthermore, inspiring from the sound seismic behavior of moment resisting frames, ISFs are expected to exhibit a ductile response. Hence, they are believed to be good candidates for seismic retrofit of deficient RC frames.

1.2 Literature Survey

The seismic retrofitting studies have been heavily investigated in the last three decades. This section presents a numbers of studies on seismic retrofitting in relevant to the focus of the study. First, the understanding of individual steel brace member behavior is explained. Afterwards, braced frame and moment resisting steel frame behavior is briefed. Finally, the use of structural steel for seismic retrofit of deficient RC frames in the literature is discussed.

1.2.1 Steel Brace Research

Popov et al. (1976) conducted a literature review on the structural steel bracing systems. In this study, studies up to 1976s on the behavior of steel brace members, steel braced frames, experimental and analytical studies of the individual steel brace member and the behavior of the concentrically braced frame under static and dynamic loading were discussed. This literature review pointed out the need of further experimental work to better understand the brace and braced frame behavior.

Black et al. (1980) performed an experimental study to determine the inelastic buckling response of the steel members. For this purpose, 24 steel members with various slenderness and range of cross-sectional shapes and end connection (fix and pin) were tested. Based on experimental results it was found that although brace members had significant axial tension capacity, after yielding, the compression capacity of the brace members dropped significantly (Figure 1.1). This drop was closely related to the brace slenderness.

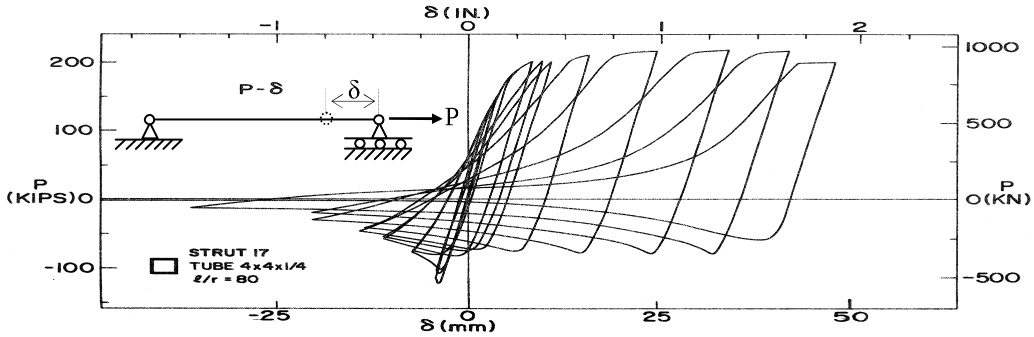

Figure 1.1 Force deformation curve of brace member taken from Black et al. 1980

Tremblay (2002) conducted a comprehensive experimental study by testing 76 brace specimens having various section types, cross section area, end conditions, brace effective slenderness, material properties, and displacement histories. It was found that except one specimen, the actual yield strength of the steel material is higher than the nominal values in all test specimens. Hence, this variation should be considered in design. Loading history had an important effect on the maximum tension force of the brace member. If a large tension excursion is applied at early stages in the tests, the highest loads could be observed. The strain hardening of braces made of tubular shapes was more effective than that of hot rolled shapes. In order to estimate the minimum brace compressive strength at a specific ductility's simple equations were proposed based on the test data for the symmetrical displacement history. The deformation response of the brace including the post buckling may be calculated by using the proposed equations derived using the test data. It was found that brace fracture for the rectangular hollow sections depends on the brace slenderness significantly. Furthermore, width-to-thickness ratio of the cross-section and the imposed displacement history has also effects on the brace fracture but not as well as slenderness.

Goggins et al. (2005) performed an experimental study on cyclic response of cold-formed hollow steel bracing members. The yield strength of the cold-formed steel members was observed to be higher than the strength usually estimated by the design codes. This seemed to be a problem for boundary elements. Both tensile (highest for members of intermediate slenderness) and compressive strength degradation was observed during the test. It was found that displacement ductility capacity of brace member increased with brace slenderness but it dropped with width to thickness ratio.

Broderick et al. (2005) conducted an experimental study on monotonic and cyclic response of the hollow and mortar filled steel members. The test results indicated that hollow sections were vulnerable to the reverse cyclic axial displacements. Due to local-buckling, brace fracture was observed during the experiments. On the other hand, the mortar infill seemed to prevent partially the brace from local buckling. Furthermore, the ductility of the brace members depends on their slenderness.

Han et al. (2007-a) tested eleven cold-formed hollow structural section (HSS) brace members by using quasi-static reversed cyclic loading. The main aim of the experimental study was to determine the effect of the width–thickness ratio on the seismic behavior of the HSS. The researchers observed that if the width–thickness ratio of the HSS brace members is low, the local buckling was delayed hence resulting in an increase of fracture life. On the other hand, the slot failure was another problem of the HSS brace member which may be seen for low width–thickness ratios. Moreover, the lower the width–thickness ratio of the HSS braces members the higher was the energy dissipation capacity.

Han et al. (2007-b) suggested a new design approach in order to prevent the slot failure observed during the tests conducted by Han et al. (2007-a). For the new design purpose, it was suggested that design fracture strength of the net section should be larger than the design yield strength of the gross section of the HSS brace member. To ensure this, the slot ends were reinforced with steel plates welded to the HSS brace member.

Uriz et al. (2008) proposed a model to predict the inelastic buckling behavior of steel braces. In this model, inelastic beam-column element with corrotational formulation of the OpenSees simulation platform was used to estimate the brace force-deformation relation. The proposed model was calibrated with the test members conducted by Black et al. (1980) in terms of initial imperfection, number of elements to represent the brace member, support conditions and number of integration points. It was found that the modeling of the second order effect along the brace is better when the number of elements to represent the brace is larger. On the other, at least two members were found to be sufficient for a reasonable global response of the brace force-deformation estimation by using force based frame elements. The initial imperfection at the mid length of the brace member (0.05–0.1% of the brace length) produced better estimations for brace behavior. The proposed modeling approach was successful in general to predict the cyclic behavior of the compact brace members.

Khatib et al. (1988) investigated the cyclic behavior of the concentric steel braced frames focusing on chevron braced frames. The main objectives of this study were to determine the parameters that influence the inelastic force redistributions in chevron braced frames (soft story is a problem in chevron braced frames) to improve the behavior of chevron braced frames, and to examine different design alternatives. For this purpose, one bay-one story and three bay-six story braced frame were examined under static and dynamic demands. It was observed that using a stiff beam at the braced bay resulted in large column axial compression forces which may causes column yielding. To prevent this, columns size needs to be increased. Furthermore, using stocky brace members did not improve the performance of the braced frame significantly. Zipper column application was also proposed to improve the response of the braced frame.

Hassan and Goel (1991) conducted nonlinear dynamic analysis in order to examine the six story concentrically braced frame structures with and without moment resisting frame. First of all, an improved hysteresis model for brace members is proposed to use in the analysis. It was proposed that in order to prevent the steel beam failure of a chevron braced frame, unbalance force after brace buckling should be considered. Moreover, the strength of the beam at the braced bay has no significant effect on the lateral strength of the non-moment concentrically chevron braced frame. For the analyzed frame, 1/3 of lateral strength was carried by the columns in the non-moment concentrically chevron braced frame. Designing a non-moment resisting frame while considering the ductility of braces and assuming a lateral force reduction factor as high as 10 resulted in excellent behavior. In addition, designing chevron braced moment resisting frames with ductile braces and assuming lateral force reduction factor as 12 resulted in acceptable performance under severe ground motions.

Remennikov and Walpole (1997) performed an analytical study on the prediction of seismic response of the low-rise X- and V-steel braced buildings. In this study, firstly, the inelastic force deformation relation of the individual brace members was developed. The proposed hysteretic behavior for individual braces was calibrated with the test data. By using the proposed model, two story-steel braced buildings were analyzed. It was proposed that ductile behavior of braced frames depends on the structural ductility factor which should not be greater than 3.

Tremblay and Robert (2001) performed an analytical study to investigate the seismic behavior of 2-, 4-, 8-, and 12-storey chevron steel braced frames. There were four type frames examined: Nominal ductility braced frame (NDBF) was designed with considering design lateral resistance R factor of 2. In this frame, beams should be designed to provide to strength sufficient at the initiation of buckling of the bracing members. The other three frames were more ductile braced frames (DBFs) designed with the R factor of 3. In the design of the beams the braced bays of these three frames were designed for 100%, 80%, and 60% of the brace yield load which led to three braced frame systems namely DBF-100, DBF-80, and DBF-60. It was found that inelastic responses of the bracing members caused significant reduction in storey shear resistance and stiffness leading to a soft story and dynamic instability problem. In order to compensate this drawback, following conclusions were reached: the numbers of story for the NDBF should be limited to up to 2. For higher stories up 4 stories, the drift and bending moments may be high. The maximum number of story of the DBF-60 and DBF-100 systems should be up to 4 and 12, respectively. Furthermore, DBF-100 systems up to 12 storeys could be used as far as beam loads due to gravity are small.

Tremblay et al. (2003) tested a total of 24 specimens which were one bay-one story X bracing and single diagonal bracing systems by using quasi static cyclic testing method. Cold-formed rectangular tubular bracing members were used as braces in the frame test. From the tests, it was observed that brace members experienced successive inelastic buckling and tension yielding. Brace fracture was observed after local buckling. The tension brace member provided a full support at the mid length of brace member for the X brace configuration hence the slenderness of the compression brace member may be evaluated by considering this support. Out of plane deformation of the X brace configuration was smaller than that of single diagonal bracing since tension brace provided supports to enable double curvature response. A model was proposed to determine the deformations for both the single diagonal and X-bracing configurations. Furthermore, the fracture of hollow section members for both bracing configurations was estimated by suggesting an empirical model which accounts for width-to-thickness ratio and effective slenderness ratio.

MacRae et al. (2004) examined the effects of continuous column flexure stiffness capacity on the concentrically braced steel frames. The relationship by using static pushover analysis for drift deformations and column moment demand were investigated for selected two-story and multistory frames. It was observed that dynamic shaking effects changed the peak drift concentration and column moment demand from the static analysis. Finally, a procedure was developed to predict the likely drift concentrations in braced frames of different heights.

Berman et al. (2005) conducted an experimental study on the braced frames and steel plate shear walls (SPSWs) in order to compare the seismic performance of them in term of stiffness, maximum displacement ductility, cumulative hysteretic energy dissipation, and energy dissipation. For this purpose, four concentrically braced frames and two light-gauge steel plate shear walls were tested by using cyclic quasi static testing procedure. It was concluded from these tests, while one of the braced frame specimens had largest initial stiffness, it was the steel plate shear wall which had the largest ductility. Up to ductility of four, braced frame and SPSW had similar capacity of the energy dissipated per cycle and the cumulative energy dissipation. After that, brace fracture occurred but SPSW reached a displacement ductility of nine.

Kim and Choi (2005) examined the overstrength, ductility, and the response modification factors of 21 special concentric braced frames (SCBFs) and 9 ordinary concentric braced frames (OCBFs). The pushover analysis was conducted to evaluate the structures with various stories and span lengths. In addition, the results of the static pushover and nonlinear incremental dynamic analysis were also compared. From the study, it was concluded that the response modification factor increases when the structure height decreased and the span length increased. Apart from three-story structures, the response modification factors of the most SCBFs model was found to be smaller that given in the code-specified value of 6.0. Similarly, the response modification factors of all OCBFs model was found to be smaller that given in the code-specified value of 5.0.

Marino and Nakashima (2006) dealt with seismic design of chevron steel braced frames. They focused on the behavior factor (q) proposed in EuroCode8 (2003) (EC8). This factor, 2.5, is constant regardless of the slenderness of braces. As well known behavior of the brace member, the axial force-deformation response of the brace members especially in post-buckling region depends on the brace slenderness. Because of this, some codes namely Japanese seismic code (BCJ) (1997) considers the brace slenderness. Hence, a method was proposed to estimate a chevron brace pair by summing of the yield strength and post-buckling strength of the brace in tension and compression, respectively. Finally, the behavior factor (q) was proposed as 3.5 in this study instead of 2.5 in the case of maximum inter-storey drift of braced frame approximately equals to that of most ductile moment resisting frames.

Johnson (2005) conducted an experimental study in order to examine the gusset plate effects on the braced frame performance. Johnson (2005) tested five full-scale SCBFs with different gusset plate applications (Figure 1.2). In this study, gusset plates were detailed by using current design methods and the proposed elliptical clearance requirement resulting in smaller gusset plates. From the tests, it was found that the using current design methods with 2t (t: gusset plate thickness) clearance resulted in a large and uneconomical gusset plate design. The frames designed by using proposed elliptical clearance had higher drift capacity due to delayed brace out plane of buckling which leads to tearing the plate and enable to experience more distribution of inelastic action in the SCBF system.

a) b)

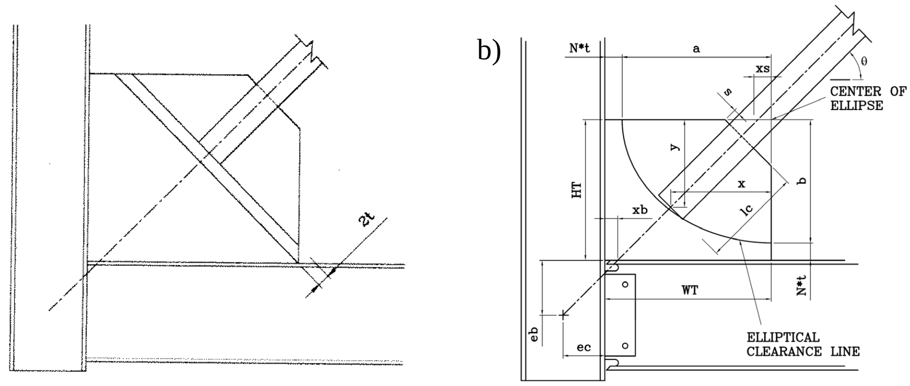

Figure 1.2 Gusset plate application, a) current design method using 2t clearance (t; gusset plate thickness), b) gusset plate with elliptical clearance (Johnson, 2005).

Kotulka (2007) performed an analytical study on the gusset plate design. The previous test frames were deeply examined. The researchers recommended the followings for a gusset plate design: 1) the gusset plate welds which were either complete-joint-penetration (CJP) welds or fillet welds, should be designed for the expected tensile yield stress of the plate. 2) A factor of 1.5 can be multiplied by the strength of the weld however, a β factor of 0.65 should be used instead of a ϕ factor of 0.75. Instead of a ϕ factor of 0.75, a β factor of 0.65 should be used to calculate the strength of the limit states of block shear fracture and Whitmore fracture of the gusset plate. 3) There is no need to check the limit states of Whitmore yielding and block shear yielding for the gusset plate design. 6t to 8t (t; gusset plate thickness) should be used to locate the end of the brace on the gusset plate.

Yoo et al. (2008) conducted a finite element study on brace frames. In this study, test frames were modeled by using inelastic finite element (FE) modeling after careful validations. Afterwards, to investigate the impact of different gusset plate connection design parameters on connection and system performance, a number of simulations were performed (Figure 1.3). The examined parameters were: the current linear 2tp (tp: gusset plate thickness) clearance requirement, elliptical clearance model, tapered and rectangular gusset plates, welded flange and shear-plate beam-to-column connections, gusset plate thickness, variations in the size of beams and columns at the gusset plate connection, weld length joining the brace to the gusset plate connection, frame geometry and brace angle of inclination.

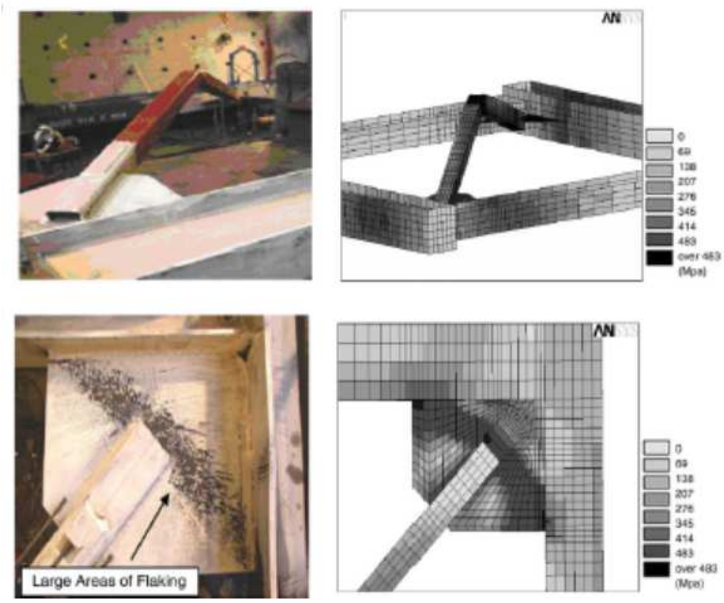

Figure 1.3 FE simulation (Yoo et al., 2008)

1.2.2 Seismic Retrofit Using Structural Steel Members

Higashi et al. (1980) conducted an experimental and analytical study on the seismic retrofitting of RC frames (Figure 1.4). The main objective of the retrofitting of existing RC building in this study was to increase the ultimate lateral strength and ductility of the RC building. For this aim, 13 1/3 scaled one bay-one story RC frames were tested with reverse quasi static testing procedure. While two of the 13 frames were reference frames the other were retrofitted with various techniques namely: infilled reinforced concrete wall cast in place, precast concrete wall panels in frame, precast concrete wall panels with door openings in frame, steel bracing in frame, steel frame in frame and steel truss in frame. Poor reinforcement ratio for flexure and shearing, and insufficient confinement for the columns were the main deficiencies of the RC frames. The concrete strength of the RC frame was reported as about 20.6 MPa. Figure 1.4 shows the retrofitted RC frames with steel members. The test results indicated that steel bracing can significantly increase the lateral strength and stiffness of the deficient RC frame.

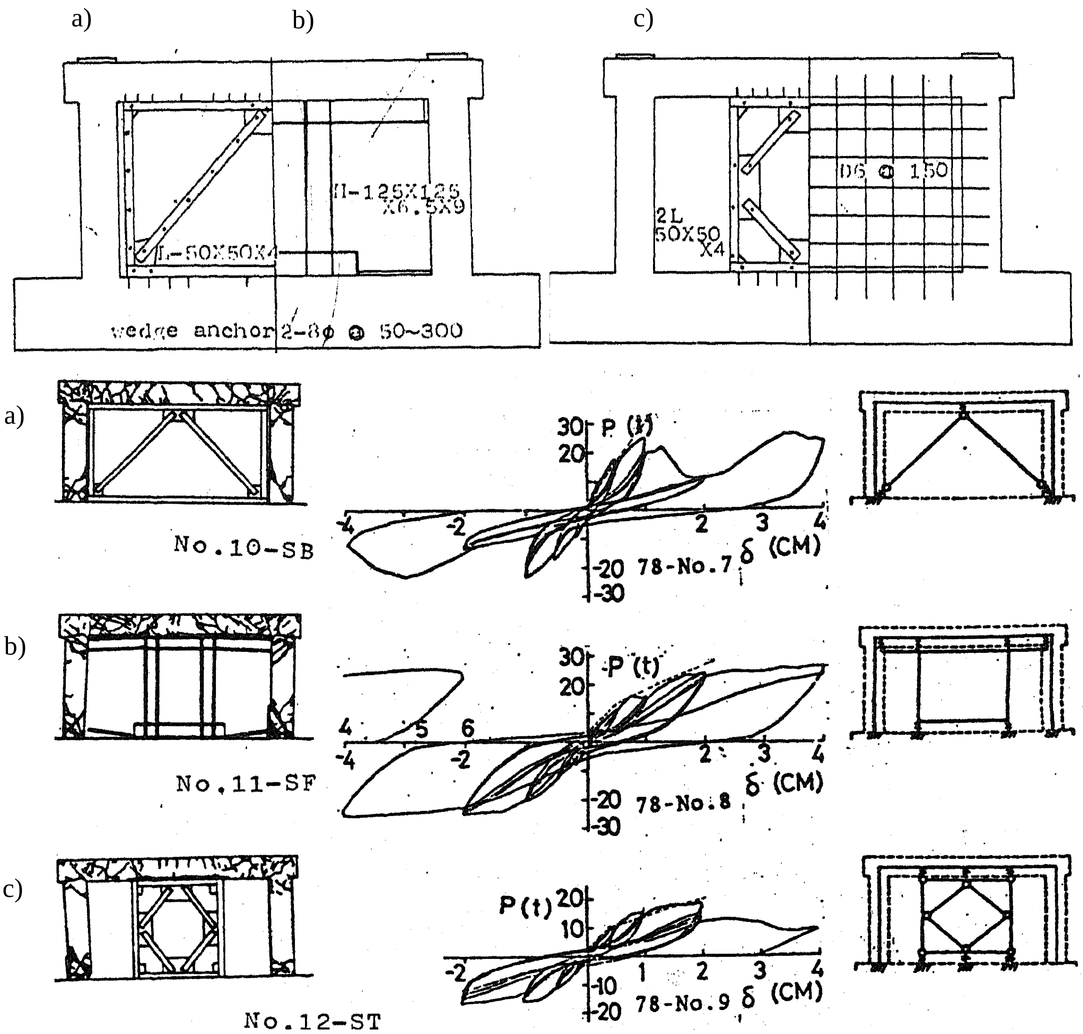

a: steel bracing in frame, b: steel frame in frame, c: steel truss in frame

Figure 1.4 Test frame and test results (Higashi et al., 1980)

Sugano and Fujimura (1980) conducted an experimental research on the seismic retrofitting of the RC frames. For this purpose, ten 1/3 scaled one bay-one story RC test specimens were tested by using quasi static testing procedure in order to investigate the various seismic retrofitting techniques namely shear wall, steel panel, cast in place concrete panel, precast concrete block and steel bracing (Figure 1.5). The RC columns had insufficient stirrups and the concrete strength of the RC frame was about 23.5 MPa. The test results indicated that the steel brace retrofitting techniques increased the lateral strength, stiffness and energy dissipation capacity of the RC frame. As can be seen in Figure 1.5 the bracing members applied large forces to the RC joints. Therefore, a suggestion to pay more attention on the RC joints was made.

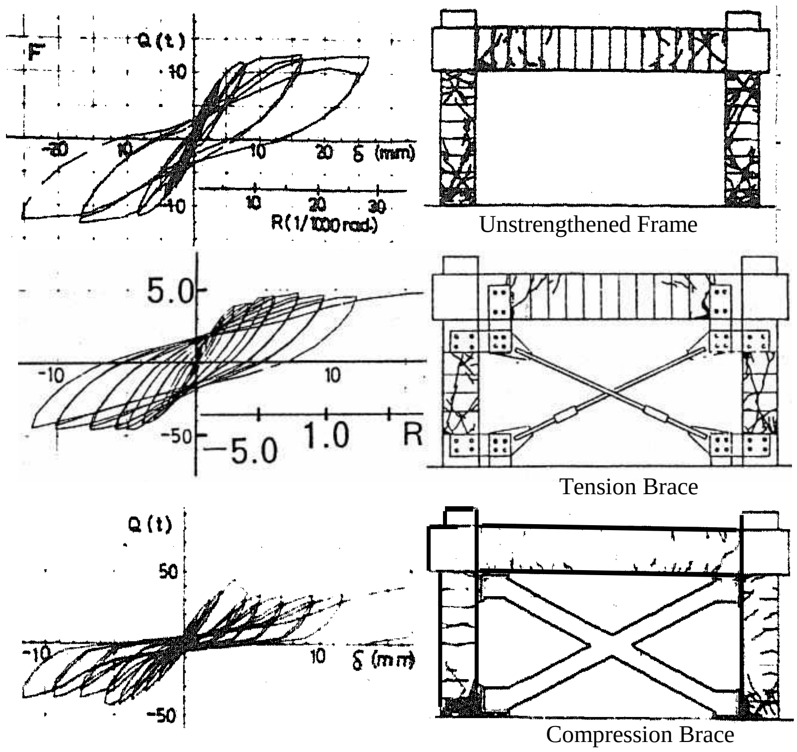

Figure 1.5 Test frame and test results (Sugano and Fujimura, 1980)

Kawamata and Ohnuma (1980) conducted a study on the design of steel braces for the retrofit purposes. An eight story pre-damaged RC building located in Japan was retrofitted by using combination of external steel bracing and shear walls. The connection between RC frame and brace members were performed by using post installed anchorage rods. The effectiveness of the proposed connection details was also tested by preparing a sub-assemble test setup. The suggested connection details performed satisfactorily according to the test results. Furthermore, in order to determine the cyclic performance of the brace members, 1/3 scaled steel braced frames were tested. With respect to performance of the connection and brace members, the design of the eight-story pre-damaged RC building was performed.

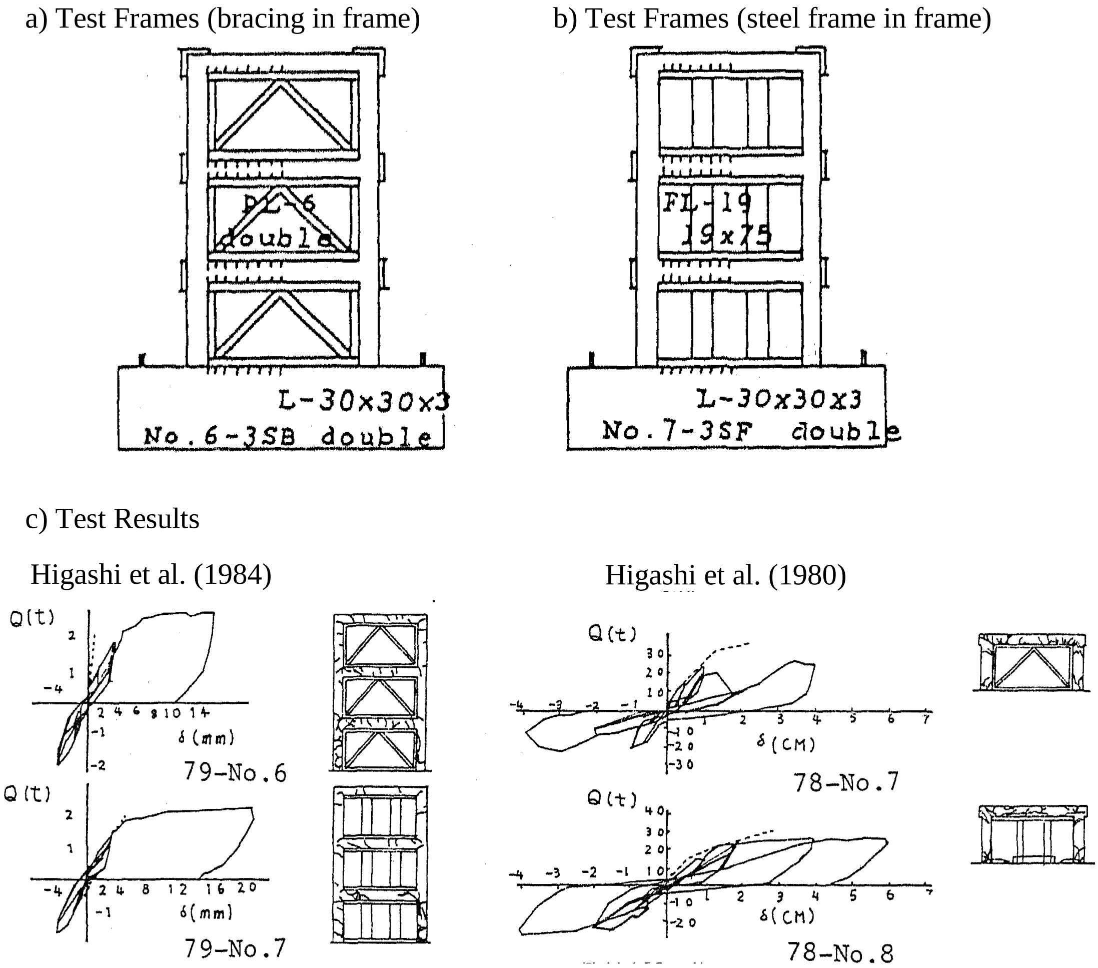

Figure 1.6 Test frames and test results (Higashi et al., 1984)

Higashi et al. (1984) tested eight 1/7 scaled one bay-three story RC frame before and after retrofit (Figure 1.6). The retrofitting technique used in this study was similar with study conducted by Higashi et al. (1980). There were four types of retrofitting techniques namely infilled reinforced concrete wall cast in place, precast concrete wall panels in frame, steel bracing in frame and steel frame in the frame investigated in this study. Insufficient confinement for the columns was the main deficiencies of the RC frames. The concrete strength of the frame was about 14 MPa. The test results indicated that the steel brace and steel frame retrofitting increased the lateral strength and stiffness of the deficient RC frames.

a) Subassemblage b) Analytical Model of Subassemblage

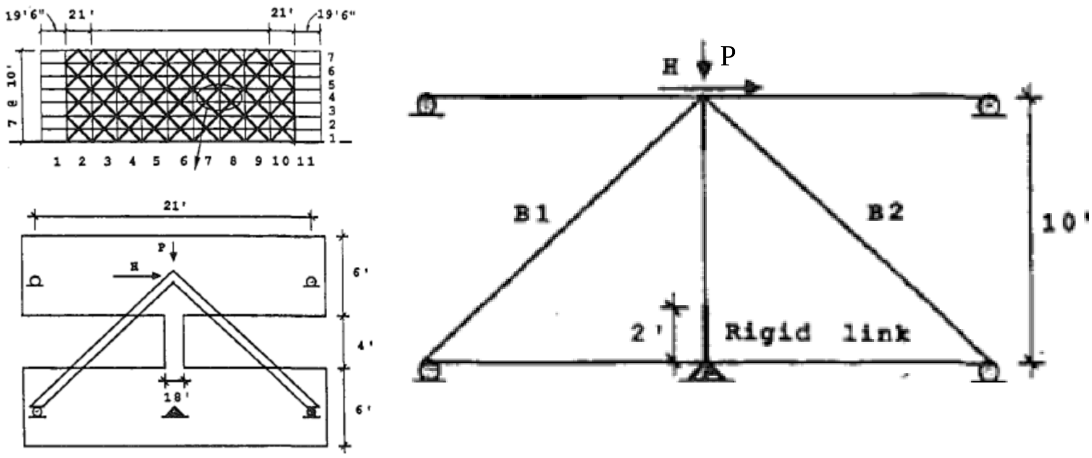

Figure 1.7 Subassemblage and analytical model (Badoux and Jirsa, 1990)

Badoux and Jirsa (1990) conducted both analytical and experimental studies to investigate the seismic retrofitting of RC frames with steel braces. In this study, deep beams and weak short columns were considered. The steel braces were installed adjacent to the exterior of the RC frame. Figure 1.7 presents the subassemblage and analytical model used in their study. The following conclusions were drawn by Badoux and Jirsa (1990): a) if the main aim of the retrofit scheme is to increase the stiffness of the structure, steel bracing is an appropriate solution, b) for seismic design, braces should be selected as a member working in the elastic range satisfying from ductility scarifying from ductility. Besides, if the brace connection is adequate, the brace yielding and buckling may provide significant hysteretic energy dissipation, c) Decreasing the slenderness of the brace enhances the inelastic behavior, hence increasing the ductility of the brace.

Bush et al. (1991) tested a two bay three story RC frame. The test frame contained deep, stiff spandrel beams and short, flexible columns (Figure 1.8). The concrete strength of the RC frame was 21 MPa. It was reported that the columns were vulnerable against the shear failures. Steel X brace technique was employed for the retrofit scheme. The brace members were attached to the exterior of the frame. The connection between RC frame and steel members were performed by utilizing epoxy-grouted treaded dowels (Figure 1.8). The test results indicated that steel bracing increased lateral strength and stiffness significantly and steel braces governed the cyclic behavior of the strengthened RC frame. In addition, it was found that after brace buckling, lateral strength dropped suddenly. The shear failure was observed at the RC column as expected. The dowel connections were performed well during the tests.

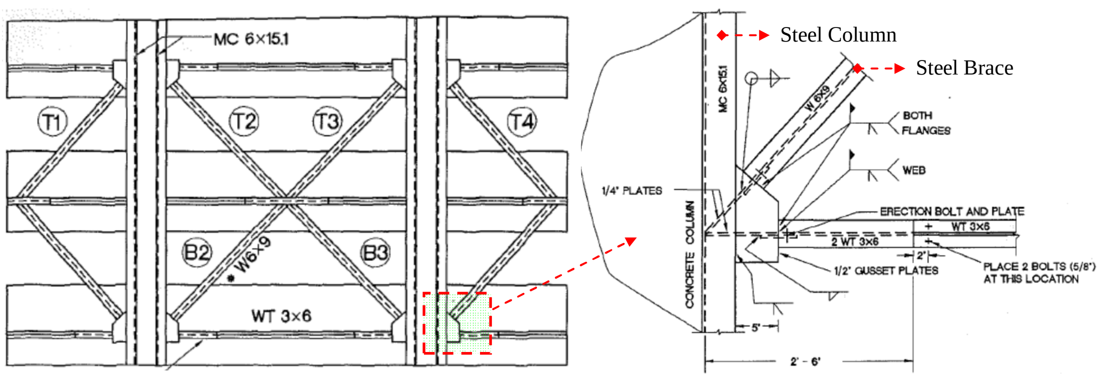

Figure 1.8 Test frame and connection details (Bush et al., 1991)

Downs (1991) examined the contribution of two retrofit schemes namely steel brace and RC infill wall applications. Two RC buildings Park Espana (ten-story built in 1960s) and Durango (twelve-story built in 1972), were strengthened by using both steel braces and RC infill wall (Figure 1.9). The concrete compressive strength of the former and latter buildings was 20.6 and 24.5 MPa, respectively. Plan irregularities, spaced stirrups, limited interstice between adjacent buildings and some construction errors were the main deficiencies of the retrofitted buildings. These buildings were damaged during the 1979 Mexico earthquake. After retrofitting, both retrofitted buildings experienced stronger 1985 earthquake. While the first earthquake caused severe damage on both buildings, the pre-damaged repaired buildings performed satisfactorily without sustaining any significant damage. The analytical study (or the earthquake) indicated that both retrofit schemes provided essential stiffness and strength increase in the buildings performed satisfactorily during the 1985 earthquake.

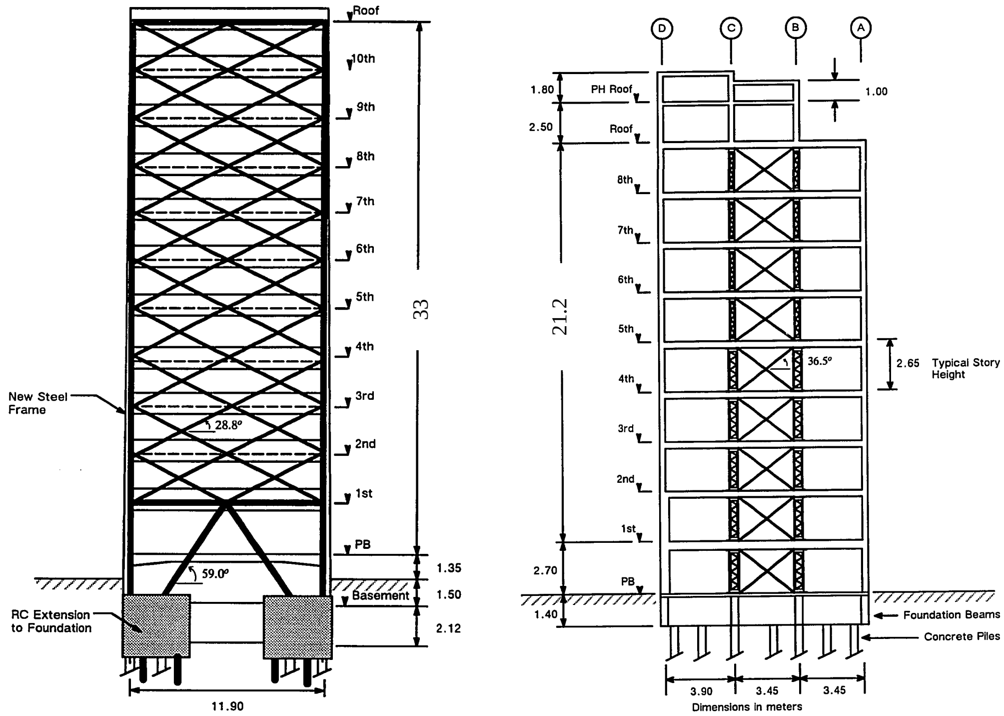

Figure 1.9 Examined buildings, Durango and Park Espana buildings (Downs 1991)

Tagawa et al. (1992) tested five ½ scaled RC frames to investigate the steel member retrofitting techniques. There were two techniques investigated in this study namely strengthened with I-section frames and corner braces besides I-section steel frame (Figure 1.10). The concrete strength of the test frames were between 21 and 25 MPa. The connection between RC and steel frame was performed by using headed studs and resin anchors. Headed studs were welded to the outside flange of steel frame, and headed resin anchors were driven into the RC frame. Then, the void between steel and RC frame were consolidated by mortar and spiral. The test results indicated that steel member retrofitted techniques used in this study increased the lateral strength and stiffness of the RC frames.

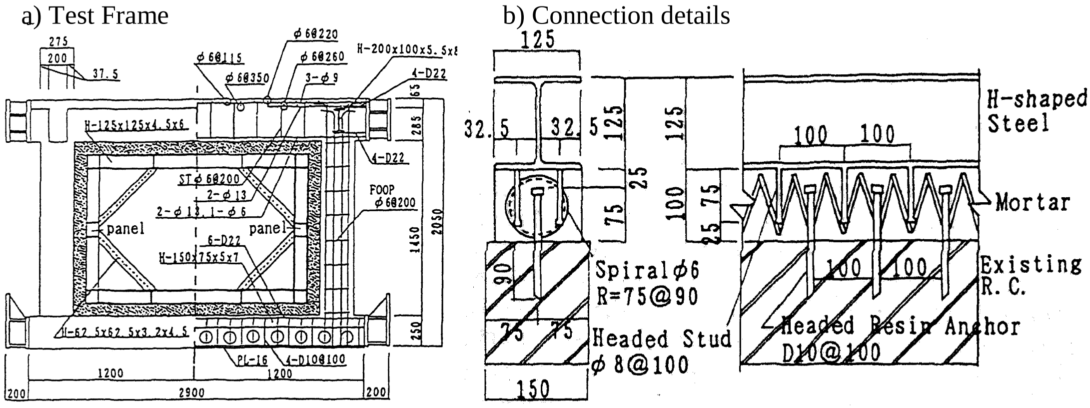

Figure 1.10 Figure test frame and connection details (Tagawa et al., 1992)

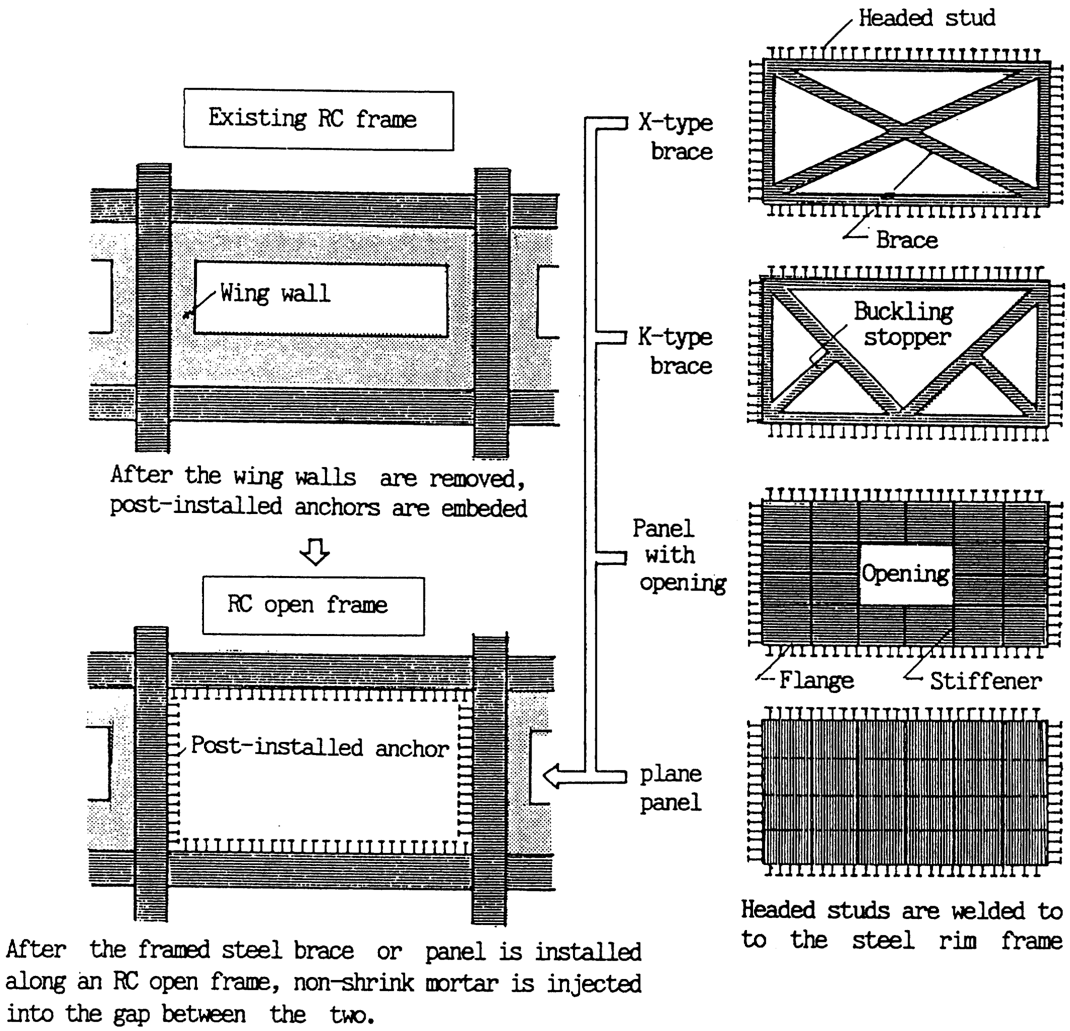

Figure 1.11 RC frame retrofitted with steel members (Yamamoto, 1993)

Yamamoto (1993) tested 16 1/3 scaled one bay-one story RC frames with retrofitting and without any retrofitting. Two of the test frames were bare RC frame and RC frame installed steel rim alone. The other specimens were retrofitted with steel brace and wall panel. Indirect connection between RC frame and steel members were performed for the retrofitting cases (Figure 1.11). The lateral reinforcement ratio was about 0.1% to simulate the insufficient confinement. The compressive strength of concrete of the RC frames was between 19.5 and 29.1 Mpa. The test results indicated that the steel brace and panel wall retrofit increased the lateral strength, stuffiness and ductility of the RC frame.

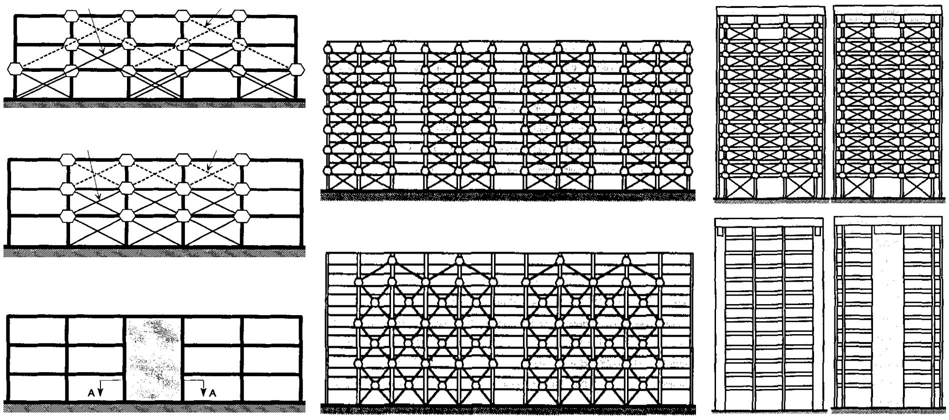
Three Story Building Seven Story Building Twelve Story Building

Figure 1.12 Retrofitted buildings (Pincheira and Jirsa, 1995)

Pincheira and Jirsa (1995) performed an analytical study on the seismic retrofitting of RC buildings with three different retrofitting techniques: Posttensioned bracing, structural steel bracing, and RC infill walls. In their analytical study, nonlinear static and dynamic analysis were performed by using five different ground motion and three different buildings which were three, seven and twelve story (Figure 1.12). The concrete strength of three, twelve and seven story buildings was 21, 35 and 21 MPa, respectively. Gravity load design, insufficient transverse reinforcement, short-lap splice at the base of columns, short anchorage lengths at the bottom of beam reinforcement, lack of confinement at the beam-column joints and short columns were the main deficiencies of the three story buildings. Soft story and a massive parapet at the roof existed in the twelve story building. Pin ended connection was assumed for the boundary condition of all strengthening brace members. The analysis indicated that all the retrofitting schemes increased both lateral strength and stiffness of the strengthened buildings. For low rise structures such as the three story building, all the retrofitting schemes performed satisfactorily. Without any strengthening, some of the existing RC member bracing systems did not experience an acceptable performance for the seven and twelve story building. On the contrary, the wall schemes performed satisfactorily for these buildings. The brace members applied additional axial load on the RC columns and it was suggested that strengthening of existing RC columns and beams of braced bays was found to be crucial for satisfactory performance of the braced strengthened frame. Consequently, it was found that superior performance of the retrofitted buildings depends on the limits of story drifts and damage of the existing gravity load carrying members.

Masri and Goel (1996) tested one-third scaled two bay-two story RC slab-column frames with and without steel brace retrofitting (Figure 1.13). The RC frame was constructed to simulate the older seismically vulnerable structures designed according to the early 1960's code requirements. The columns were strengthened by using steel angles and batten plates (Figure 1.13). The test results indicated that the steel bracing increased the lateral strength, stiffness and energy dissipation capacity of the retrofitted RC frames significantly.

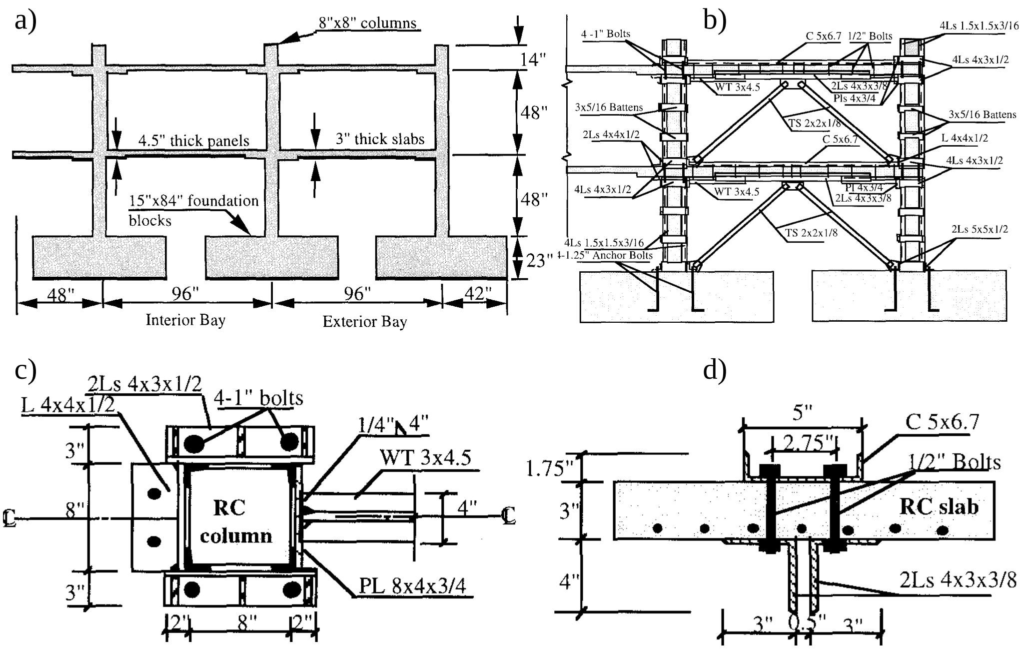

Figure 1.13 a) RC frame, b) Brace frame, c) Column section, d) slab section (Masri and Goel, 1996)

Maheri and Sahabi (1997) tested square RC frames with given dimension in Figure 1.14. The test frames were strengthened with steel brace diagonals. The proposed details of the connection between RC frame and steel braces were performed by two application procedures. While one of them was suitable for the existing frames, the other can be installed prior to concrete casting (Figure 1.14). Test results revealed that the steel diagonals increased the in-plane shear strength of the RC frame.

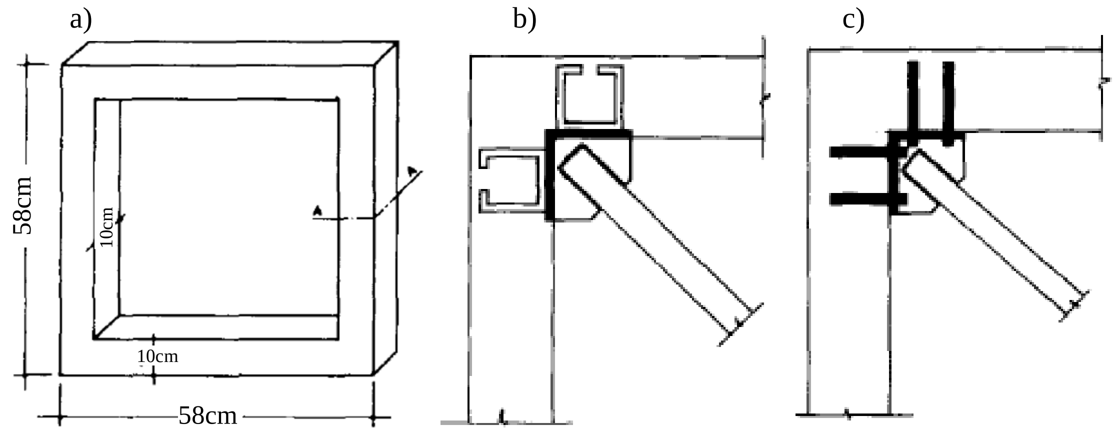

Figure 1.14 a) Test frame, b and c) connection details (Maheri and Sahabi, 1997)

Ghobarah and Elfath (2001) performed an analytical study in order to strengthen a three story RC office building by using an eccentric steel bracing system with a vertical steel link member (Figure 1.15). In the analytical study the seismic performance of the RC building retrofitted with steel braces is examined by using nonlinear static and dynamic time history analysis. Besides the effect of the eccentric steel brace distribution over the story of the three story of RC office building was also examined. The building was designed with respect to gravity loads only. The concrete strength of the building was 21 MPa. The connection details of the vertical steel link are shown in Figure 1.15. The analysis results indicated that steel braces with vertical links increased the lateral strength and stiffness of the RC building. The link deformation angle was found to be an important parameter. As long as the link deformation angle was limited under lateral demands the eccentric brace rehabilitation was expected to have better seismic performance than the concentric braces.

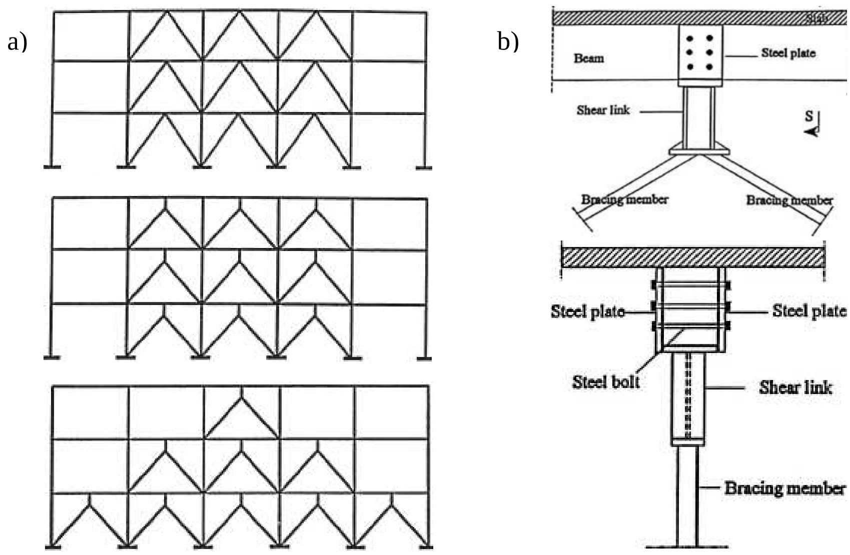

Figure 1.15 a) Frame view, b) connection details (Ghobarah and Elfath, 2001)

Maheri and Hadjipour (2003) conducted experimentals to study the connection details between RC frame and steel braces (Figure 1.16). A corner RC frame-steel brace joint was tested in their experimental program. The minimum concrete compression strength of the test members was 41 MPa. There were mainly three types of connections namely type a, b and c as seen in Figure 1.16. While two of them (type a and c) are not proper connection for the existing structures, the proposed connection type of c may be used for a retrofit case.

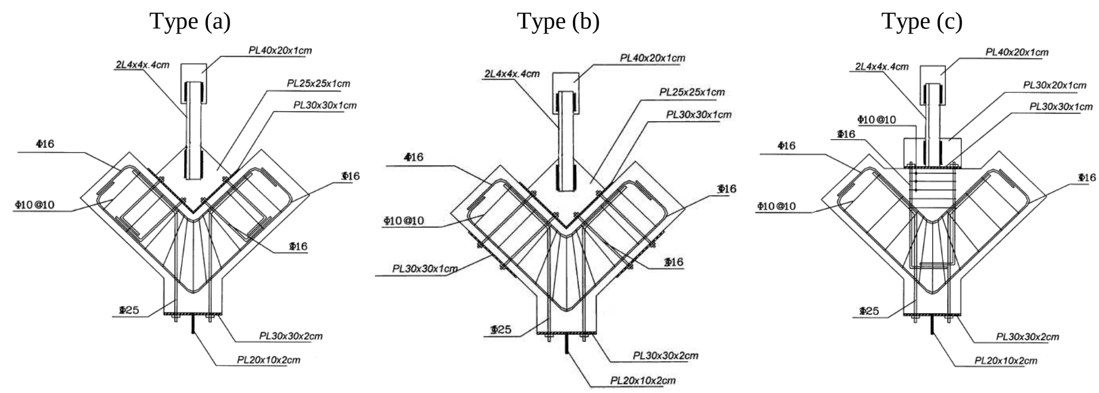

Figure 1.16 Connection types (Maheri and Hadjipour, 2003)

Bartera and Giacchetti (2004) tested single story RC frames retrofitted with dissipater bracing systems in the form of high damping rubber pad (HDRD) and a shape memory alloy wire assemblage (SMAD). It was concluded that both the HDRDs and the SMADs were capable of increasing the equivalent damping ratio of the braced frame. The hysteretic behavior of SMADs was found to be unstable and showed a progressive decay of the energy dissipated.

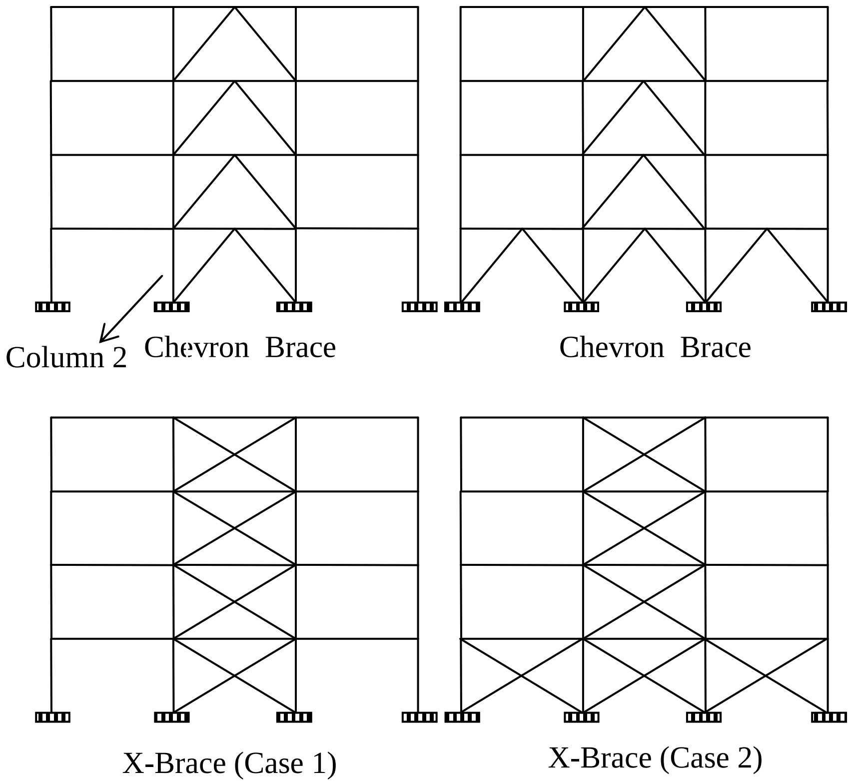

Figure 1.17 Frames retrofitted with X-brace and chevron brace (Ozcelik and Binici, 2006)

Ozcelik and Binici (2006) conducted nonlinear time history analysis in order to determine the performance of the retrofitted RC frame with the X-brace and chevron braces (Figure 1.17). For this purpose, a three bay-four story RC frame before and after retrofitting were examined under Duzce and Kocaeli earthquake demands. The concrete strength of the frame was assumed as 25 MPa and the columns had widely spaced stirrups (equal the smaller dimension of the columns section). Five different steel brace sections with two different arrangements (X-braces and chevron braces) were employed in the parametric studies. From the analysis, followings were concluded: 1) the interstory drift profiles of the retrofitted frame depend on the ground motion significantly. 2) The interstory drifts of the retrofitted frames were much less than that of deficient frame. Hence, steel braced frames were found to be effective lateral load resisting systems to control the story deformations. 3) Deformations in the retrofitted structures remained below the un-retrofitted case, indicating that interstory drift control can easily be achieved with the use of steel braces. 4) Upon scaling the ground motion it was observed that column curvature demands were limited up to a certain threshold value, beyond which curvature demands increased drastically. Hence it was possible to identify the performance points with incremental dynamic analyses and monitoring longitudinal rebar strains of columns. 5) As expected fundamental period of the buildings were inversely proportional with the brace cross-sectional areas and they were less influenced from the bracing pattern. It was observed that at shorter periods, i.e. for larger brace cross sections, ductility demands increased corresponding to an approximate R value of 2 to 4. Peak ground acceleration (PGA) of scaled ground motions at performance points was inversely proportional with the fundamental periods of the buildings. However, the relationships of PGA versus periods for Koaceli and Duzce ground motions were different due to difference in the frequency content of the two motions.

Youssef et al. (2007) investigated the use of steel braces in a newly constructed RC frames. There were two RC frames: one of them was designed as a moment resisting frame with respect to current code, the other was designed with steel braces to compare the performance of the both system. The connection between RC frame and steel braces were established by using anchorage rods which were placed before the concrete casting. The results indicated that the braced RC frame size calculated using the force reduction factors used in a conventional RC moment frame with moderate ductility may perform satisfactorily during an earthquake event. Finally, the RC frame and steel members can be designed by using available RC and steel structure design methods.

Mazzolani (2008) carried out full-scale experimental tests on different innovative seismic upgrading techniques based on the use of yielding steel components. For this purpose a two story existing RC building designed and constructed at the end of 1970s was examined. The steel upgrading methods were as follows; base isolation with rubber bearings, buckling restrained braces, composite fiber-reinforced materials, eccentric braces, shape memory alloy braces and shear panels (both in steel and pure aluminum). It was observed that effectiveness of the examined metal systems were more successful to improve the original capacity of the RC structure in terms of strength, stiffness and ductility.

It was observed from the literature view that there is further need to study the performance of structural steel retrofitted RC buildings (especially with deficiencies commonly seen in Turkey). Hence, the RC frame with and without any steel strengthening is considered to be topic of the research. The following items are sought to be properties of the RC frame which will be examined before and after retrofitting.

- The RC frame with low concrete compressive strength (approximately 10 MPa).
- The post installed direct connection between steel members and existing RC frame and the effect low concrete compression strength on this connection.
- The RC frame with insufficient transverse reinforcement for the columns and beam-column joint and improper stirrup details
- Using plain bar for the longitudinal reinforcement.

1.3 Aim of the Study

The seismic performance of the exiting RC buildings in developing countries needs to be assessed and strengthened by using modern engineering techniques. This is necessary to prevent the catastrophic effects of the earthquakes on structures in urban areas. Most of the existing RC buildings constructed prior to modern codes are vulnerable against the imposed lateral load demands. There is still an urgent need to develop rapid, safe and economical retrofitting technique to improve the seismic performance of the existing deficient RC building. The techniques must be rapid, safe and economical since there are thousands of vulnerable RC buildings in the developing countries. A compressive research program was conducted at the Middle East Technical University within the scope of this thesis. For this purpose, extensive experimental and numerical study was performed to investigate steel member retrofit.

The main objectives of the experimental study are:

- To observe lateral strength, deformation and energy dissipation capacity enhancement.

- To observe performance limits of the RC frame upgraded by structural steel members.
- To determine alternatives for connection and performance based design.

The main objectives of the numerical simulations are:

- To estimate the behavior of the test frames and to propose methods for this purpose
- To compare the estimated performance levels of the test frames by using available member deformation limits with test observations
- To demonstrate the use of proposed strengthening schemes on a case study building

In Chapter 2, one bay-one story RC frames without any retrofit and with retrofit were tested by using reverse quasi static test procedure. In this section, two reference frames, five chevron braced frames, six internal steel frames, one X-braced frame and one column with shear plate frame were tested. The test results are presented and critically discussed.

In Chapter 3, three bay-two story RC frames were tested by using pseudo dynamic (PsD) testing procedure. One of three RC frames was reference frame without any retrofitting and two RC frames were retrofitted with chevron brace and internal steel frames. The reference frame had an infill wall at the interior bay and this frame was tested by Kurt (2010).

In Chapter 4, the numerical simulation of the test frames performed in Chapter 2 and 3 was conducted. The reverse cyclic tests were simulated by conducting an inelastic nonlinear pushover analysis. Then, the performances of the test frame were determined by using strain limits suggested by Turkish Earthquake Code (TEC) (2007) and American Society of Civil Engineering (ASCE/SEI 41) (2007) document. For the PsD test, nonlinear time history analysis was performed and the performance of the test frame were evaluated based on the TEC (2007) and ASCE/SEI 41 (2007). Finally, a 5-story existing deficient RC building was evaluated with respect to TEC (2007) and ASCE/SEI 41 (2007) against the demand of Duzce ground motion.

In Chapter 5, summary and important conclusions of the experimental and numerical results are presented. For a seismic retrofitting scheme, a simple design flow chart is suggested.

CHAPTER 2

2. CYCLIC TESTS ON ONE BAY ONE STORY FRAMES

2.1 Introduction

Strengthening of 1/3 scaled one bay-one story test frames with structural steel members were examined in this chapter. These tests were conducted on small scale one bay-one story structures in order to rapidly evaluate and understand the force transfer mechanisms and relations of damage to deformation. These tests were not indented to simulate the system behavior in actual buildings except first story. Conversely, they were merely tested to examine the performance of steel strengthened specimens. The test schedule (Figure 2.1) shows that strengthening of deficient RC frames with structural steel members can be divided into two techniques, namely internal strengthening and external strengthening. The study of external strengthening technique is outside the scope of this chapter and described elsewhere Özkök (2010).

This chapter deals with the internal strengthening techniques by using chevron braces, internal steel frames (ISFs), X brace and column with shear plate. One bay-one story RC test frames were used for the reference and strengthened frames. Within the scope of the experimental study, there are a numbers of parameters whose effects on RC test frame and individual steel members should be investigated.

Steel braces are known to be effective in providing lateral strength and stiffness for steel frames. However, they experience severe strength degradation as a result of tension-compression cycles (Tremblay, 2002; Marino and Nakashima, 2006). This effect is reflected in the seismic codes through the use of relatively low response modification (or behavior) factors compared to those used for other structural systems. On the other hand, use of steel braces is very economical for low rise frame structures for seismic resistance as mentioned in Chapter 1. Noting the fact that most of the deficient RC frames lack deformation capacity, it is a sound approach to use steel braces in controlling deformation demands within the range of moderate ductility demands. Furthermore, the use of steel braces for seismic retrofit is worth evaluating due to advantages such as addition of minimal mass to the structure, little disturbance on the functioning of the building, and its ability to accommodate openings for architectural purposes. The objective of this chapter is to investigate the performance of chevron braces when they are used in the upgrade of such deficient RC frames. In this way, possible design methods and limitations of chevron braces in seismic retrofits of low to mid-rise frames can be established.

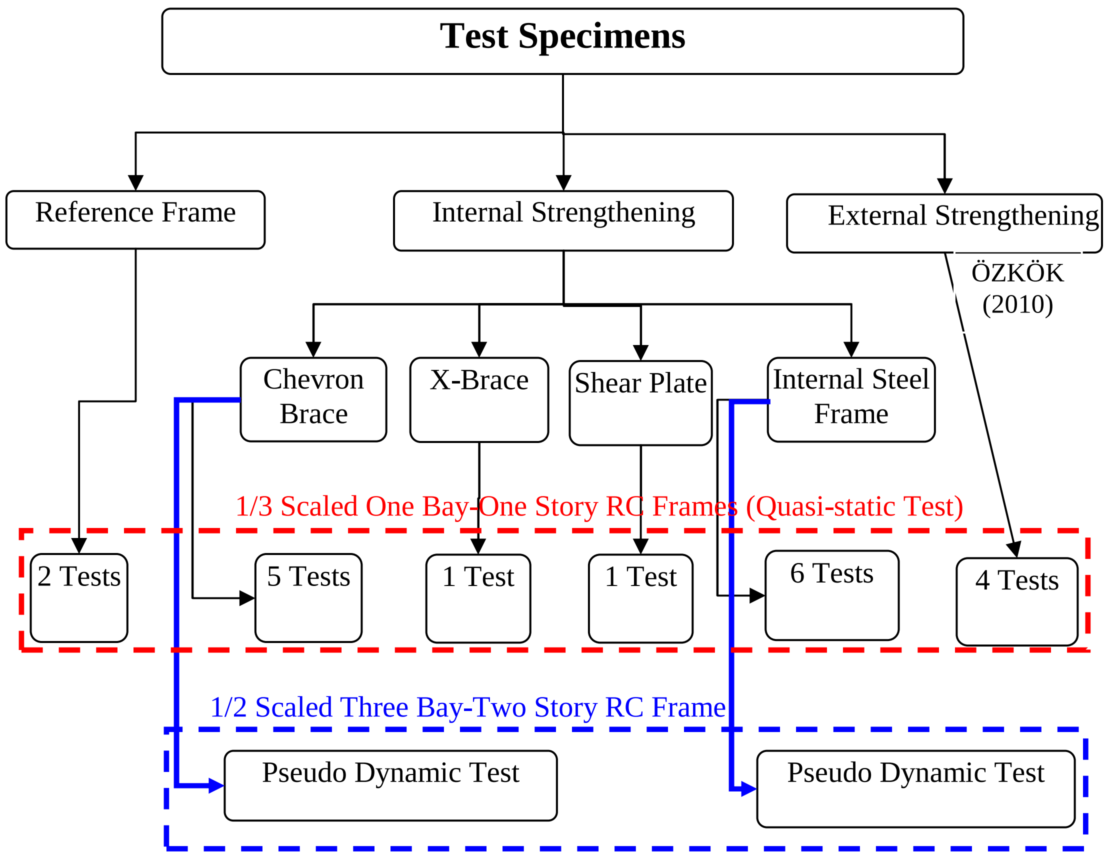

Figure 2.1 Schedule of the strengthening frames with structural steel members

Unlike chevron braced frames, inspiring from the satisfactory seismic behavior of moment resisting frames, ISFs are expected to exhibit a ductile response. The ISFs are intended to easily accommodate wall openings for architectural requirements. In addition, an X-braced RC frame was tested to investigate the performance of the different bracing configuration. The RC frame with steel column with shear plate was tested in order to determine the steel retrofitting efficiency. In this upgrading system, it was desired to enhance the seismic performance of the RC frame by providing shear yielding of the plate. In the following parts of this chapter, application details and test results of reference frames, chevron braced frames, ISFs, X-braced and column with shear plate frames will be presented.

2.2 Test Specimens and Setup

Fifteen 1/3 scaled one bay-one story RC test frames were constructed to investigate the retrofitting techniques with structural steel members. The RC frames tested during the course of experiment are: two reference frames, five frames strengthened with chevron braces, six frames strengthened with ISFs, one X-braced frame and one steel column with shear plate.

The test frames represented approximately 1/3 scale of a prototype structure previously studied by Ozcelik and Binici (2006) (Figure 2.2-a). It was previously shown by some researches (Maheri and Sabebi, 1997; Youssef et al., 2007; Bertero et al., 1984; Aktan and Bertero, 1984; Benjamin and Williams, 1958; Vintzileou et al., 1999) that such scaled RC specimens can represent the expected load-deformation response of their full-scale companions as long as similitude laws are followed when deciding on member dimension and material properties. Figure 2.2-a indicates that the first story of the analyzed three bay-four story RC frame was considered to examine before and after retrofit. In addition, the laboratory constraints also determined the dimension of the test frame and cross section of the RC members. Furthermore, strong axis of the column was also considered in order to provide small section limitations for the connection application i.e. drilling of the RC columns, anchorage rod installation. Consequently, a primary design to determine the dimensions of the RC frame was performed by using Opensees simulation platform Mazzoni et al. (2010) by using distributed plasticity modeling. Figure 2.2-b and c indicates the numerical simulation and results of the pre-dimensioned test frame. In this numerical simulation Kent and Park (1971) concrete model was utilized for the columns and beam. Longitudinal bar buckling was modeled by employing the backbone curve of Dhakal and Maekawa (2002). The concrete compression strength was assumed to be 8 MPa. The yield strength of the reinforcement was taken as 330 MPa. The main deficiencies of the primary designed RC frame were:

a) Insufficient confinement such as 100 mm spacing at the column plastic hinge regions.
b) Insufficient volumetric confinement ratio with respect to TEC (2007)
c) Low concrete strength (7-10 MPa).
d) Violation of the strong column-weak beam formulation with respect to TEC (2007).

It can be concluded that the expected plastic mechanism occurs by the formation of column plastic hinges. Furthermore, the estimated lateral capacity of the test frame was about 17.6 kN.

Accordingly, the center-to-center span length was decided as 1400 mm and the column height was 1000 mm in test frames (Figure 2.3). The 100 mm × 150 mm columns were provided with four 8-mm diameter longitudinal reinforcement plain bars resulting in about 1.33 % longitudinal reinforcement. The longitudinal bars were welded to steel plates embedded in the top end of the column in order to prevent anchorage failure of the longitudinal bars (Appendix 1, section A1.1). 4 mm diameter plain bars were used for stirrups. Although TEC (2007) requires stirrups to be anchored using 135 degree hooks, 90 degree hooks were used for all columns and beam to simulate the detailing deficiency of the Turkish construction practice before the establishment of the modern seismic codes. The stirrup spacing of the columns was equal to the smaller dimension of the column section (100 mm) to simulate insufficient confining details (that was 500 mm in the analytical model). The 100 mm × 150 mm beam was cast with a 450-mm wide, 55-mm thick slab. In addition to including slab effects, the slab was used as a platform to directly support the steel blocks that applied a constant gravity load. A 70-mm transverse reinforcement spacing was used for the beams. The RC beam-column joint had only one column stirrup extending into the joint. The picture of the test setup is shown in Figure 2.4. Design and construction details and drawing about test frames and setup is given in Appendix 1.

Material properties

The average yield strength of the 4-mm and 8-mm diameter reinforcement bars was determined as 270 and 330 MPa, respectively, by conducting uniaxial tension tests according to American Society for Testing and Materials E8 (ASTM) (2004). These values were determined from five 4 mm and fifteen 8 mm coupon tests. The testing apparatus and measured stress-strain response of the reinforcing bars are presented in Figure 2.5 and Appendix 1.

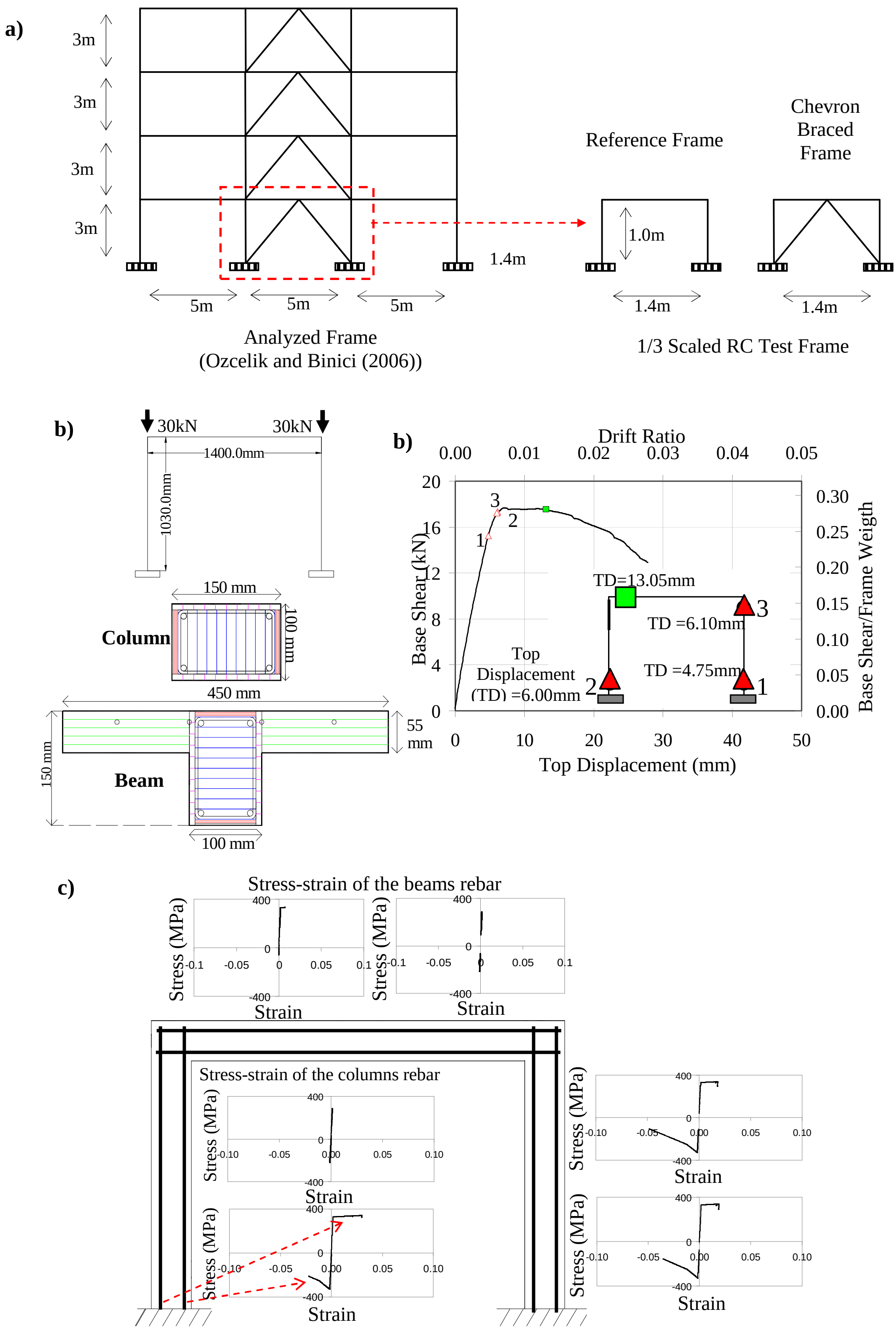

Figure 2.2 a) prototype structure, b) numerical simulation of the RC frame (distributed plasticity model), c) strain at the longitudinal bars

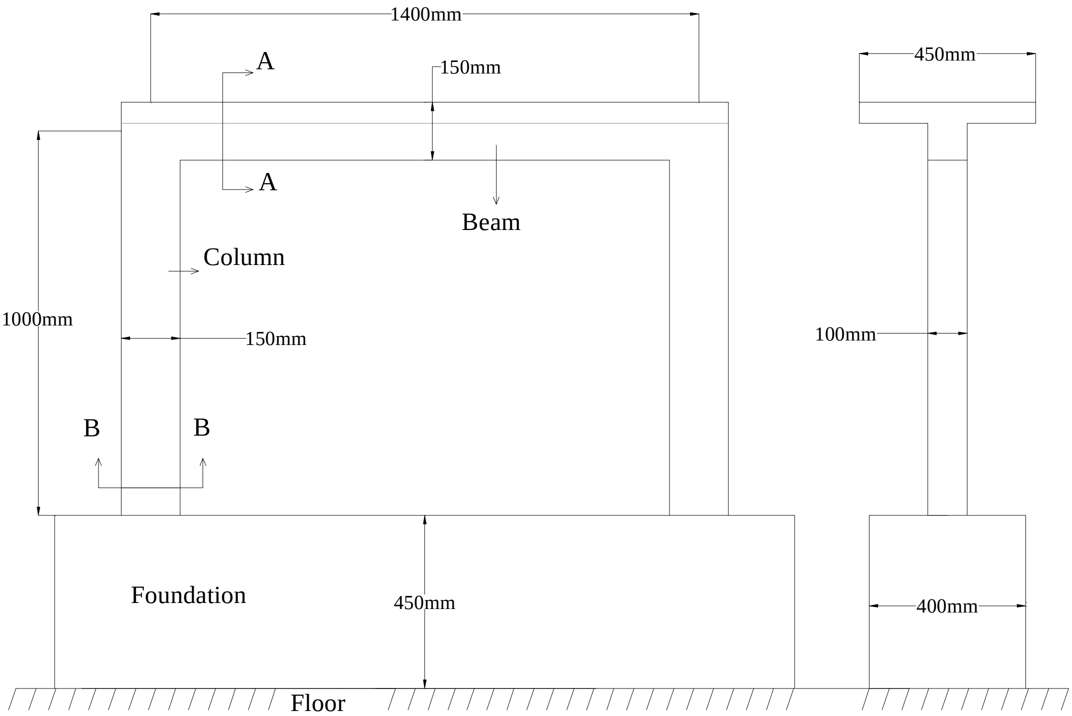

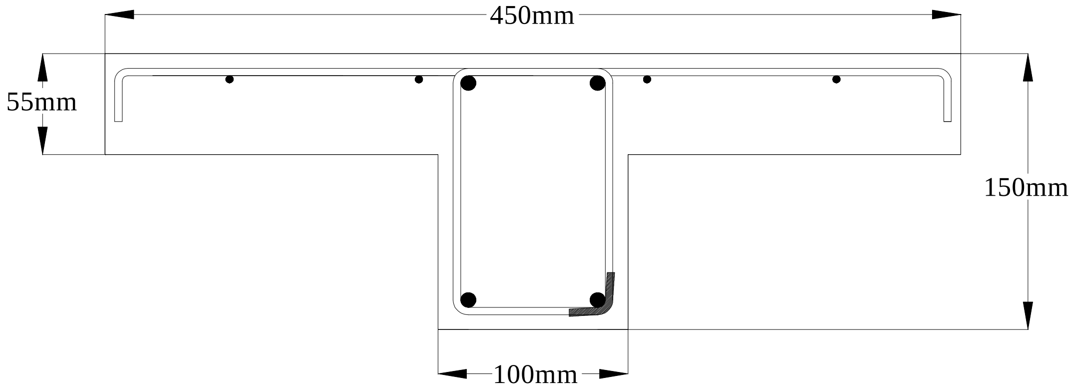

Longitudinal bar; 4-ϕ8 and 4-ϕ4, Stirrup; ϕ8/70mm

Section A-A

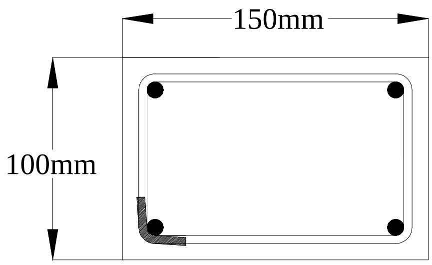

Longitudinal bar; 4-ϕ8, Stirrup; ϕ8/100mm

Section B-B

Figure 2.3 Dimensions of the test frame

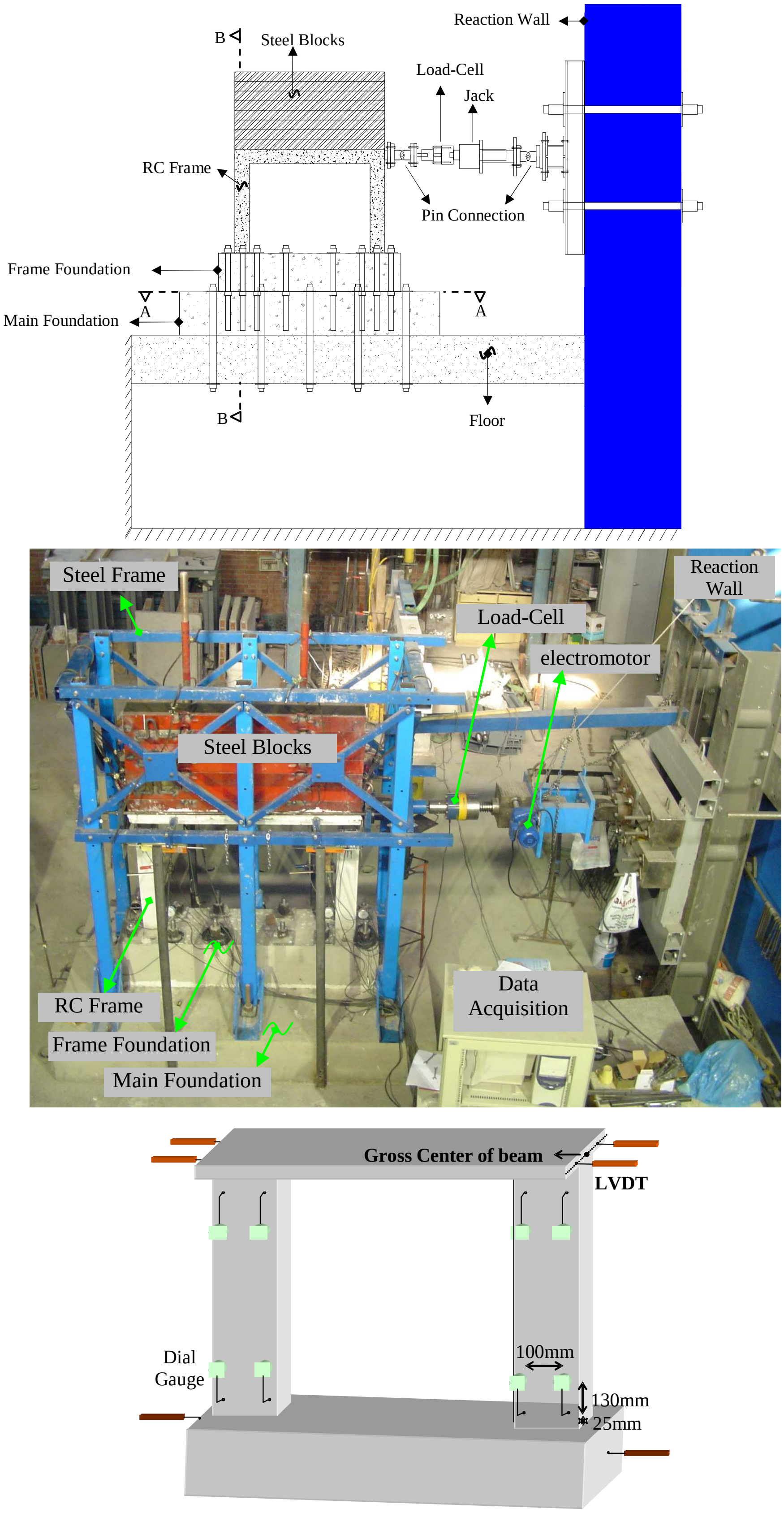

Figure 2.4 Test setup and instrumentation

The concrete had a maximum aggregate size of 7 mm with a target 28-day cylinder compressive strength of 8-10 MPa. This simulates the concrete strength in existing deficient structures of the Turkish RC building stock as reported by the field investigations (Çağatay, 2005; Tezcan and İpek, 1995; Doğangün, 2004). The mixture of the concrete is given in Table 1. The measured concrete strength at the day of testing coincided quite well with the target strength of 8-10 MPa.

Loading system

An additional steel frame was constructed around the RC frame as a precaution in the case of a sudden gravity collapse (Figure 2.4). Each steel block approximately weight 6 kN was attached loosely to the steel frame with cable. The cable was slack enough to enable the RC frame to perform lateral displacement. Steel frame was designed to carry all steel blocks under dynamic type sudden loading.

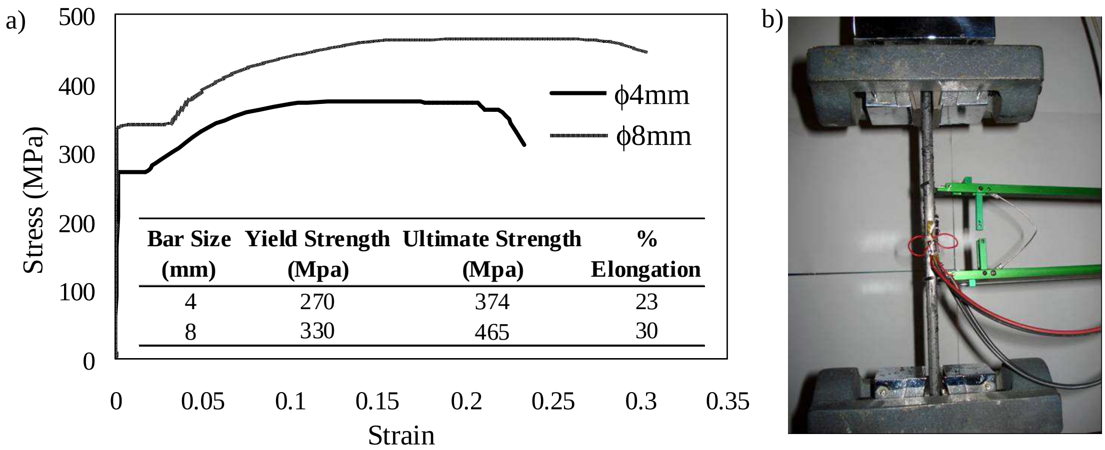

Figure 2.5 a) Stress-Strain response for transverse and longitudinal reinforcement, b) Picture of member ϕ8mm bar during the test

Table 2.1 Concrete Mixture

Mixture Component	Weight (kg)	Proportions by weight (%)
Cement	50	10.9
Water	50	10.9
0-3 mm aggregate	140	30.4
3-7 mm aggregate	220	47.8

The lateral excursion was applied to the frame with an electromotor driven jack with a maximum speed 0.2 mm/sec (Figure A1.7). Four 200mm-Linear Variable Differential Transducers (LVDTs) and a 200KN-load cell were attached on the RC frame along the direction of gross centre of beam to obtain horizontal top displacement and lateral forces, respectively (Figure 2.4). Two electronic dial gauges were placed on the top and bottom of each column to measure displacement. Measured displacement at the columns ends enabled to determine curvatures of the columns. Cyclic lateral loading was imposed by controlling the drift ratio (DR): Two cycles were introduced at drift ratios increased to ± 0.5, 1.0, 1.5, 2.0, 3.0, 4.0, and 5.0% in an increasing manner. Afterwards, the DR was increased by ± 1% and one cycle was applied at each DR. The loading protocol is showed in Figure 2.6.

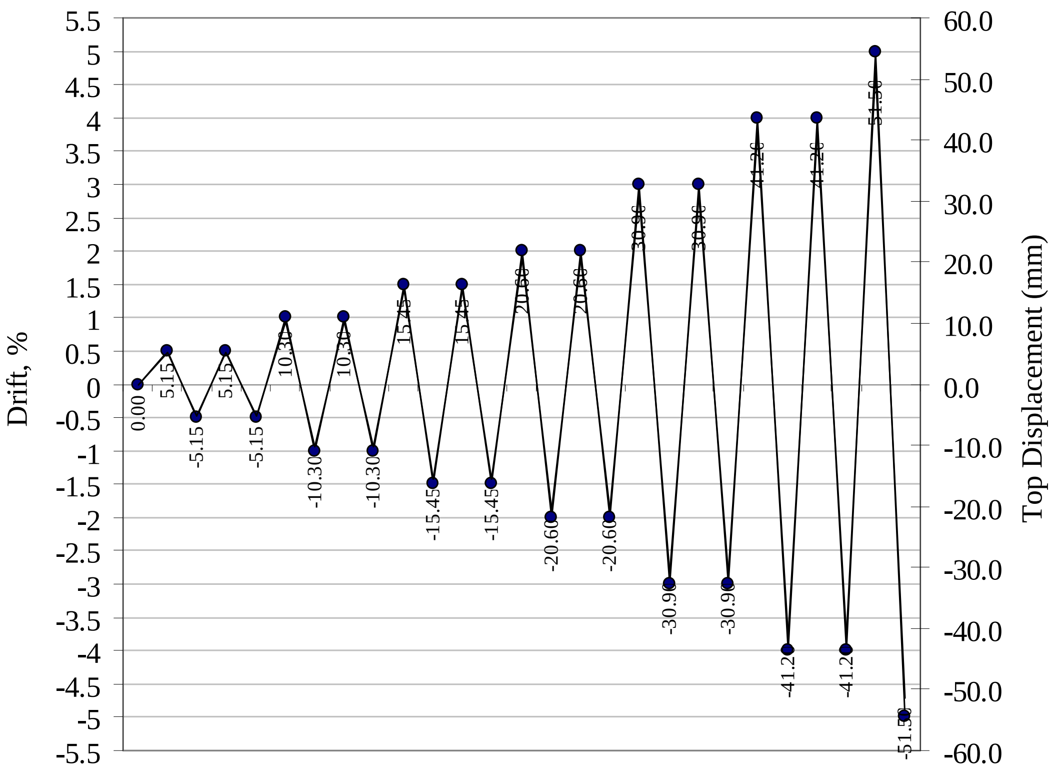

Figure 2.6 Loading protocol

2.3 Reference Frames

All of the RC frame specimens were similar in terms of dimensions and reinforcement ratios to allow a uniform basis of comparison. Two reference (or bare) frames which were not strengthened were tested for sake of comparison between strengthened frames and reference frame. In this study, reference frames were encoded as R_axial load ratio (%)_concrete compressive strength. For example, R_13_10 labels the reference frame which had 10 MPa concrete compressive strength with column axial load ratio of 13 %. The column axial load ratio was defined as the ratio of the sum of column axial loads to the column axial load carrying capacities (computed simply as the concrete compression strength times gross section area of columns). The main difference between reference frames was the axial load level (21 kN and 30.6 kN were applied as a gravity load on each columns for the R_13_10 and R_25_8.1, respectively) on the columns as indicated in Table 2.2. Figure 2.7 presents the frame before the test.

Table 2.2 Experimental program of the reference frames

Specimen	Concrete Compressive Strength (MPa)	Axial Load Ratio
R_13_10	10.0	0.13
R_25_8.1	8.1	0.25

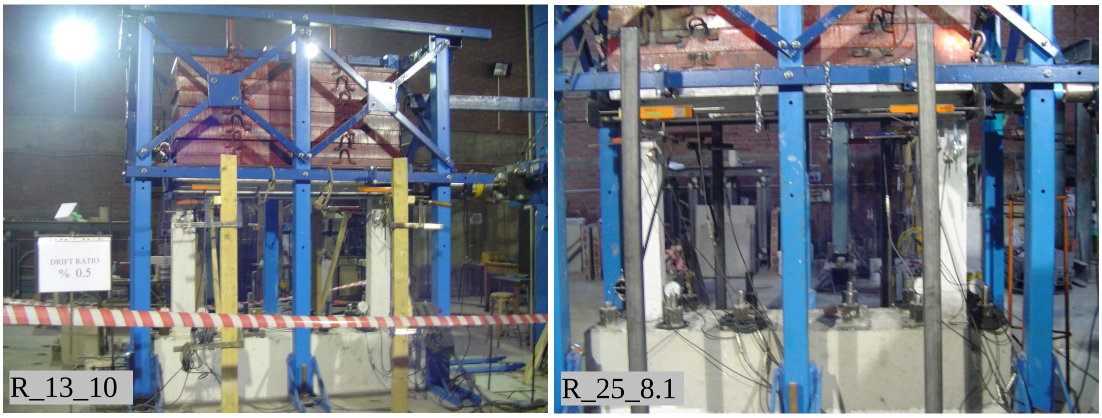

Figure 2.7 Pictures of the reference frames before the test

2.4 Strengthened Frames

Internal strengthening was accomplished by four different methods: Chevron braces, Internal Steel Frame, X-braced frame and column with steel shear plate. Five, six and one for each strengthened frames were tested for chevron brace, internal steel frame, x-braced frame and column with shear plate, respectively. The specimens' details and application procedures are explained in the following section following that test results are presented.

2.4.1 Chevron Braced Frames

Chevron brace strengthening methods are commonly used in the steel frames to resist against the lateral demands. These braces are implemented into the frame as "V" or "inverted V" configuration. This section deals with the latter configuration.

Application details of the chevron brace

In the chevron brace strengthening, an inverted V steel brace system was installed by using three connections between RC frame and chevron brace members. While two connections were at the bottom of the column and the other connection was at the mid span of the beam. Figure 2.8 indicates the general view of the braced frame and connection details. The strengthening started after the placement of the steel blocks as dead weight to simulate existing structures. The steel members used for connection between the brace and the RC frame are indicated in Figure 2.9. The design of the brace and application procedure are given in the upcoming sections with complete details in Appendix 1. Strengthening steps were the same for all braced frames and are as follows:

1) Connection application at the column: First, the anchorage holes were drilled into RC column and foundation. Subsequently, these holes were cleaned up at three steeps: i) air blowing, ii) brushing and iii) air blowing in order to establish the anchorage rod connections (Figure 2.10). Then, epoxy primer was injected into these holes followed by the insertion of the anchorage rods. The diameter of the anchorage rods and holes were 6 mm and 8 mm, respectively, whereas the depths of anchorages were 120 mm from the member face. The gaps between the rods and holes were filled with epoxy to obtain flat and smooth bonding surfaces. Finally, plate 6 and 7 were tightened to provide successful force transfer from the braces to the RC member (Figure 2.8 to 2.10).

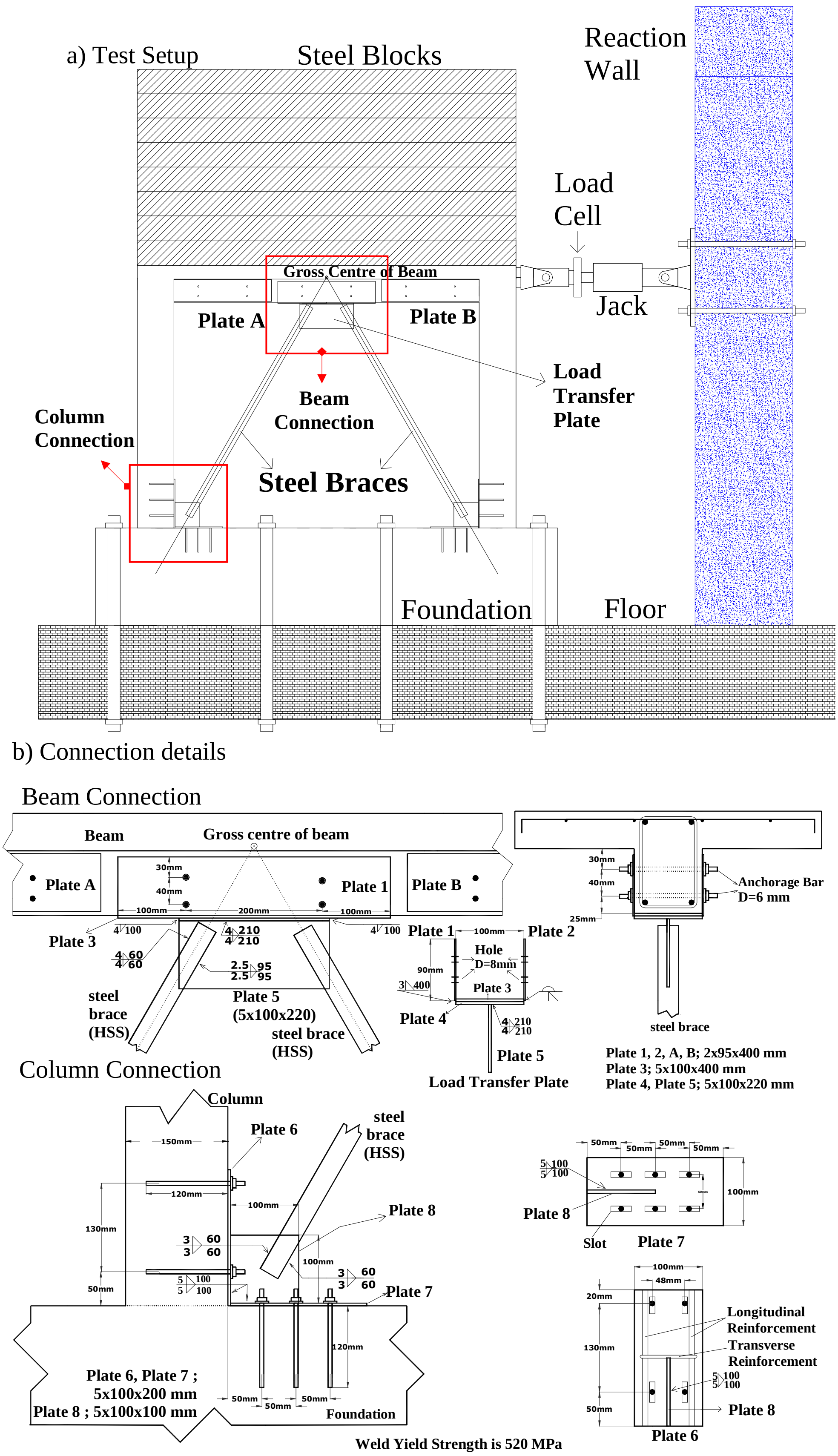

Figure 2.8 Chevron braced frame test setup, b) Connection details

2) Connection application at the beam: It was considered that the braces attached at the mid span of the beam induce unbalanced shear force upon brace buckling. Hence shear strengthening of the beams was performed by bonding 2 mm thick side steel plates and providing side anchorages to transfer forces from the braces to the beam. First, anchorage holes extending from one face to other were drilled at the beam. For side plates (Plate A and B), epoxy primer was injected into these holes followed by the insertion of the anchorage rods (Figure 2.11). Then a thin layer of repair putty was applied to obtain a smooth bonding surface on the sides of the beam and then epoxy was wiped on both sides of the member surface and side steel plates. Finally, side anchor rods were tightened to finalize the connection between side plates and RC beam (Figure 2.11). At the mid span of the beam, a load transfer steel member (Figure 2.9) was manufactured consisting of five steel plates connected by welding. For the load transfer member connections, a thin layer of repair putty was applied to obtain a smooth bonding surface on the sides of the beam. Side plates had four holes extending from one face to the other and used to install side anchors for successful shear transfer from the braces to the RC member. Then, epoxy was wiped on both sides of the member surface and steel plates. Finally, side anchor rods were tightened to provide successful shear transfer from the braces to the RC member. The connection details and beam of the braced frame design is given in Appendix 1 (section A1.2).

Material properties

The mechanical properties of the two different anchorage rods (Rod 1 and Rod 2) and brace members are given in Table 2.3 and Figure 2.12. It was observed from these table and figure that although the steel grade of the HSS sections was ST 37 (TS 648, 1980) gives nominal yield and ultimate strength is 235 and 363 MPa, respectively) with respect to TS 5317, the expected yield strength was quiet higher than nominal yield strength.

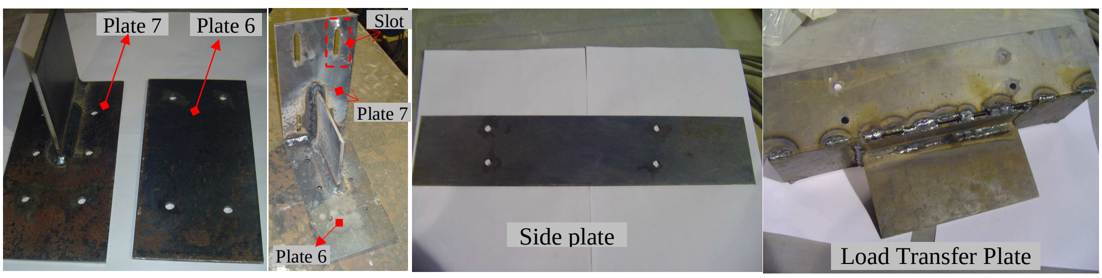

Figure 2.9 Steel members used for connection between brace and RC frame

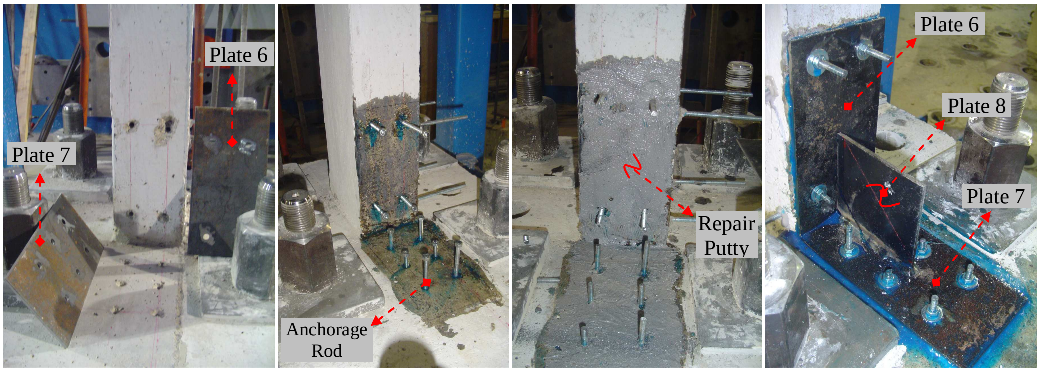

Figure 2.10 Connection at the bottom of the column

a) connection details at both ends of the beam

b) connection details at the midspan of the beam

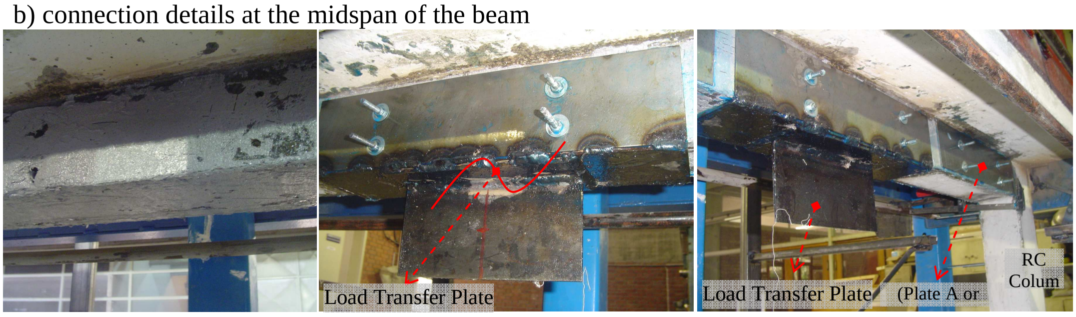

Figure 2.11 Connection details a) connection details at the both ends of the beam, b) connection details at the midspan of the beam

Table 2.3 Mechanical properties of the steel members for the chevron brace strengthening

Member	Yield Strength (Mpa)	Ultimate Strength (Mpa)	Elongation (%)
HSS 30x30x2.6 TS 5317	405	415	1.2
HSS 30x30x2 TS 5317	395	415	11.5
HSS 40x40x3.2 TS 5317	410	445	7.9
Plate 30x5	280	425	15.0
Plates 5, 8 (Gusset Plate)	350	470	26.4
Plates A, B, 1, 2	213	297	36.0
R1 (Φ6)	786	802	1.5
R2 (Φ6)	945	1120	11.0

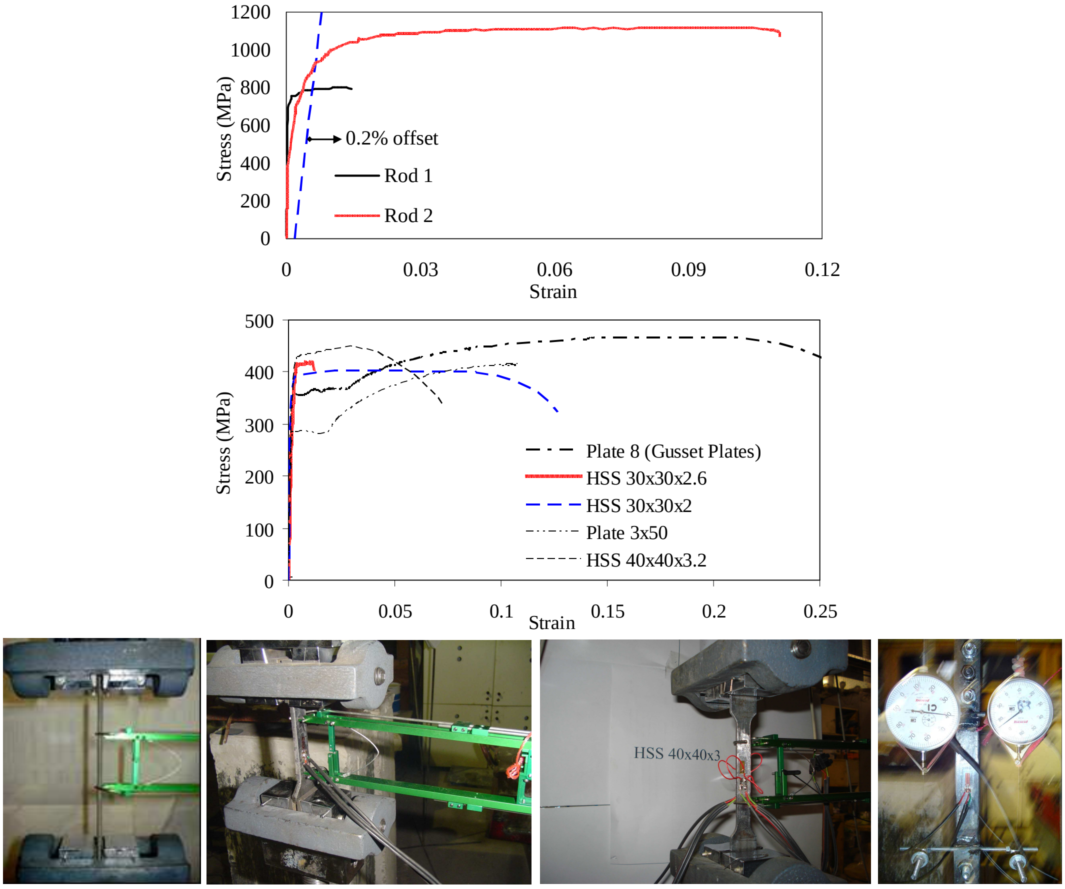

Figure 2.12 Stress-Strain response for anchorage rods and steel brace members

Test Specimens

Table 2.4 presents the specimen details of the chevron braced strengthened frames. In this table, the chevron braced frame names are abbreviated as C (Chevron braced frame)_axial load ratio (%)_concrete compression strength (MPa)_ anchorage type (R1 and R2 are brittle and ductile anchorage rods, respectively.)_slenderness (λ, equation 2.1)_cross section area (mm^2). For example, C_13_10_R1_91_262 defines the chevron braced frame with 13% column axial load ratio. The concrete strength of this frame is 10 MPa and connection between brace and RC frame was supplied with R1 type anchorage rod. The brace slenderness and brace cross sectional area of this frame were 91 and 262 mm^2, respectively.

$$\lambda = kl/i \tag{2.1}$$

Where, λ is the slenderness, k is the effective length ratio, *l* is the brace length, *i* is the radius of gyration.

Table 2.4 Experimental program of the chevron braced frames

Specimen Name	Brace Dimension (mm)	Brace Cross Section Area (mm2)	Anchorage Rod			Concrete Compressive Strength (Mpa)	Axial Load Ratio
			Type	Number of Anchorage on			
				Column	Foundation		
C_13_10_R1_91_262	HSS 30x30x2.6	262	Rod 1	4	6	10	0.13
C_24_8.5_R1_91_262	HSS 30x30x2.6	262	Rod 1	4	6	8.5	0.24
C_24_8.5_R2_89_210	HSS 30x30x2	210	Rod 2	4	6	8.5	0.24
C_24_8.5_R2_68_436	HSS 40x40x3.2	436	Rod 2	6	6	8.5	0.24
C_22_9.4_R2_1147_300	Steel Plate 30x5	300	Rod 2	4	6	9.4	0.22

In specimen C_24_8.5_R2_89_210, the brace section HSS 30x30x2 was used unintentionly. In this specimen, HSS 30x30x2.6 was desired to be used instead of HSS 30x30x2.6.

Specimens C_13_10_R1_91_262, C_24_8.5_R1_91_262, C_24_8.5_R2_89_210 and C_22_9.4_R2_1147_300 were designed to have lateral load carrying capacities of about 60 kN (case 1 and case 2 in Appendix 1, section A1.2). Hence, the desired lateral strength enhancements of these specimens were about three times that of the reference frame. On the other hand, the chevron brace size in specimen C_24_8.5_R2_68_436 was selected such that lateral strength of the retrofitted frame was about 100 kN (Appendix 1, section A1.2). This corresponds to a lateral strength of about five times that of the reference frame. The target lateral strength of this frame is highest among all specimens. Detailed design calculations are presented in Appendix 1 for these specimens. The other test variables among specimens besides the target lateral strength enhancement are (Figure 2.13):

a) The axial load ratio: There were two different target axial load ratios (13 % and 24%) as indicated in Table 2.4. The axial load ratio of the first and second chevron braced frames in Table 2.4 was different on the other hand all other parameters were same for both specimens. Furthermore, the target axial load ratio (24%) for all specimens except C_13_10_R1_91_262 was similar.

b) Anchorage rod type; Rod 1 (R1) anchors were lower cost and strength but brittle (about 1.5 % ultimate strain), whereas Rod 2 (R2) anchors were more expensive (costs approximately five times that of Rod 1) and ductile (about 11 % ultimate strain).

c) Brace member size; two different brace cross sections such as square hollow structural steel HSS (brittle material and low slenderness) and steel plate (ductile material and high slenderness) were used.

Brace member size dictates the slenderness and brace cross section area. Except slenderness of the brace used in specimen C_22_9.4_R2_1147_300, all of the brace member slenderness values were within the limit state (250) suggested by the TS 648 (1980) for compression members. Specimen C_22_9.4_R2_1147_300 was designed to determine the contribution of the shear strength of the RC beam on the cyclic performance of the chevron braced frame in addition to slenderness effect. Specimens C_24_8.5_R2_89_210 and C_24_8.5_R1_91_262 had the same axial load ratio but they had different anchorage rods. Specimen C_24_8.5_R2_68_436 had braces with lower slenderness and higher cross sectional area than C_24_8.5_R1_91_262 in order to achieve the target lateral strength enhancement.

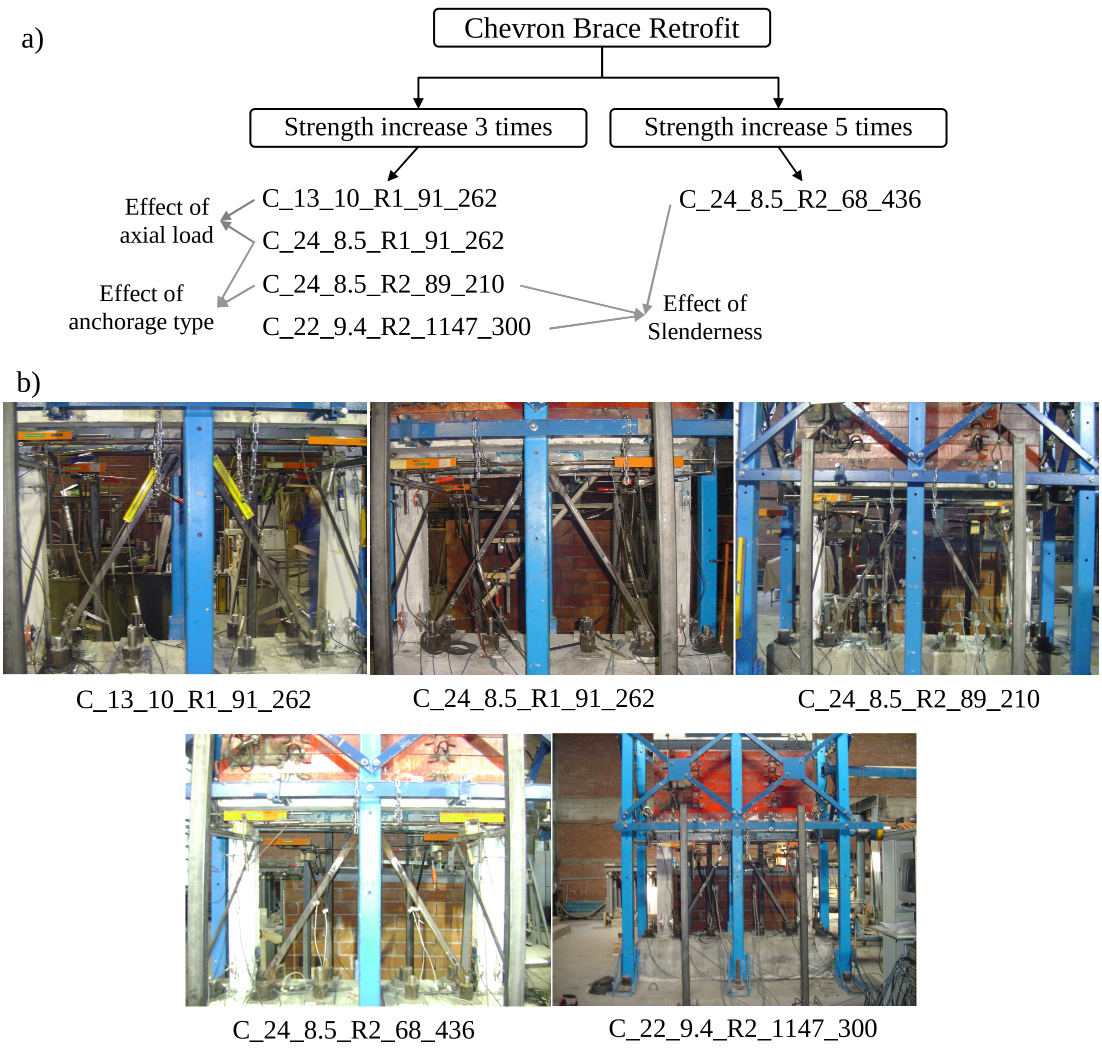

Figure 2.13 a) Test parameters b) pictures of the braced frames before the test

In addition to test parameters explained above, followings minor differences exist between specimens C_13_10_R1_91_262 and C_24_8.5_R1_91_262 and other chevron brace retrofitted specimens. Plate 7 and 8 were welded outside before placing on the RC frame and then Plate 6 was welded to the Plate 7 and 8 (Figure 9 and 10) for the specimens C_13_10_R1_91_262 and C_24_8.5_R1_91_262. Plate 8 was welded to the Plate 6 and 7 at the outside before placing on the RC frame for the other braced frames. The attachment was provided with slots on the Plate 6 and 7 (Figure 9 and 10). With slotted plate connection, adverse effect of the welding on epoxy due to heating was eliminated. The pictures of the braced frames before the test are indicated in Figure 2.13-b.

2.4.2 Internal Steel Frames

The internal steel frame (ISF) were composed of steel columns and beams installed within the bay of the deficient RC frame. The general view of test specimens is given in Figure 2.14.

The ISFs are intended to easily accommodate wall openings for architectural requirements upon retrofitting. Installation methods that minimize the use of anchors between the ISF and RC members are explored by conducting a number of tests. The ISF was composed of rigidly connected beams and columns ensured welded connections. End plates at the top and bottom of the column and angles were used to construct a rigid connection between the beam and column. In order to simulate actual retrofit conditions, the ISFs were implemented after constant gravity load was applied on the RC frame.

Test Specimens

The experimental program details for ISF strengthened specimens is given in Table 2.5. In this table, the ISF specimens are abbreviated as ISF_ axial load ratio (%)_concrete compression strength_the ISF installation method (three methods, I, II, III as explained below)_ steel member type (HSS or I section (IS))_energy dissipation system (if dissipation system is available, it will be written with letter E followed by its rod height such 150 mm and 75 mm). For example, specimen ISF_27_7.5_I_HSS is abbreviation of ISF with 27 percent axial load ratio. The concrete strength of this frame is 7.5 MPa and method I was used as an installation of ISF. The steel member type was HSS and no energy dissipating rods were used. The main parameters analyzed in ISF were:

a) The ISF installation method: Three installation methods mentioned above were used for ISF.

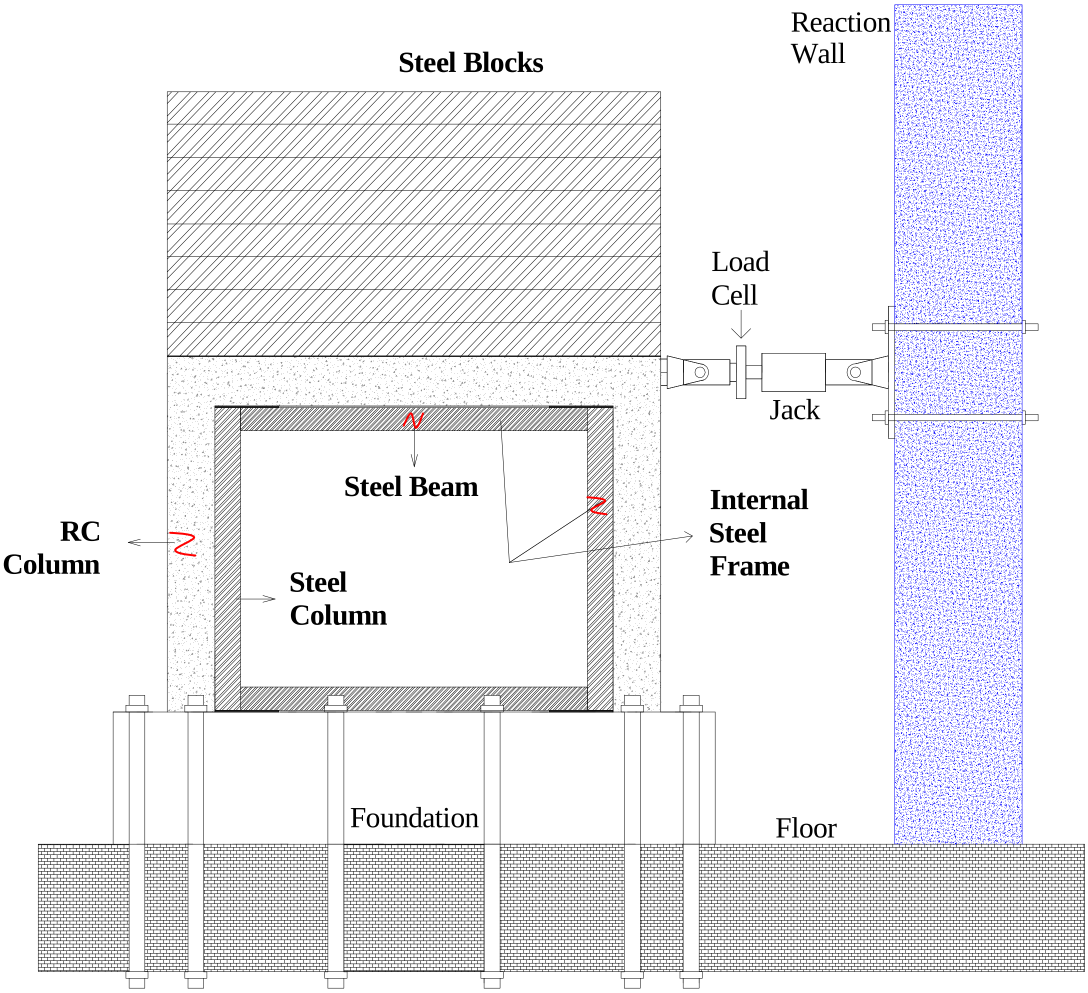

Figure 2.14 Test setup of the ISF

Table 2.5 Experimental program of the ISF

Specimen Name	Steel Frame Member Dimension (mm)		Steel Frame Member Cross Section Area (mm2)		Concrete Compressive Strength (MPa)	Axial Load Ratio
	Column	Beam	Column	Beam		
ISF_27_7.5_I_HSS	80x80x4	70x70x3.2	1160	820	7.5	0.27
ISF_20_10.6_I_IS	I-140	I-120	1820	1420	10.6	0.20
ISF_24_8.7_II_IS	I-140	I-120	1820	1420	8.7	0.24
ISF_28_7.4_III_IS	I-140	I-80	1820	757	7.4	0.28
ISF_27_7.5_I_HSS_E150	80x80x4	70x70x3.2	1160	820	7.5	0.27
ISF_26_8.0_I_HSS_E75	80x80x4	70x70x3.2	1160	820	8.0	0.26

b) The member type used for the ISF (HSS and IS). The HSS steel was notably less ductile than the IS steel. However, the HSS supplied approximately 1.5 times larger contact area compared to the IS. The measured mechanical properties of the steel members are given in Figure 2.15 and Table 2.6.

c) The use of energy dissipaters: Two specimens whose details are given in Figure 2.17 were strengthened with energy dissipaters.

Material properties

The mechanical properties of the steel members used during the construction of the ISF are indicated in Figure 2.15 and Table 2.6 by conducting uniaxial tension tests according to ASTM E8 (2004).

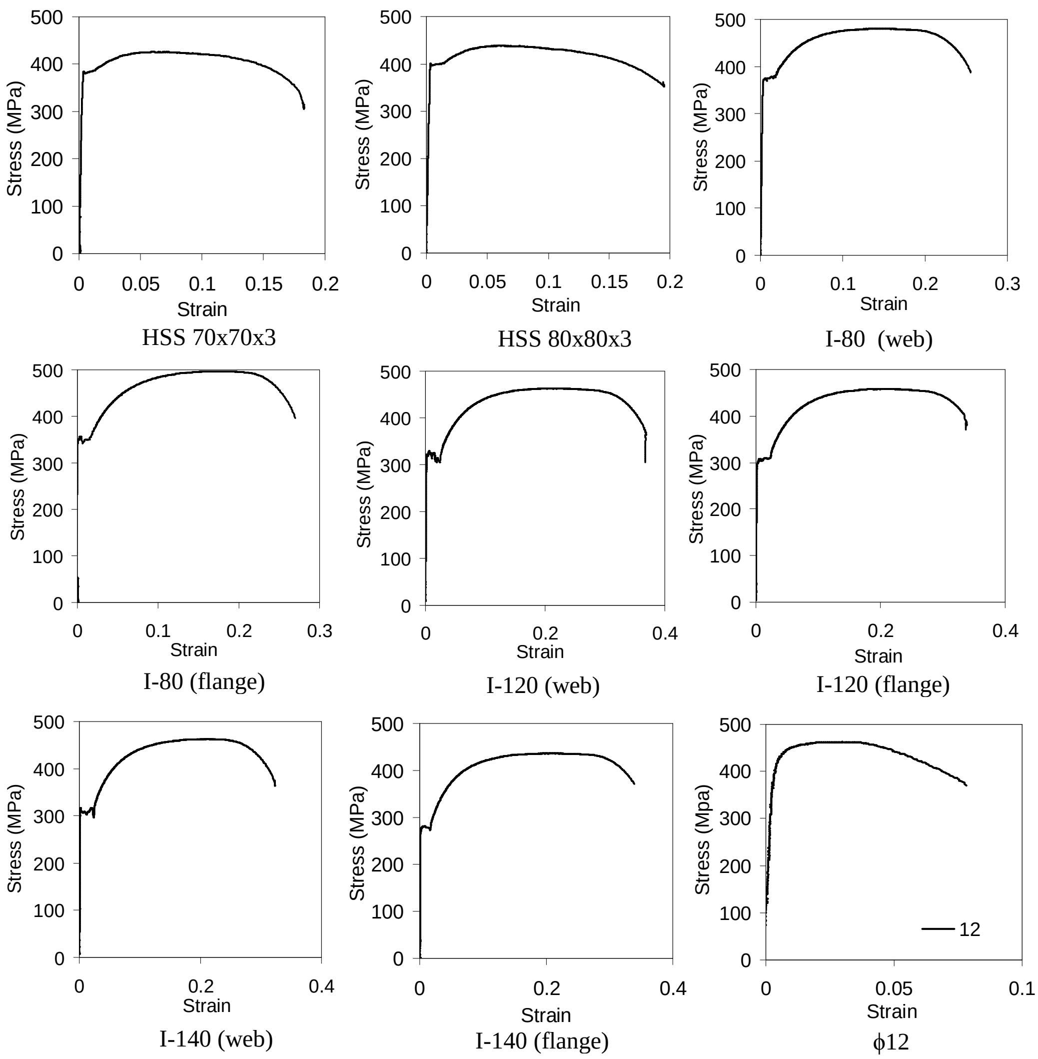

Figure 2.15 Stress-strain response of the ISF steel members (from left to right HSS70x70x3, HSS 80x80x4, I-80 web, I-80 flange, I-120 web, I-120 flange, I-140 web, I-140 flange, energy dissipater rod ϕ12)

Table 2.6 Mechanical properties of steel members

Steel Members	Yield Strength (MPa)	Ultimate Strength (MPa)	% Elongation
HSS 80x80x4	398	439	18.5
HSS 70x70x3	385	426	17.2
I-140	313^{w} / 282^{f}	463^{w} / 437^{f}	32^{w} / 34^{f}
I-120	320^{w} / 300^{f}	463^{w} / 458^{f}	36^{w} / 34^{f}
I-80	373^{w} / 350^{f}	480^{w} / 496^{f}	25^{w} / 26^{f}
Energy Dissipater Rod (ϕ12)	415	463	7.8
Anchor Rod (R2)	945	1120	11.0

w and f; coupons extracted from web and flange of I-section, respectively.

Application details of the ISFs

Three different methods were used to install the ISFs. Figures 2.16 to 2.19 show the details of the installation methods, while Figure 2.20 shows the photographic views of the ISFs installed in the RC frames and Figure 2.21 shows specimens before the test. The application methods are as follows:

Method I: As seen in Figure 2.16 no anchors were used between the RC frame and ISF. Prior to installation, a thin layer of repair putty was applied on all surfaces of the RC frame to obtain a smooth bonding surface. The individual steel members were attached to the RC frame using epoxy. Epoxy is used in these specimens only to ensure that ISF remains stable and standing inside the frame without any out of plane instability. After the epoxy had cured for three days, the steel beams were welded to the steel columns following the weld size requirement in the Turkish Standard TS 3357 (1979).

Method II: In addition to the epoxy bond used in method I, anchor rods were used to enhance force transfer between the top of the ISF beam and bottom of the RC beam (Figure 2.17). Hence, it can be viewed as a semi-composite assemblage of the ISF to the RC frame. The number of the anchors was sufficient to enable lateral force transfer from RC beam to ISF by ensuring that total shear strength of the anchors were higher than the lateral strength of the ISF. Method II was achieved in two stages. In the first stage, anchor holes were drilled into the bottom side of the RC beams and cleaned up by brushing and air blowing. Then, epoxy primer was injected into these holes and the anchor rods were inserted and left for curing for at least three days. In the second stage, a thin layer or repair putty was applied on the RC member on all surfaces that contact the ISF, as in method I. Before the epoxy cured, the anchor rods were tightened to fasten the individual steel members to the RC frame.

Finally, the steel beams were welded to the steel column using the same welding procedure as in method I. The diameter of the anchor rods and holes were 6 mm and 8 mm, respectively. The anchors were embedded 120 mm into the RC beam with epoxy filling. Anchorage rods were identical with the Rod 2 used in chevron braced frames (Chapter 2.4.1).

Method III: In this method, it was aimed to achieve fully-composite action between the RC frame and ISF (see Figure 2.18). Anchor rods were installed along the columns in addition to the beam as done in method II. 42 column and 32 beam anchor rods were used to provide the shear strength transfer between the RC and steel frames. The numbers of anchors were calculated for the ultimate shear force that can act on the composite member based on the formation of plastic hinges at member ends (i.e. similar to the capacity design principle). For the ultimate shear force demand, *V*, on beam and columns, the number of shear connectors (anchor rods) was calculated using the elastic shear flow equation as given below:

$$n \geq \frac{V \times Q \times L_m}{I \times V_a} \qquad (2.2)$$

where *n* is the required number of anchor rod, *Q* is the first moment of the area above the RC-Steel section interface of the composite section, L_m is the member clear length and V_a is the shear strength of the anchor rods, which was assumed to be 0.6 times the strength of the rods in tension.

The energy dissipating system shown in Figure 2.19 was inserted at mid-height of the HSS-columns at the specimens ISF_27_7.5_I_HSS_E150 and ISF_27_7.5_I_HSS_E75. The energy dissipating system was composed of six 12-mm diameter threaded rods. The measured mechanical properties of the rods are given in Table 2.6. The length of the energy dissipater rods was different for the two specimens ISF_27_7.5_I_HSS_E150 and ISF_27_7.5_I_HSS_E75 to control the strength of the supplementary ISF system. Specimens ISF_27_7.5_I_HSS_E150 and ISF_27_7.5_I_HSS_E75 were designed to concentrate inelastic action and damage in the rods while maintaining the rest of the ISF remains elastic.

The ISF members were proportioned with the strong column-weak beam concept to limit damage in the ISF columns. Estimated moment capacities of beams, columns of the RC frame, ISF and the composite sections are provided in Table 2.7.

Method I

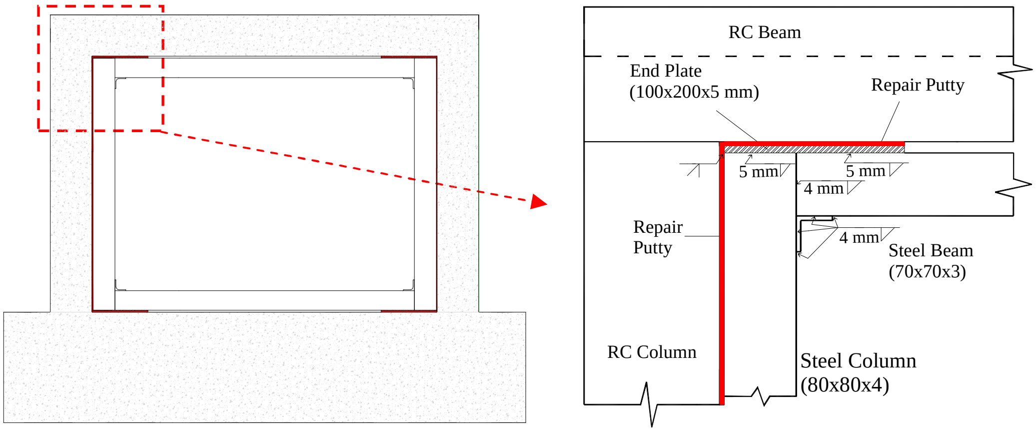

ISF_27_7.5_I_HSS

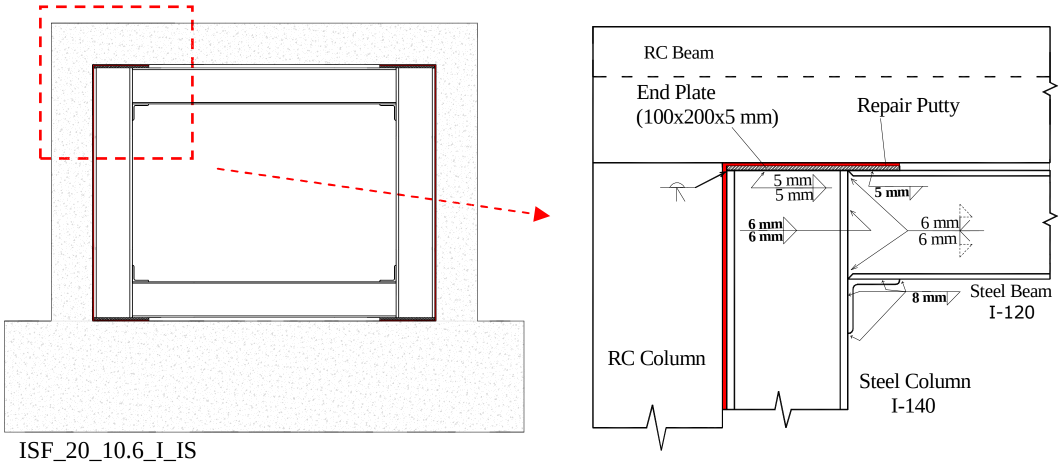

ISF_20_10.6_I_IS

Figure 2.16 Connection details of ISF for Method I

Method II

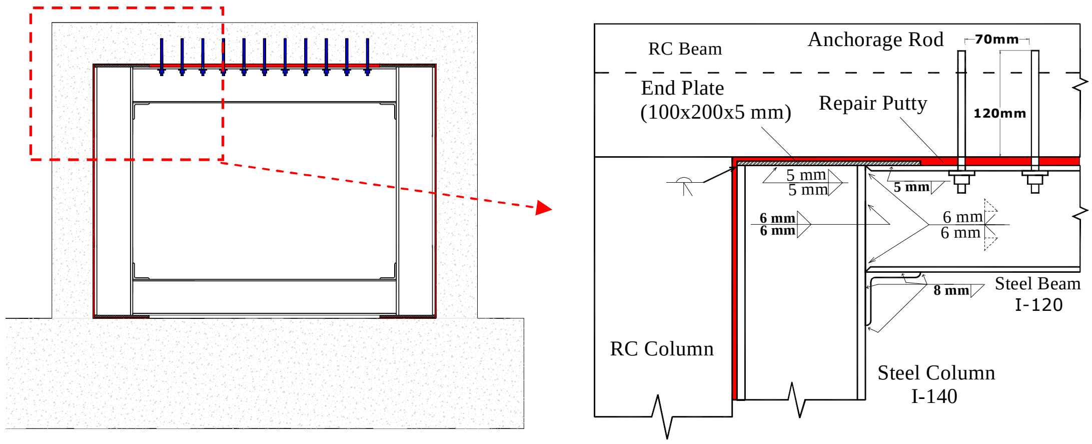

ISF_24_8.7_II_IS

Figure 2.17 Connection details of ISF for Method II

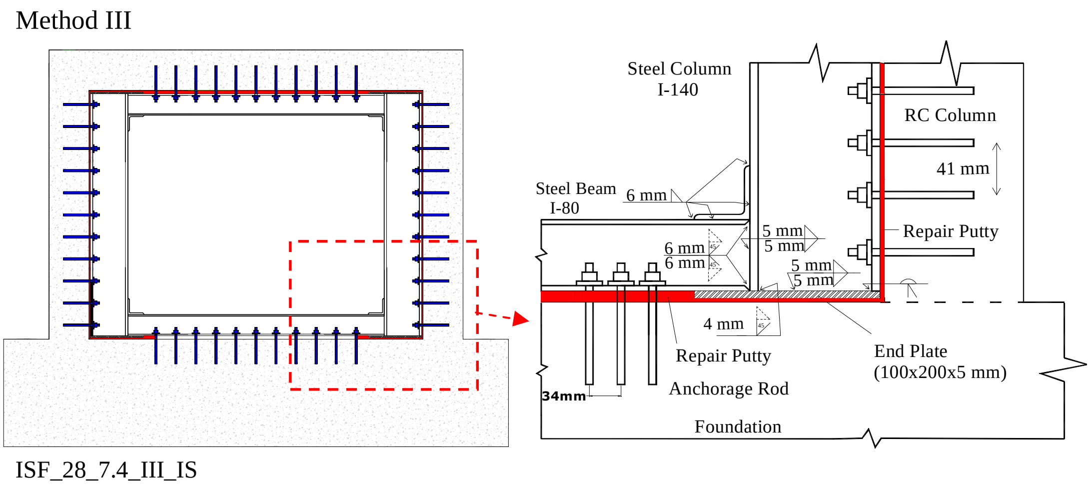

Figure 2.18 Connection details of ISF for Method III

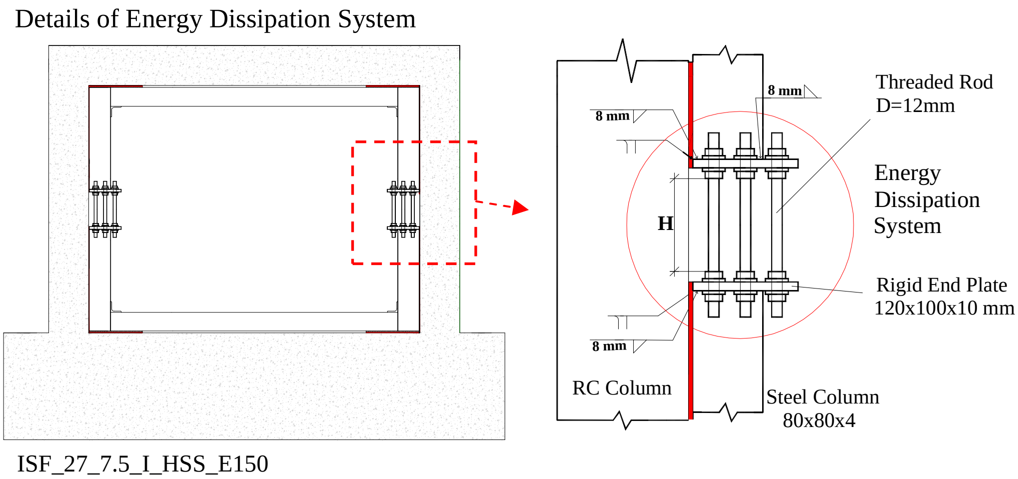

Figure 2.19 Connection details of ISF for energy dissipation system

Table 2.7 Moment capacity of the members

Member	Moment Capacity (kN-m)	
	Positive (+)	Negative (-)
RC Column[a]	5.30	5.30
RC Beam	4.50	5.30
HSS 80x80x4	13.80	13.80
HSS 70x70x3	7.78	7.78
I-140	28.17	28.17
I-120	19.51	19.51
Composite Column	40.85	36.40
Composite Beam	37.50	16.75
Energy Dissipater Rods	0.12	0.12

a; Calculated considering the axial load

Figure 2.20 Application details of ISF. a) Method I, Specimen ISF_27_7.5_I_HSS, b) Method I, Specimen ISF_20_10.6_I_IS, c) Method II, Specimen ISF_24_8.7_IS, d) Method III, Specimen ISF_87_7.4_III_IS, e and f)Energy dissipation system, Specimen ISF_27_7.5_I_HSS_E150 and Specimen ISF_26_8.0_I_HSS_E75

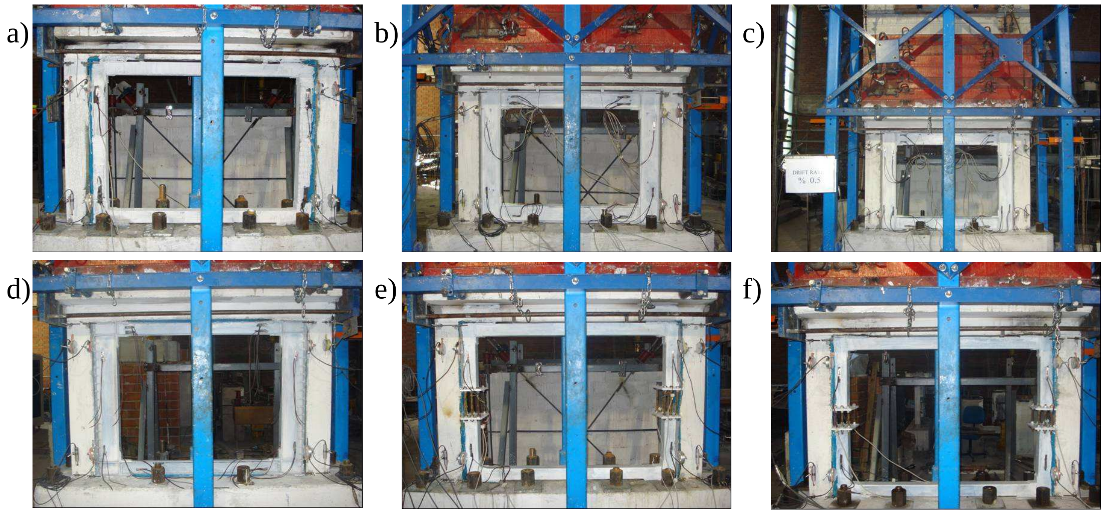

Figure 2.21 Application details of ISF. a) Method I, Specimen ISF_27_7.5_I_HSS, b) Method I, Specimen ISF_20_10.6_I_IS, c) Method II, Specimen ISF_24_8.7_IS, d) Method III, Specimen ISF_87_7.4_III_IS, e and f)Energy dissipation system, Specimen ISF_27_7.5_I_HSS_E150 and Specimen ISF_26_8.0_I_HSS_E75

2.4.3 X-Brace Strengthened Frame

The X-Brace strengthened frame was tested in order to compare the performance of X-brace and chevron brace retrofit technique. The application details of the X-brace were similar to that of chevron braced frame. The main difference of the X-brace and chevron brace frame is while the X-brace application has four connection locations between RC frame and steel brace, the chevron brace has three connection locations. Figure 2.22 and 2.23 indicate the test setup and connection details of the X-brace retrofitted RC frame, respectively. The steel brace member was a steel plate with a significant high slenderness. This plate was same plate used for specimen C_22_9.4_1147_300. The concrete strength of the X-braced frame was 8.5 MPa.

2.4.4 Column with Shear Plate

The column with shear plate strengthening was conducted to examine an innovate steel retrofit system. In such a system, the main objective was to introduce a new lateral load carrying steel column connected only to the beam of the existing bays. The main advantage of such system is the easy of connection and absence of introducing additional demands on

RC column and joints. The test setup of the column with the shear plate frame is indicated in Figure 2.24. As seen in this figure, there is a steel column post-installed at the mid-span of the beam and foundation. The steel column was not continuous but it was cut into two parts at the mid length (Figure 2.25). Between these two half length columns there is a plate welded to each column part. It was desired to enhance the lateral strength of the RC frame by providing the shear plate yielding under shear deformation demands.

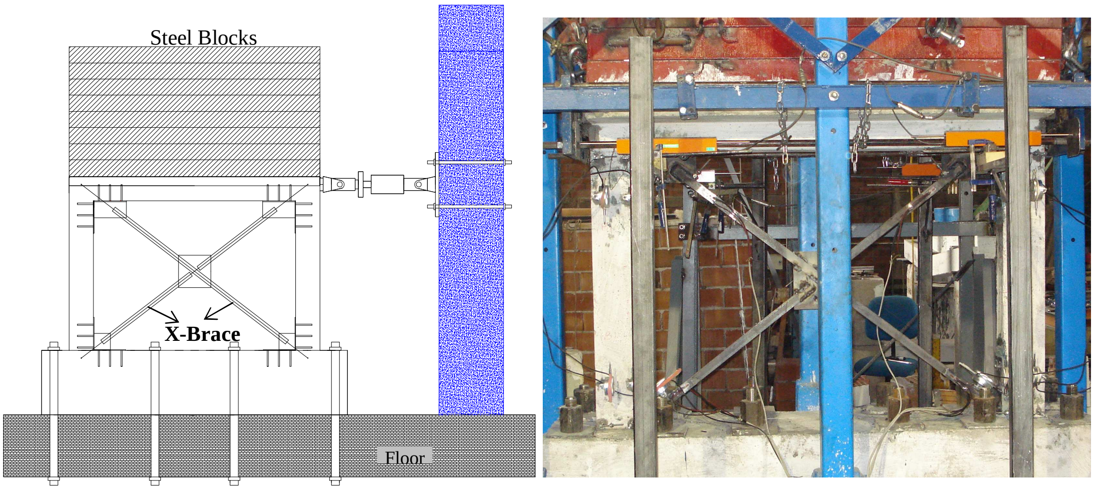

Figure 2.22 Test setup for X-Braced frame

The application details can be summarized as follows: first of all, anchorage rods were installed to the bottom of the beam and foundation of the RC frame with the similar procedures explained in previous chevron brace application. Then, the half length column (I-140 section) was welded to rigid steel plates at both its ends. This welding was done outside to prevent the adversely effects of welding heat on the repair putty and epoxy. One of the plates had already punched with respect to anchorage rods already embedded into the RC beam and foundation. Then, thin layer repair putty was applied on the RC frame face followed by epoxy. Finally, the anchorage rods were tightening to fasten the steel columns to the RC frame. The shear plate was welded to the two rigid plates which were welded to the steel columns. The desired lateral strength enhancement was calculates as below:

$$F_{SP} = 0.6 \times t \times b \times \sigma_y \,,\ \{F_{SP} = 0.6 \times 4 \times 78 \times 270 = 42120N = 42.12kN\} \qquad (2.3)$$

Where, F_{SP}: Shear strength of the shear plate, t: thickness of the shear plate, b: width of the shear plate, $\sigma_{y:}$ yield strength of the shear plate

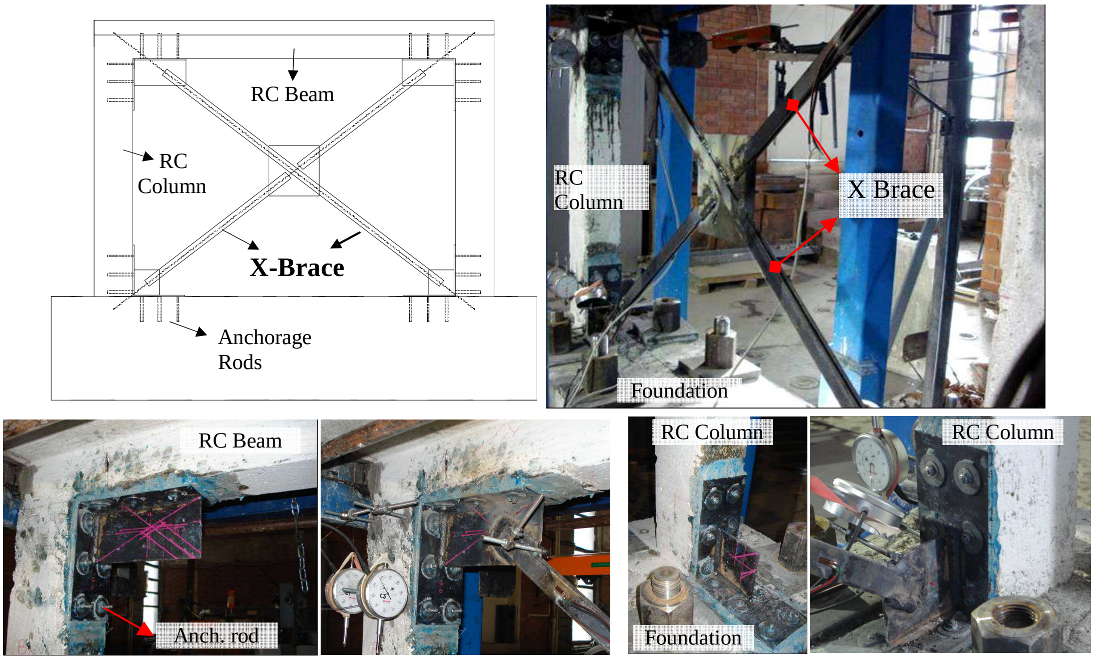

Figure 2.23 Connection details of the X-Braced frame

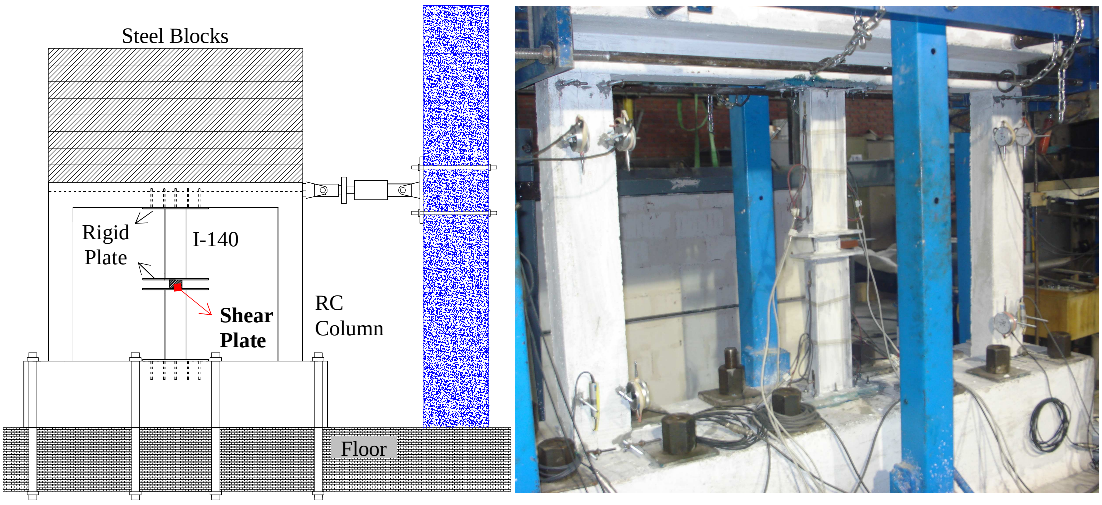

Figure 2.24 Test setup for the column with shear plate frame

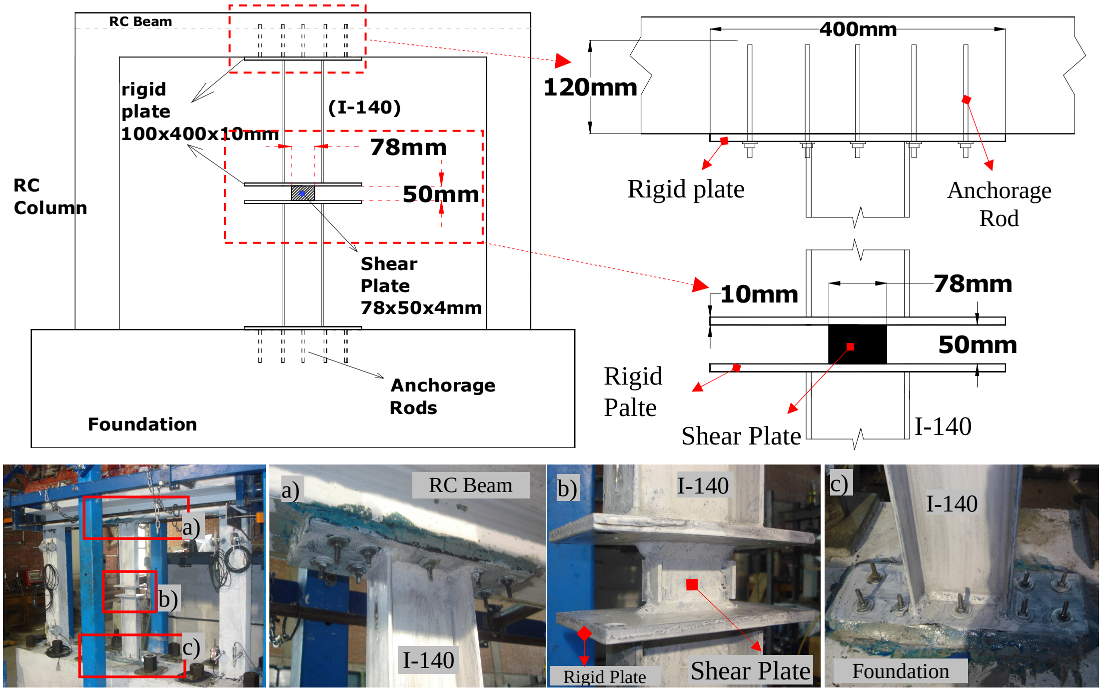

Figure 2.25 Connection details of the column with shear plate

2.5 Test Results

Test results are given in terms of cyclic response of the frames. The cyclic response is presented in terms of lateral force versus lateral displacement. In addition, the figure of the hysteretic response indicates the important events such as plastic hinge formation in the RC columns, brace buckling, anchorage rod failure, brace fracture, gravity collapse, beam shear failure, fracture initiation of ISF elements, fracture initiation of energy dissipater rods, and joint failure of the RC frame. Plastic hinge formation of the RC columns was defined as the stage when the measured curvature exceeded the curvature at first yield based on standard sectional analysis. In addition to cyclic response, observed damage and pictures of the test frame is presented. Test results are summarized in tables including the ultimate lateral strength, lateral stiffness, DR capacity, displacement ductility, dissipated energy, DR at failure, and observed failure modes. Lateral stiffness is defined based on the peak positive and negative loading points during the first cycle (± 0.5% DR). The DR capacity is defined as the drift when the lateral load capacity dropped to 85% of the ultimate lateral strength. Displacement ductility is defined as the drift capacity divided by the DR when any of the column critical section exceeds the estimated yield curvature (average value calculated from both pull and push directions). Dissipated energy is calculated by summing the area enclosed by the hysteretic loop up to ± 4% DR cycles. Failure is defined as the state when the lateral load dropped to 85% of the maximum measured lateral load value.

2.5.1 Reference Frames

Figure 2.26 shows the hysteretic response obtained from reference specimens. The test results are summarized in Table 2.8. The ultimate lateral strength and stiffness for specimen R_13_10 was 12.9 kN and 1.75 kN/mm, respectively. The displacement ductility and DR capacity for specimen R_13_10 were about 3.9% and 4%, respectively. The ultimate lateral strength and stiffness for specimen R_25_8.1 was 13.7 kN and 2.48 kN/mm, respectively. The displacement ductility and DR capacity for specimen R_25_8.1 were about 2.5% and 2%, respectively. High axial load placed on R_25_8.1 caused in this specimen to perform higher lateral strength and lateral stiffness than R_13_10. On the contrary, Specimen R_25_8.1 exhibited severe strength degradation upon observation of the first plastic hinge at a DR of 1% due to the presence of a higher axial load ratio (Figure 2.26). A plastic mechanism was formed at a DR slightly higher than ± 2%. Upon further increase in loading amplitude, pinching behavior and severe stiffness degradation was observed. Reference specimen R_25_8.1 lost its lateral strength very rapidly after developing a plastic mechanism. Furthermore, because the plastic hinges formed in the columns, the RC frame could be quite vulnerable to collapse. Figures 2.27 and 2.28 indicate the damage observed during the tests for specimens R_13_10 and R_25_8.1, respectively. As it is clearly seen in this figure, hinges occurred at the top and bottom of the columns for both reference specimens.

Table 2.8 Test results of the reference specimens

Specimen Name	Ultimate Lateral Load (kN)	Lateral Stiffness (kN/mm)	Dissipated Energy (kN.mm)	Displacement Ductility Direction		Drift Ratio (%) Capacity Direction		Failure Modes	Drift Ratio (%) at Failure
				Right	Left	Right	Left		
R_13_10	12.9	1.75	2100	4.75	3.88	5.0	4.0	Column Mechanism	4.0
R_25_8.1	13.7	2.48	2082	2.51	2.51	2.0	2.0	Column Mechanism	2.0

V_u: Ultimate lateral strength, K_{LS}: Lateral stiffness, E: Dissipated energy

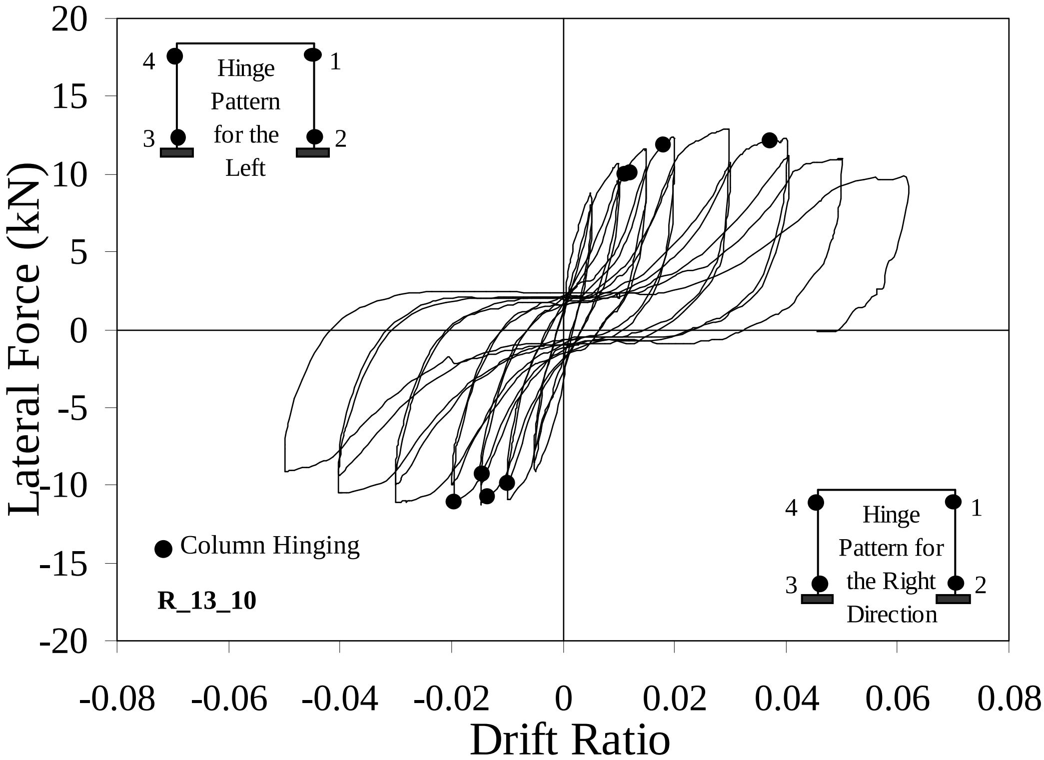

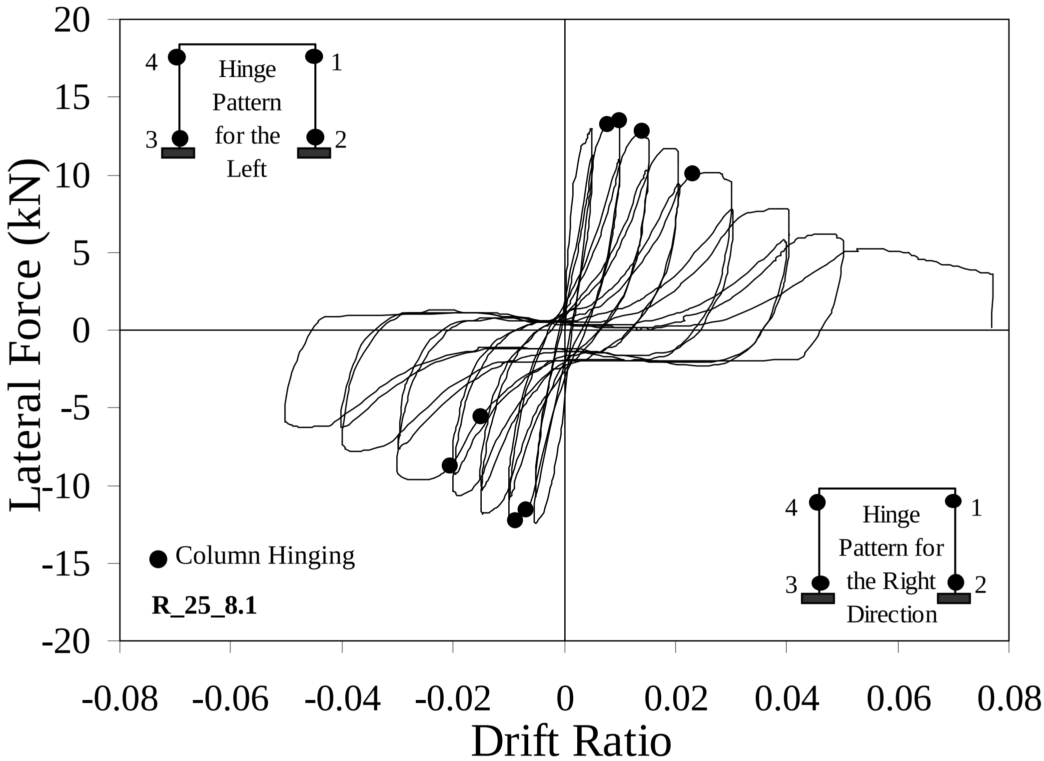

Figure 2.26 Cyclic response of the reference specimens R_13_10 and R_25_8.1

Figure 2.27 Pictures of the specimen R_13_10 during the test

Figure 2.28 Pictures of the specimen R_25_8.1 during the test

2.5.2 Test Results of the Chevron Brace Strengthened Frames

The cyclic response of the chevron braced strengthened test specimens are presented in Figures 2.29 to 2.33. These figures also show the important events of experiments such as plastic hinging sequence, brace buckling and failure events (formation of a plastic mechanism, anchorage rod failure, brace fracture, gravity collapse, and beam shear failure). Test results are summarized in Table 2.9, including the ultimate lateral strength, lateral stiffness, displacement ductility, dissipated energy, DR capacity, DR at failure, observed failure modes.

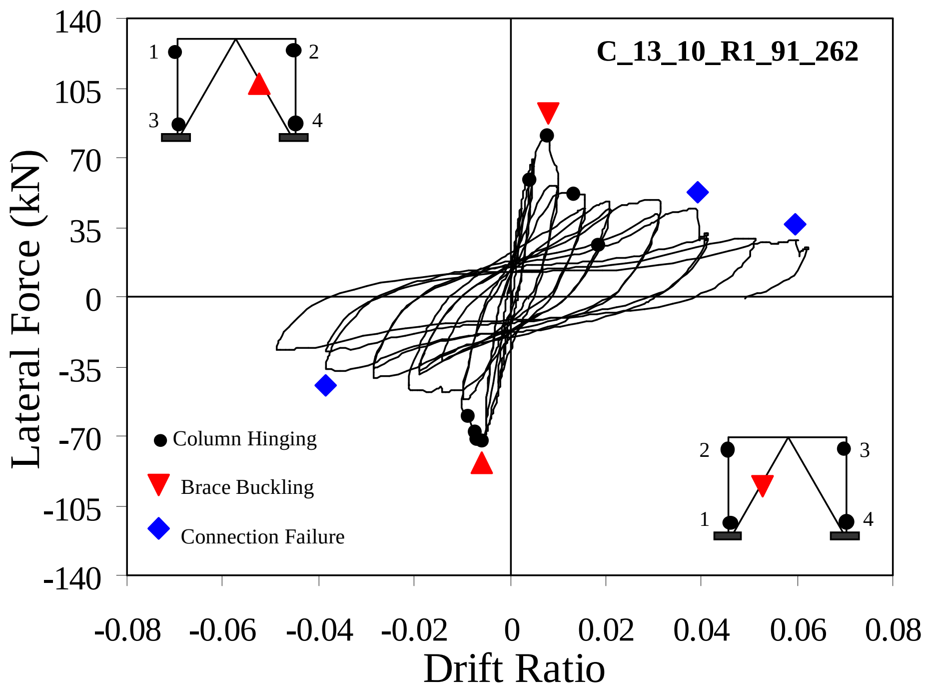

Figure 2.29 Cyclic response of the specimen C_13_10_R1_91_262

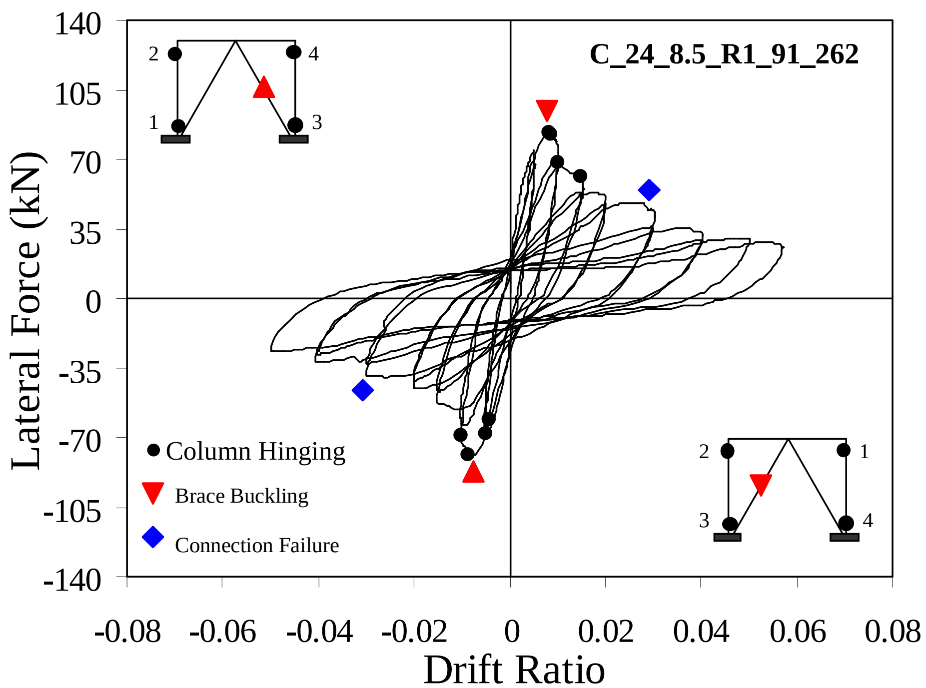

Figure 2.30 Cyclic response of the specimen C_24_8.5_R1_91_262

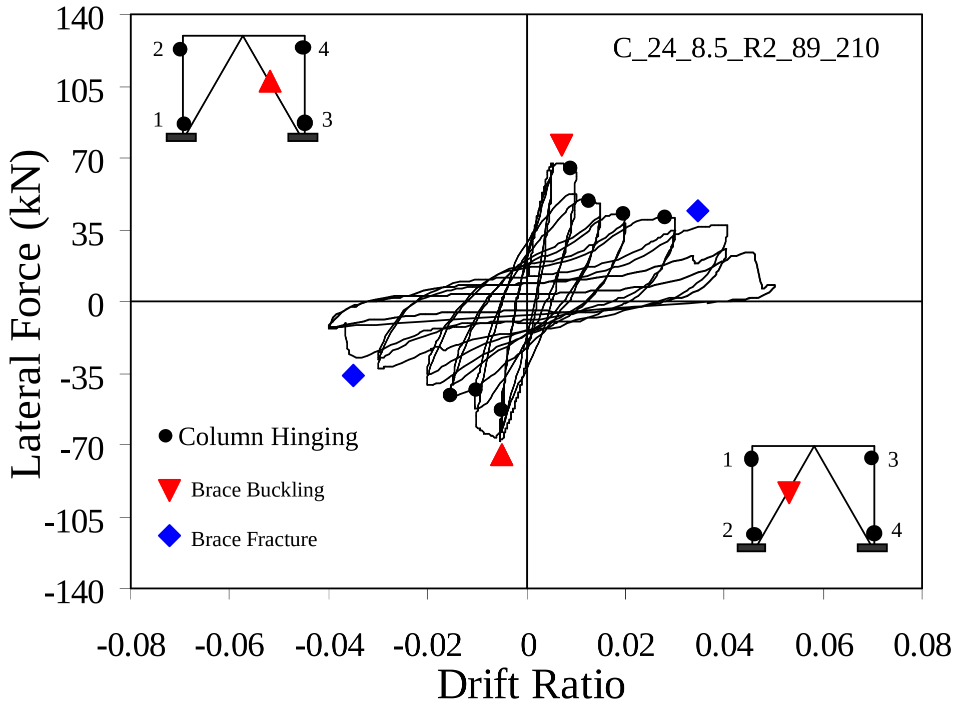

Figure 2.31 Cyclic response of the specimen C_24_8.5_R2_89_210

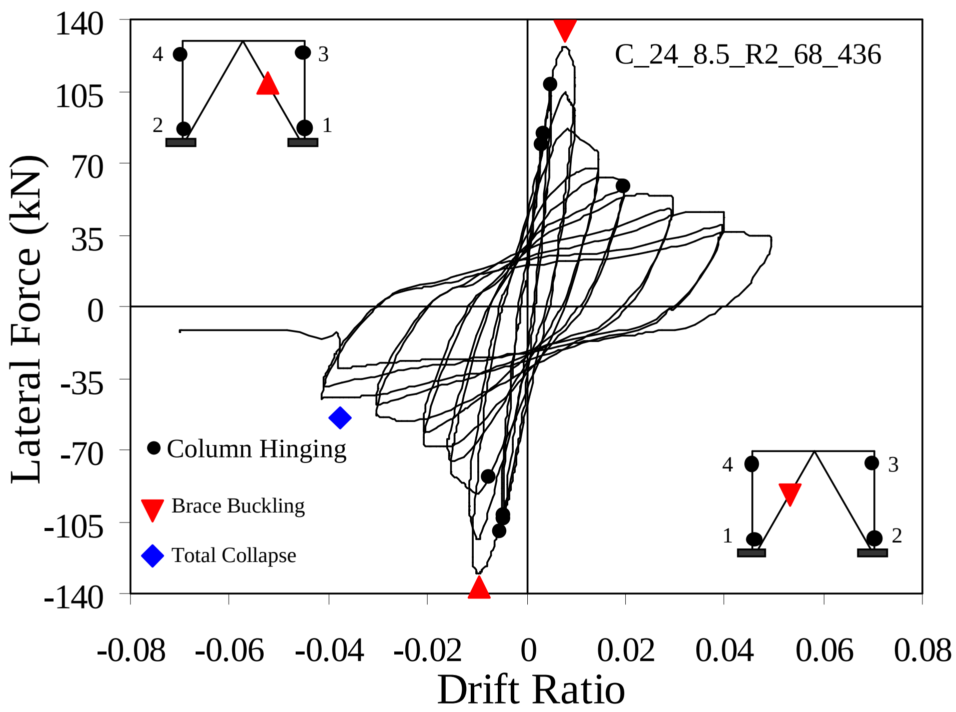

Figure 2.32 Cyclic response of the specimen C_24_8.5_R2_68_436

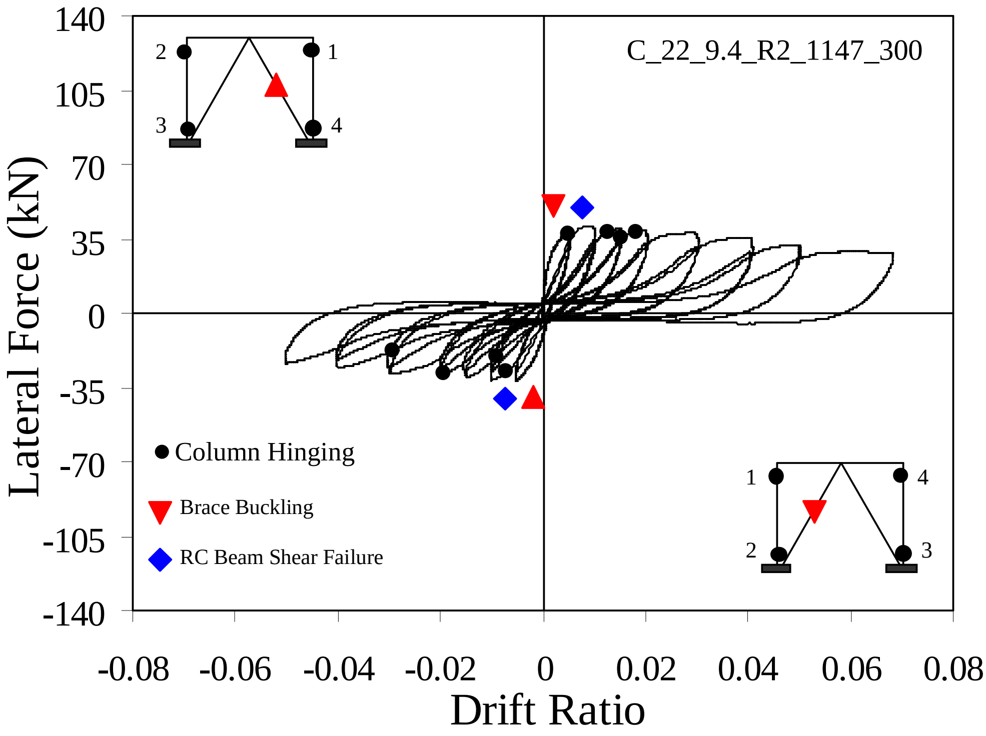

Figure 2.33 Cyclic response of the specimen C_22_9.4_R2_1147_300

The last three columns of Table 2.9 list the normalized strength, stiffness, and dissipated energy with respect to the corresponding values measured from the reference specimens (R_13_10 and R_25_8.1). Pictures of test specimens after failure are presented from Figure 2.34 to 2.38.

All of the chevron braced frames with square HSS exhibited a similar load-deformation response. A nearly elastic response up to buckling of the compression brace (Figure 2.34) was observed followed by severe strength degradation. Upon brace buckling, the lateral strength and stiffness of these specimens decreased significantly. However, the lateral load carrying capacity was maintained (Figure 2.29 to 2.33). After brace buckling, post-buckling capacity of the brace members dictated the cyclic performance of the braced frame. It was also observed that brace buckling triggered flexural-shear cracks at the mid-span of the beam (Figure 2.35). As soon as brace buckling occurred, shear cracks started to open up. Up to about ±3% DR, shear cracks were controlled by the presence of bonded side plates.

Table 2.9 Test results of the reference and chevron braced frames

Specimen Name	Vu (kN)	KLS (kN/mm)	Displacement Ductility Direction		E (kN.mm)	Drift Ratio (%) Capacity Direction		Drift Ratio (%) at Failure	Failure Modes	$\frac{V_u}{V_{u(reference)}}$	$\frac{K_{LS}}{K_{LS(reference)}}$	$\frac{E}{E_{(reference)}}$
			Rigth	Left		Rigth	Left					
R_13_10	12.9	1.75	4.75	3.88	2100	5.0	4.0	4.0	[1]	1.00	1.00	1.00
R_25_8.1	13.7	2.48	2.51	2.51	2082	2.0	2.0	2.0	[1]	1.00	1.00	1.00
C_13_10_R1_91_262	81.5	13.30	5.37	3.58	14547	3.0	2.0	2.0	[2]	6.33	7.60	6.93
C_24_8.5_R1_91_262	83.5	14.10	2.47	2.31	13939	1.5	1.4	1.4	[2]	6.08	5.69	6.70
C_24_8.5_R2_89_210	68.1	12.90	2.85	2.14	11092	2.0	1.5	1.5	[3]	4.95	5.20	5.33
C_24_8.5_R2_68_436	130.4	21.20	3.24	3.01	21874	1.3	1.2	1.2	[4]	9.49	8.55	10.51
C_22_9.4_R2_1147_300	40.7	6.60	6.67	5.0	5817	4.0	3.0	3.0	[5]	2.96	2.66	2.79

[1]; Column mechanism, [2]; Connection Rod Failure, [3]; Brace Fracture, [4]; Gravity Collapse, [5]; Shear failure at the mid-span of the beam.

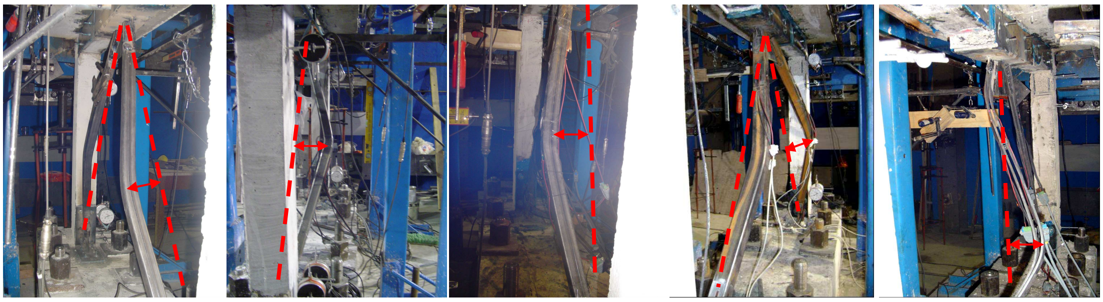

C_13_10_R1_91_262 C_24_8.5_R1_91_262 C_24_8.5_R2_89_210 C_24_8.5_R2_68_436 C_22_9.5_R2_1147_300

Figure 2.34 Brace buckling for braced frames

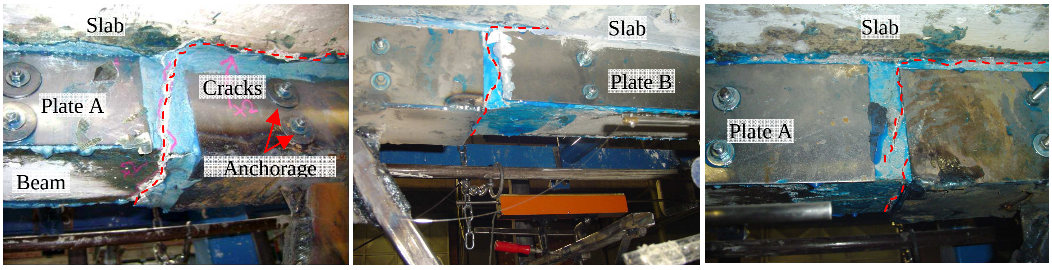

C_13_10_R1_91_262 C_24_8.5_R1_91_262 C_24_8.5_R2_89_210

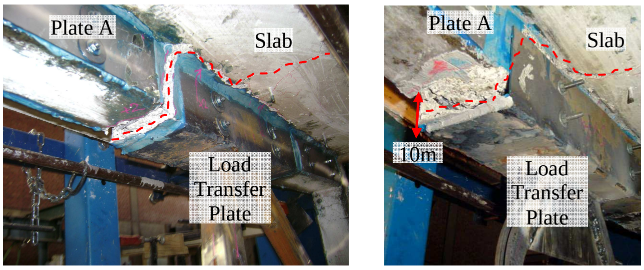

C_24_8.5_R2_68_436 C_22_9.5_R2_1147_300

Specimen Name	Drift Ratio (%)
C_13_10_R1_91_262	2.0
C_24_8.5_R1_91_262	1.5
C_24_8.5_R2_89_210	1.5
C_24_8.5_R2_68_436	3.0
C_22_9.4_R2_1147_300	4.0

Figure 2.35 Shear deformation at the mid-span of the beam for braced frames

C_13_10_R1_91_262 C_24_8.5_R1_91_262

Figure 2.36 Connection failure for specimens C_13_10_R1_91_262 and C_24_8.5_R1_91_262

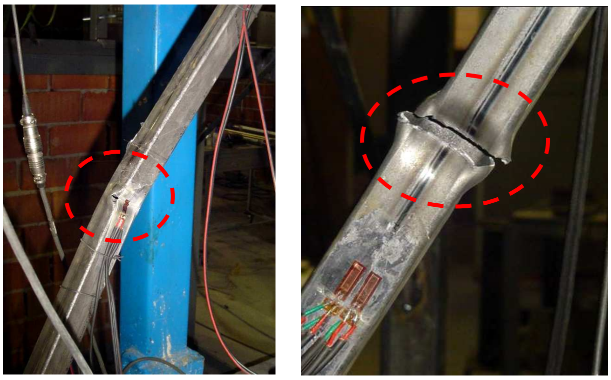

C_24_8.5_R2_89_210

Figure 2.37 Brace fracture for specimen C_24_8.5_R2_89_210

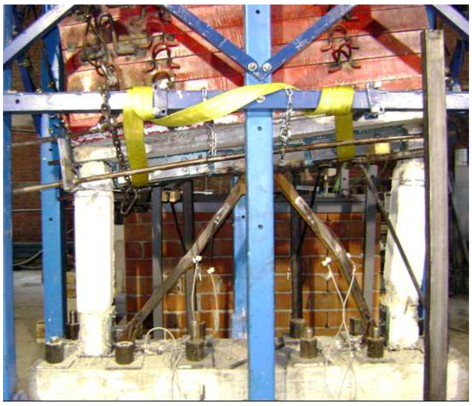

C_24_8.5_R2_68_436

Figure 2.38 Gravity collapse for specimen C_24_8.5_R2_68_436

Specimen C_13_10_R1_91_262

The ultimate lateral strength and lateral stiffness of the specimen C_13_10_R1_91_262 was 81.5 kN and 13.3 kN/mm, respectively. The increase in ultimate lateral strength and lateral stiffness of C_13_10_R1_91_262 were 6.3 and 7.6 times that of the reference frame, R_13_10, respectively. Plastic hinge mechanism of the columns and brace buckling were observed for C_13_10_R1_91_262 at about 0.9 % and 0.8 % DRs, respectively (Figure 2.29 and 2.34). A lateral load carrying capacity of approximately 45 kN (about 3.5 times the capacity of specimen R_13_10) was maintained up to about ± 4%. The connection failure and fracture of anchorage rods occurred at the 4 % DR followed by the drop of 30 kN (Figure 2.29 and 2.36).

Specimen C_24_8.5_R1_91_262

The ultimate lateral strength and lateral stiffness of the specimen C_24_8.5_R1_91_262 was 83.5 kN and 14.1 kN/mm, respectively. The increase in ultimate lateral strength and lateral stiffness of C_24_8.5_R1_91_262 were 6.1 and 5.7 times that of reference frame, R_25_8.1, respectively. Plastic hinge mechanism and brace buckling were observed for C_24_8.5_R1_91_262 at about 1 % and 0.8 % DRs, respectively (Figure 2.30 and 2.34). A lateral load carrying capacity of approximately 45 kN (about 3.5 times the capacity of specimen R_25_8.1) was maintained up to about ± 3.5 %. The connection failure, fracture of anchorage rods, occurred at the 3 % DR and then lateral load dropped to 30 kN (Figure 2.30 and Figure 2.36).

Specimen C_24_8.5_R2_89_210

The ultimate lateral strength and lateral stiffness of the specimen C_24_8.5_R2_89_210 was 68.1 kN and 12.9 kN/mm, respectively. The increase in ultimate lateral strength and lateral stiffness of C_24_8.5_R2_89_210 were 5.0 and 5.2 times that of reference frame, R_25_8.5, respectively. Plastic mechanism and brace buckling were observed for C_24_8.5_R2_89_210 at about 1.5 % and 0.5 % DRs, respectively (Figure 2.31 and Figure 2.34). A lateral load carrying capacity of approximately 35 kN (about 2.6 times the capacity of specimen R_25_8.5) was maintained up to about ± 3.0 %. Fracture initiation started at the 3% DR following the brace fracture at the 3.5 % DR (Figure 2.37). Connection failure, fracture of anchorage rods, did not occur for this braced frame.

Specimen C_24_8.5_R2_68_436

The ultimate lateral strength and lateral stiffness of the specimen C_24_8.5_R2_68_436 was 130.4 kN and 21.20 kN/mm, respectively. The increase in ultimate lateral strength and lateral stiffness of C_24_8.5_R2_68_436 were 9.5 and 8.6 times that of reference frame, R_25_8.5, respectively. Plastic mechanism and brace buckling were observed for C_24_8.5_R2_89_210 at about 1 % and 0.8 % DRs, respectively (Figure 2.32 and Figure 2.34). A lateral load carrying capacity of approximately 55 kN (about 4.0 times the capacity of specimen R_25_8.5) was maintained up to about ± 3.0%. Connection failure, fracture of anchorage rods, did not occur for this braced frame. After completion of the -4% DR excursion, a sudden gravity collapse occurred at the end of the second cycle (Figure 2.38).

Specimen C_22_9.4_R2_1147_300

The ultimate lateral strength and lateral stiffness of the specimen C_22_9.4_R2_1147_300 was 40.7 kN and 6.60 kN/mm, respectively. The increase in ultimate lateral strength and lateral stiffness of C_22_9.4_R2_1147_300 were 3.0 and 2.7 times that of reference frame, R_25_8.5, respectively. Plastic mechanism was observed for C_22_9.4_R2_1147_300 at about 1.8 % DR. Brace buckling occurred at the first cycle, 0.5 % DR excursion (Figure 2.34). This is because the slenderness of the brace member, steel plate, was very high resulted in negligible brace compression capacity. Shear cracks at the mid span of the RC beam was observed due to the lack of balance between the tension and compression brace (Figure 2.35). Severe pinching response was observed. The combined flexural shear cracking of the beam near the connection region helped in dissipating the energy without any significant loss of strength up until a 2 mm shear crack width was observed. No anchorage rod failure was observed for specimen C_22_9.4_R2_1147_300. Connection failure, fracture of anchorage rods, did not occur for this braced frame.

It was observed that the axial load ratio had no significant effect on the cyclic performance of the chevron braced frames. In fact, the cyclic performance of the chevron braced frame was found to be governed by the brace area and slenderness.

Envelope Response and Energy Dissipation

Figure 2.39 compares the envelope of lateral load versus deformation response obtained from all specimens, reference and braced frames. Figure 2.40 presents the cumulative energy dissipated at completion of each DR.

Table 2.9 summarized the total dissipated energy up to ± 4 % DR completion of each DR. If the seismic energy induced by the ground motion is desired to be dissipated by the structure, the reference frames or specimens R_13_10 and R_25_8.0 had poor seismic energy dissipation with a rapid strength degradation requiring upgrades. Upon upgrading, mainly due to strength enhancement, less pinching and stiffness degradation, larger energy dissipation was observed. It can be observed that highest energy dissipation was observed for specimen C_24_8.5_R2_68_436 with the largest brace cross sectional area and lateral force carrying capacity. For specimen strengthened using steel plates (C_22_9.4_R2_1147_300), energy dissipation was smallest among all braced frames.

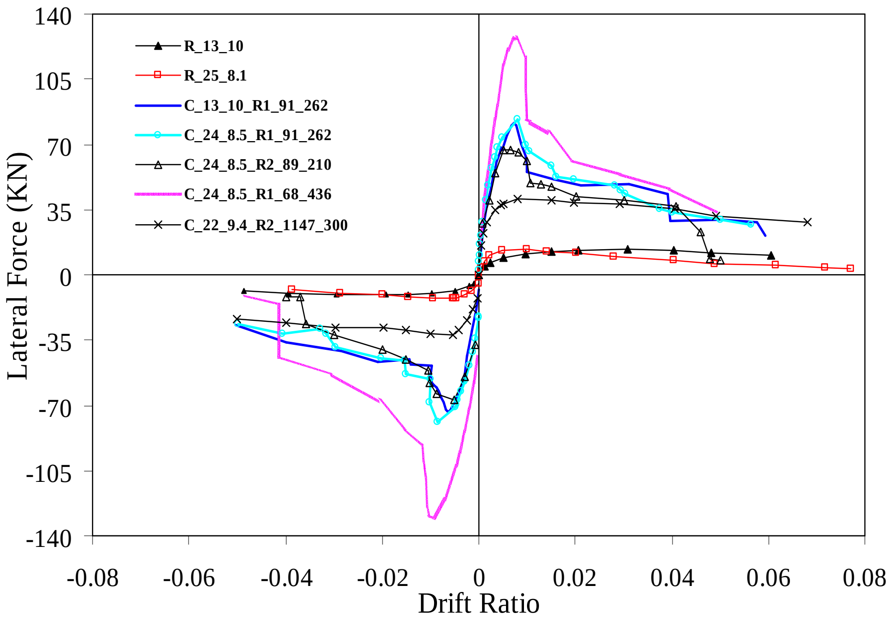

Figure 2.39 Envelope response of the reference and chevron braced frames

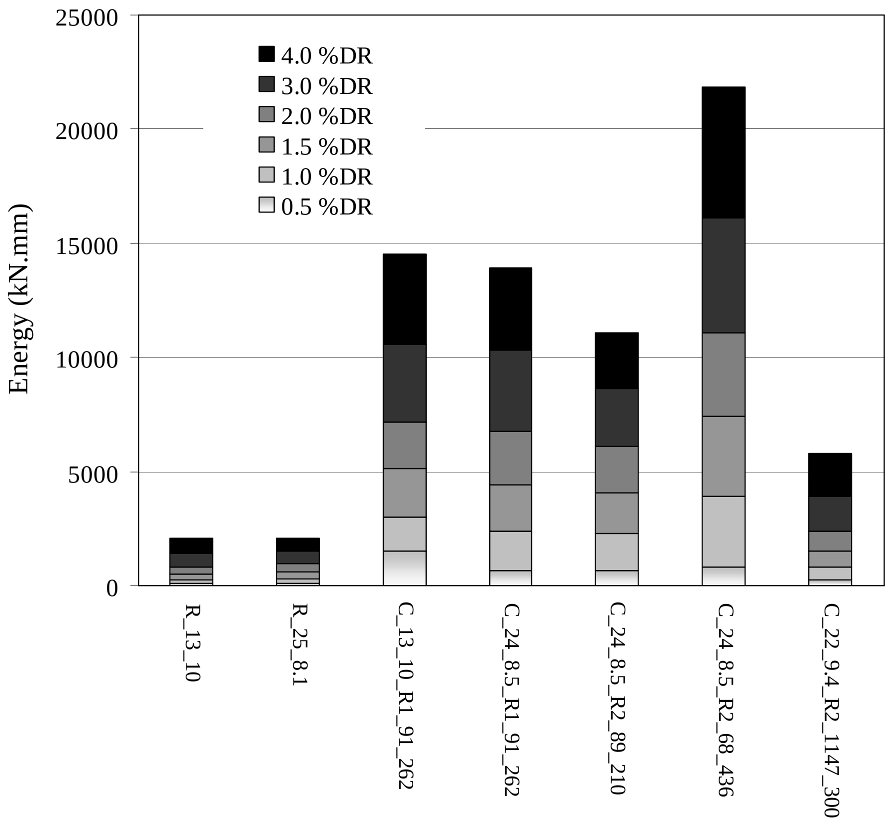

Figure 2.40 Energy dissipation capacity of the reference and chevron braced frames

2.5.3 Test Results of the ISF Strengthened Frames

The cyclic response of the test specimens are presented in Figures 2.41 to 2.46. These figures also indicate important events such as plastic hinge formation in the RC columns, fracture initiation of ISF elements, fracture initiation of energy dissipater rods, and joint failure of the RC frame. Pictures of test specimens after failure are presented in Figures 2.47 and 2.48.

Test results are summarized in Table 2.10, including the ultimate lateral strength, lateral stiffness, displacement ductility, dissipated energy, DR capacity, DR at failure, observed failure modes. During the dissipated energy calculation, an exception was made for specimen ISF_20_10.6_I_IS, where the summation was taken up to completion of the ± 3% DR cycles during when the specimen failed. The last five columns of Table 2.10 list the normalized strength, stiffness, and dissipated energy with respect to the corresponding values measured from specimen R_25_8.1, estimated lateral strength of the strengthened frame and ratio between estimated and measured lateral strength of strengthened frame.

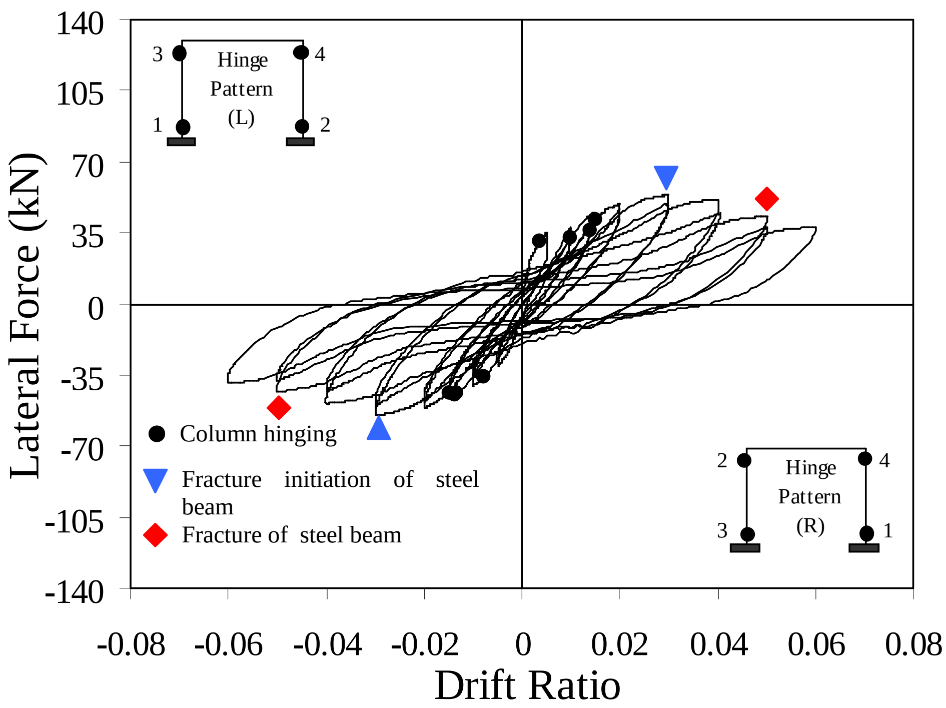

Figure 2.41 Cyclic response of the specimen ISF_27_7.5_I_HSS

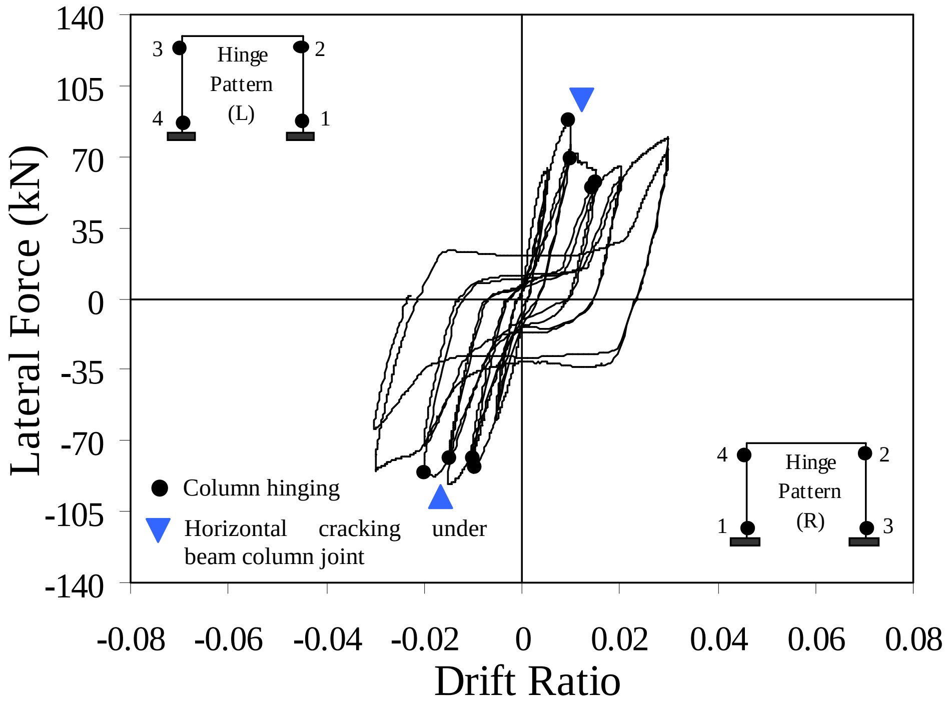

Figure 2.42 Cyclic response of the specimen ISF_20_10.6_I_IS

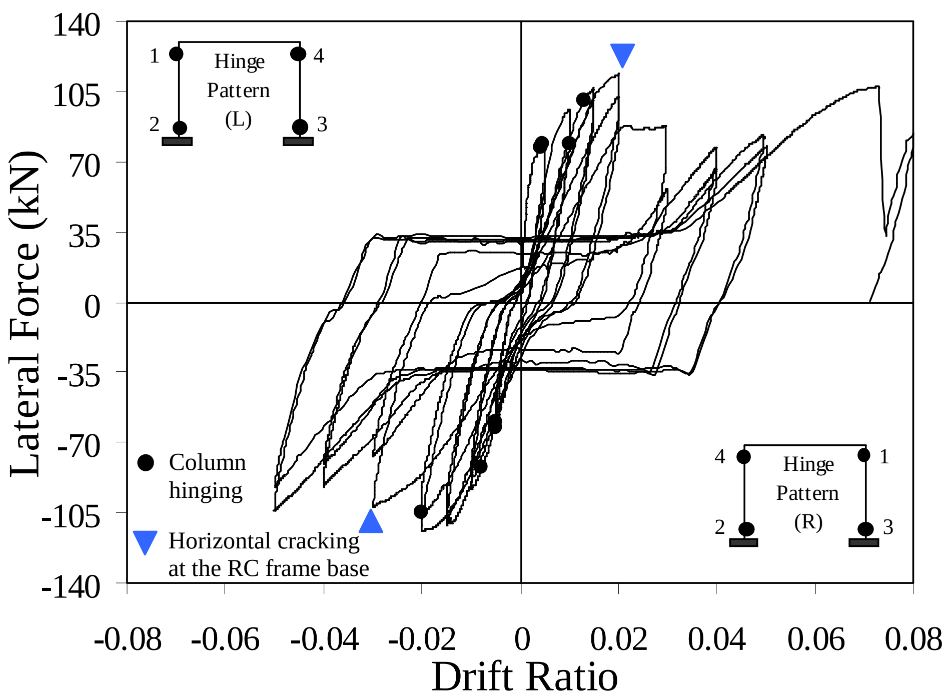

Figure 2.43 Cyclic response of the specimen ISF_24_8.7_II_IS

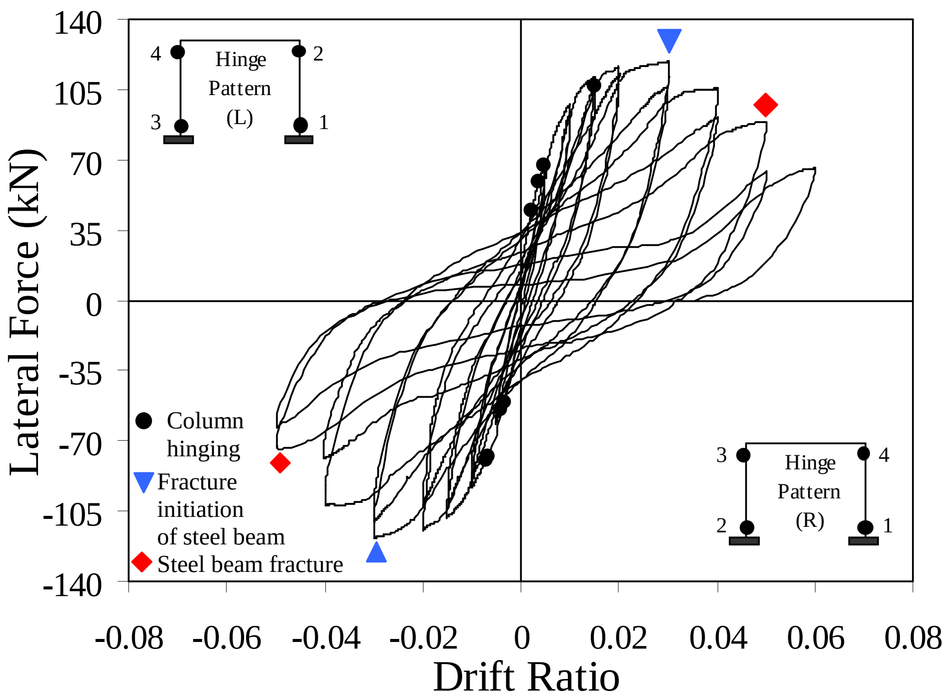

Figure 2.44 Cyclic response of the specimen ISF_28_7.4_III_IS

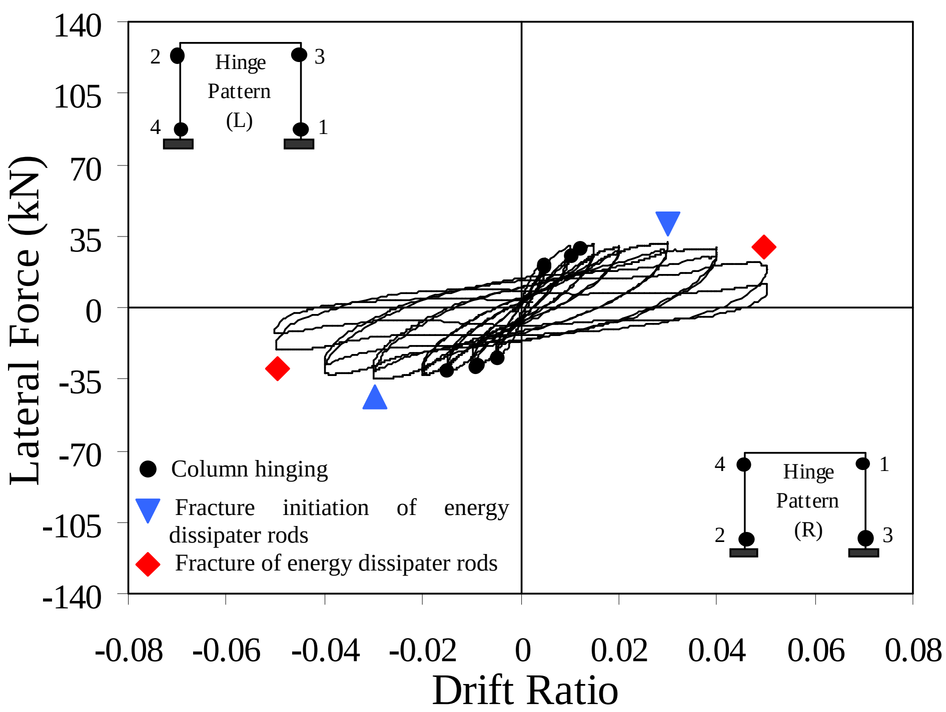

Figure 2.45 Cyclic response of the specimen ISF_27_7.5_I_HSS_E150

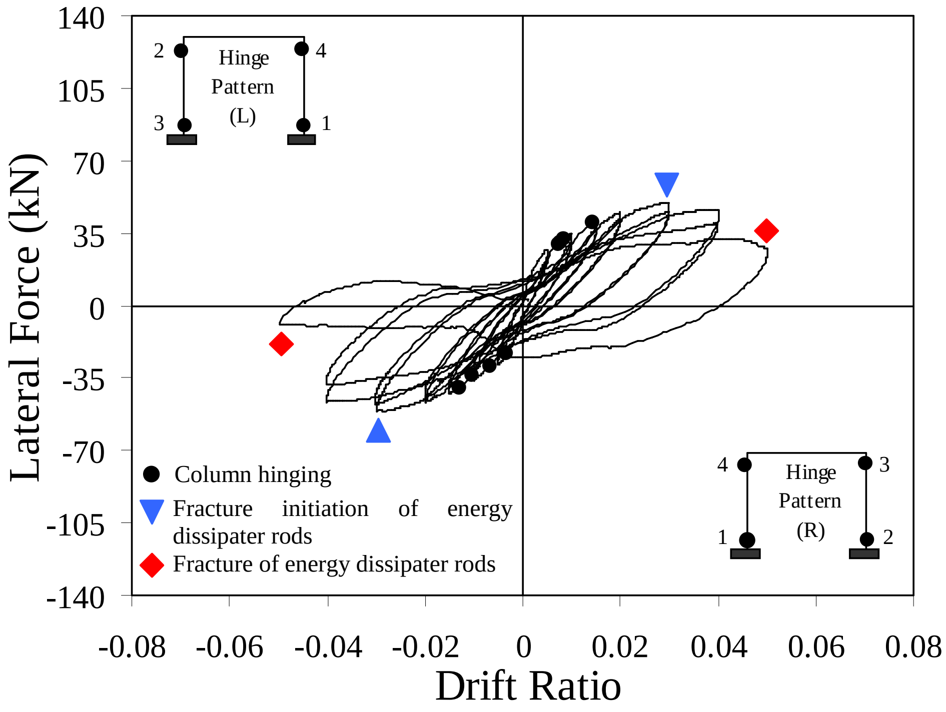

Figure 2.46 Cyclic response of the specimen ISF_26_8.0_I_HSS_E75

Specimen ISF_27_7.5_I_HSS

Specimen ISF_27_7.5_I_HSS developed an ultimate lateral strength of 55.0 kN (4 times the reference frame, R_25_8.1) and lateral stiffness of 6.37 kN/mm (2.6 times the reference frame, R_25_8.1). Separation between the ISF and RC column was observed after ±2% DR. At ±3% DR, fracture initiation of the ISF (HSS section) occurred at both ends of the beam along the fillet weld connecting the beam to the column. Prior to fracture in the ISF beams, while increasing plastic hinge rotation was measured at the RC columns, limited damage was observed in the RC frame. Plastic mechanism at RC columns occurred at 1.5% DR. Fracture of the steel beams (see Figure 2.41 and 2.47) led to gradual decrease in lateral strength after 3% DR. The displacement ductility of this ISF retrofitted specimen was about two times the displacement ductility of the reference specimen (Table 2.10).

Specimen ISF_27_7.5_I_HSS

Specimen ISF_20_10.6_I_IS

Specimen ISF_24_8.7_II_IS

Specimen ISF_28_7.4_III_IS

Specimen ISF_27_7.5_I_HSS_E150

Specimen ISF_26_8.0_I_HSS_E75

Figure 2.47 Picture of failure observed in each specimen

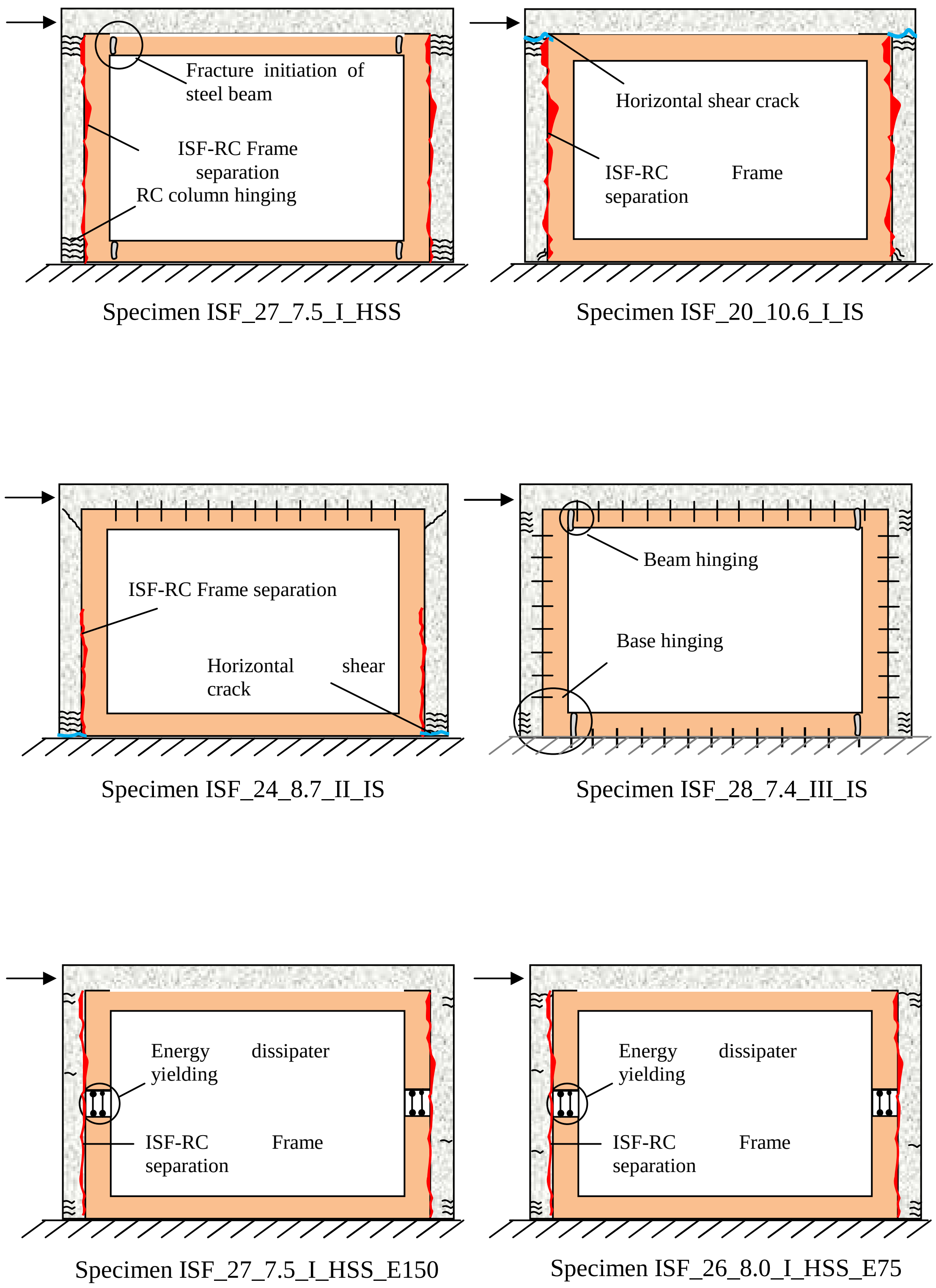

Figure 2.48 Close-up views of failure observed in each specimen

Table 2.10 Test results of the reference frame and ISF

Specimen Name	V_u (kN)	K_{LS} (kN/mm)	Displacement Ductility Direction		E (kN.mm)	Drift Ratio (%) Capacity Direction		Drift Ratio (%) at Failure	Failure Modes	$\frac{V_u}{V_{u(reference)}}$	$\frac{K_{LS}}{K_{LS(reference)}}$	$\frac{E}{E_{(reference)}}$	V_{sf}	$\frac{V_{sf}}{V_u}$
			Rigth	Left		Rigth	Left							
R_25_8.1	13.7	2.48	2.51	2.51	2082	2.00	2.00	-	[1]	1	1	1	-	-
ISF_27_7.5_I_HSS	55.0	6.37	7.05	7.05	10184	4.00	4.00	4.00	[2]	4.00	2.57	4.89	50.7	0.92
ISF_20_10.6_I_IS	91.8	11.90	1.11	3.13	11043	1.00	3.00	1.00	[3]	6.68	4.80	7.23	67.7	0.74
ISF_24_8.7_II_IS	114.1	13.72	4.29	6.44	22151	2.00	3.00	2.00	[4]	8.30	5.53	10.64	111.9	0.98
ISF_28_7.4_III_IS	118.89	12.68	14.12	14.12	24553	4.00	4.00	4.00	[5]	8.65	5.11	11.79	131.0	1.10
ISF_27_7.5_I_HSS_E150	35.04	4.74	8.69	8.69	7501	4.00	4.00	4.00	[6]	2.55	1.91	3.60	32.8	0.94
ISF_26_8.0_I_HSS_E75	51.14	5.39	7.58	7.58	9192	4.00	4.00	4.00	[6]	3.72	2.17	4.42	51.9	1.02

V_u: Ultimate lateral strength, K_{LS}: Lateral stiffness, E: Dissipated energy, V_{sf}: Estimated lateral strength of the strengthened frame, [1]: RC Column mechanism, [2]: ISF beam mechanism, [3]: Horizontal cracking under beam column joint, [4]: Horizontal cracking at the RC frame base, [5]: Composite frame beam mechanism. [6]: Fracture of energy dissipater rods.

Specimen ISF_20_10.6_I_IS

Specimen ISF_20_10.6_I_IS developed an ultimate lateral strength of 91.8 kN (6.7 times) and a lateral stiffness of 11.9 kN/mm (4.8 times the reference frame). Separation between the ISF and RC frame was first observed at ± 1.5 % DR. Specimen ISF_20_10.6_I_IS failed due to excessive damage at the beam-column joints of the RC frame (Figure 2.47). Because load transfer between the RC frame and the ISF relied on bearing between one RC column and the ISF, the transferred load was limited by the horizontal shear strength of the RC beam-column joint. Horizontal shear cracks were observed at both RC beam-column joints, along the top of the ISF, after ± 1% DR. Observations suggest that the horizontal shear strength of the RC beam-column joint was mainly due to the frictional resistance of concrete and dowel resistance of longitudinal column bars. As the DR was increased beyond 1.0%, horizontal shear cracks widened (Figure 2.42 and 2.47), and the lateral strength deteriorated by about 20%. It is hypothesized that the lateral strength increases beyond ± 2% DR was due to strain hardening of the highly stressed longitudinal bars. The displacement ductility of specimen ISF_20_10.6_I_IS was lowest among all specimens with an ISF. No fracture was observed in the ISF during the test. The performance of specimen ISF_20_10.6_I_IS indicates that the benefit of ISF may be limited if failure in the beam-to-column joint of the RC frame cannot be controlled. The lateral strength observed beyond 2% DR might be developed only if the longitudinal bars are well anchored without any splice deficiencies.

Specimen ISF_24_8.7_II_IS

Specimen ISF_24_8.7_II_IS developed an ultimate lateral strength of 114.1 kN (8.3 times the reference frame) and a lateral stiffness of 13.7 kN/mm (5.5 times the reference frame). In specimen ISF_24_8.7_II_IS, separation between the ISF and RC column was observed at ± 2%. Failure of the RC beam-column joint did not occur in specimen ISF_24_8.7_II_IS. It appeared that a substantial portion of the lateral load was transferred from the RC beams to the ISF through the anchor rods, and thereby, the shear force transferred to the RC beam-column joint was limited. On the other hand, at the base of the RC columns, where force transfer between the ISF and RC frame depended only on epoxy bonding and frictional resistance, concentrated damage eventually led to complete loss of RC columns as shown in Figure 2.47 and 2.48. No anchor failure was observed during the test. The cyclic response in Figure 2.43 indicates an increase in lateral strength beyond ± 4% DR similar to the cyclic response of specimen ISF_20_10.6_I_IS beyond ± 1.5% DR. It is noted that even after such severe damage to the RC columns, the specimen maintained its gravity load carrying capacity owing to the reserve capacity of the ISF, hence acting as a backup axial load carrying system (Figure 2.47).

Specimen ISF_28_7.4_III_IS

Specimen ISF_28_7.4_III_IS developed an ultimate lateral strength of 118.9 kN (8.7 times the reference frame) and a lateral stiffness of 12.7 kN/mm (5.1 times the reference frame). Specimen ISF_28_7.4_III_IS was designed to develop composite action in the beam and two columns. Cracks in the concrete widened during each loading excursion that produced tension in the concrete portion of the composite section. Figure 2.47 and 2.48 shows cracks developing in the column as the bending moment produces tension in the closer side of the column. Unlike any of the other specimens, no separation was observed between the ISF and RC frame. No anchor failure was observed during the test. Horizontal shear cracking at the column base observed in specimen ISF_24_8.7_II_IS did not occur in specimen ISF_28_7.4_III_IS. The specimen failed due to fracture of the welded beam-to-column connection that initiated at ± 3% DR (Figure 2.47). Among all specimens, specimen ISF_28_7.4_III_IS achieved the largest lateral strength and displacement ductility. Superior performance of this specimen can be attributed to the anchor connection provided between ISF and RC frame all around the inner boundary.

Specimen ISF_27_7.5_I_HSS_E150

Specimen ISF_27_7.5_I_HSS_E150 developed an ultimate lateral strength of 35 kN (2.6 times the reference frame) and a lateral stiffness of 4.7 kN/mm (1.9 times the reference frame). The use of energy dissipater rods resulted in a 34% and 57% decrease in stiffness and lateral strength compared to Specimen ISF_27_7.5_I_HSS, respectively. Similar to specimen ISF_27_7.5_I_HSS, separation between the ISF and RC column was seen after ± 2% DR. All potential plastic hinges at the RC columns of specimen ISF_27_7.5_I_HSS_E150 formed at 2% DR with no other visible damage. ISF_27_7.5_I_HSS_E150 failed due to fracture of the energy dissipater rods at 5% DR. At this stage, flexural-shear cracking was observed in the RC columns at ISF contact locations (Figure 2.47 and 2.48). ISF_27_7.5_I_HSS_E150 had a displacement ductility of about 8.7 which 3.8 times that of reference frame and 1.7 times that of ISF_27_7.5_I_HSS. As intended in design, while the threaded rods underwent substantial plastic deformation, no yielding occurred in the remaining portion of the ISF.

Specimen ISF_26_8.0_I_HSS_E75

Specimen ISF_26_8.0_I_HSS_E75 developed an ultimate lateral strength of 51 kN (3.7 times the reference frame) and a lateral stiffness of 5.4 kN/mm (2.2 times the reference frame). The use of energy dissipater rods resulted in 18% and 8% decrease in stiffness and lateral strength compared to Specimen ISF_27_7.5_I_HSS, respectively. Similar to specimen ISF_27_7.5_I_HSS, separation between the ISF and RC column was seen after ± 2% DR. All potential plastic hinges at the RC columns of specimen ISF_26_8.0_I_HSS_E75 formed at 2% DR with no other visible damage. ISF_26_8.0_I_HSS_E75 failed due to fracture of the energy dissipater rods at 5% DR. At this stage, flexural-shear cracking was observed in the RC columns at ISF contact locations (Figure 2.46 and 2.47). ISF_26_8.0_I_HSS_E75 had a displacement ductility of about 7.6 which was merely three times that of reference frame and approximately equal that of ISF_27_7.5_I_HSS.

Envelope Response and Energy Dissipation

Figure 2.49 compares the envelope of lateral load versus deformation response. Figure 2.50 presents the cumulative energy dissipated at completion of each DR. The proposed upgrade schemes of adding an ISF increased the lateral strength of the RC frame (represented by reference specimen R_25_8.1) by 2.6 to 8.7 times. More importantly, the energy dissipation capacity increased by a factor of about 3 to 12 times the bare frame due to less pronounced pinching, stiffness and strength degradation. On the other hand, specimens ISF_20_10.6_I_IS and ISF_24_8.7_II_IS exhibited unstable cyclic performance (Figure 2.41 and 2.42), low displacement ductility and smaller energy dissipation capacity (Table 2.10). In addition, the extensive RC beam-column joint and column base damage due to high shear demands in these specimens discourage the use of ISF when the horizontal shear strength of the RC beam-column joints is smaller than the lateral strength of the ISF. Although same installation method, method I, was used for Specimens ISF_27_7.5_I_HSS_E150 and ISF_26_8.0_I_HSS_E75, they had different envelope response because of the dissipater rod height. The inelastic action on the dissipater rods resembles the plastic mechanism of a fixed-fixed steel column (Figure 2.51). The lateral force carrying capacity of the energy dissipater rods is determined by the plastic moment capacity and length of the section. Hence, decreasing in the rod length resulted in an increase in the strength of the retrofit system. The largest degree of enhancement in energy dissipation, strength, and displacement ductility was achieved by Specimen ISF_28_7.4_III_IS implemented anchors between the ISF and RC frame to achieve fully composite action.

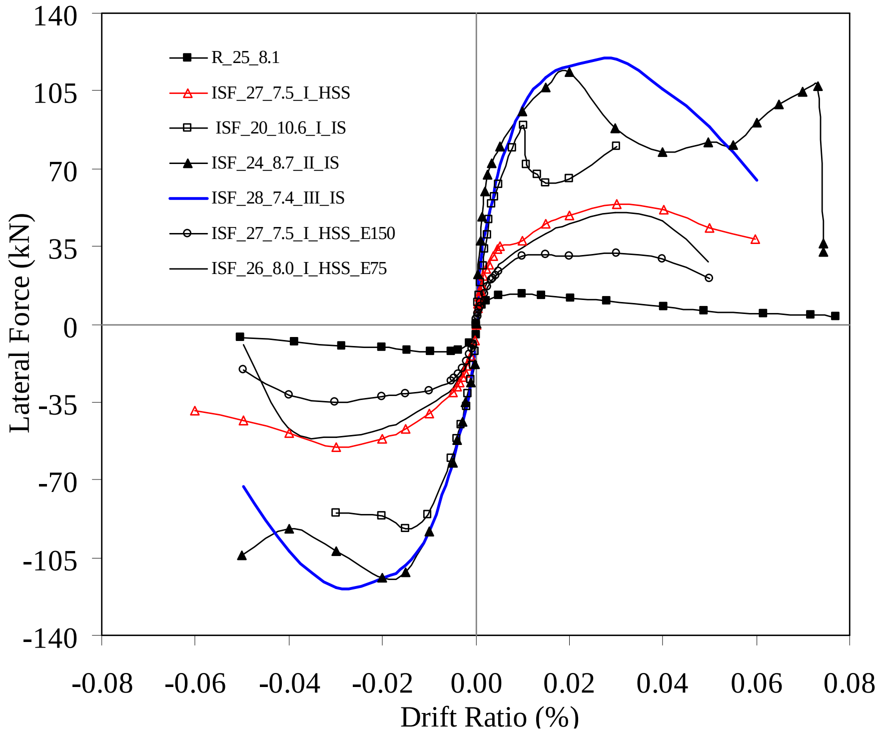

Figure 2.49 Envelope response of test specimens

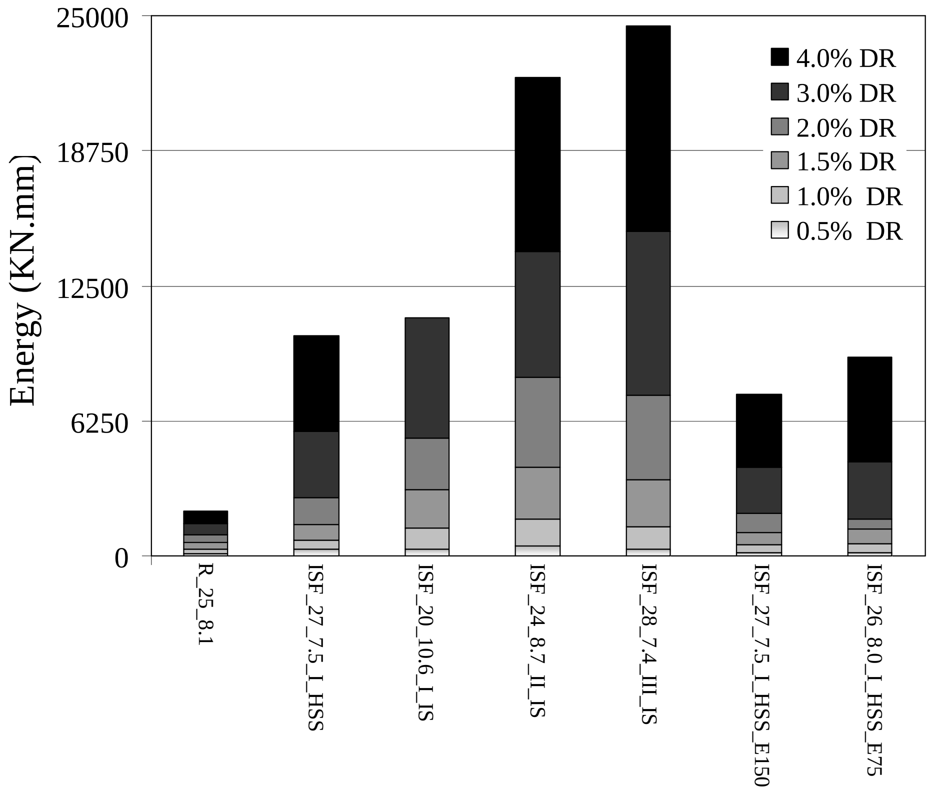

Figure 2.50 Energy dissipation capacity of the reference and ISFs

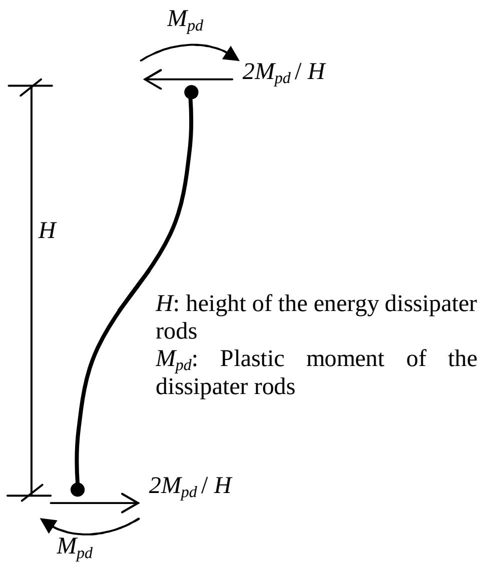

Figure 2.51 Plastic deformation of dissipater rods

Strength Evaluation of the Test Specimens

The observed failure modes of the specimens with ISF are illustrated in Figure 2.47 and 2.48. The failure modes suggest that the strength of the specimen was governed by the following limit cases for each specimen: (a) sum of the plastic strengths of the RC frame and ISF (specimen ISF_27_7.5_I_HSS); (b) horizontal shear strength of the RC beam-column joint (ISF_20_10.6_I_IS), shear strength of the column base (ISF_24_8.7_II_IS); or (c) plastic strength of the composite frame (ISF_28_7.4_III_IS) and (d) the strength of the energy dissipaters (ISF_27_7.5_I_HSS_E150 and ISF_26_8.0_I_HSS_E75). The last column of the Table 2.10 compares the measured strength against the prediction based on simple calculations.

The estimated strength in Table 2.10 was obtained by summing the measured strength of reference R_25_8.1 with the plastic strength of the ISF. For specimens ISF_27_7.5_I_HSS, ISF_20_10.6_I_IS, ISF_27_7.5_I_HSS_E150 and ISF_26_8.0_I_HSS_E75 which did not use anchors, the following equations were used:

$$V_{sf} = V_{bf} + \min(V_j\ , V_{ISF}) \tag{2.4}$$

$$V_{ISF} = \begin{cases} \min\left(\dfrac{4M_p}{L_{ISF}}, N\dfrac{2M_{pd}}{H}\right) \text{ with energy dissipater} \\ \dfrac{4M_p}{L_{ISF}} \text{ without energy dissipater} \end{cases} \tag{2.5}$$

where V_{sf} is the estimated lateral strength of the strengthened frame, V_{bf} is the measured lateral strength of the RC frame (taken from Specimen R_25_8.1), V_j is the horizontal design shear strength of the RC beam-column joint (computed based on TEC (2007) as 0.45 × measured concrete compressive strength listed in Table 2.4 x joint height x joint width) and V_{ISF} is the design lateral strength of the ISF. V_{ISF} is computed as the smaller of the plastic strength of the ISF and the plastic strength of the energy dissipating system. In Equation 2.5, M_p and M_{pd} (Figure 2.51) are the plastic moment of the ISF beams and dissipater rods, respectively, H and L_{ISF} are the heights of the energy dissipater rods and ISF, respectively and N is the number of dissipater rods.

Specimen ISF_24_8.7_II_IS was designed to avoid failure at the RC beam-column joint. Lateral strength was estimated by considering plastic capacity of the steel beam mechanism (Equation 2.4). In the case of ISF installed with anchors (i.e. specimen ISF_24_7.4_III_IS), horizontal shear strength of the RC beam-column joint did not govern the ultimate load. Hence, lateral load capacity was calculated based on a beam mechanism using the capacity of the composite beam and column sections presented in Table 2.7. Table 2.10 indicates that strength increase achieved by ISFs in each specimen, except specimen ISF_20_10.6_I_IS, was predicted within 10 % by these simple calculations.

Above calculations show that the strength of ISF at formation of a failure mechanism depends on the presence of anchor rods. If no anchors are used (i.e. installation method I), then the capacity of the system is limited by the horizontal strength of the region below the RC beam-column joint. Hence, there is no benefit in providing an ISF with the lateral capacity of it greater than the horizontal shear strength of the RC beam-column joint. Upon providing sufficient anchors, it was found that collapse mechanism can be estimated by the strength of the composite frame.

2.5.4 Test Results of the X-Braced Frame

The cyclic response of the X-Braced frame is shown in Figure 2.52. This figure also indicates the cyclic response of the specimen C_22_9.4_R2_1147_300 (having the same brace section used in chevron braced frame) for comparison. These two frames are similar in terms of the connection details and brace members which were steel plates. Specimen X-Braced frame developed an ultimate lateral strength of 42.5 kN (3 times the reference frame, R_25_8.1) and lateral stiffness of 7.95 kN/mm (3.3 times the reference frame, R_25_8.1).

The cyclic response of the X-Braced frame was not stable due to excessive damage at the joints (Figure 2.53). The 15% lateral strength drop was observed up to +1% and -0.5% DR for pull and push directions, respectively. It can be observed that chevron braced frames exhibited a superior performance compared to the X-brace system. This can be attributed to anchoring the braces to RC beam rather than attaching then to joints that are extremely vulnerable. Moreover, it should be kept in mind that the beam strengthening is more applicable than the joint strengthening due to easy of access and architectural concerns.

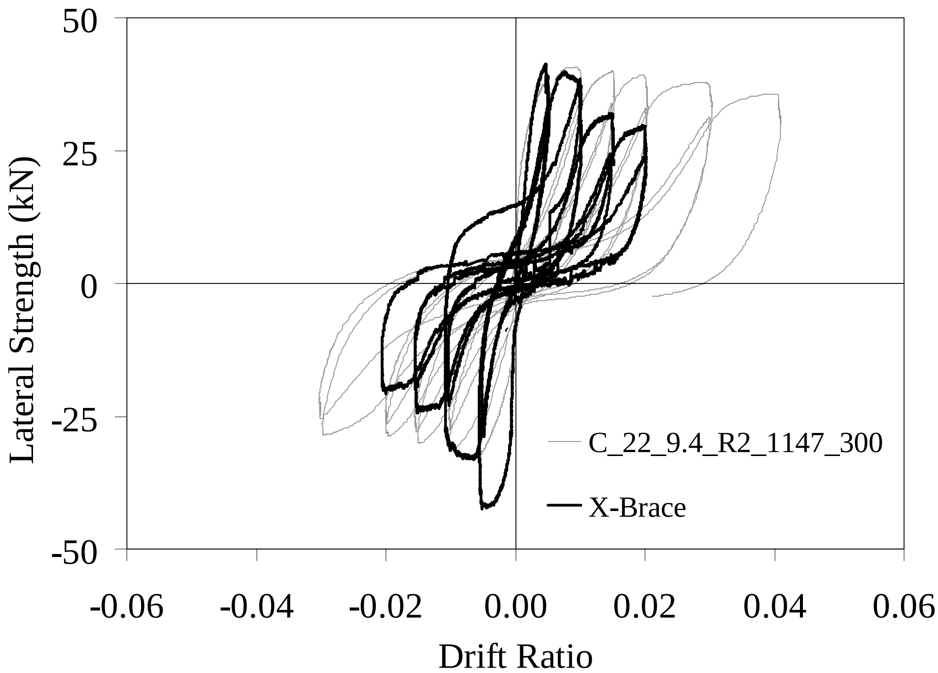

Figure 2.52 Cyclic response of the specimen X-Braced Frame

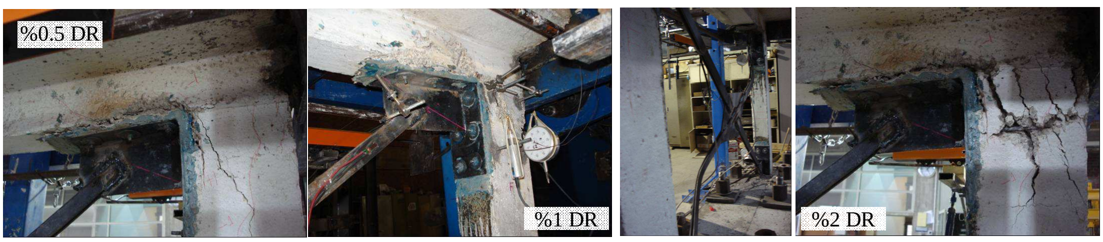

Figure 2.53 Picture of the X-Braced frame damage

2.5.5 Test Results of the Column with Shear Plate Frame

The cyclic response of the column with shear plate frame is given in Figure 2.54. Specimen column with shear plate frame developed an ultimate lateral strength of 31.5 kN (2.3 times the reference frame, R_25_8.1) and lateral stiffness of 4.1 kN/mm (1.7 times the reference frame, R_25_8.1). The desired lateral strength enhancement was not obtained for this specimen due to excessive damage on the RC beam and shear plate (Figure 2.55). The shear plate imposed additional flexural demands on the RC beam which did not have strength to resist this additional demand. Hence, excessive beam damage occurred during the test. In addition, the shear plate had in and out of plane stability problem with increasing lateral excursions. The physical dimension of the shear plate is so small that the alignment problem is considered to be main problem of this stability problem. This test indicated that to design a shear plate for a real retrofit case may be difficult due to physical concerns which should be provided shear yielding of the steel plate instead of flexure yielding. Steel column, I-140 section, behaved elastically up to end of the test.

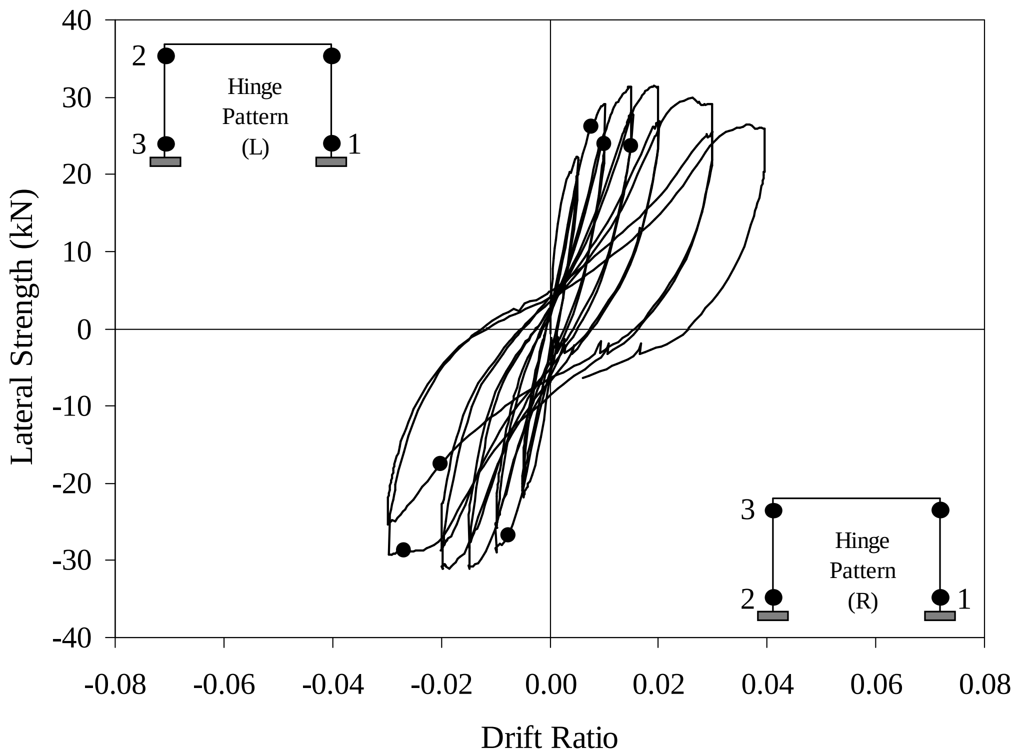

Figure 2.54 Cyclic response of the specimen column with shear plate frame

Figure 2.55 Picture of column with shear plate frame

2.6 Evaluation of the Test Frames

The cyclic response of 1/3 scaled one bay-one story RC frames indicated that the chevron braces frames and the ISF are possible candidates in seismic retrofit of deficient low rise building frames. The chevron braces increased the lateral strength, stiffness and energy dissipation capacity of the deficient RC frames significantly (Figures 2.39 and 2.40). This is clearly an important contribution since the deficient buildings in Turkey lack lateral strength and stiffness. In this way, the lateral displacement demands of columns and beams can be relieved. The chevron braces have three connections between braces and RC frame rather than four connections for the X braced RC frame. The lower number of connections is more appealing for a retrofit scheme. The chevron braces are installed to mid-span of the RC beams and the foundation in one story frames. This is an obvious advantage over X braces since the demand on beam-column connections is not significantly affected. In structures having more than one story, the connections to joints becomes a necessity for chevron braces and the performance of such cases are examined in Chapter 3 and 4.

The connection between RC and steel brace members were performed by using post-installed anchorage rods (Figures 2.8, 2.17 and 2.18) for the chevron brace retrofits. The anchor depth of 20ϕ or 0.8*h* (ϕ: diameter of the anchorage rod and *h*: column depth thought the drilling direction) was determined to be adequate in order to provide force transfer from steel braces to RC members. The threaded rods were found to be useful in order to provide easy connection and better bonding surface. The strengthening of the beam may be needed in the case of large unbalance forces in beam to brace region. It was found that the steel plates can be attached to the RC beam by using anchorage rods, epoxy and repair putty effectively. The shear strengthening of the beam by means of appropriate methods can be designed for the force difference between the vertical component of brace yield force and vertical component of brace post buckling capacity (see Appendix 1). The brace post buckling capacity can be determined from Load and Resistance Factor Design (LRFD) (1994) or ASCE/SEI 41 (2007) documents. Furthermore, the connections may be designed for a higher over strength factor. As indicated in Table 2.3, the yield strength of the HSS sections was higher than nominal strength of the used steel grade which is ST 37 (TS 648, 1980). The over strength factor was found to be between 1.4 and 2. When the brace slenderness is higher than 250 (allowed by TS 648 (1980) or other limits suggested by the ASCE/SEI 41 (2007), LRFD (1994) can be used) it was observed that the system can exhibit a ductile response by yielding the RC beam (strengthened with steel plates, see Figure 2.33 and 2.39). However, extensive damage in form shear crack opening was observed for such a design (see Figure 2.35). Hence, slenderness limitations in the design guideline could be obeyed when designing such retrofits.

ISFs increased the stiffness, strength, and energy dissipation capacity of seismically deficient RC frames effectively (Figures 2.49 and 50). For the ISF, there were two cases examined:

1) If the lateral strength enhancement provided by the ISF is lower than the horizontal shear strength of the RC beam-column joint, the ISF without any anchorage (Method I) can be used for seismic retrofit.

2) If the lateral strength enhancement provided by the ISF is higher than the horizontal shear strength of the RC beam-column joint, the ISF should be constructed to function compositely with the RC frame (Method III) in order to limit the force imposed on the RC beam-column joints. For fully composite members, the connection strength should be adequate in order to provide force transfer between RC and steel members. The numbers of the anchorage rods can be determined safely by using the methods described in Section 2.4.2.

The energy dissipation system was observed to be beneficial in increasing the lateral strength, stiffness and energy dissipation capacity of the deficient RC frame. However, the out of plane stability and damage introduced in the mid-span of RC columns suggested the need of further investigations for such systems with different type of dissipaters.

The X-braced and column with shear plate system retrofits were not sought further in this thesis, as they introduced excessive beam-column joint and beam damage, respectively.

CHAPTER 3

3. PSEUDO DYNAMIC TESTS ON STEEL STRENGTHENED RC FRAMES

3.1 Introduction

Strengthening of the deficient RC frames with structural steel members were examined by pseudo dynamic testing of three two story-three bay RC frames in this chapter. First frame was the reference frame tested and explained in detail by Kurt (2010) without any strengthening. Two additional specimens were strengthened with structural steel members and tested. Based on the knowledge gained from the test results presented in Chapter 2, it was considered to strengthen the 3 bay-2 story RC frames with chevron brace and ISF with fully composite section. The frame with infill wall specimen of Kurt (2010) was used as a reference for economy purposes. The steel strengthened specimens simulate the strengthening of a realistic RC frame building by removing the infill walls and installing new structural steel components. The objective of testing a two story structure with PsD test methods are:

1) To realistically simulate the seismic demand.

2) To observe multi-bay multi-story system behavior as opposed to one bay-one story structures.

3) To observe the connection performance in upper stories where the brace is connected to the beam-column joint.

4) To determine possible redistribution after sudden member failures (for example brace failure or excessive plastic hinge damage).

5) To investigate the performance of ISF composite columns in a two story structures.

3.2 RC Frames and Test Setup

The test frame was scaled to ½ from a prototype RC frame building with infill walls tested by Kurt (2010) (see Figure 3.1). As seen in Figure 3.1, the test specimen was extracted from the interior bays of the prototype building (Kurt, 2010). Both live (300 kg/cm^2) and dead (250 kg/cm^2) loads were considered in the design of prototype building. These loads produced about 13 and 23 % column axial load ratio at the first story exterior and interior columns, respectively. These ratios were 8 and 15 % for the second story exterior and interior columns, respectively.

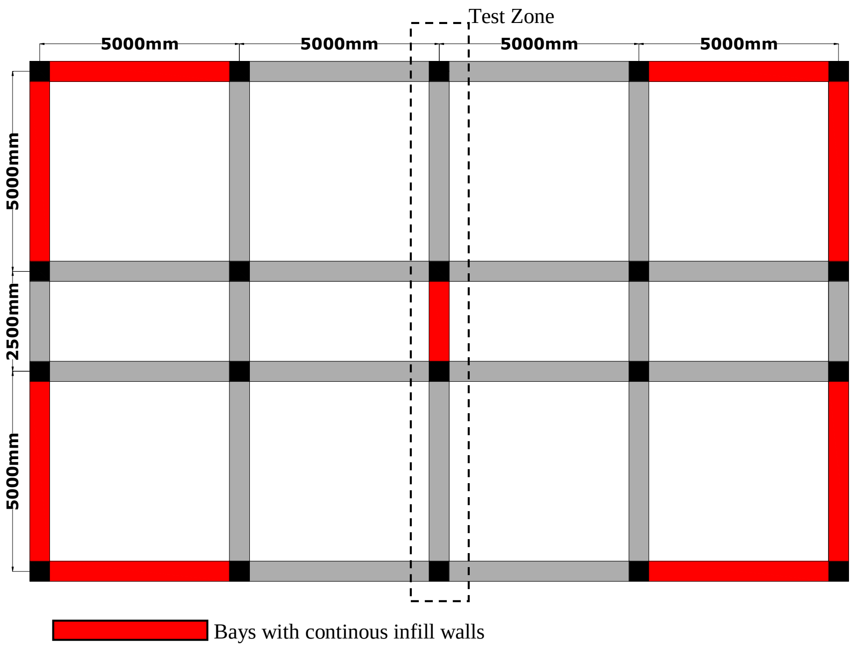

Figure 3.1 Plan view of prototype building (adopted from Kurt, 2010)

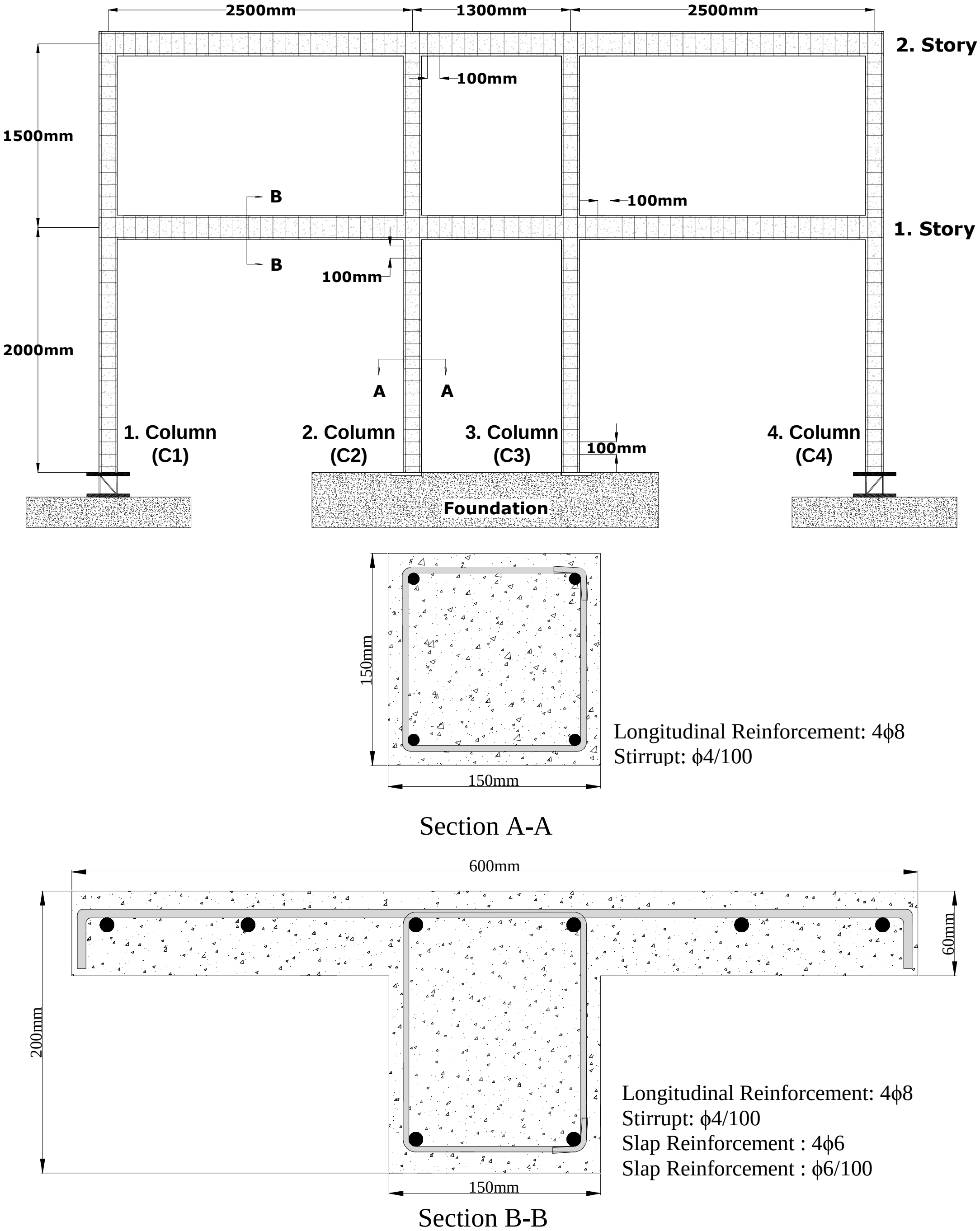

Figure 3.2 RC test frame

Figure 3.2 shows the elevation view of the test specimens excluding the strengthening component or the infill. The exterior and interior bay of the test specimen was 2500 mm and 1300 mm, respectively. The height of the first and second story was 2000 mm and 1500 mm, respectively. The 150 mm × 150 mm columns were provided with four 8-mm diameter longitudinal reinforcement plain bars resulting in about 1.0 % longitudinal reinforcement ratio (Figure 3.2). The column longitudinal reinforcement was welded to the 25 mm thick base plate (Figure 3.3-b). The base plates were fixed to the concrete foundation with anchor rods placed before concrete casting in the foundation (Figure 3.3-b) for columns C2 and C3 (Figure 3.2). The base plates of columns C1 and C4 were connected to the force transducers designed by Canbay et al. (2004).

Four mm diameter plain bars were used for stirrups of both columns and beams (Figure 3.2 and 3.3-b and d). Although the TEC (2007) requires stirrups to be anchored using 135 degree hooks, 90 degree hooks were used for all columns and beams to simulate the detailing deficiency of the Turkish construction practice before the establishment of the modern seismic codes (Figure 3.2 and Figure 3.3-b, d and f).

The stirrup spacing of the columns was 100 mm in the plastic hinge regions to simulate insufficient confining details (Figure 3.2). This produced 0.16% volumetric ratio of transverse reinforcement which was smaller than that required by the TEC (2007) (ρcode=0.25%).

The 150 mm × 200 mm beams were cast with a 600-mm wide, 60-mm thick slab (Figure 3.2). In addition to including the slab effects, the slab was used as a platform to directly support the steel blocks that imposed gravity loads. Transverse reinforcement of the beams was composed of 4 mm diameter stirrups with 100 mm spacing. The beams had four 8 mm diameter longitudinal reinforcement in addition to the four 6 mm diameter reinforcement (Figure 3.2 and 3.3-e). The slab had 6 mm reinforcing bars with spacing 100 mm along the slab width (Figure 3.3-e). Bottom and top beam longitudinal reinforcements were welded to each other at the third column and mid of the interior span of the frame to provide the continuity of longitudinal reinforcement, respectively. The RC beam-column joint had no stirrup extending into the joint to simulate insufficient construction details (Figure 3.3-d and j).

The view of the frame, before removing the steel molds is shown in Figure 3.3-n. After removing the molds, second story steel blocks were placed on the frame than the contraction of test frame was completed as seen in Figure 3.4. This figure shows original case before the construction of the infill wall and strengthening cases. The RC frame was constructed on three foundations (Figure 3.4). These foundations were fixed to the strong floor. To fix the foundation to the floor ϕ50mm rods were used. Four and eight rods were used for the exterior and interior foundation, respectively.

a) before the construction of the molds, b) reinforcement details at the bottom of the column (2. column), c) 1. story mold constructed, d) joint, e) 1. story before the concrete casting, f) 1. story concrete casting, g) placing the steel blocks on the 1. story, h) 2. story mold construction, i) 2. story before the concrete casting, j) joint, k) 2. story concrete casting, m) after concrete casting, n) curing, 1) longitudinal reinforcement of the column, 2) transverse reinforcement, 3) rc foundation, 4) base plate for RC frame, 5) anchorage rod, 6) steel mold, 7) long. reinforcement of the beam, 8) slab reinforcement parallel to the beam longitudinal reinforcement, 9) slab reinforcement perpendicular to the beam longitudinal reinforcement, 10) steel frame

Figure 3.3 RC frame and construction details

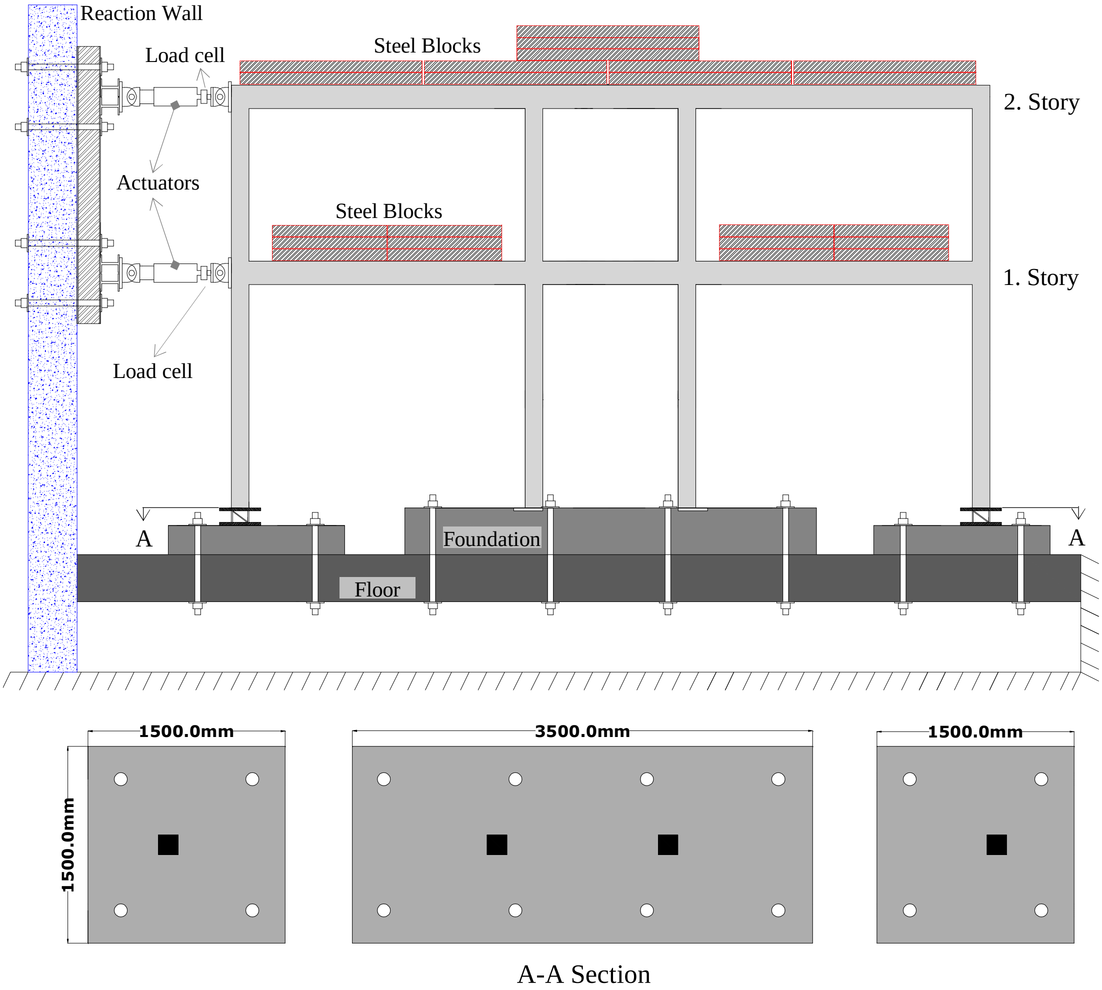

Figure 3.4 RC frame test setup and foundation

Instrumentation and loading system

Figure 3.5 indicates the instrumentations and loading systems. Two computer controlled actuators were used to impose lateral displacement demands to the RC frame (Figure 3.5-a). Pulling on the RC frame was conducted by the help of four ϕ30mm-high strength rods connected to the frame ends.

These 7000 mm length-rods were fastened to the 25 mm steel plate which was connected to the RC frame at both end of the frame on the first and fourth columns (C1 and C4, see Figure 3.5-a, c and f). 500-kN-load cells were placed between actuators and RC frame to measure the lateral force at each story level. Two LVDTs and heidenheim were used to measure the floor displacement at first and second floors (Figure 3.5-f). Two LVDTs were used to measure the elongation and contraction of the column to calculate the column curvature (Figure 3.5-b and d). Two special manufactured transducers (Figure 3.5-e) were placed under the exterior columns (C1 and C4, see Figures 3.2 and 3.5) to acquire column moment, shear and axial force. The details about the transducer production and calibration are available elsewhere Canbay et al. (2004).

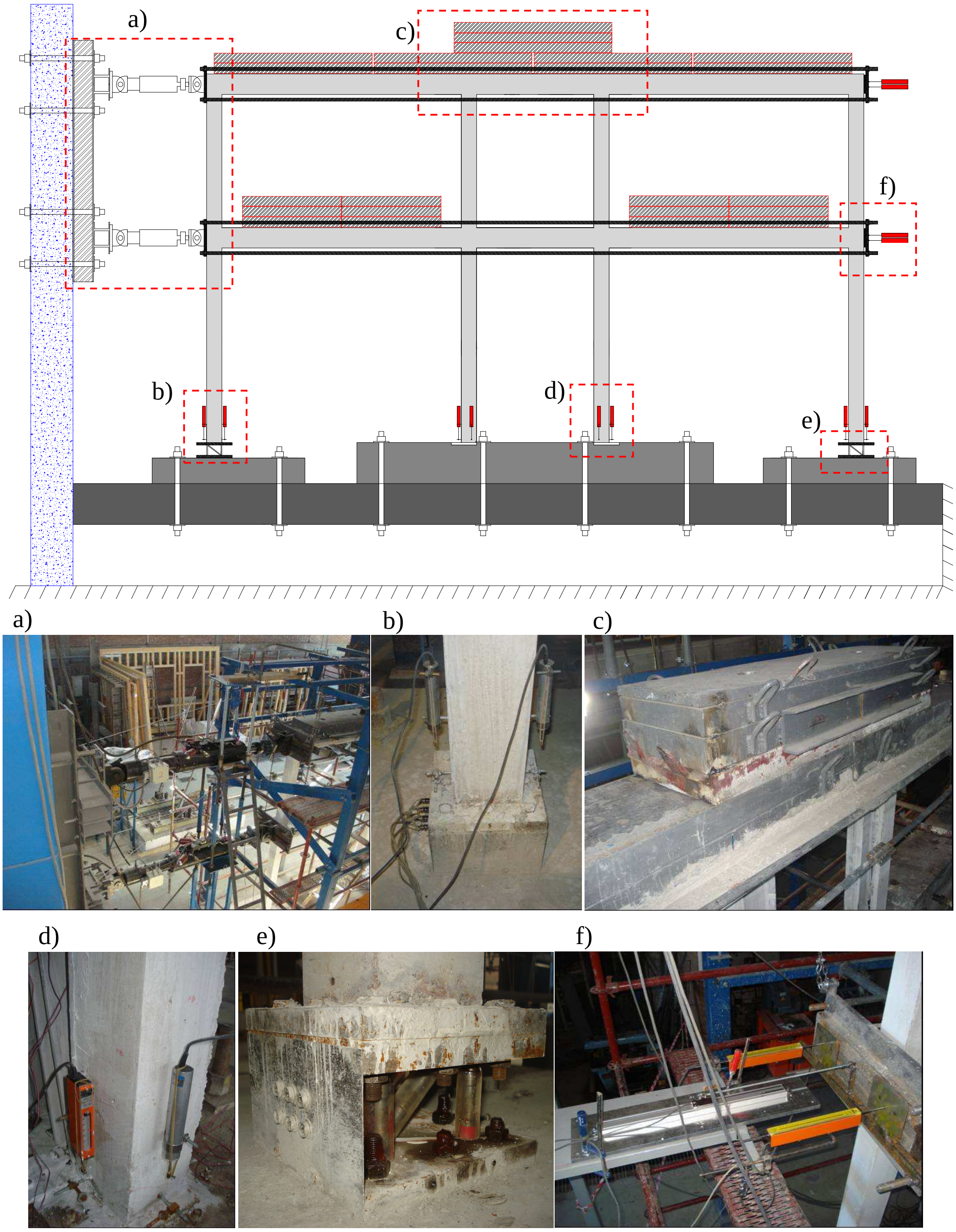

Figure 3.5 Loading and instrumentation

The axial load on the column was applied by using steel blocks (Figure 3.5-c). One group of steel blocks had 100x450x1000 mm dimension. Blocks were placed on the first and third span of the first story. The other types of steel blocks were 100x450x1550 mm and they were placed on the full span of the second story. Infill wall and strengthening techniques were only applied to the interior span of the frame. Therefore, steel block was not placed in the interior span of the first story. A steel frame was constructed around the RC frame to act as a safety during a possible sudden collapse. The steel blocks were connected to the steel frame with adequate slack which enabled RC frame to experience displacement without any artificial restrain.

Material properties

The concrete had a maximum aggregate size of 12 mm with a target 28-day cylinder compressive strength of 7.5 MPa. This simulates the concrete strength in existing deficient structures of the Turkish RC building stock as reported by the field investigations (Tezcan and Ipek, 1995; Dogangun, 2004; Cagatay, 2005). The mixture of the concrete is given in Table 3.1. The concrete strength of the each specimen during the testing day of specimens is indicated Table 3.2.

Table 3.1 Mix design

Mixture component	Weight (kg)	Proportions vs weight (%)
Cement	254	11.1
Water	254	11.1
0-3 mm aggregate	658	28.9
3-7 mm aggregate	608	26.7
7-12 mm aggregate	506	22.2

The mechanical properties of the longitudinal and transverse reinforcement by conducting uniaxial tension tests according to ASTM E8 (2004) is given in Table 3.3. Material properties of the other materials (such as structural steel anchors etc.) used during construction are available in the relevant parts of this chapter.

Table 3.2 Concrete strength

Ground Motion	Reference	Chevron 1.story/2.story	ISF 1.story/2.story
50%	7.4	7.8 / 7.4	7.5 / 7.3
100%	7.4	7.8 / 7.5	7.5 / 7.3
140%	7.4	7.8 / 7.5	7.5 / 7.3
180%	-	8.0 / 7.7	7.7 / 7.6
220%	-	8.0 / 7.9	-

Table 3.3 Mechanical properties of reinforcement

Reinforcement	Yield Strength (Mpa)	Ultimate Strength	Max. Elongation (%)
$\phi 8$	330	465	30
$\phi 4$	270	374	23

3.3 Reference Frame

The details of the reference frame were explained in detail by Kurt (2010). Hence only a brief summary is presented herein to enable a basis of comparison with the strengthened frames. The steel blocks at the first story were placed before concrete casing of the second story. After concrete casting of the second story, other steel blocks were placed on that story. The bricklaying of the interior bay of the RC frame was conducted under axial loaded conditions to simulate the situation in existing structures. The reference frame had infill walls made from hollow clay brick into its interior span. Figure 3.6 indicates the test setup for the reference frame. The size of the hollow clay brick is presented in Figure 3.7. The infill wall was laid center in to the RC columns so that no out of plane eccentricity existed. As seen in Figure 3.7, the width of the brick was 105 mm, hence a 20 mm gap was covered with plaster to achieve the infill wall to be aligned with the column face.

The uniaxial compressive strength of the hollow clay brick was 14 MPa in the direction along voids. The uniaxial compressive strength of brick laying mortar and plaster were 12 MPa. These data was taken from Kurt (2010).

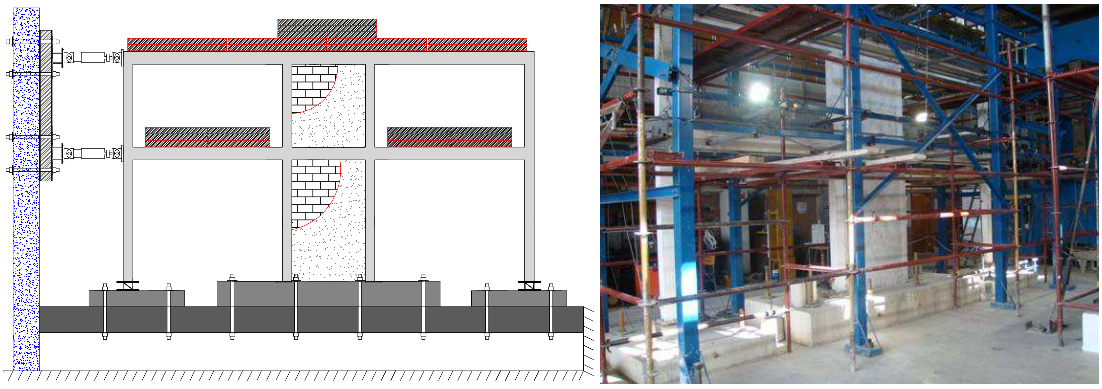

Figure 3.6 Test setup for reference frame

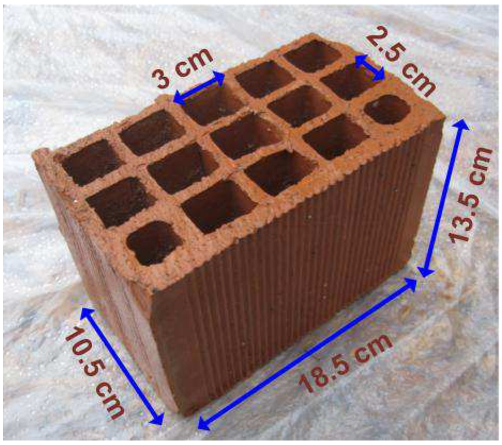

Figure 3.7 Hollow clay brick used in experiments (taken from Kurt, 2010)

3.4 Chevron Braced Frame

The main purposes of the tests were to examine the performance of the RC frame, steel members and the connection under more realistic seismic demands. The deformation and damage levels of the steel brace, gusset plate and RC members were aimed to be examined from low to high intensity earthquake simulations. It was observed in Chapter 2 that inelastic performance of the brace members are not stable after brace buckling due to significant strength drop. In other words, the post buckling capacity dictates the performance of the braced frame. Although the chevron braces increase the lateral strength and stiffness significantly, the ductility of system due to buckling is limited. The lateral strength enhancement of the braced frame depends on the brace members which act as axial load carrying members with high axial stiffness. It should be reminded that the existing RC buildings have already poor ductile columns and beams. To improve the ductility of the all columns may not be an economical and feasible approach for retrofit schemes. Hence, braced frames are considered to be economical candidates in providing stiffness and strength. In the brace design of this specimen, slight deviations from the conceptual design of braced frame specimen of Chapter 2 was made. These differences are:

1) Anchorage design was conducted by using the uniform force methods of the LRFD (1994) as opposed to elastic design presented in Chapter 2.

2) The brace slenderness was lower than the stockiest section used in Chapter 2 to achieve the target lateral strength.

3) The RC beam strengthening was conducted by using top and bottom steel plates as opposed to side and bottom plates used in Chapter 2 (see Figure 2.8). This enabled a more practical way of connection the braces to the beams and provided shear and flexure capacity to the existing beam.

Figure 3.8 indicates the test setup for chevron braced frame. The strengthening started after the placement of the steel blocks to simulate the presence of dead weight on the existing structures. Chevron braces had three critical connections in each floor namely connection at the bottom of the column or base plate (Figure 3.9), at the mid span of the beam (Figure 3.10) and at the RC beam-column joint (Figure 3.11). The connection details between RC frame and steel brace was slightly different from that of previous chevron brace application examined in Chapter 2. In this part, no side shear plates were used. Instead, two 10 mm thick plates at the bottom and top surface of each beam were installed.

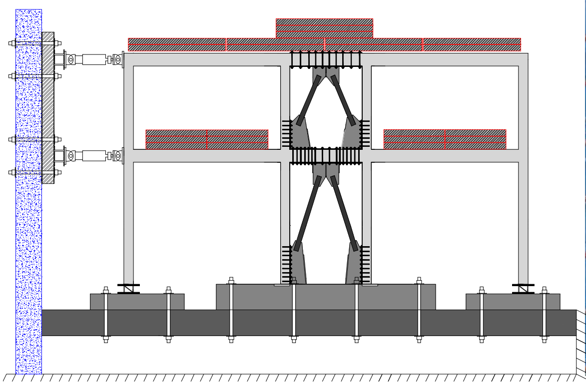

Figure 3.8 Test setup for braced frame

1) Connection application at the bottom of the column and base plate (Figure 3.9): First of all, an additional base plate for brace connection was anchored on the RC frame inside the interior span (Figure 3.9-a). The anchorage holes were drilled into RC column then these holes were cleaned up in three steps; namely air blowing, brushing and again air blowing (Figure 3.9-b and c). Then, epoxy primer was injected into these holes followed by the insertion of the anchorage rods (Figure 3.9-d). The diameter of the anchorage rods and holes were 10 mm and 12 mm, respectively, whereas the depth of anchorages was 120 mm from the member face. The gaps between the rods and holes were filled with epoxy to obtain flat and smooth bonding surfaces. Plate 1 and Plate 2 (Figure 3.9) were welded outside to prevent adverse effect of the welding heat on the epoxy. Then a thin layer of repair putty approximately 3 mm was applied to obtain a smooth bonding surface on the face of the column and then epoxy was wiped on both face of Plate 2 and RC column member. Anchor rods were tightened to provide successful connection between Plate 2 and RC column. Plate 1 was welded to the base plate 1 in placed followed by the welding of the stiffeners and brace members (Figure 3.9-e and f). It should be mentioned that the brace angle with respect to horizontal axis was 72^{o}. In the current design guide lines (for example LRDF, 1994) this angle is defined between 30^{o} and 60^{o}. In this study this rule was violated because the intention of the study was not to design a new chevron brace frame structure but to retrofit a deficient existing RC frame by using chevron braces with the minimum number of connections.

2) Connection application at the mid span of the beam (Figure 3.10): The connection at the mid span of the beam was started by drilling anchorage holes for RC beam from top surface to bottom surfaces (Figure 3.10-a) followed by Plate 4 and Plate 5 according to this anchorage holes. Plate 3 was welded to the Plate 4 and then stiffeners were welded to both Plate 3 and Plate 4 (Figure 3.10-b). Repair putty was smeared to the top and bottom of surface of the beam to ensure a smooth attachment surface. Finally, Plate 4 and Plate 5 were tightened by using anchorage rods (Figure 3.10-c and d).

3) Connection application at the joint (Figure 3.11): Firstly, the anchorage holes were drilled into RC column (Figure 3.11-a). Then, epoxy primer was injected into these holes followed by the insertion of the anchorage rods. The depth of anchorages was 120 mm from the joint face. Plate 6 and Plate 7 were welded prior to the installation of the system to prevent adverse effect of the heat on the epoxy. Putty was smeared on the RC column face to provide a smooth bonding surface. Plate 4 and Plate 5 were already in their places during the connection at the mid-span of the beam. Plate 6 was tightened to RC column by using the anchors (Figure 3.11-b) and welded to the Plate 5 followed by welding of the stiffener and brace member (Figure 3.11-c, d and e).

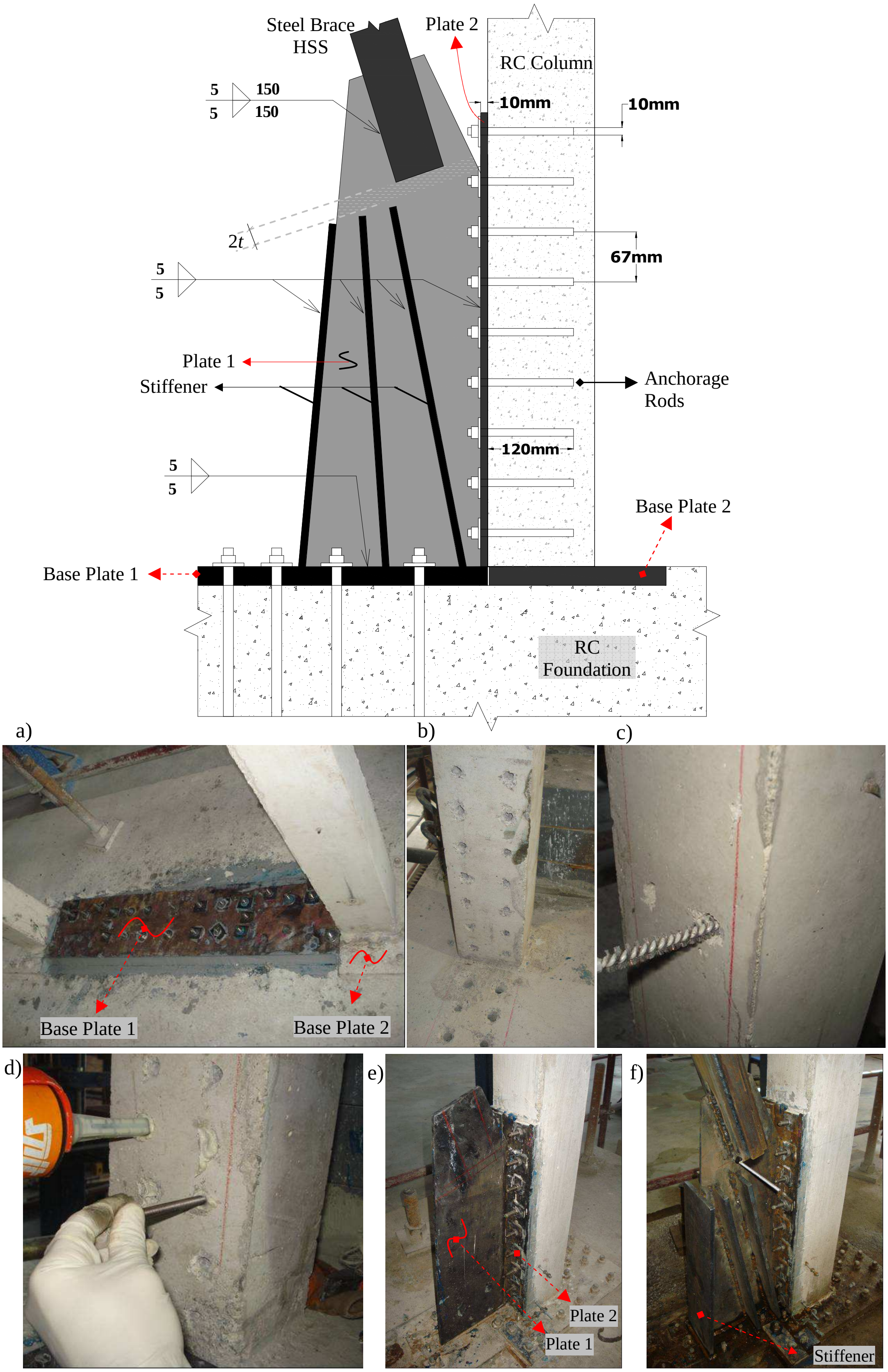

Figure 3.9 Connection details at the bottom of the column

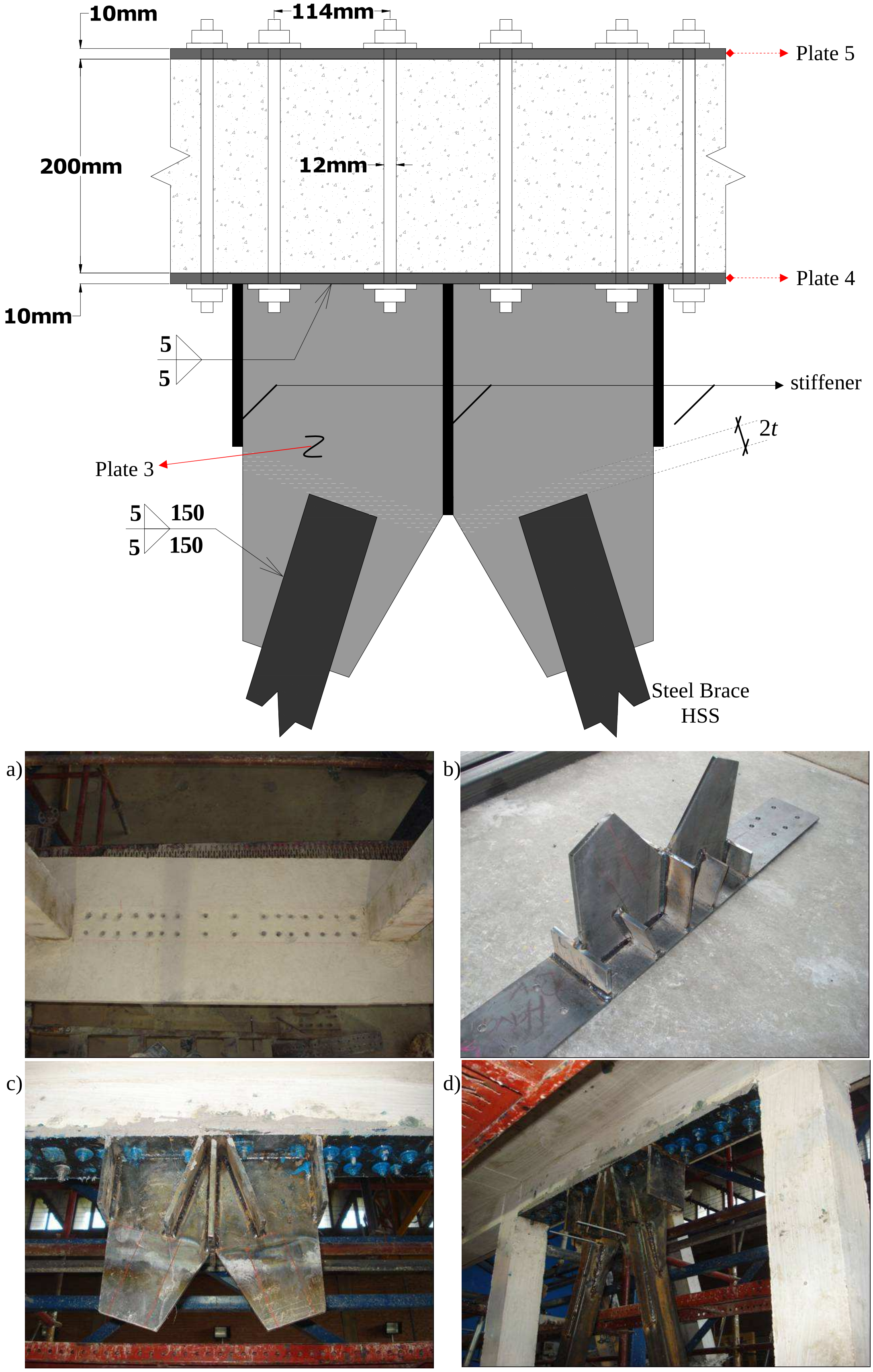

Figure 3.10 Connection details at the mid span of the beam

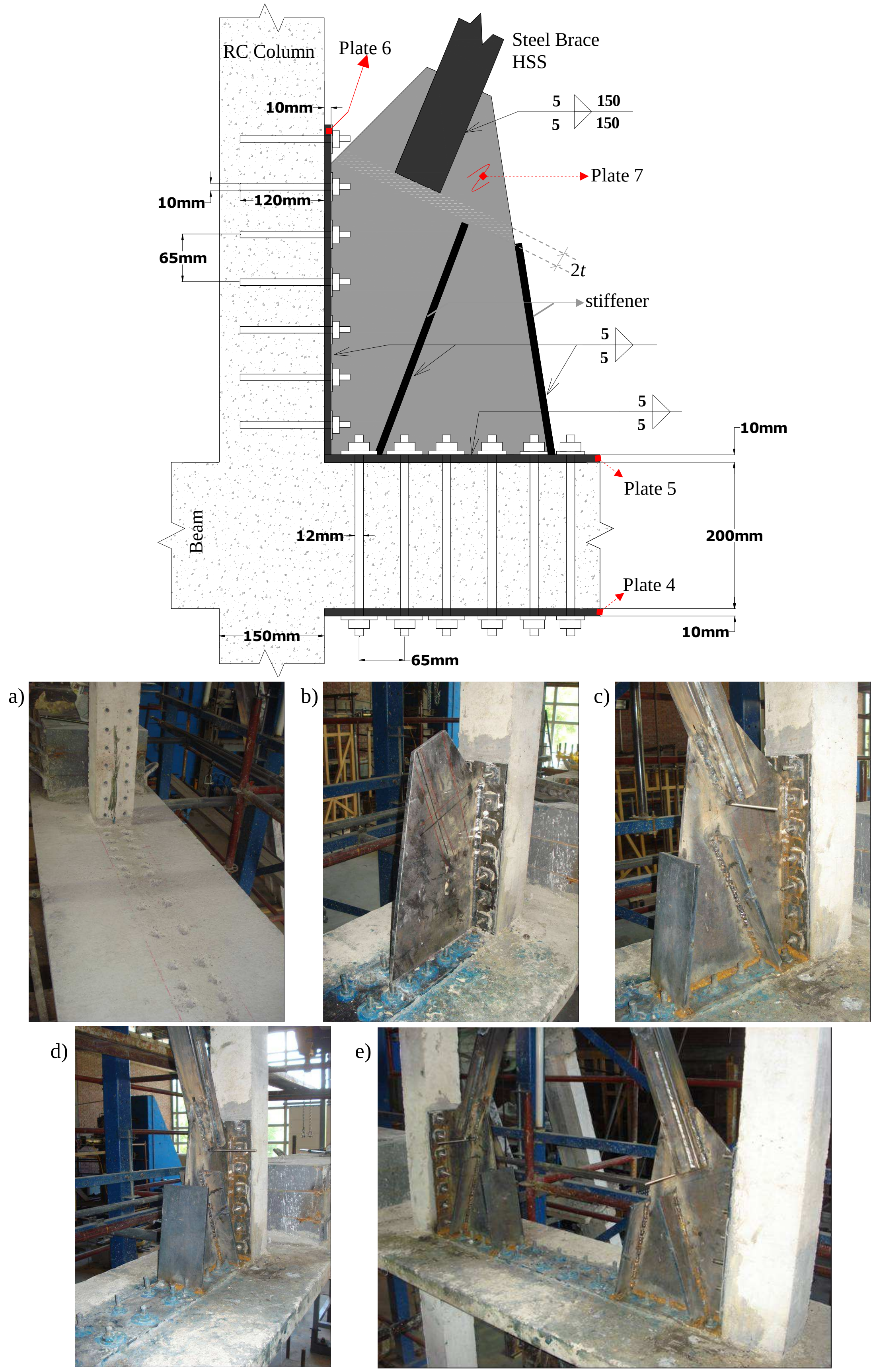

Figure 3.11 Connection details at the joint

Estimated Base Shear Capacity of the Braced Frame

The steel brace members were square hollow structural steel (HSS). This brace type was defined in the Turkish standard “Welded Square and Rectangular Steel Tubes (TS 5317)”. According to TS 5317 the steel brace member was 70x70x4 TS 5317-Fe 37 6000-s. The cross section properties of this member were 70x70 mm sections with a 4 mm wall thickness. The area and moment of inertia of the member was 1000 mm^2 and 70.4 10^4 mm^4. The nominal yield and tensile strength of the steel brace and steel plates (Plate 1 to 7) were 235 and 363 MPa, respectively (TS 648, 1980). Although lateral strength or base shear capacity of the braced frame was evaluated here, the connection design of the brace member and connection are explained in Appendix 2. The target base shear capacity increment of the braced frame was 3 and 2 times that of reference frame before and after brace buckling, respectively. The base shear capacity of the braced frame was calculated from two force contributions namely plastic hinges of the first story columns and horizontal component of the first story brace forces (Figure 3.12). The moment capacities of the RC columns were about 5 kNm (Since the braces limits the storey drift, the columns may not reach their capacities). The brace forces was evaluated for two cases: In the first case, while one of the braces has tension force, the other brace has compression force and this case occurred just before the compression brace buckles (In this case both braces have equal tension and compression force). In the second case, while one of the braces buckles (the axial force of the brace member is assumed as 0.3 and 0.5 times the brace buckling capacity within the post buckling region with respect to LRDF (1994) and ASCE/SEI 41 (2007), respectively.) and the other brace yields in tension. For both cases, case 1 and case 2, the base shear of the braced frame were calculated as 206 kN (3.1 times that of reference frame) and 175 kN (2.6 times that of reference frame), respectively. It was important to emphasize that the ratio, 0.5, to calculate post buckling capacity of the brace member is a simple assumption to estimate the brace post buckling capacity. Post buckling capacity of the brace members may be calculated by using more involved methods or analysis. In the design of the tests such an approach was not sought. Conversely, target capacity range (175-206 kN) was found to be satisfactorily lateral strength of comparing target strength with the reinforced concrete infill wall strengthening of Kurt (2010). As a result, the target base shear strength increment, 3 times that of reference frame, seemed to be satisfied by using HSS-70 brace members.

Case 1

$$V_{base} = 4 \times Vc + 2 \times 301 \times \cos 72 = 206 kN, (Vc = 5 \text{ kN in Figure 3.12})$$

Case 2

$$V_{base} = 4 \times Vc + \left(0.5 \times 301 + 350\right) \times \cos 72 = 175 kN, (Vc = 5 \text{ kN in Figure 3.12})$$

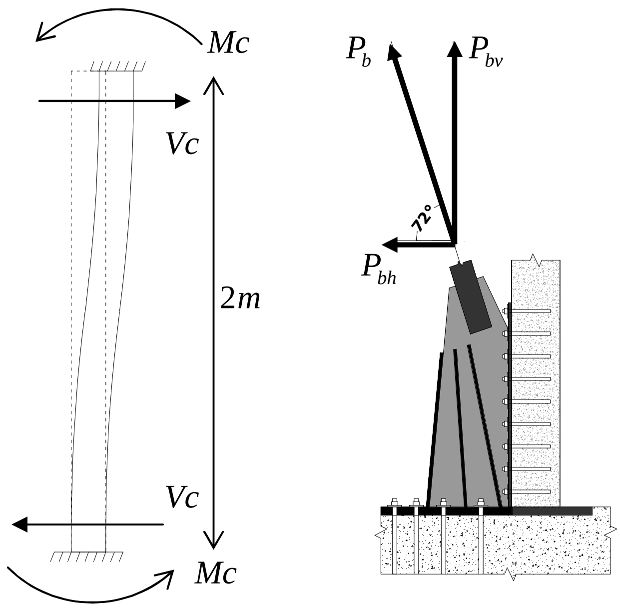

$$Mc = 5kNm$$
$$Vc = \frac{2Mc}{2m} = Mc$$
$$Vc = 5kN \text{ for each column}$$
$$\mathrm{P_{bh}} = \mathrm{P_b} \cos 72$$
$$P_b \rightarrow P_{bt} \text{ or } \mathrm{P_{bc}}$$
$$\mathrm{P_{bt}} = 350\mathrm{kN}$$
$$\mathrm{P_{bc}} = 301\mathrm{kN}$$

Figure 3.12 Lateral strength estimation

3.5 Internal Steel Frame

The main purposes of the tests were to examine the performance of the ISF and their connections under simulated earthquake motions. The deformation and damage levels of composite column and beam members were aimed to be examined from a low to high intensity earthquake simulation. In the design of this specimen following differences were introduced compared to the ISF strengthened frames presented in Chapter 2.

1) Instead of I sections used in ISF of one bay-one story frames (Figures 2.18), top and bottom steel plates were employed in order to satisfy strong column-weak beam design of the retrofitted specimen (Figure 3.14 to 3.16).

2) The number of shear anchor dowels were designed based on limit states of RC columns/beams and steel members in this specimen (Equations 3.1 to 3.5). A more conservative elastic design was employed in Chapter 2 (Section 2.4.2, equation 2.2).

The Internal Steel Frame was examined in Chapter 2 by testing six one bay-one story frames. The results from these smaller scaled specimen tests revealed that ISF with full composite connection produced a remarkable performance. Hence ISF with full composite connection was tested by the PsD test procedure. Figure 3.13 exhibits the test setup for ISF strengthened RC frame. Figure 3.14 shows the composite column and beam sections. Strengthening started after placing the steel blocks on the RC frame. Composite members were produced by attaching steel members next to the existing RC frame members with anchorage rods. The RC columns were converted to composite columns by attaching steel I sections. This section is called as IPOG 200x100x8.5 TS 910/5, Fe37, 12000 and medium wide flange I beams (IPE200) in the Turkish Standard TS 910 (1986) and international standard, respectively.

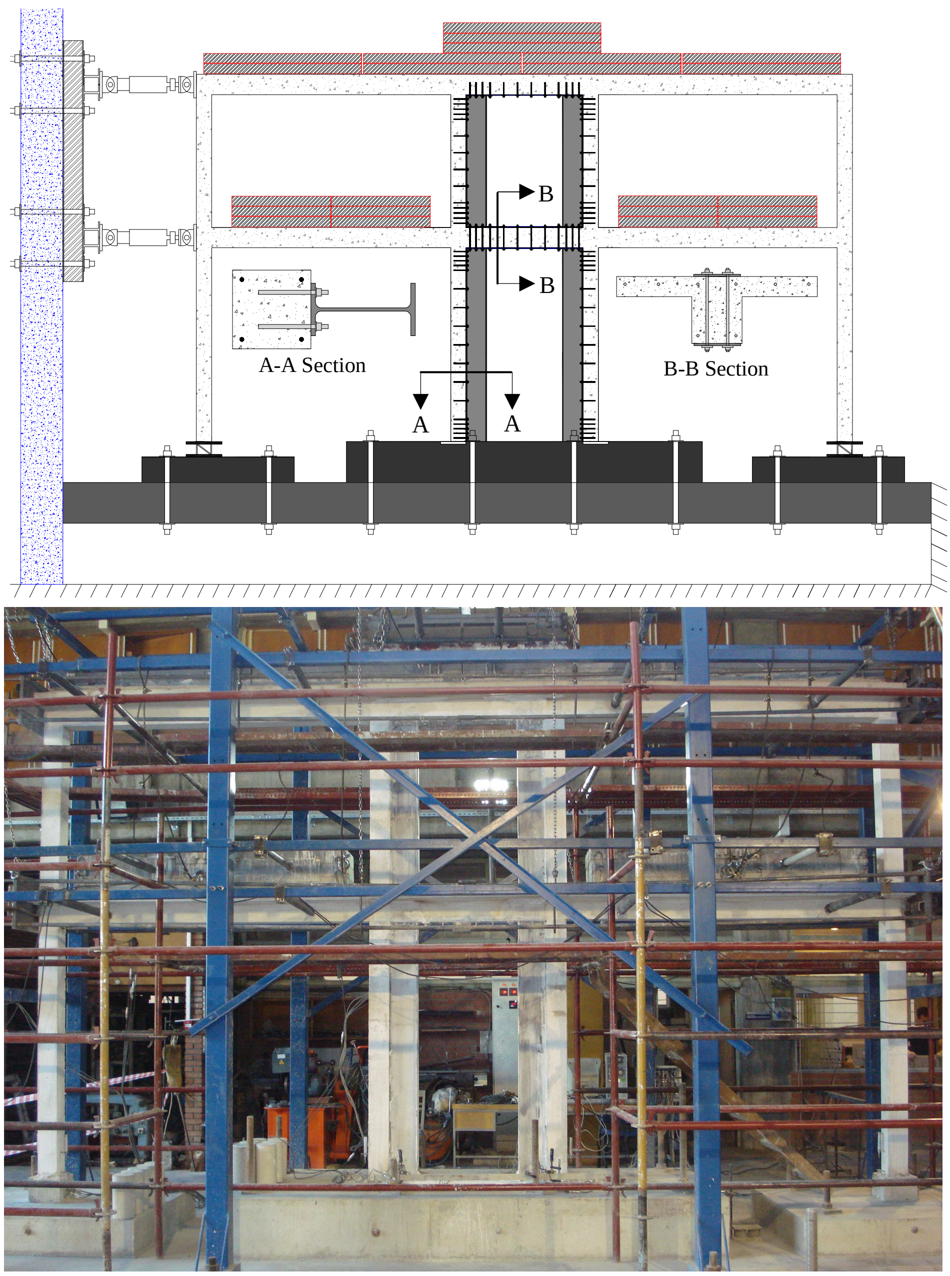

Figure 3.13 Test setup for ISF

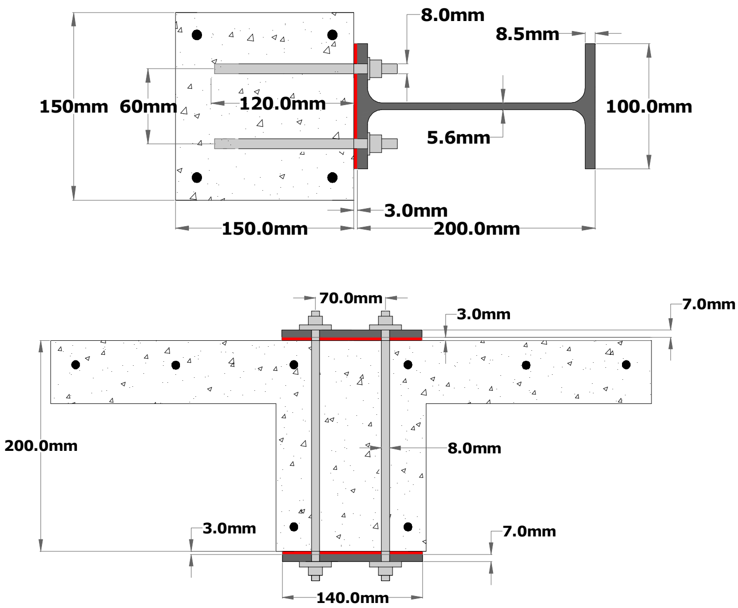

Figure 3.14 Composite column and beam member

The ISF had three critical connections namely connection at the beam (Figure 3.15), at the bottom of the column or base plate and at the RC beam-column joint (Figures 3.16 and 3.17). The connection details between RC frame and steel members was slightly different from that of previous ISF application examined in chapter 2.

1) Connection details at the beam: Steel plates having 7x140 mm dimensions were attached to bottom and top surface of the RC beam at the interior span of the RC frame. First, anchorage holes were drilled into bottom side of the RC beam at the second story. The anchorage holes were cleaned at three stages, air blowing, brushing and air blowing to achieve a perfect smooth bonding surface (details about cleaning was mentioned at the chevron brace application). Then, epoxy primer was injected into these holes followed by the insertion of the anchorage rods (Figure 3.15) and left for curing three days. The diameter of the anchorage rods and holes were ϕ12 - ϕ8 and 14 - 10 mm, respectively, whereas the depth of anchorage wholes was 120 mm from the bottom face of the beam. A thin layer of repair putty was applied on the RC member surfaces. Then epoxy was wiped on both face of steel plate 1 and bottom of the RC beam. Before the epoxy cured, the anchor rods were tightened to connect the individual steel plate 1 to the RC beam (Figure 3.15). First story beam connection was started by drilling the beam from top to bottom surfaces. Drilled holes were cleaned up at three steps as mentioned above. Epoxy primer was injected into these holes followed by the insertion of the anchorage rods (Figure 3.15-c, d and e). A thin layer of repair putty was applied on the RC member on all surfaces that contact the steel Plate 2 and Plate 3. Then epoxy was wiped on both face of steel plates and bottom of the RC beam. Before the epoxy cured, the anchor rods were tightened to fasten the individual steel Plates 2 and Plate 3 to the RC beams (Figure 3.15-f, g, h and i).

2) Connection details at the column: Figure 3.16 and 3.17 exhibit the connection details at the RC beam-column joint and at the bottom of the column C3. Anchorage holes were drilled into the RC column. Subsequently these holes were cleaned up at three steps; namely air blowing, brushing and again air blowing. Then, epoxy primer was injected into these holes followed by the insertion of the anchorage rods and left for three days for curing. The diameter of the anchorage rods and holes were 8 mm and 10 mm, respectively, whereas the depth of anchorages was 120 mm from the member face. Then a thin layer of repair putty was applied to obtain a smooth bonding surface on the face of the column and then epoxy was wiped on both face of IPE200 and RC column. Anchor rods were tightened to complete the connection between IPE200 and RC column. Finally, IPE200 was welded to the base plate 1 (Figure 3.16) and Plate 3 (Figure 3.15 and 16) at the first story. This plate was then welded to Plate 1 and Plate 2 (Figure 3.15) at the second story. The adverse effect of welding on epoxy was not significant since six 12 mm diameter anchor rods connect two plates (Plates 2 and Plate 3) effectively. In other words, these plates were used to construct to obtain a composite member via anchorage rods rather than relying on bond capacity between plates and concrete for composite action.

ISF Design

The ISF design had two parts namely anchorage rod design and achieving the target base shear capacity of the ISF. The former was based on calculating the adequate numbers of anchors used between steel and RC frame members. The latter was found by assuming plastic hinge mechanism.

Anchorage rod design:

The number of anchorage rods was calculated such that shear at the interface between RC member and steel member can be transferred safely. Figure 3.18 shows the limit state force distribution on composite column and beam member at its limit state. For composite column (Figure 3.18) anchorage rods are required to resist the maximum shear forces developed between interface of the RC column and IPE200 members. This shear force between RC column and IPE200 is the maximum tension and/or compression force (or capacity) on the IPE200 and RC column, respectively.

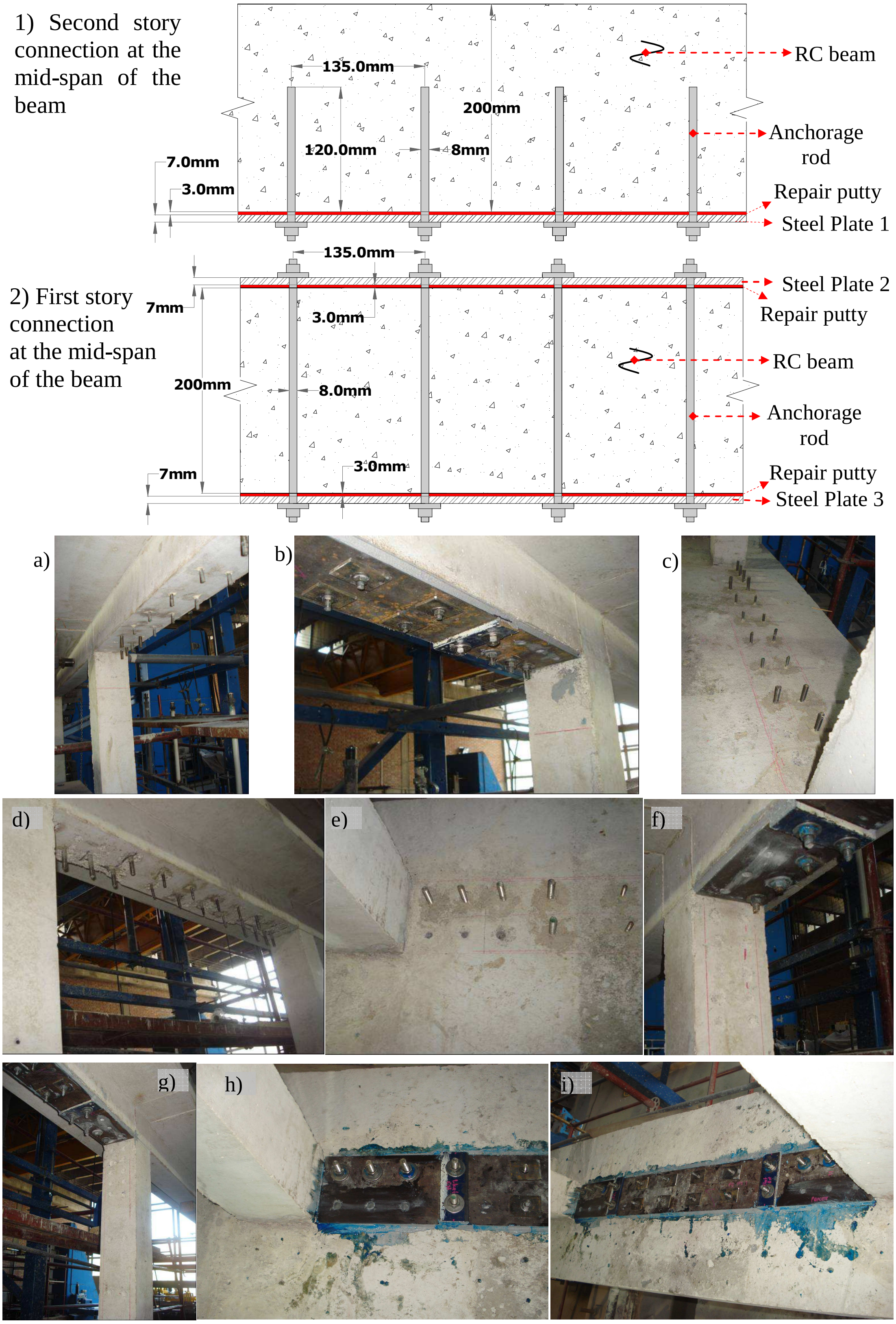

a) 2 story bottom of the beam, b) 2. story bottom of the beam, c) 1story top of the beam, d) 1story bottom of the beam, e) 1story top of the beam, f) and g) 1story bottom of the beam, h) and i) 1story bottom of the beam.

Figure 3.15 Connection details at the mid-span of the first and second story beam

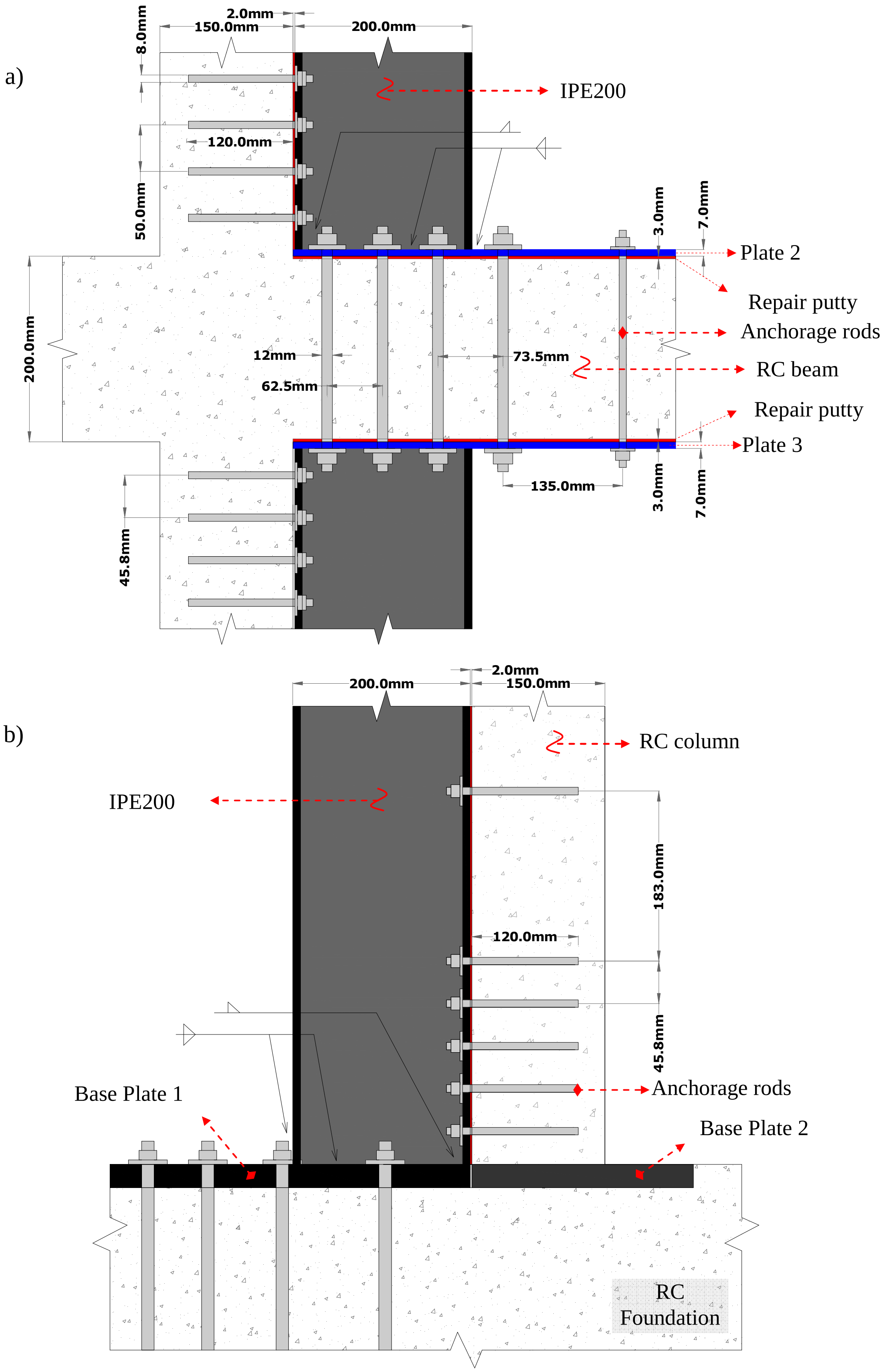

Figure 3.16 Connection details; a) beam-column joint, b) column-base plate.

a) 2 story top of the bottom of column, b) 2. story column, c) 2 story joint, d) 1story column, e) 2 story bottom of the column (1. story joint), f) 1 story top of the column (1. story joint), g and h) 1 story bottom of the column or connection at the base.

Figure 3.17 Connection details at the column

Assuming inflection point of the composite column is at the mid height, for the half length of the composite column, the smaller capacity (P_1 and P_2) is the design force for the anchorage rods (see Salmon et al., 2009). For the full length of the composite column, the design force for anchorage rods was $P_A = (P_1+P_2)$.

$$P_{com} = 0.85 \times b_c \times h_c \times f_c + A_s \times f_y \tag{3.1}$$

$$P_{ten} = A_s \times f_y \tag{3.2}$$

$$P_{IPE\,200} = A_{IPE\,200} \times f_{IPE\,200} \tag{3.3}$$

$$P_{com} = 0.85 \times 150 \times 150 \times 7.5 + 200 \times 330 = 209kN$$

$$Pt_{en} = 200 \times (330) = 66kN$$

$$P_{IPE\,200} = 2850 \times 235 = 670kN$$

P_1 = smaller value of $(P_{com}, P_{IPE\,200})$ for the first half length of the composite column,

P_2 = smaller value of $(P_{ten}, P_{IPE\,200})$ for the second half length of the composite column,

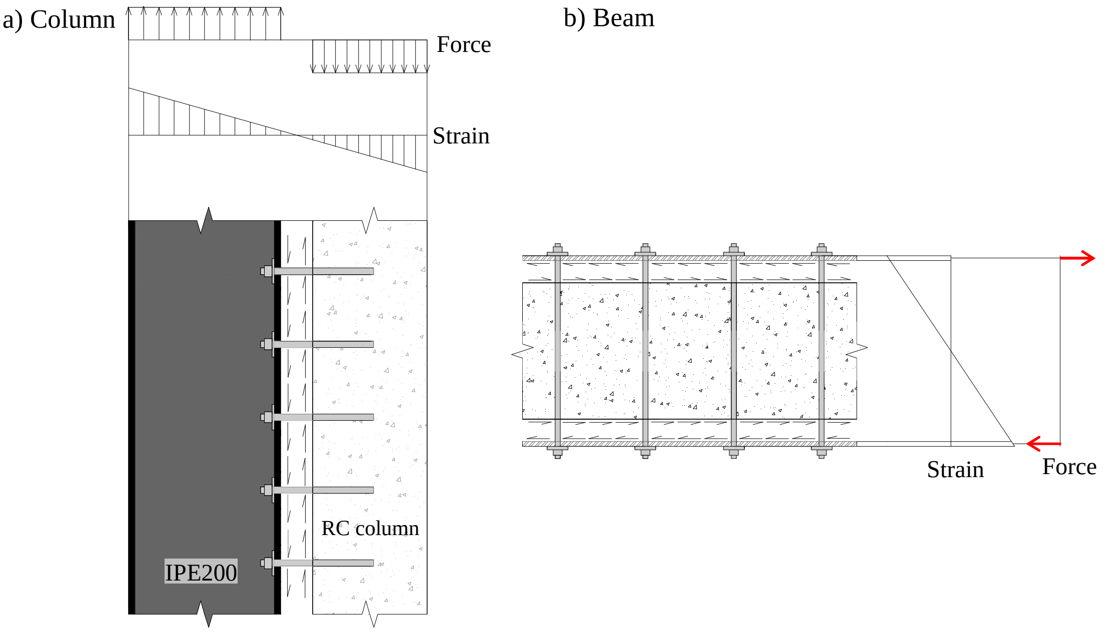

Figure 3.18 Force distribution on composite members

From the uniaxial material test, the shear strength (0.6 times the axial capacity) of the 8 mm diameter anchorage rods was 15 kN (Table A2.4 and Figure A2.9). Hence the required numbers of the anchorage rods were 19 as seen below.

$$P_A = P_1 + P_2$$

$$P_A = P_1 + P_2 = 209 + 66 \rightarrow P_A = 275kN$$

$$N_{Anc} > \frac{275}{15} = 18.3 \rightarrow 19$$

Where

P_{com}: axial compression capacity of the column

b_c: column width

h_c: column height

A_s: column longitudinal reinforcement area

F_y: yield strength of the reinforcement

P_{ten}: tension capacity of the column

P_{IPE200}: tension capacity of the IPE200

P_A: design force for anchorage rods for full length of the composite column

N_{Anc}: minimum required number of anchorage rods

Low concrete strength required the bearing capacity to be checked in design in the RC frame member. The anchorage hole was 10x120 mm and bearing capacity of the holes was 9kN (equation 3.4).

$$V_B = d_{Anc} \times h_{Anc} \times f_c \tag{3.4}$$

$$V_B = 10 \times 120 \times 7.5 = 9kN$$

$$N_{Anc} > \frac{275}{9} = 30.5 \rightarrow 31$$

Where,

V_b: bearing capacity of the anchorage hole

d_{Anc}: diameter of the anchorage hole

h_{Anc}: depth of the anchorage hole

As seen above, the minimum required number of the anchorage rods for composite columns was 31. At each story, top and bottom of the composite column, five lines of anchorage rods (two for each line) were used. At this location, Figure 3.19 indicates the anchorage rod spacing which is approximately 50 mm. On the other hand, the 14 anchorage rods (in 7x2 arrangements) with spacing were 183 and 163.5 mm throughout height of the first and second story composite columns, respectively (Figure 3.19). In this case total number of the anchorage rods for whole length of composite column was 34.

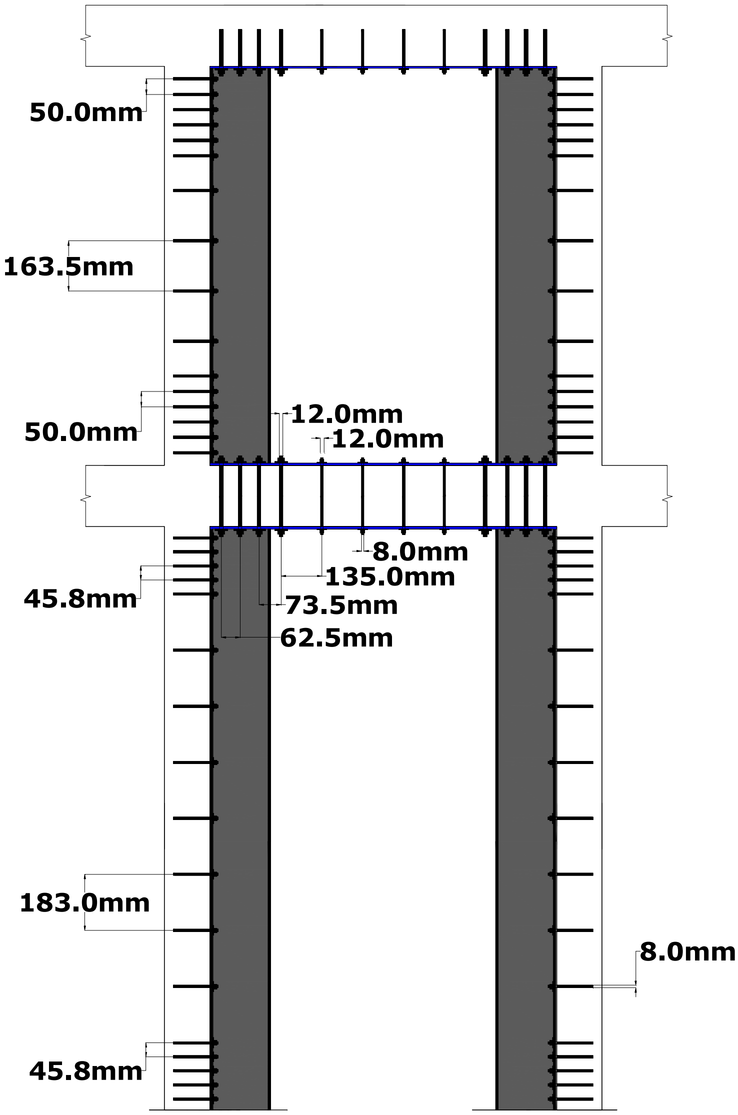

Figure 3.19 Anchorage rod distribution

The number of anchorage rods for the composite beam was determined differently from the anchorage strength calculation of composite column. The force transfer occurred between steel plates (Plate 2 or Plate 3 in Figure 3.15) and RC beam. Hence, the axial load capacity of the steel plates must be lower than the total shear capacity of the anchorage rods for the mid-length of the beam. The following equations indicate that 10-ϕ12 and 2-ϕ8 anchorage rods were adequate to construct composite beam for the half length. While the former was used at the beam-column joint, the latter was used up to the mid length of the beam.

$$P_{plate} = t_{plate} \times b_{plate} \times f_{yplate} \qquad (3.5)$$

$$P_{plate} = 7 \times 140 \times (1.4 \times 235) = 322kN$$

$V_{\phi 12} = 40kN, V_{\phi 8} = 15kN$ (Table A2.4 and Figure A2.9)

use 10-ϕ12 and 2-ϕ8 anchorage rods up to mid-length of the beam

$$10 \times \mathrm{V}_{\phi 12} + 2 \times \mathrm{V}_{\phi 8} = 10 \times 40 + 2 \times 15 = 430kN > P_{plate} \rightarrow ok$$

Where,

P_{plate}: plate axial load capacity

t_{plate}: plate thickness

b_{plate}: plate width

f_{yplate}: nominal yield strength of the plate

Base shear capacity estimation of the ISF

The target base shear capacity of the ISF was designed to be two times (similar to the chevron braced fame after buckling) that of reference frame. This capacity is also similar to the capacity of the specimen with shear RC wall tested by Kurt (2010). Hence, the composite column and beam capacity was determined for this target lateral strength. The moment capacity of the column was determined by considering extreme fiber of the concrete strain of 0.003. Figure 3.20-a indicates the strain and stress distribution and the moment capacity of the composite column which was calculates as 72.1 kNm. In addition, the moment capacity of the composite column was about 60 kNm when the extreme fiber of the concrete was assumed to be in tension. A steel plate with dimensions of 7x140 mm was designed on both top and bottom sides of the RC beam. The moment capacity was calculated based on yielding of these two plates at limit state. Figure 3.20-b exhibits stress and strain profile when the extreme fiber at the top of the beam is in tension. For this case, the moment capacity of the composite beam member was calculated as 58 kNm whereas for opposite case it was 53 kNm. TEC (2007) requires strong column weak beam in order to provide beam hinging instead of column hinging.

TEC (2007) explains strong column weak beam as “ In structural systems comprised of frames only or of combination of frames and walls, sum of ultimate moment resistances of columns framing into a beam-column joint shall be at least 20% more than the sum of ultimate moment resistances of beams framing into the same joint”. The following equation indicates that the composite column and beam obeys the strong column-weak beam limitation requirement as indicated in Figure 3.21.

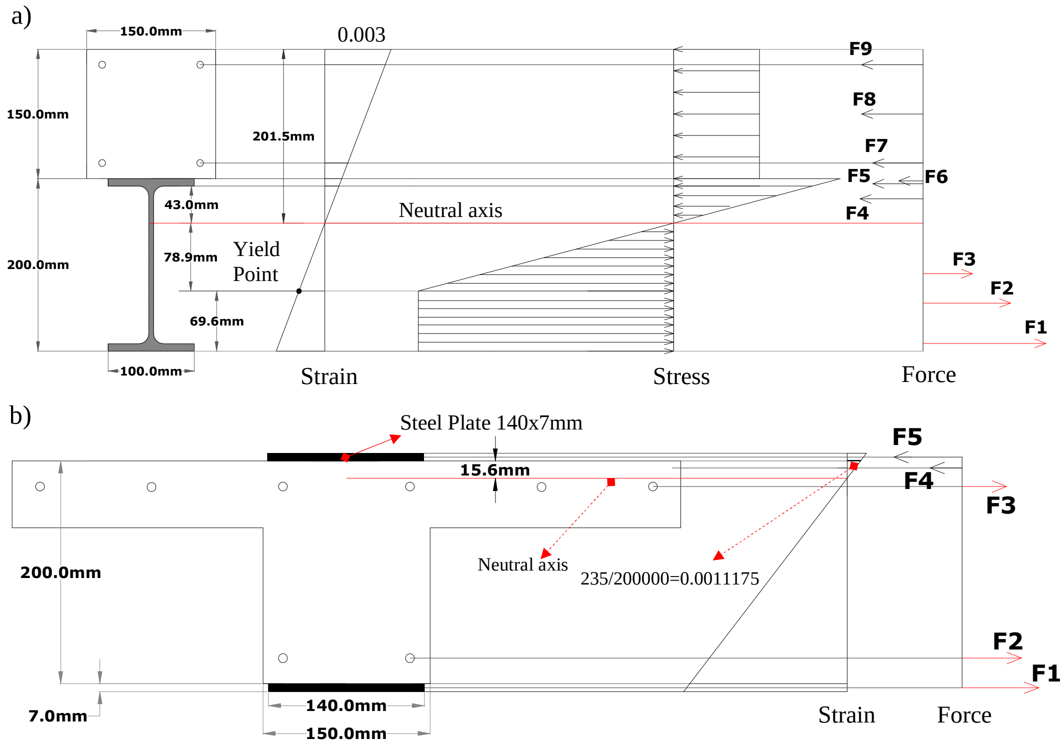

a)

$$Ft = F1 + F2 + F3$$

$$Fc = F3 + F4 + F5 + F6 + F7 + F8$$

$$Ft = 322088N, Fc = 322088N \rightarrow Ft = Fc$$

$$Mr = 72.1kNm$$

b)

$$Ft = F1 + F2 + F3$$

$$Fc = F4 + F5$$

$$Ft = 270927N, Fc = 270927N \rightarrow Ft = Fc$$

$$Mr = 58kNm$$

Figure 3.20 Moment capacity of the composite column and beam

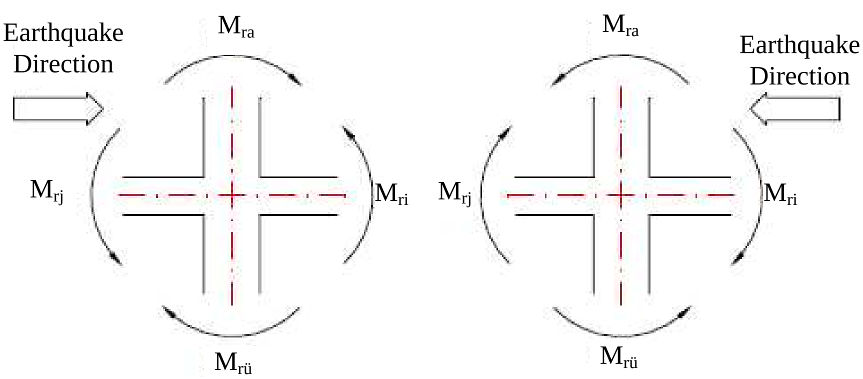

Figure 3.21 Strong column weak beam case (taken from TEC, 2007)

$M_{ra} = 60kNm$
$M_{rü} = 72kNm$
$M_{rj} = 12kNm$
$M_{rj} = 58kNm$
$M_{ra} + M_{rü} = 60 + 72 = 132\text{kNm}$
$(\text{M}_{\text{rj}} + \text{M}_{\text{ri}}) = 12 + 58 = 70\text{kNm} \rightarrow 1.2 \times (\text{M}_{\text{rj}} + \text{M}_{\text{ri}}) = 84\text{kNm}$

$$M_{ra} + M_{rü} \geq 1.2 \times (\text{M}_{\text{rj}} + \text{M}_{\text{ri}}) \rightarrow 132 \geq 84 \rightarrow \text{Strong column - weak beam} \tag{3.6}$$

To calculate the lateral strength of the ISF it was assumed that hinges occurred at the beams and columns a seen in Figure 3.22. This figure shows that hinges occurred at the bottom of the first story composite columns. On the other hand, beams occurred hinges at the interior joints because of strong column-weak beam construction. The lateral force for each story was calculated by considering each story mass and height. Both of these forces give the base shear capacity of the ISF. It is important that the hinge mechanism indicated in Figure 3.22 gives the upper bound solution and the estimated shear capacity of the ISF considering the nominal strength of the steel members was 139 kN which was two times the base shear capacity of the reference frames.

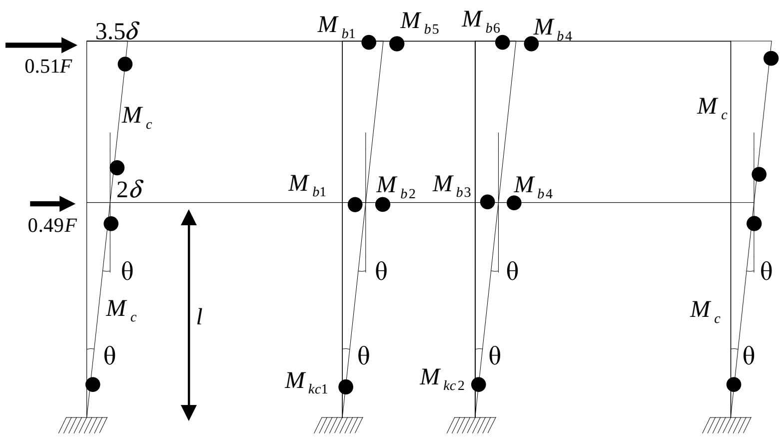

$M_c = 5kNm$
$M_{kc1} = 60kNm$
$M_{kc2} = 72kNm$
$M_{b1} = 12kNm$
$M_{b2} = 58kNm$
$M_{b3} = 53kNm$
$M_{b4} = 6kNm$
$M_{b5} = 45kNm$
$M_{b6} = 13kNm$
$\theta = \dfrac{2\delta}{l} \rightarrow \delta = \theta \times l/2$

$\text{External Work} = 0.49F \times 2\delta + 0.51F \times 3.5\delta = 2.765F \times \delta$
$ExternalWork = 2.765F \times \theta \times l/2$
$\text{Internal Work} = \sum \theta_i M_i$
$BaseShearForce = F$
$InternalWork = \left(M_c \times \theta \times 2 + M_{kc1} \times \theta + \left(M_{b1} + M_{b2}\right) \times \theta + M_{kc2} \times \theta + (M_{b3} + M_{b4}) \times \theta + M_c \times \theta \times 2\right)$
$+ \left(M_c \times \theta \times 2 + \left(M_{b1} + M_{b5}\right) \times \theta + (M_{b6} + M_{b4}) \times \theta + M_c \times \theta \times 2\right) = 385\theta$
$385\theta = 2.765F \times \theta \times l/2 \rightarrow F = 139 \rightarrow BaseShearForce = 139kN$

Figure 3.22 Plastic hinge mechanism of the ISF

Further details of the initial ISF design including the shear capacity check for the composite members and lateral buckling of the steel members are presented in Appendix 2.

3.6 Pseudo Dynamic Test Procedures

Pseudo dynamic testing technique requires a simultaneous control of an on-line computer and test frame structure. PsD testing has two processes namely calculation and loading process (Figure 3.23). Calculation process needs the software and the hardware working in collaboration to solve the equation of motion of the system.

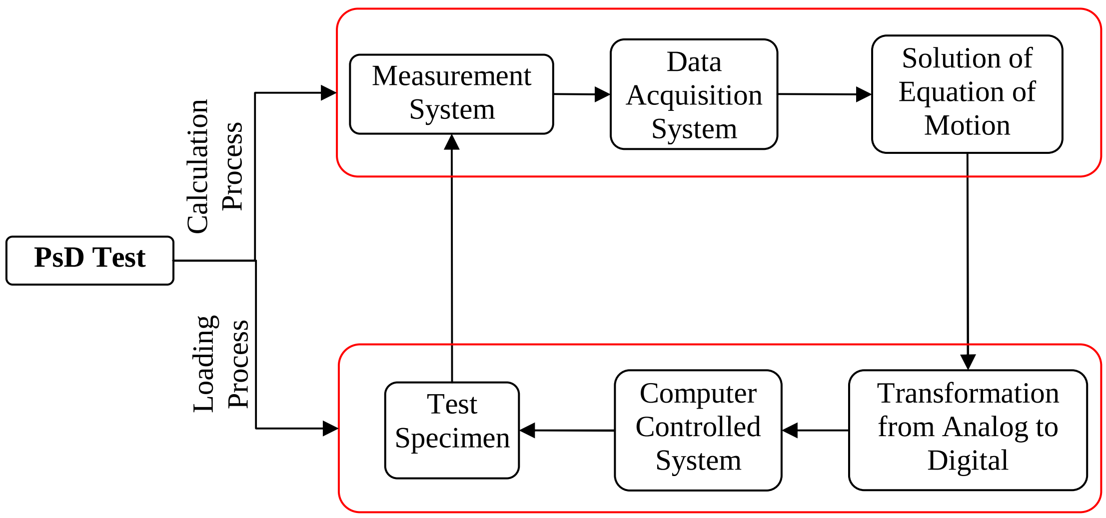

Figure 3.23 Loading and calculation sections of PsD testing (adapted from Kurt, 2010)

The PsD method has been used as an alternative to shaking table tests in the last thirty years (Takanashi et al., 1975; Mahin et al., 1989, Nakashima et al., 1992). In this first application, properties of the structural namely mass and damping is mathematically modeled whereas the rest of the structure is tested in parallel with the mathematical model. A well-established step by step time integration methods is utilized during a PsD test. At each step of the PsD test the followings are determined. First, the test specimen is imposed a deformation resulted from a specified ground motion, and then the lateral resisting forces are measured by using computer controlled actuators. After proceeding in the measured force at each computational time interval, new displacements are computed from the discrete parameter model and this displacement is imposed to the test frame. Finally, this step is repeated at end of the ground motion.

The restoring forces and displacements for each story are directly measured from the test specimen by means of static test procedure, mass, damping and the ground motion properties, on the other hand, are assumed for the PsD test. The measured forces from load-cell are then used in the numerical integration of the governing second order differential equations of motion of the test specimen. After than nodal displacement history is implemented for further steps.

The equation of motion for time step "i" may be written as:

$$M \times a^{i} + C \times v^{i} + R^{i} + K \times d^{i} = -M \times a_{g}{}^{i} \tag{3.7}$$

Where;

M: Mass matrix

C: Viscous damping matrix

R_i: Nodal restoring forces at time "i"

K: Geometric stiffness matrix

a_i, v_i, d_i: Nodal accelerations, velocities and displacements, respectively, at time i

a_{gi}: Ground acceleration at time "i"

A numerical solution in a stepwise manner (R_i is the restoring force measured from the test specimen) is performed for the equation of motion above. This solution results in the displacement which computer controlled actuators shall apply to the specimen at each node. To solve equation of motion during a PsD test both implicit and explicit integration algorithms can be utilized. Explicit integration algorithm employ the structure at the beginning of each step to assess the response of the structure at the end of that step, on the other hand, implicit integration algorithms calculate the response of the test specimen by using the knowledge of the response at the target displacement.

Test procedure and ground motions

The continuous PsD testing method proposed by Molina et al. (1999) was utilized for the PsD experiments. To eliminate possible relaxation errors integration process was executed continuously during the test. A 2x2 lumped mass matrix was used for numerical integration.

The mass of the first and second story was 5000 and 7000 kg, respectively. Instead of a synthetic ground motion a real ground motion was found to simulate the hazard level that could be expected for the prototype building. For the PsD tests north-south component of 7.1 moment magnitude 1999 Duzce ground motion was used. PsD tests were performed about 1000 times slower compared to the real time motion. The peak ground acceleration of Duzce was scaled at four different scale factors from low to high seismic intensity. 50%, 100%, 140% and 180% scaling was used to various damage states. In fact, these damage states were decided prior to the testing of the reference frame. Figure 4.24 and Figure 4.25 display the acceleration time series of the motion and the pseudo acceleration spectrum of the motion, respectively. The scaling was enabled to investigate the response at three different hazard levels expected for the reference frame with infill wall:

a) 50% Duzce: Spectral acceleration value for 50% Duzce is approximately similar to the base shear capacity ratio (base shear capacity divided by structure weight) of the bare frame at the structure's fundamental period. Hence, it is expected that structure will remain near or below yielding considering the presence of infill walls. It can be stated that this level should produce immediate occupancy compatible damage levels (Kurt, 2010).

b) 100% Duzce: Use of the actual Duzce ground motion recorded in 1999 Adapazari earthquake can represent the hazard level realistically for less frequent events Kurt (2010).

c) 140% Duzce: This hazard level will correspond to a severe and rare earthquake and has approximately similar Sa value with the Turkish Earthquake Design Spectrum for Zone 1 on firm soil conditions at the pre-test estimated fundamental period of the structure Kurt (2010).

d) 180% Duzce: This hazard level will correspond to a severe and rare earthquake and has higher Sa value with the Turkish Earthquake Design Spectrum for Zone 1 on firm soil conditions at the pre-test estimated fundamental period of the structure.

It should be kept in mind that recent studies on the seismicity of the region state that Turkish Earthquake Design Spectrum can give design Sa values well above those estimated by using realistic attenuation relationships (Kalkan and Gülkan, 2004)

Consequently, 100, 140 and 180% ground motion tests were conducted on damaged specimens. It is believed that as long as the structure remained below minimum and moderate damage states for these two levels, respectively, the results of experiments could serve the purpose of relating damage with the displacement demand. The original ground motion is compressed in time by a factor of $1/\sqrt{2}$ to incorporate scale effects according to similitude law (Bertero et al., 1984; Elkhoraibi and Mosalam, 2007).

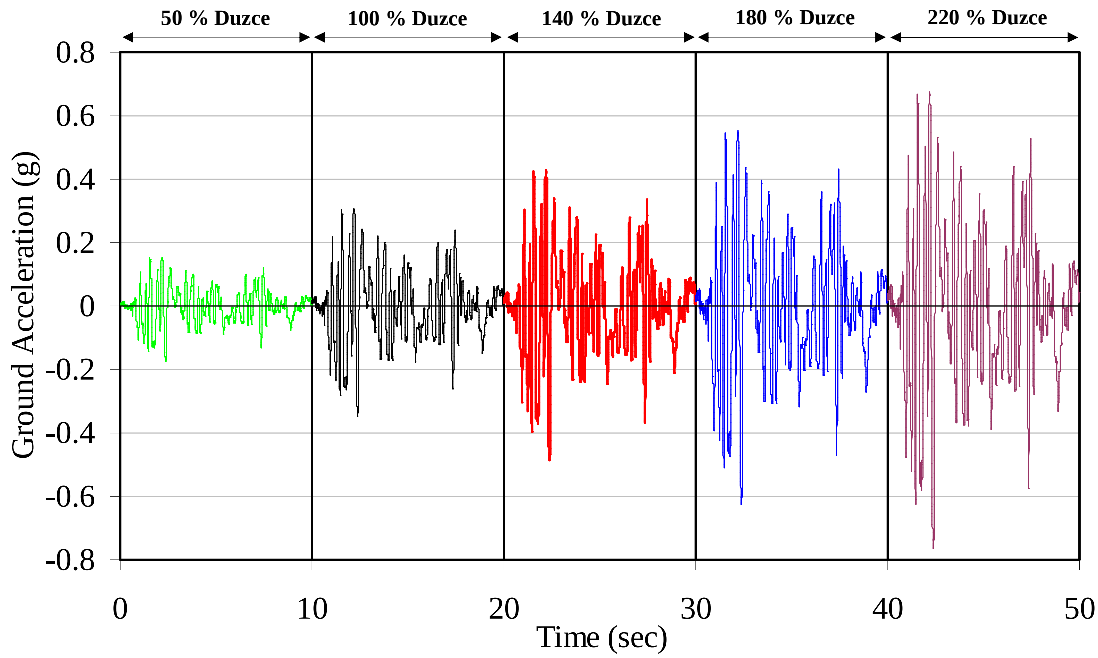

Figure 3.24 Ground acceleration time history

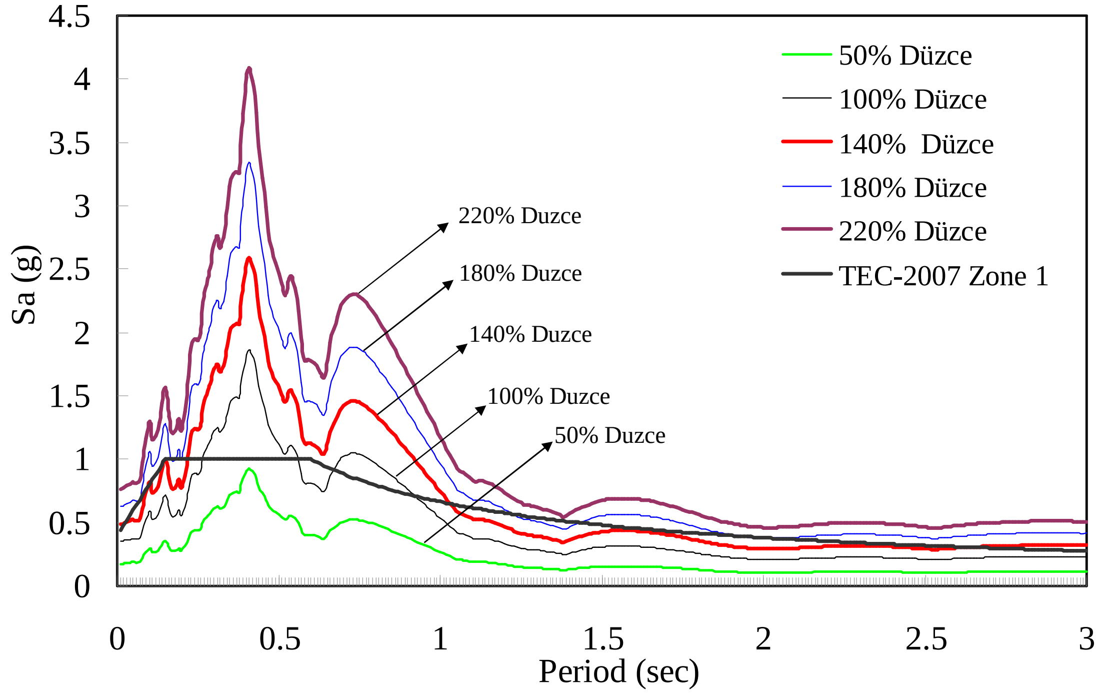

Figure 3.25 Spectrum of scaled ground motions

3.7 Test Results and Observations

Test results are presented in this chapter. During the tests there were 55 channels that monitored the frame deformations and imposed forces. All this data are presented from the point of view of structural engineering with the objective of contributing to the understanding of physical phenomena. With respect to data acquired from the tests, many figures including displacement response, base shear-deformation, damage extent, floor displacements, inter-story drift ratios (IDRs), base shear, axial, shear and moment forces of the columns, curvatures at column bases, floor accelerations, identified damping ratio and initial periods of the test specimen are presented. Floor displacement was monitored from the LVDTs placed at each floor. The IDR was calculated as dividing each relative floor displacement to story height. The lateral force was monitored by using load-cell placed at each story. The data acquired from these load-cells give each story shear forces. Force transducer enabled to monitor the end forces at the bottom of the columns, C1 and C4. In addition, LVDTs placed at the bottom of the columns was used to calculate the curvatures of at the bottom of all columns. The observed physical damage is given by the help of the photos taken during the experiments. The test results are given one by one for each of the three specimens namely reference, chevron and ISF. At the end of the chapter a comprehensive comparison between reference and strengthened frames is also presented.

3.7.1 Reference frame

In this study, reference frame was not tested. Instead, the reference frame tested by Kurt (2010) is employed. The following results are directly taken from Kurt (2010). Further details can be found in that reference.

Figure 3.26 indicates the time history of the test results in terms of story displacements. The story displacement of the first and second story were 15 and 23 mm for 50 % Duzce, 35 and 49 mm for 100 % Duzce, 85 and 94 mm for 140 % Duzce test, respectively.

Figure 3.27 indicates the time history of the test results in terms of IDRs. The maximum IDRs of the first and second story was 0.7 and 0.6% for 50% Duzce, 1.8 and 1.1% for 100 % Duzce, 4.5 and 1.4% for 140 % Duzce test.

Figure 3.28 indicates the time history response of the base shear force. The maximum base shear force was 60.4 kN for 50% Duzce, 67.9 kN for 100% Duzce, 54.5 kN for 140% Duzce tests.

Figure 3.29 indicates the force-deformation response of the reference frame for the three ground motion. In this figure there are two axes describing the lateral force vs. lateral top displacement and top DR vs. base shear ratio (ratio between lateral strength (or base shear) and frame weight). Kurt (2010) determined that the yield displacement (Δ_y) of the reference frame as 15 mm. Based on extending a line from origin and passing through a point on the initial loading curve that corresponds to 75% of the ultimate load carrying capacity.

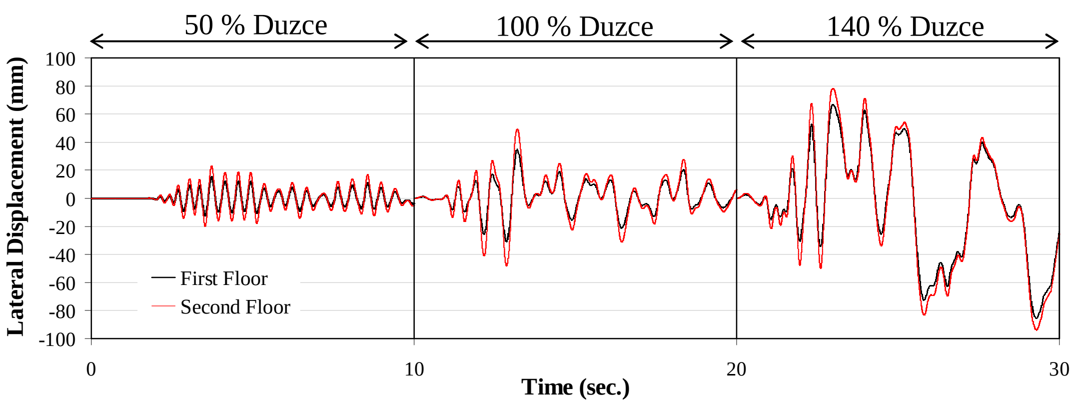

Figure 3.26 Time history of floor displacements for reference frame

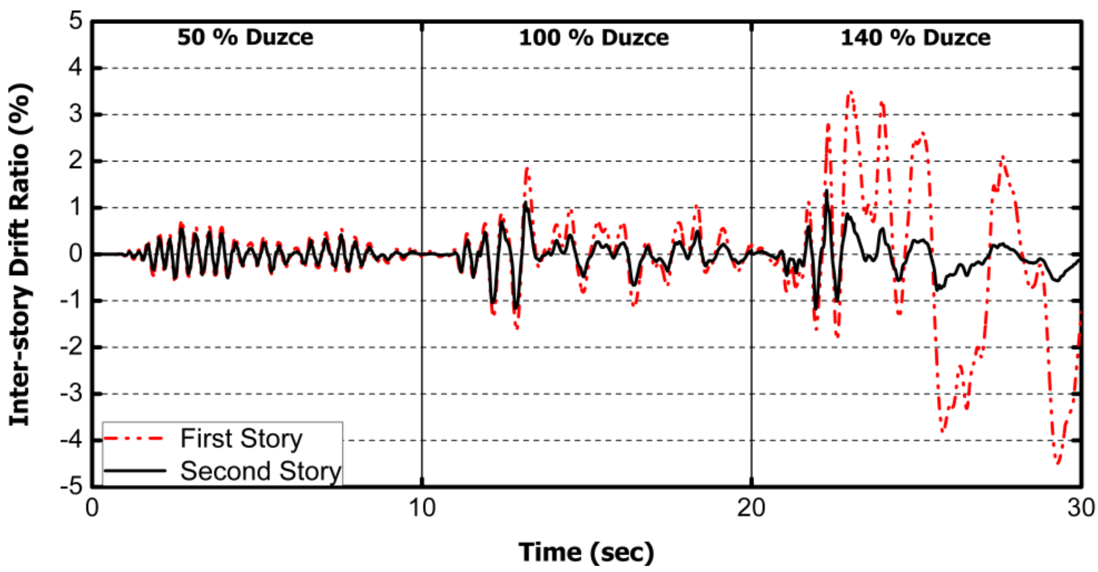

Figure 3.27 Time history of inter-story DRs for reference frame

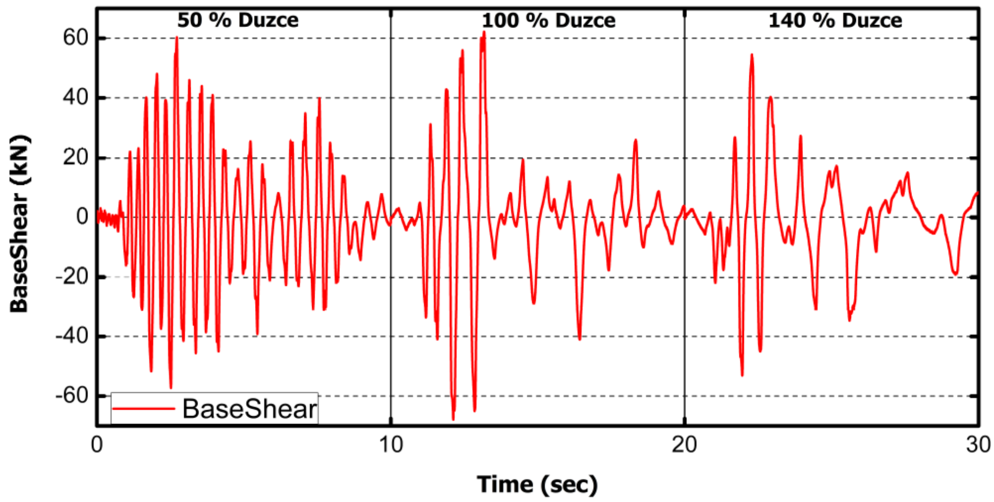

Figure 3.28 Time history of base shear for reference frame

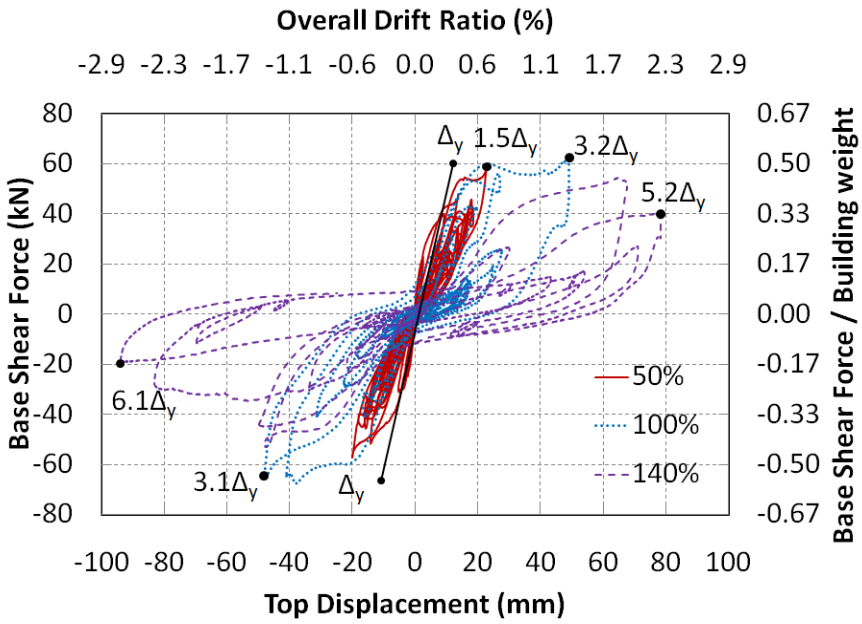

Figure 3.29 Force-Deformation response of the reference frame

Kurt (2010) mentioned that the base shear capacity of the reference frame without any significant lateral strength drop was observed during the 100% Duzce test. On the other hand, lateral strength (or base shear) dropped to about 30% of the frame maximum lateral capacity at 140% Duzce test. Figure 3.30 indicates the moment-curvature response of columns 1 and 4 for these experiments. This figure also shows the curvature performance levels, immediate occupancy (ϕ_{IO}), life safety (ϕ_{LS}) and collapse prevention (ϕ_{CP}) as described in TEC (2007). The moment and curvatures was calculated from the measurements gained from transducers and LVDTs at the bottom of the column. Although there was no significant loss of column lateral load carrying capacity, plastic deformation occurred at the bottom of the column C1 and C4. The measured maximum curvature ductility demands were about 9 for column C1 and 11 for column C4.

Figure 3.31 exhibits the moment interaction response of columns C1 and C4. This figure indicates that axial load on columns C1 and C4 varied between 7 and 15 % axial load ratio. Figure 3.32 presents variation of the axial load, shear force and moment at the bottom of the columns C1 and C4 for all Duzce tests. The values in this figure were calculated by using a converter matrix and measurements from the force transducer. Maximum variation on axial load was 14.2 kN for tension at column C1 and -9.6 kN for compression at column C4. Maximum variation on shear force was 5.8 and 4.4 kN for columns C1 and C4, respectively.

Maximum values of bending moment on columns C1 and C4 were -6.1 and 5.7 kNm, respectively. The overturning effect resulted in reverse measured demands for the axial load, shear force and moment. While one of the exterior column's axial loads increased, the other exterior column's axial load decreased simultaneously. Figure 3.33 indicates the axial load, shear force and moment demands on the both exterior columns C1 and C4 during the all Duzce tests. These values were obtained by adding the force variation given in Figure 3.33 to initial forces on the columns C1 and C4.

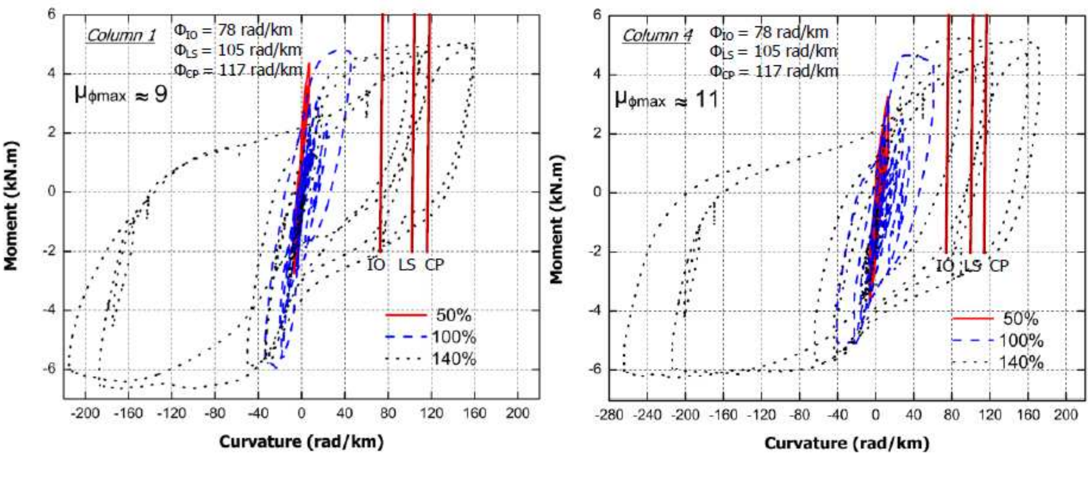

Figure 3.30 Moment-Curvature diagrams of columns C1 and C4 for reference frame

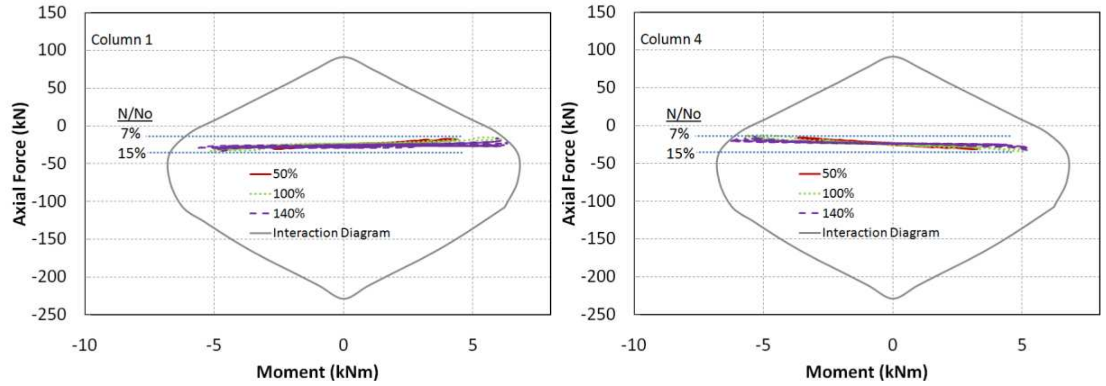

Figure 3.31 Moment interaction response of columns C1 and C4 for reference frame (Response 2000)

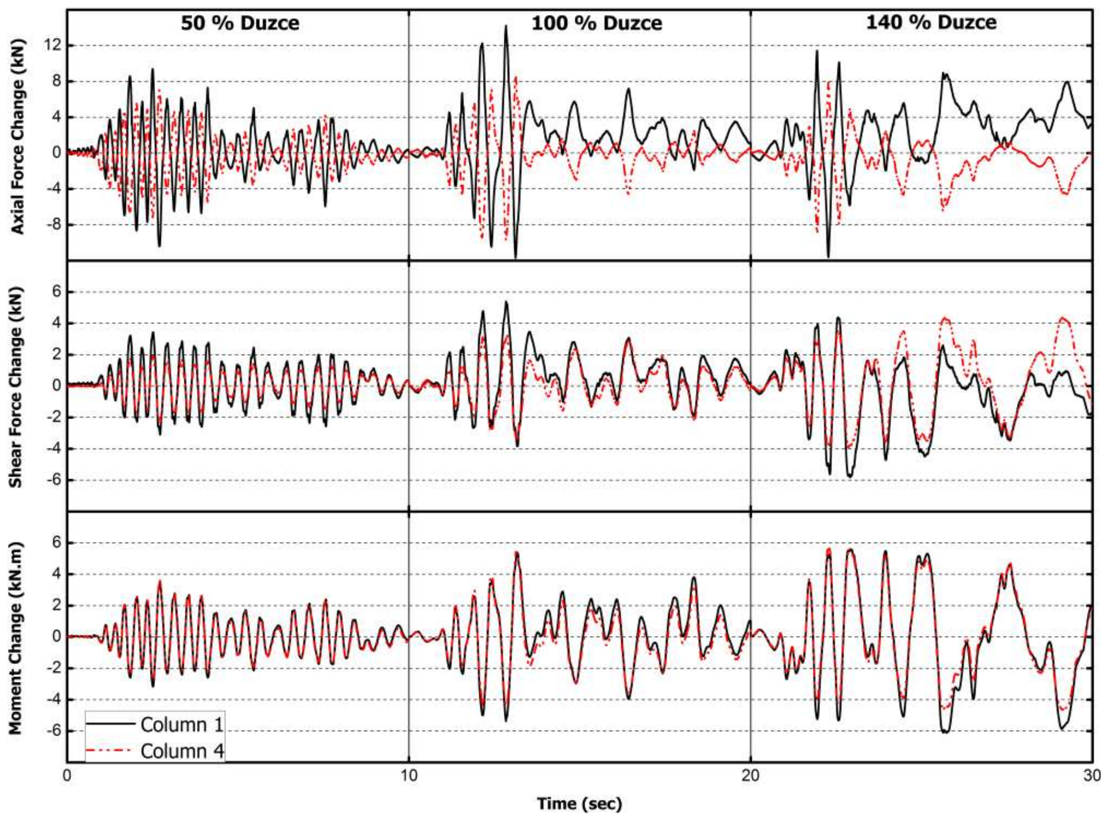

Figure 3.32 Time histories of axial, shear and moment forces change for reference frame

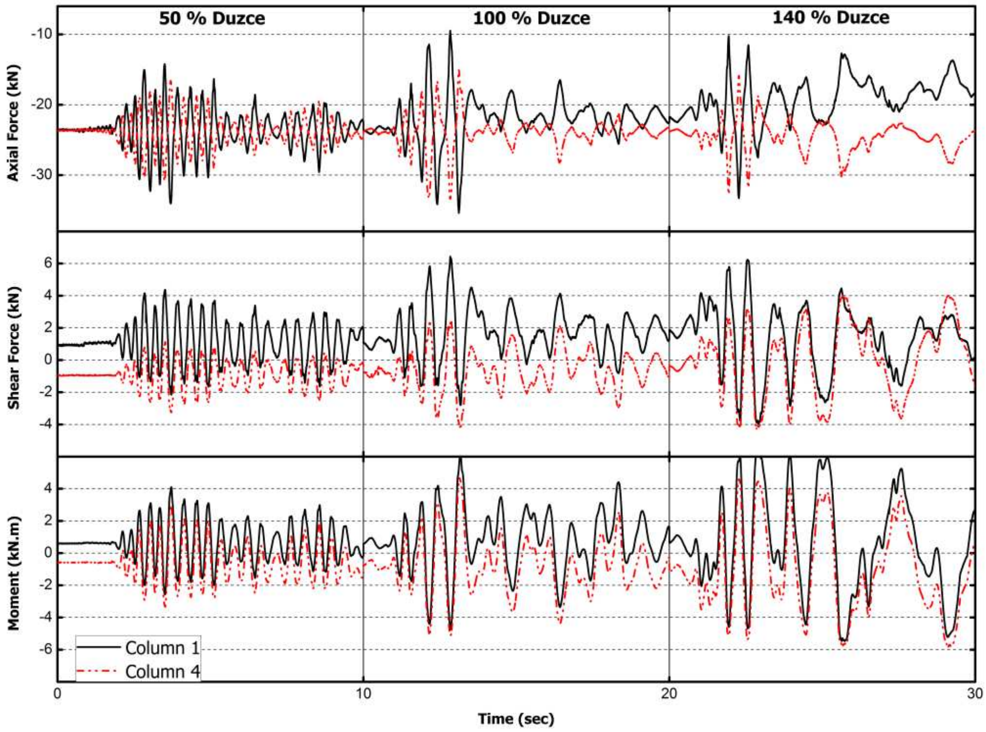

Figure 3.33 Time histories of axial, shear and moment forces for reference frame

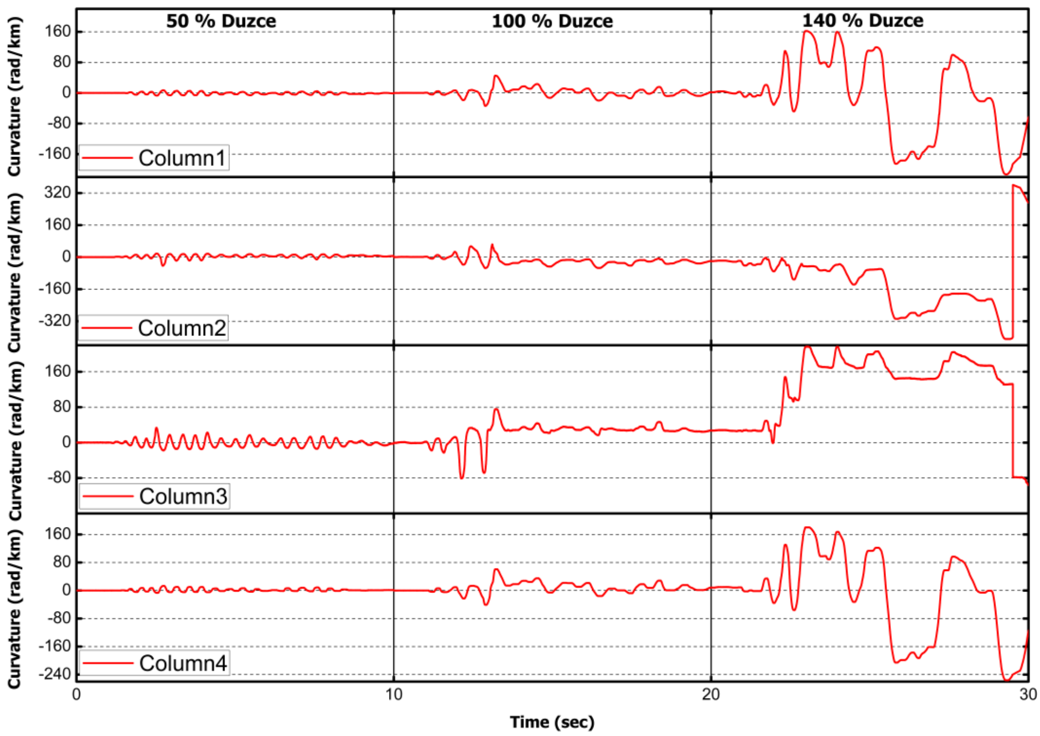

Figure 3.34 Time histories of curvatures for all columns for reference frame

Figure 3.34 represent the measured curvatures from the LVDTs at the bottom of the columns. Column curvatures at the bottom of the columns were affected by the infill wall damage. Infill-wall damage triggered the increase of the curvatures not only at the exterior but also at the interior columns. Maximum curvatures were observed after infill wall failure and their values were 215, 123, 390 and 264 rad/km for columns C1, C2, C3 and C4, respectively.

Figure 3.35 shows the floor accelerations measured from all Duzce tests. Floor acceleration response when added to the base excitation may be used as damage estimation parameters. The maximum floor acceleration was observed as 5.71 m/s^2, 7.22 m/s^2 and 8.68 m/s^2 at the 50, 100 and 140% Duzce test, respectively. Figure 3.36 and 37 present the time dependent dynamic properties, namely period and equivalent viscous damping for the first mode, respectively. They were determined with the procedure proposed by Molina et al. (1999). The maximum damping ratios were around 14, 25 and 90% at the 50, 100 and 140% Duzce tests, respectively. During 50% Duzce test, initial period was determined as 0.17 seconds. During this excitation minor damage occurred at the frame and then period was raised up to 0.43 seconds. It was 0.75 at the end of the 100% Duzce test.

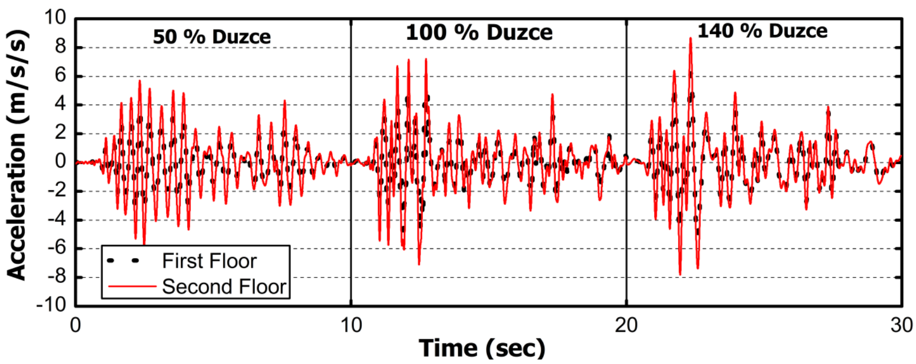

Figure 3.35 Floor accelerations for reference frame

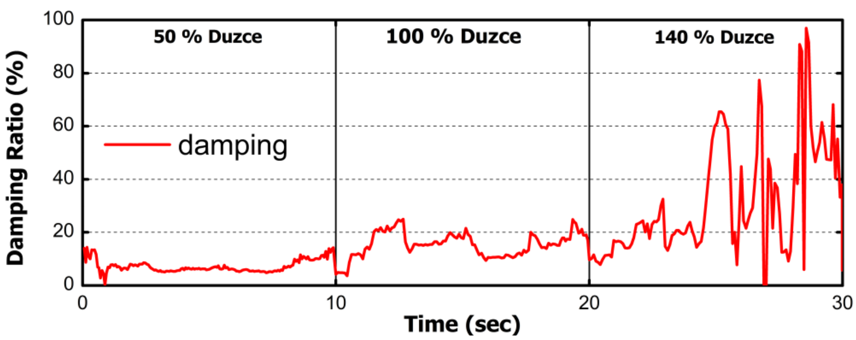

Figure 3.36 Identified damping ratio for reference frame

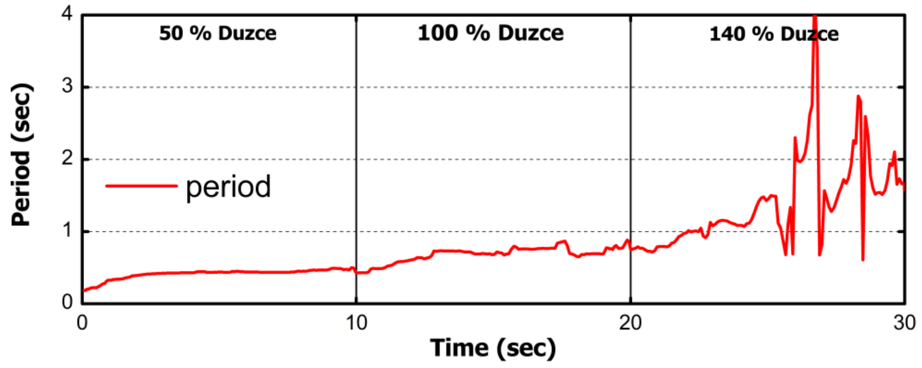

Figure 3.37 Identified period of the test specimen for reference frame

Figure 3.38 indicates IDRs and observed damage states. The damages observed during the tests were marked on the time-series response to better represent the occurrence time. The marked damage on the figure can be described as (Kurt, 2010): A; flexural cracks on interior columns and interface cracks between infill wall and surrounding columns at first floor, B; spalling of concrete and longitudinal bar buckling, C; compression strut formation, D; bar buckling at two regions, final state; global buckling of the first story interior columns and failure of infill wall.

The global and local demand parameters obtained during whole Duzce test are presented in Table 3.4. As results, the following can be deduced from the test results. During the 50% Duzce test, cracks occurred at maximum moment regions of the first story columns and interface cracks were observed at the infill wall-frame boundaries indicating the separation of the infill walls along one diagonal. Compression strut action was the only load carrying mechanism for the infill wall. Hence, damage or cracks occurred on the infill wall was governed mainly by the lateral stiffness and strength of the test frame. Besides such cracking, no other significant damage was observed. With respect to observed damage and measurements the test frame has experienced minor damage and remains functional.

It was suggested that minor repair to this frame would be needed after the 50% scale excitation. Based on the measured demand parameters and judgment of the observed damage state, immediate occupancy level damage criterion was declared by Kurt (2010).

Although there was no significant damage at the 50% Duzce test, significant damage occurred at 100% Duzce test. The main damage was; the concrete crushing at column base of interior columns followed by longitudinal bar buckling and significant diagonal cracking along the diagonals of the first story infill wall. The lateral strength of the test frame was sustained up to about 50 mm of top displacement. On the other hand, plastic hinges was observed at the columns' base. Severe pinching occurred due to opening and closing of diagonal cracks on the first story infill walls.

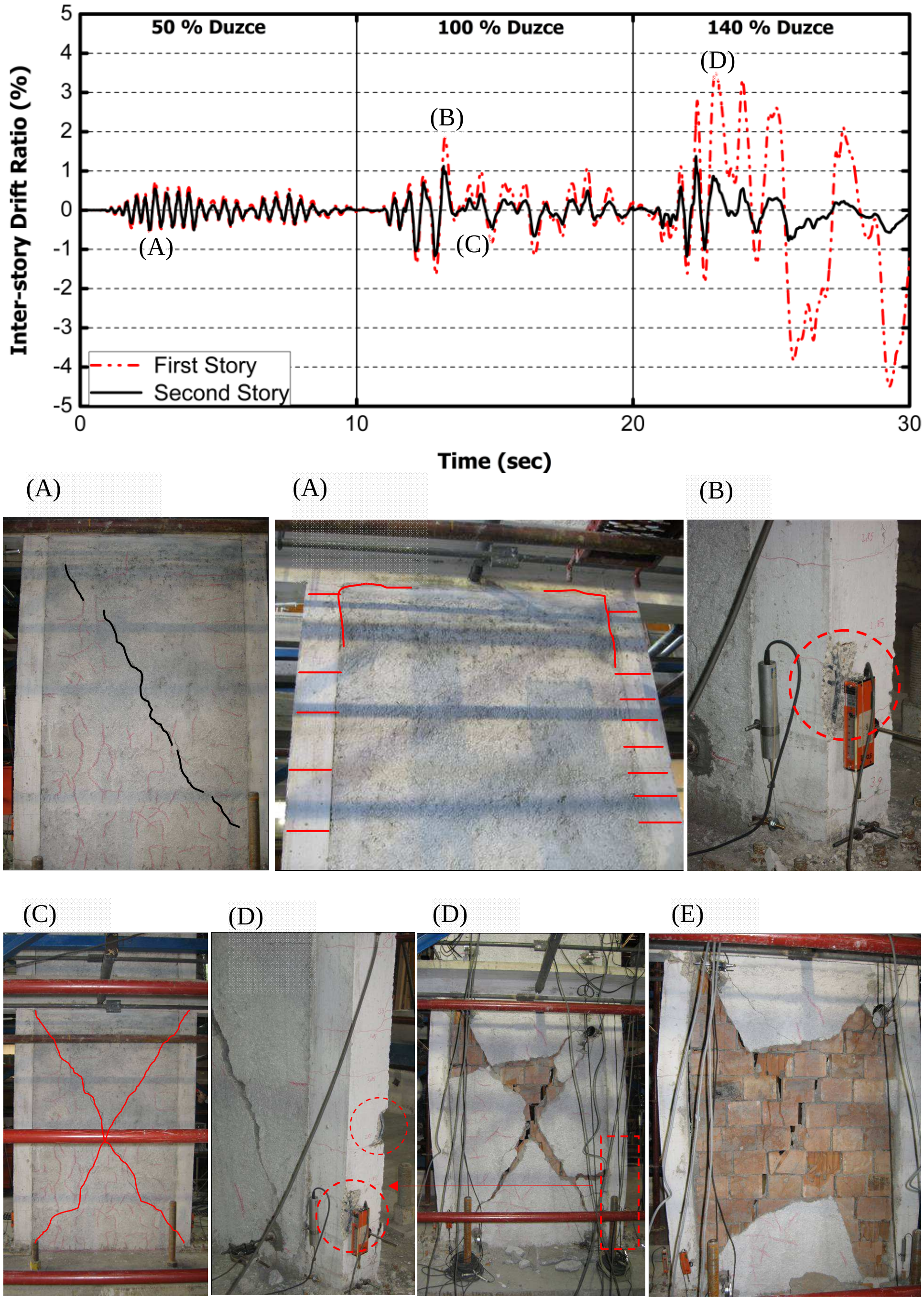

A; Infill frame interface cracks and diagonal crack initiation, B; Spalling and bar buckling, C; Diagonal cracks, D; Two bar buckling regions, E; Final State

Figure 3.38 Drift ratio and observed damage for reference frame

The structure was judged to be capable of withstanding the deformation demands without any significant drop of lateral strength and could be occupied after strengthening despite the significant damage. As a result, the structure was proposed to satisfy the life safety performance criterion based on engineering judgment (Kurt, 2010). At the 140% Duzce test, the maximum IDR of the first and second story was 4.5% and 1.8%, respectively. This indicates that a soft story was observed, where the second story sustained drift levels were at relatively low levels (1.4% DR). Lateral strength of the frame dropped to 30% of its lateral strength merging to the bare frame response. Such a decrease in lateral strength made the structure seriously vulnerable for life safety. The infill wall damage with diagonal cracking and separation of plaster from infill wall surface was the main reason of the severe decrease of the lateral strength. Extended diagonal cracking and separation of plaster from infill wall surface was observed. In addition, top and bottom plastic hinges of the interior columns longitudinal bar buckling occurred. Results show that the test frame was unsafe for occupancy purposes and declared to be at the verge of collapse (although no gravity collapse took place) due to the following reasons (Kurt, 2010).

1) The infill wall was susceptible to out of plane collapse for any out of plane disturbance.

2) Lateral strength had significantly deteriorated.

3) Repair was not possible due significant damage in the structural and non-structural elements.

4) A stability problem could have risen with small disturbance.

Table 3.4 Summary of test results for reference frame (taken from Kurt, 2010)

Ground Motion	Maximum Displacement Demand (mm)		Maximum Interstory Drift Ratio (%)		Maximum Story Base Shear Force (kN)		Column Plastic Rotation Demands			
							θ_{p1}	θ_{p2}	θ_{p3}	θ_{p4}
	1st Story	2nd Story	1st Story	2nd Story	1st Story	2nd Story	$\mu_{\phi 1}$	$\mu_{\phi 2}$	$\mu_{\phi 3}$	$\mu_{\phi 4}$
50 % Düzce	15	23	0.7	0.6	60.4	27.6	0 0.3	0.003 1.9	0.001 1.5	0 0.6
100 % Düzce	35	49	1.8	1.1	67.9	58.2	0.004 2.0	0.006 2.8	0.008 3.5	0.006 2.6
140 % Düzce	85.3	93.8	4.5	1.4	54.5	52.9	0.038 9.4	0.055 16.9	0.025 8.3	0.036 11.5

ϕ; curvature determined from bottom of the columns.
μ_ϕ; curvature ductility (ratio between ultimate curvature (ϕ_u) and yield curvature (ϕ_y))
θ_p; plastic rotation (determined as (ϕ_u-ϕ_y) × l_p)
l_p; plastic hinge length, 130 mm (this length is the monitored length by the LVDTs for curvature estimation at the bottom of the column.)

3.7.2 Chevron Braced Frame

Although reference frame was tested for the 50, 100 and 140% scaled Duzce ground motion, the chevron brace upgraded frames was tested for 50, 100, 140, 180 and 220% scaled Duzce ground motions. Figure 3.39 indicates the time history of the test results in terms of story displacements. The story displacement of the first and second story were 1.66 and 2.45 mm for 50 % scaled, 4.69 and 7.29 mm for 100 % scaled, 13.18 and 22.06 mm for 140 % scaled, 18.17 and 34.92 mm for 180 % scaled Duzce test, respectively.

Figure 3.40 indicates the time series response of the chevron braced frame for IDR. The maximum IDRs of the first and second story was 0.1% for 50 % scaled, 0.2% for 100 % scaled, 0.7% and 0.6% for 140% Duzce test, 0.9% and 1.1% for 180% Duzce test, respectively. As can be seen, the IDRs were very similar in both floors. This indicates that no soft story behavior was observed unlike the reference frame and a nearly linear deflection profile was attained. The lateral force distribution for floors was approximately a triangular distribution.

Figure 3.41 indicates the time history of the test results in terms of maximum base shear. The estimated base shear capacity for case 1 and 2 are also shown in this figure. The base shear was 39.94 kN for 50% Duzce, 89.12kN for 100% Duzce, 178.98 kN for 140% Duzce and 206.06 kN for 140% Duzce test, respectively. The lateral strength drop did not occur for all tests up to the 220% Duzce test. The reason of this behavior was the stable response of the braced system.

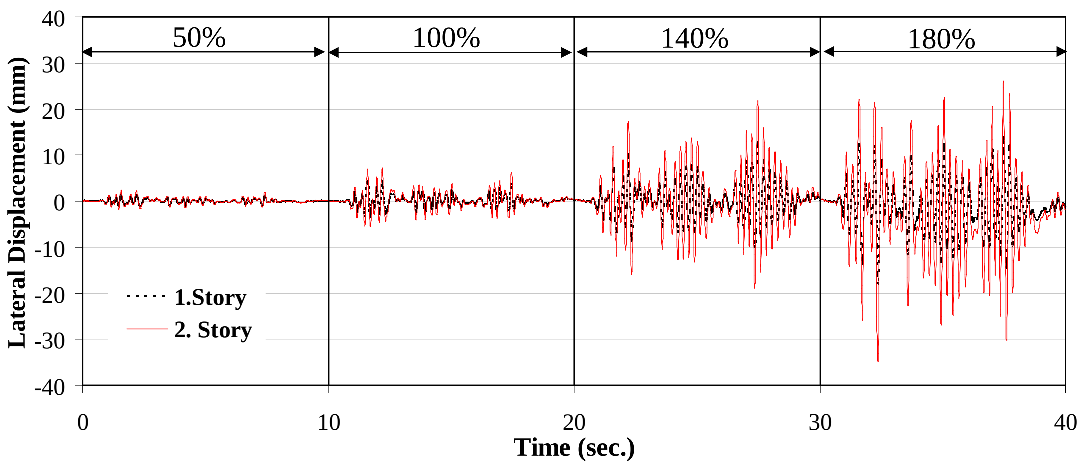

Figure 3.39 Time history of floor displacements for chevron braced frame

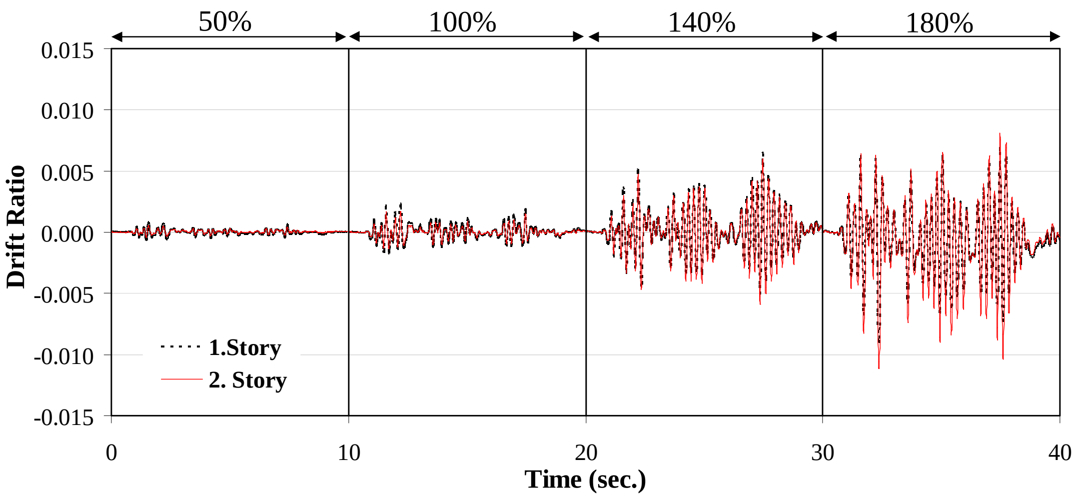

Figure 3.40 Time history of inter-story DRs for chevron braced frame

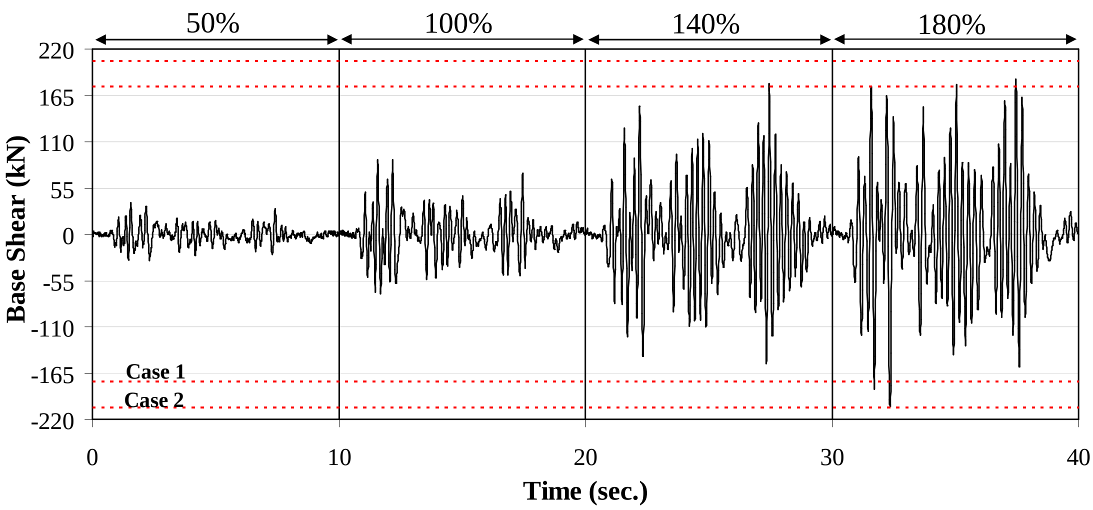

Figure 3.41 Time history of base shear for chevron braced frame

Figure 3.42 indicates force-deformation response of the chevron braced frame. Top DR was slightly higher than 1% and the base shear ratio was about 1.72 at the end of the 180% Duzce test. To observe the limit state of this specimen, further lateral demand was imposed to the frame. The 220% Duzce test was conducted and the failure of the column C3 was observed at about 2.5 sec. The yield displacement, Δ_y, was found by extending a line from the origin and passing through 75% of the ultimate load carrying capacity (maximum base shear observed at 220% Duzce test) as previously explained and referenced to Kurt (2010).

The braced frame was almost elastic during the 50, 100 and 140% Duzce tests. The maximum ductility demands were 1.48 and 1.67 for the 140 and 180% Duzce test, respectively. The maximum base shear ratio was about 1.83 during the 220% Duzce test.

Figure 3.43 presents the moment curvature relation obtained from force transducer and LVDTs at the bottom of the columns C1 and C4. Moment-curvature relation obtained from sectional analysis is also indicated for two axial load ratios which are 5 and 18%. Since the chevron braces were capable of controlling the lateral deformation of the frame, plastic hinges did not occurred at the exterior columns C1 and C4 for all tests (Figure 3.43).

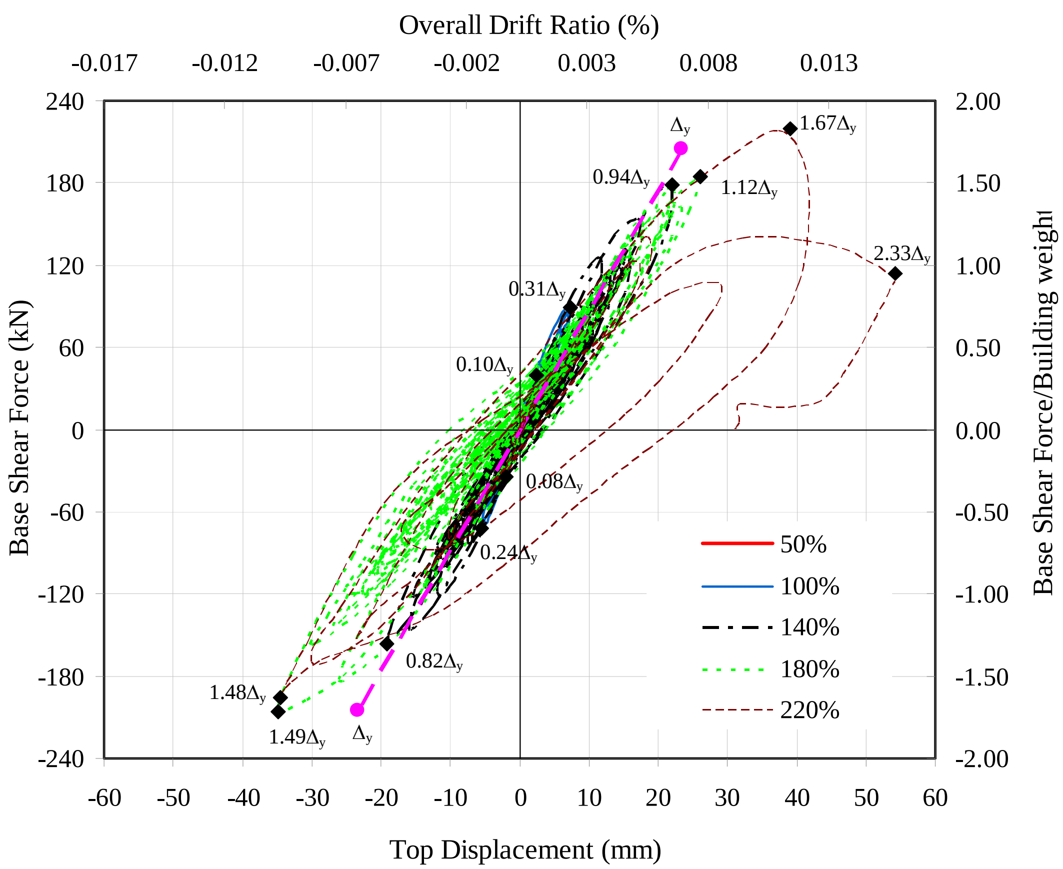

Figure 3.42 Force-Deformation response for chevron braced frame

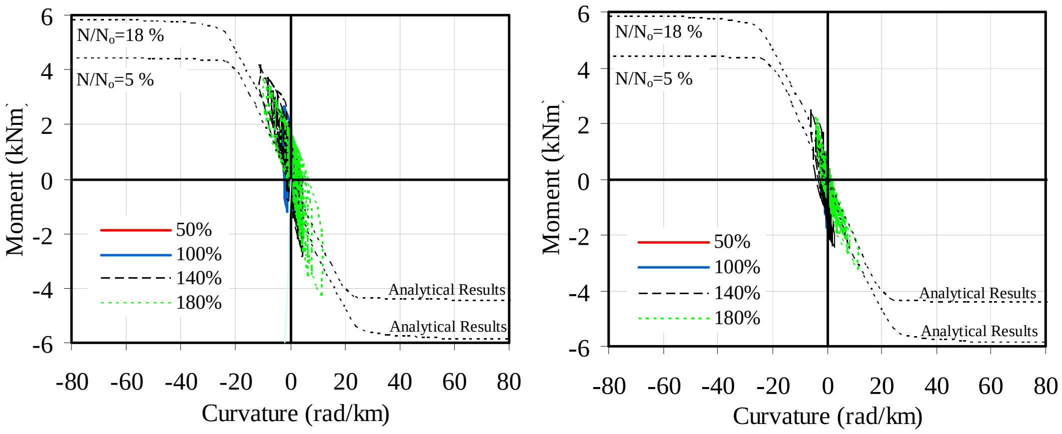

Figure 3.43 Moment-Curvature diagrams of columns C1 and C4 for chevron braced frame

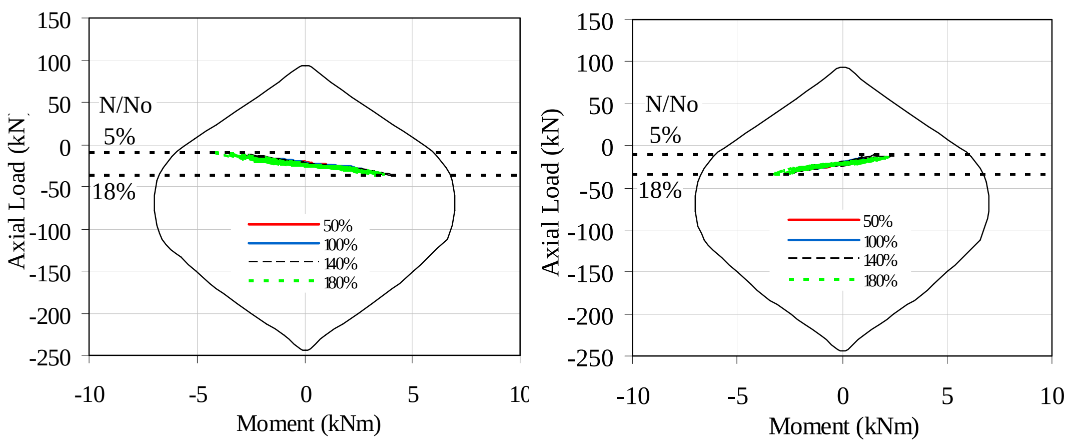

Figure 3.44 Moment interaction response of columns C1 and C4 for chevron braced frame

Moment interaction response of the columns C1 and C2 are indicated in Figure 3.44. The maximum and minimum axial load ratios were 5 and 18% during the experiment due to overturning effect.

The maximum variation for all tests in axial load, shear force and bending moment were 15.9, 10.6 kN, 5.3, 0.8 kN and 5.0, 2.8 kNm at the bottom of the columns C1 and C4, respectively. These variations are presented in Figure 3.45.

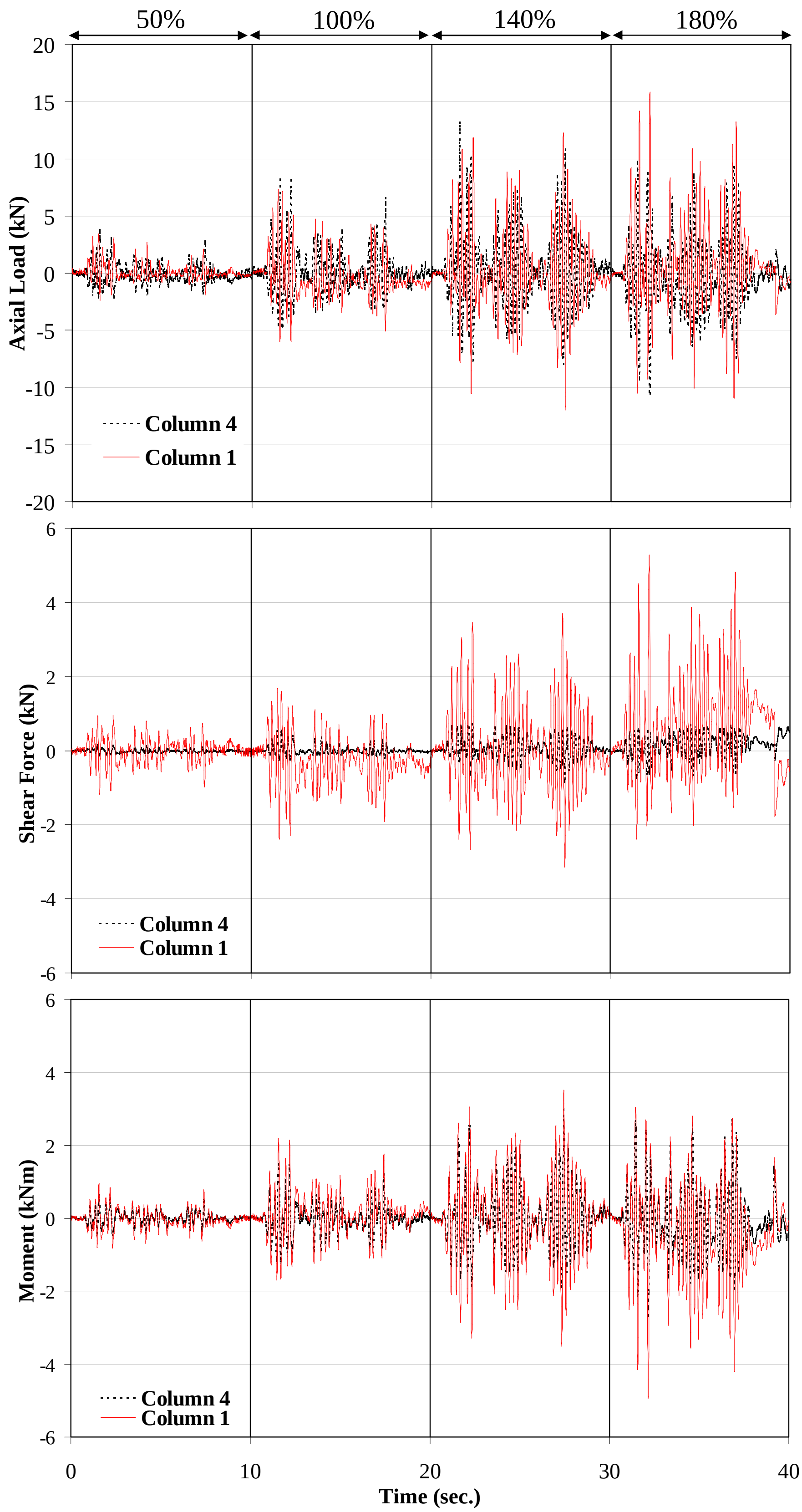

Figure 3.45 Variation at time histories of axial, shear forces and bending moment

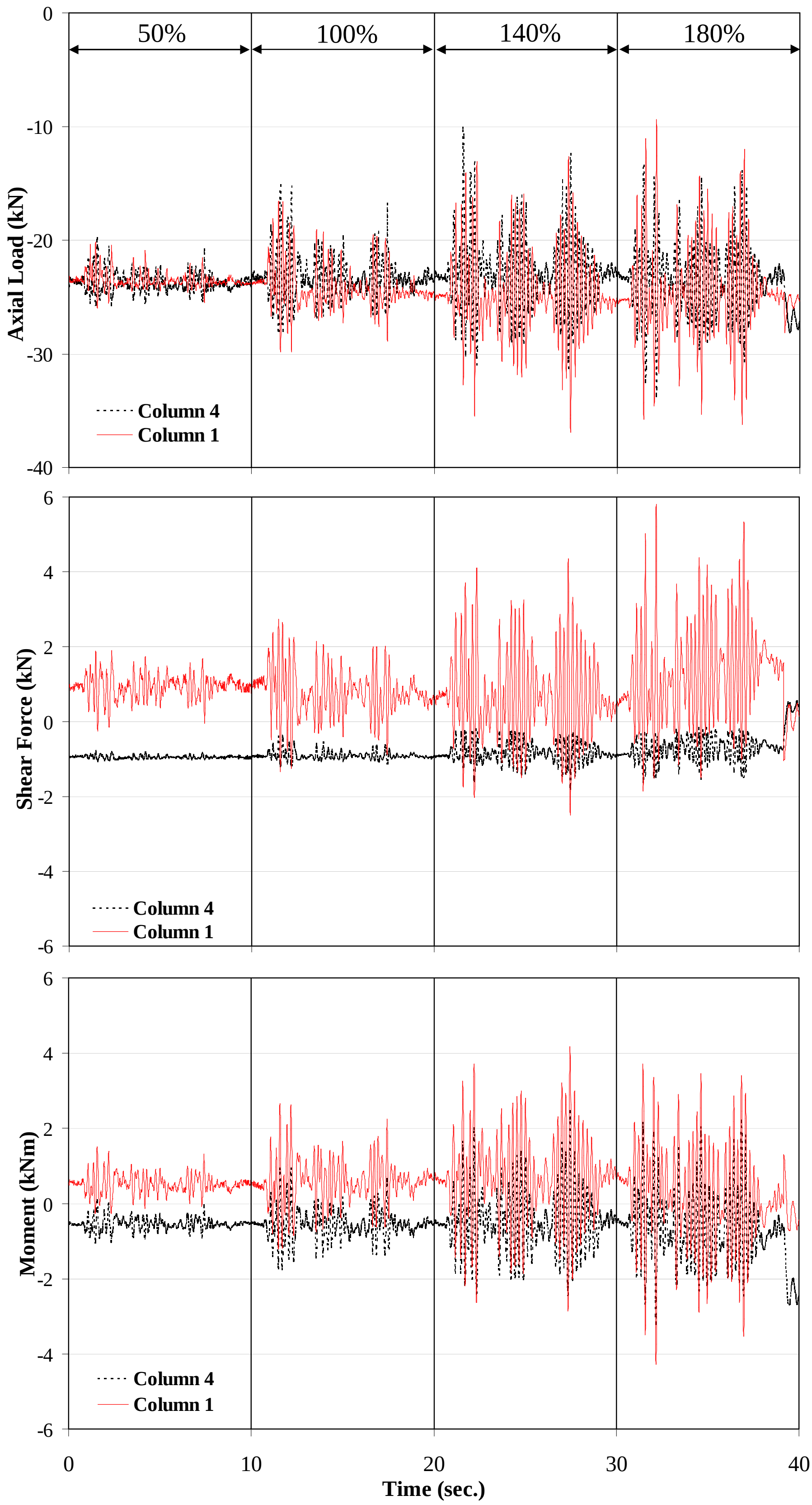

Figure 3.46 Time histories of axial, shear forces and bending moment

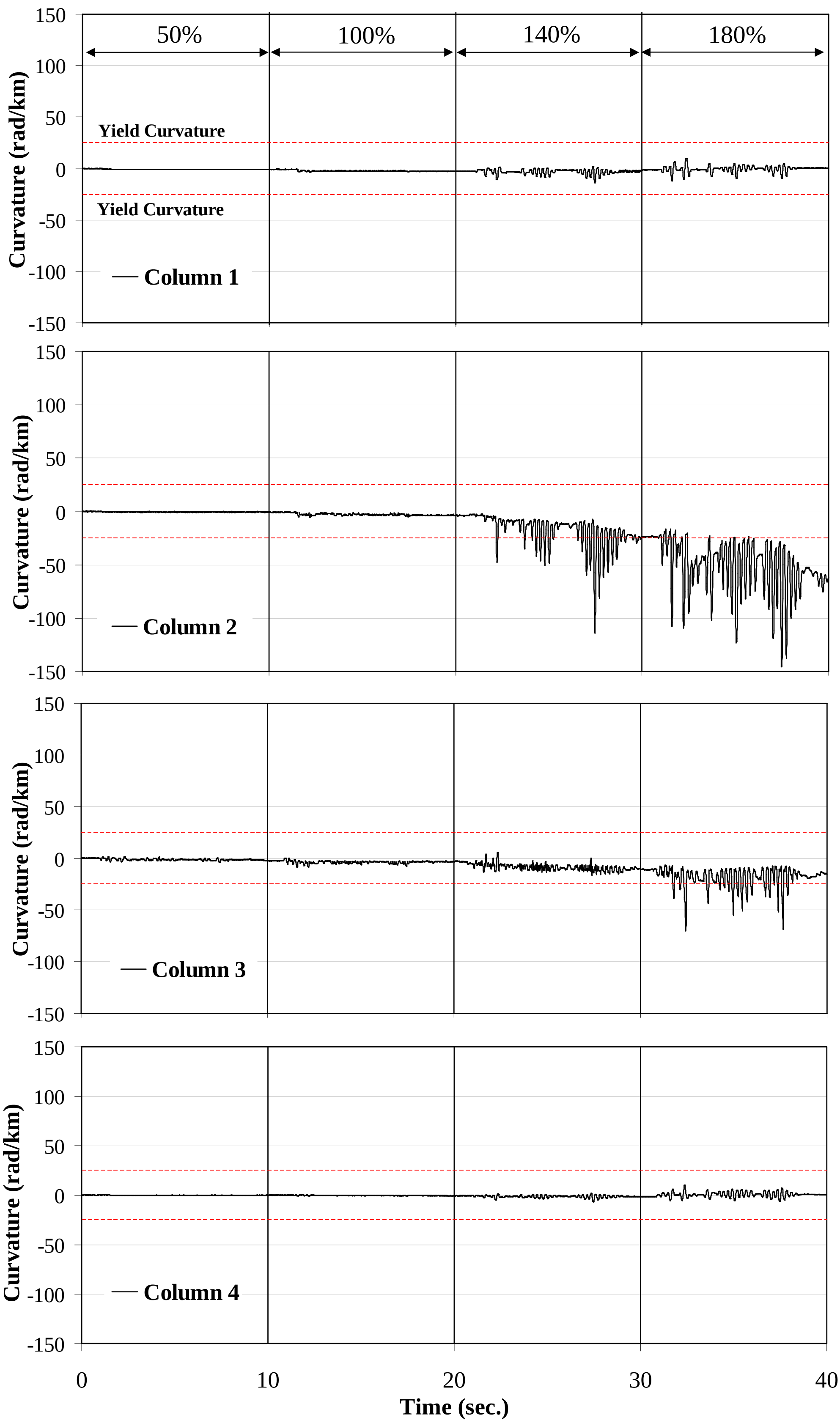

Figure 3.47 Time histories of curvatures at column bases.

The exterior columns base reaction (axial load, shear force and moment) monitored during all experiments are plotted in Figure 3.46. The upper and lower bound of the axial load were -9.4, -36.4 kN and -10.1, -33.8 kN for columns C1 and C4, respectively.

Curvatures measured from the bottom of the columns C1 to C4 are presented in Figure 3.47. While curvatures of the exterior columns C1 and C4 were lower than the estimated yield curvature, the interior columns were higher than the estimated yield curvature from the sectional analysis results shown in Figure 3.43. These results are consistent with moment-curvature plots in Figure 3.43. Maximum curvatures obtained from all tests for columns C1 to C4 were 12.0, 146.4, 71.0 and 10.5 rad/km, respectively.

Time dependent dynamic properties, namely period and equivalent viscous damping, of the chevron braced frame were determined for this specimen as well as reference frame (Molina et al., 1999). The variation of the period for the first mod is given in Figure 3.48. The initial period of the frame was 0.125 sec. Since the braced frame experienced nearly elastic behavior during the 50% Duzce test, the variation in period was not significant and at the end of this test it was 0.126 sec. The period at the end of the 100%, 140% and 180% Duzce test were 0.17, 0.22 and 0.25 sec, respectively. The variation of the damping ratio of first mode is exhibited in Figure 3.49. The peak damping ratio at the 50% Duzce test was 78% and it dropped during the rest of the test. The peak damping ratio during 100%, 140% and 180% Duzce test were 63, 23 and 23%, respectively.

Table 3.5 summarizes the test results for chevron braced frame. The physical damage correlation with the cyclic behavior of the test frame is presented in Figure 3.50.

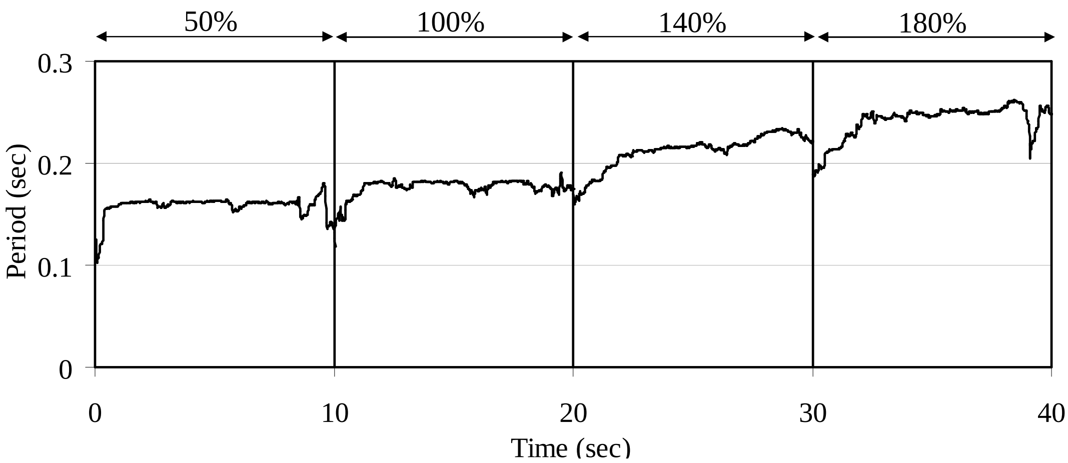

Figure 3.48 Identified period of the test specimen

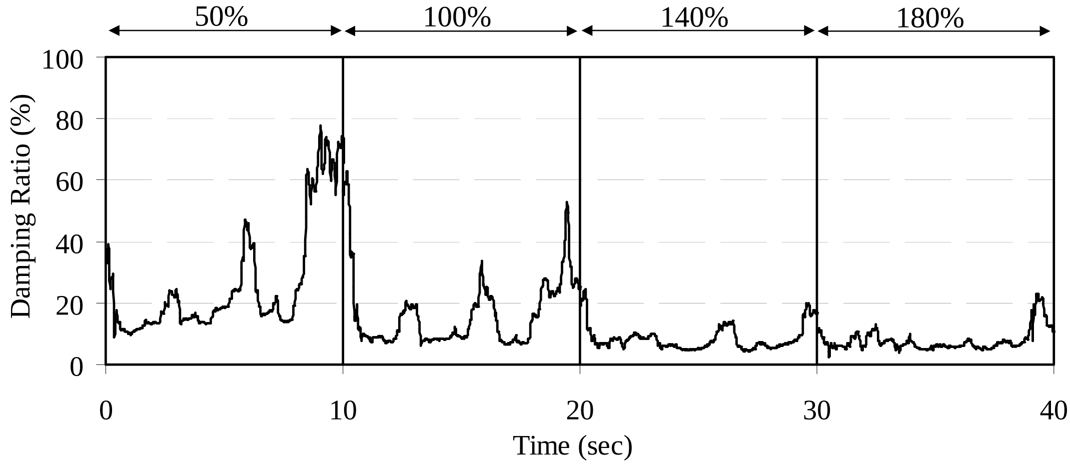

Figure 3.49 Identified damping ratios

Table 3.5 Summary of test results for chevron braced frame

Ground Motion	Maximum Displacement Demand (mm)		Maximum Interstory Drift Ratio %		Maximum Story Force (kN)		Base Shear Force (kN)	Base Shear Ratio (kN/kN)	Column Plastic Rotation Demands			
	1st Story	2nd Story	1st Story	2nd Story	1st Story	2nd Story			θ_{p1}	θ_{p2}	θ_{p3}	θ_{p4}
									$\mu_{\phi 1}$	$\mu_{\phi 2}$	$\mu_{\phi 3}$	$\mu_{\phi 4}$
50% Düzce	1.66	2.45	0.1	0.1	17.88	27.51	39.94	0.33	0	0	0	0
									0	0	0	0
100% Düzce	4.69	7.29	0.2	0.2	33.98	62.92	89.12	0.74	0	0	0	0
									0	0	0	0
140% Düzce	13.18	22.06	0.7	0.6	69.07	120.38	178.98	1.49	0	0.011	0	0
									0	4.4	0	0
180% Düzce	18.17	34.92	0.9	1.1	71.51	141.22	206.06	1.72	0	0.013	0.005	0
									0	4.9	2.4	0

ϕ; curvature determined from bottom of the columns.

μ_ϕ; curvature ductility (ratio between ultimate curvature (ϕ_u) and yield curvature (ϕ_y))

θ_p; plastic rotation (determined as (ϕ_u-ϕ_y) × l_p)

l_p; plastic hinge length, 130mm (this length is the monitored length by the LVDTs for curvature estimation at the bottom of the column.)

Since the braces resisted and limited the lateral deformation of the frame, there was no damage on braces, gusset plates and RC joints and members during the 50% Duzce test. The braced frame was elastic during the test. As seen in Table 3.5, there were no plastic hinges occurred at the bottom of the first story columns and the maximum IDR was limited. Because of elastic behavior of the braced frame and limited damage on the braced frame, this frame was observed to be in the immediate occupancy performance level. This frame can be used after such an earthquake without any repairing.

Limited flexural cracks at the bottom of the interior columns C2 and C3 were observed at the 100% Duzce test. These were the cracks shown with blue lines in Figure 3.50 and their widths were less than 0.5 mm. During this test, no damage on braces, gusset plates and RC joints and members were observed. Since there was no lateral strength drop the frame had an elastic behavior during the test. As a result, this frame was observed to be in the immediate occupancy performance level. This frame can be used after such an earthquake without any repairing.

At the 140% Duzce test, numbers of hair line cracks (black line in Figure 3.50) occurred through the first story interior columns C2 and C3 height. In addition, limited numbers of minor cracks were observed at the RC joint and slab. During this test, no damage on the braces, gusset plates and RC joints and members were observed. Since there was no lateral strength drop the frame had an elastic behavior during the test. As seen in Table 3.5, while plastic hinges occurred one of the first story columns, the others were elastic during the test. Based on the damage on the braced frame and maximum IDR being limited, this frame was observed to be in the immediate occupancy performance level. This frame can be used after such an earthquake without any repairing.

The severe damage, longitudinal bar buckling, occurred at the bottom of the column C3 at the 180% Duzce test. In contrast to longitudinal bar buckling at the bottom of the column C3, the base shear capacity did not drop and no stability problem was arisen because it was observed that Plate 2 (Figure 3.9) provided stability to the bottom of the RC column. During this test, no damage on braces, gusset plates and RC joints and members were observed. As a result, this frame was observed to be in the life safety performance level. This frame can be used after such an earthquake with limited repairing.

The 220% Duzce test was terminated because the failure of the column C3 was observed at about 2.5 sec (Figure 3.51). In addition to column failure, brace buckling was observed at this test (from the measurements of the strain gages given in Appendix 2). The descending part of the lateral load seen in Figure 3.42 was resulted from the failure of column C3. Although there was no gravity collapse, the lateral strength dropped to half of the maximum lateral capacity observed during such test. The maximum base shear of the braced frame was 218 kN which was 3.2 times the base shear of the reference frame (This result proved that the design criteria was successful). As seen in Figure 3.51, the maximum IDR was about 1.0 and 2.6 % for the first and second story, respectively. The reason of such high IDR was the excessive damage on the column C3. The main reason of the

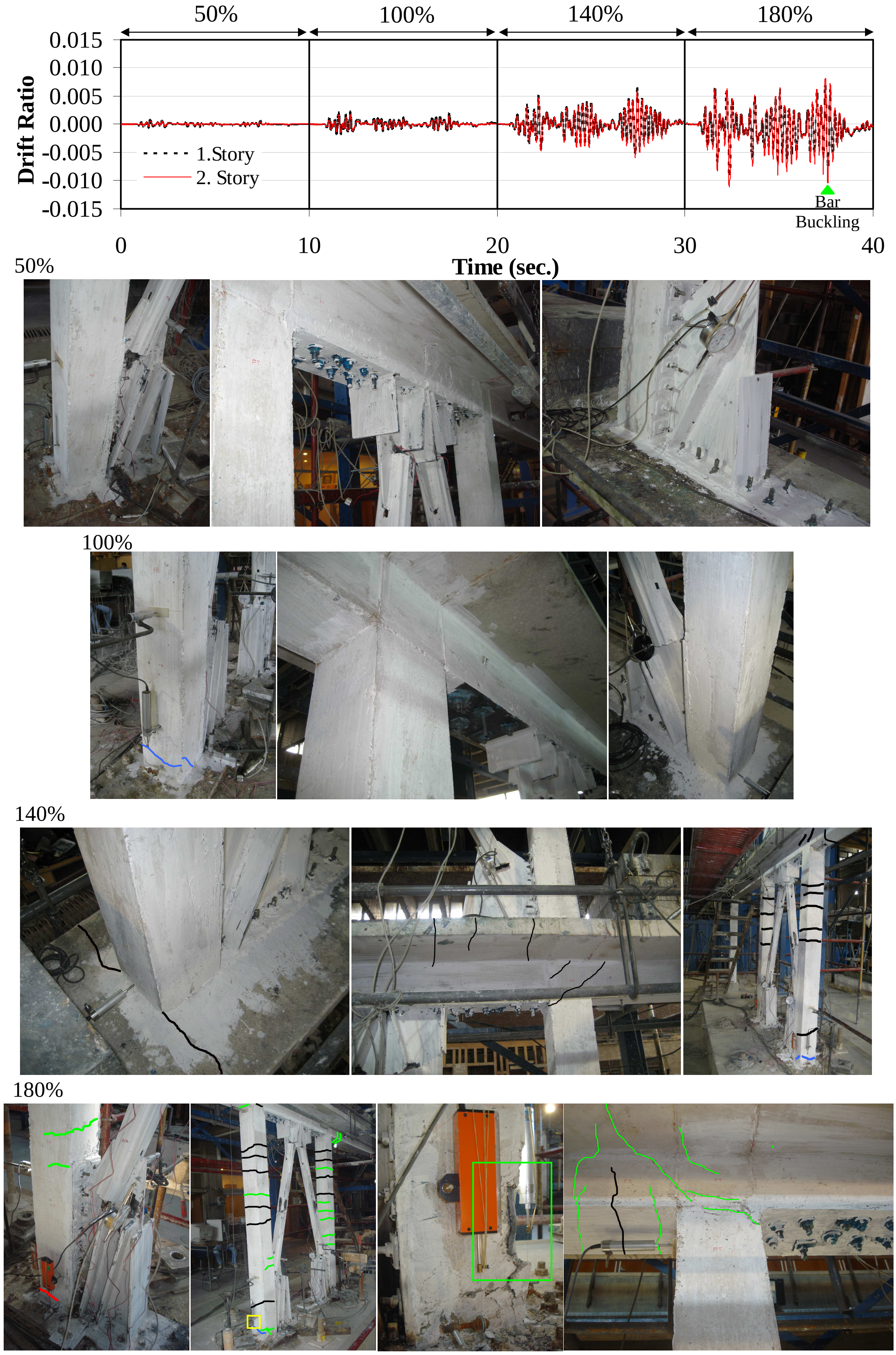

Figure 3.50 Physical damage observed during the all test

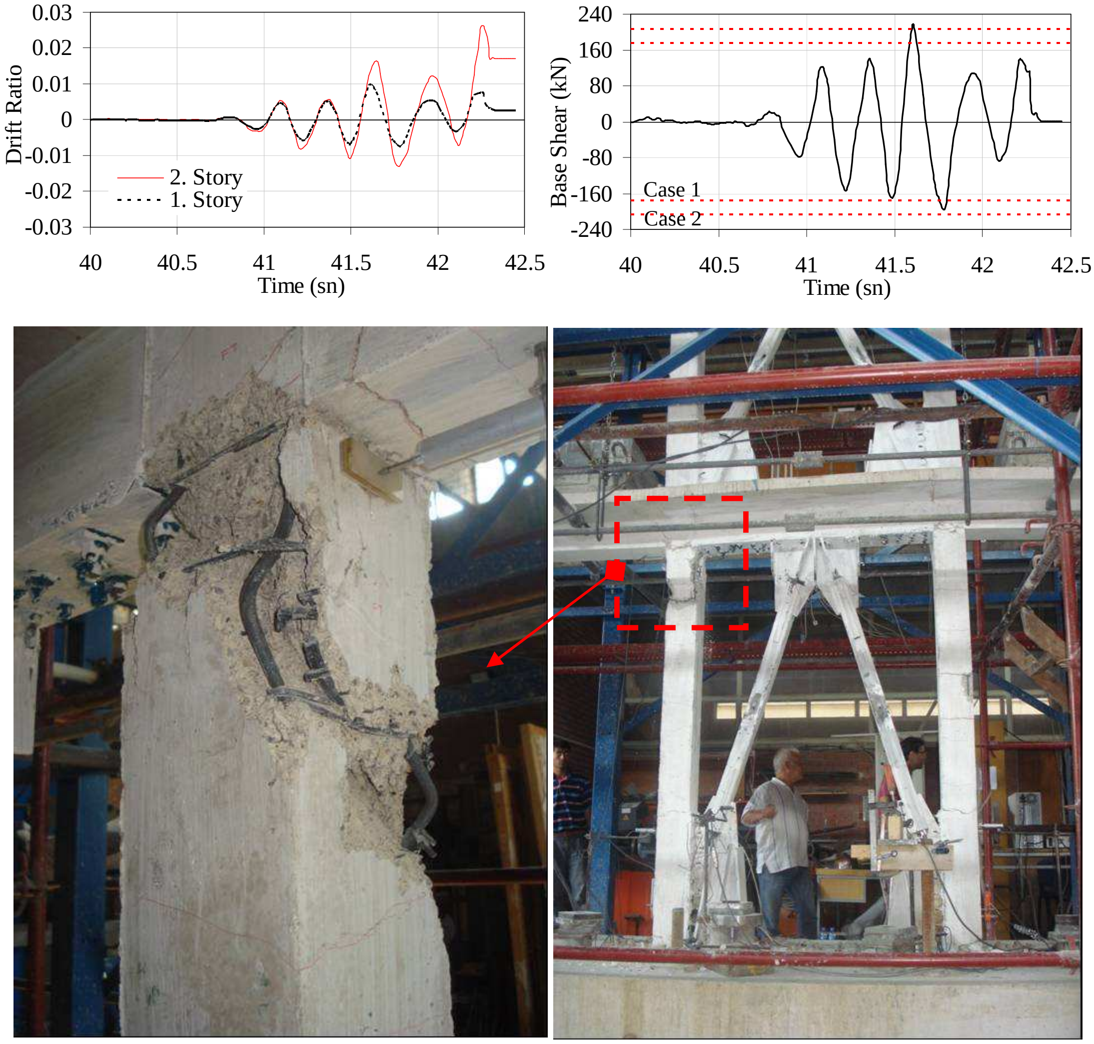

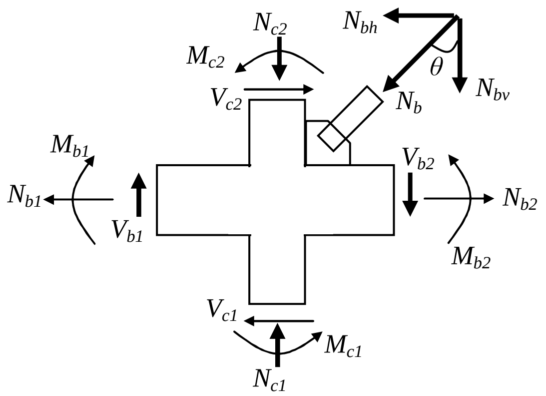

$N_{c1} = V_{b1} - V_{b2} + N_{bv}$

$N_{bv} = N_b \times \cos\theta$

N, V, M; Axial, shear force and bending moment, respectively

N_b; axial force on brace

Figure 3.51 Failure at the top of the column 3 during the 220% Duzce test

column damage was the additional demand on first story interior columns due to the transfer of axial force from the braces on the second story. When the second story brace is under compression, the vertical component of that brace produced extra axial load (N_{bv} see Figure 3.51) on the column C3. When the vertical total force on the column (N_{c1}) exceeded the axial load capacity of the column C3, failure occurred as seen in Figure 3.51. As a result, this frame was observed to be beyond the collapse prevention performance level. This frame can not be used after such an earthquake and repairing was almost impossible.

As a result, the test results in term of measurements and observed damage stated that the chevron braced frame can be used without any repair after 140% Duzce test. According to engineering judgment, this result is valid for 180% Duzce test, although column longitudinal rebar buckling was observed. In light of measured demand parameters and observed damage state, chevron braced frame can be considered within the immediate occupancy and life safety performance level criteria after 140 and 180% Duzce tests, respectively. On the other hand, the frame was beyond the collapse prevention performance level criteria for the 220 % Duzce test.

3.7.3 Internal Steel Frame

Figure 3.52 indicates the time history of the test results in terms of story displacements. The story displacement of the first and second story was 12.6 and 21.8 mm for 50% Duzce, 21.7 and 39.7 mm for 100% Duzce, 40.8 and 75.6 mm for 140% Duzce, 57.6 and 111.9 mm for 180% Duzce test.

Figure 3.53 indicates the time history of the test results in terms of IDRs. The IDRs of the first and second story was 0.6% and 0.7% for 50% Duzce, 1.1 and 1.2 for 100% Duzce, 2.0% and 2.3% for 140% Duzce, 2.9% and 3.7% for 180% Duzce test.

Figure 3.54 indicates the time history of the test results in terms of maximum base shear. The base shear was 67.6 kN for 50% Duzce, 88.2 kN for 100% Duzce, 116.6 kN for 140% Duzce, 123.2 kN for 180% Duzce test.

Figure 3.55 indicates force-deformation response for ISF. Top DR was slightly higher than 3.0% and the base shear ratio was about 1.03 at the end of the 180% Duzce test. The yield displacement, Δ_y, was found by extending a line from origin and passing through 75% of the ultimate load carrying capacity (maximum base shear observed at 180% Duzce test). According to Figure 3.55, RC frame strengthened with ISF was almost elastic during the 50 and 100% Duzce test. On the other hand, nonlinear behavior was observed at the 140 and 180% Duzce tests. The maximum displacement ductility demands were 1.34 and 2.21 for the 140 and 180% Duzce testes, respectively.

Figure 3.56 presents the moment curvature relation obtained from force transducer and LVDTs at the bottom of the columns C1 and C4. Moment-curvature relation obtained from the sectional analysis is also indicated for the two axial load ratios which is 5 and 19% in Figure 3.56. Unlike chevron braced frame, during ISF tests, curvatures measured at the bottom of columns C1 and C4 exceeded yield curvatures (25 rad/km) determined from the sectional analysis.

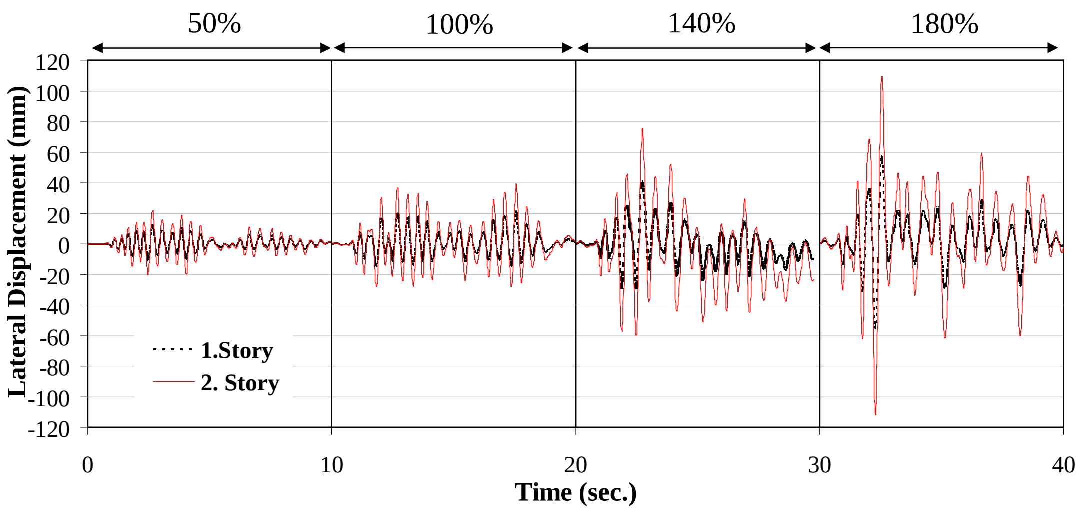

Figure 3.52 Time history of floor displacements for ISF

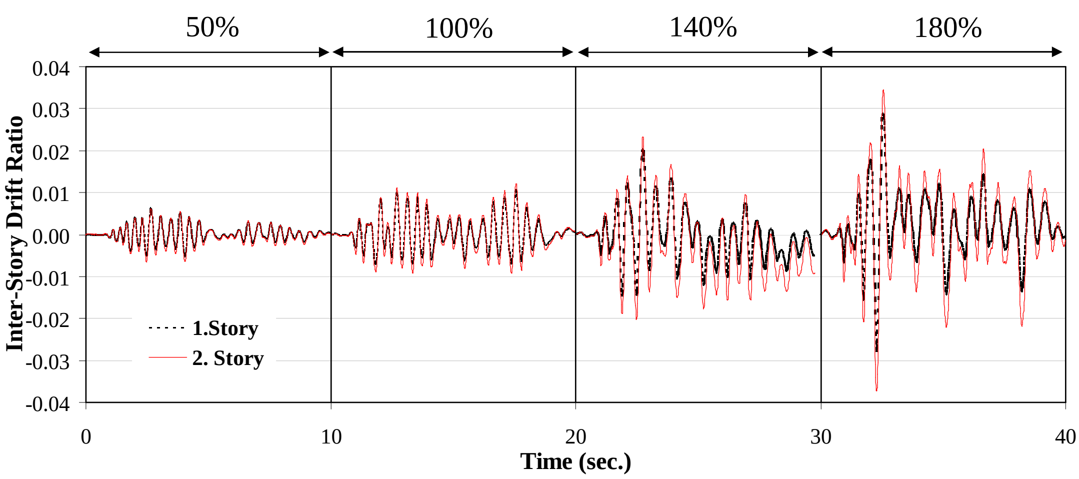

Figure 3.53 Time history of inter-story DRs for ISF

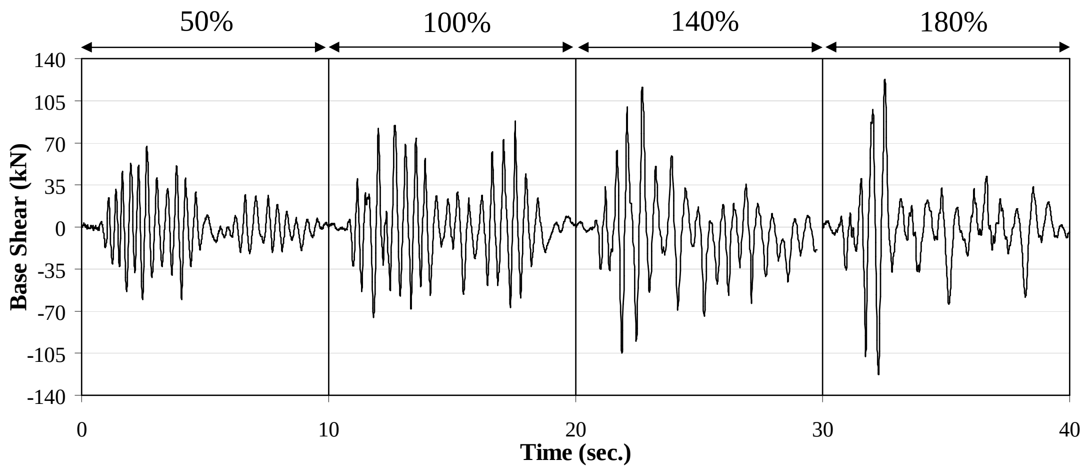

Figure 3.54 Time history of base shear for ISF

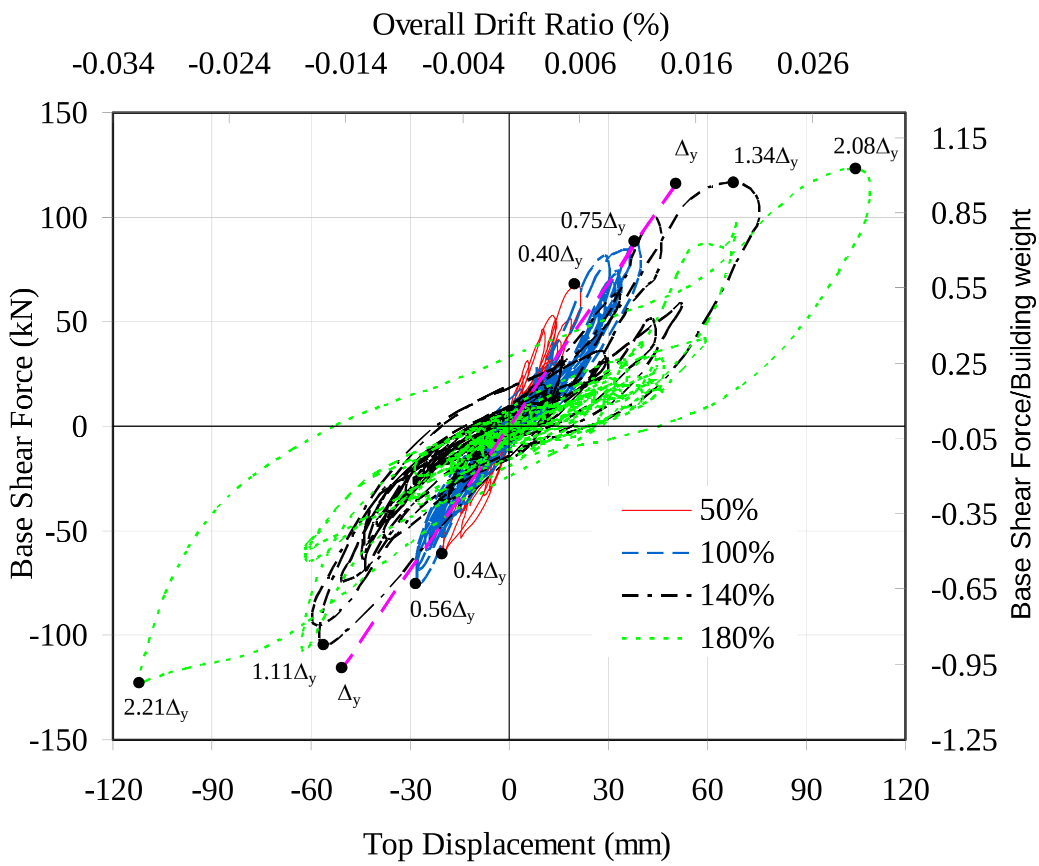

Figure 3.55 Force-Deformation response for ISF

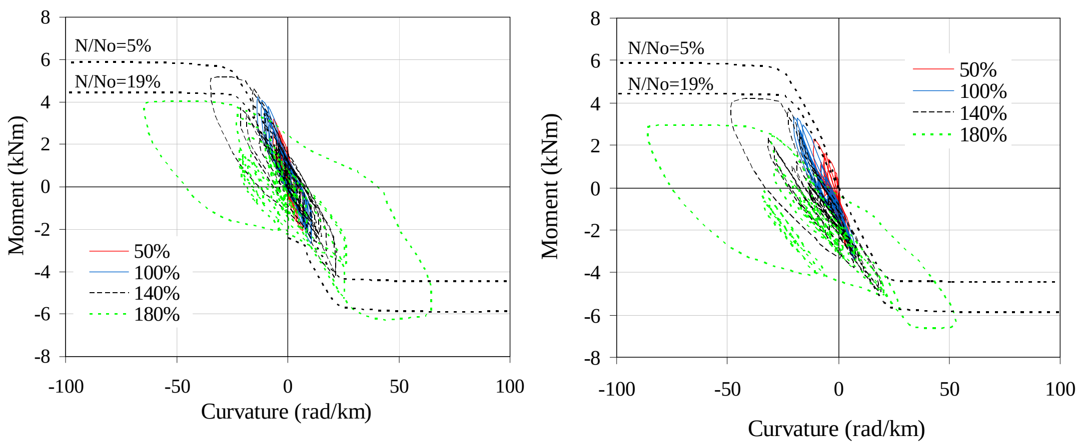

Figure 3.56 Moment curvature diagrams of columns C1 and C4 for ISF

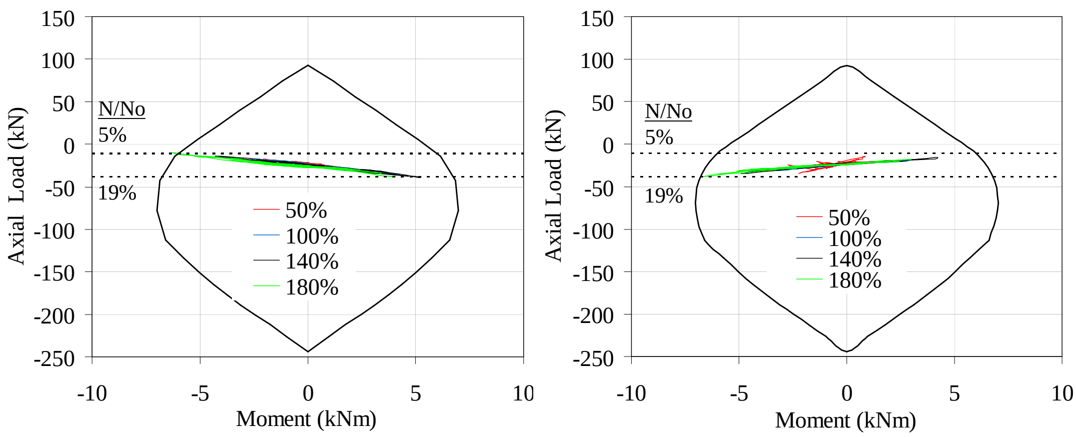

Figure 3.57 Moment interaction of columns C1 and C4 for ISF

Moment interaction response of the columns C1 and C4 are indicated in Figure 3.57. The maximum and minimum axial load ratios were 5 and 19% during the experiment due to the overturning effects.

Figure 3.58 presents the variation of axial force, shear force and moments for the columns C1 and C4. The maximum variations observed during all tests were 14.3 and 11.6 kN in axial load, 5.7 and 2.6 kN in shear force and 5.9 and 5.1 kNm in moment for columns C1 and C4, respectively. As indicated in this figure, due to overturning effect, the variation of the axial loads for columns C1 and C4 were reverse of each other. The existing end forces monitored during all tests is plotted in Figure 3.59. The lower and upper bound of the axial load were -10.3 and -39.4 kN for column C1 and -16.1 and -38.1 kN for column C4, respectively.

Curvatures measured from the bottom of the columns C1 to C4 are presented in Figure 3.60. While curvatures of the all columns are lower than the yield curvature determined from section analysis (25 rad/km) at 50 and 100% Duzce tests, they were beyond the yield curvature at 140 and 180% Duzce tests. Maximum curvature obtained from the all tests for columns C1 to C4 were 65.1, 84.8, 111.8 and 86.2 rad/km, respectively.

Time dependent dynamic properties, namely period and equivalent viscous damping, of the test frame are determined according to the procedure proposed by Molina et al. (1999) as described in Kurt et al. (2011). The variation of the period for the first mod is given in Figure 3.61. The initial period of the frame was 0.22 sec. During the 50% Duzce test, the period increased to 0.4 sec. The reason of the elongation seems to be the cracks observed on RC members. The 100% Duzce test started with a period about 0.4 sec and ended with a period about 0.45 sec. The variation of period during the 50 and 100% Duzce tests were not significant. During 140% Duzce test, period varied between 0.3 and 0.5 sec. On the other hand, there was a gradually increase in period at 180% Duzce test and at the end of the test, it was up from 0.52 sec. to 0.70 sec.

The damping ratio was between 3% and 20% at the 50 and 100% Duzce tests (Figure 3.62). On the other hand, there was a fluctuation at the 140% Duzce test. For the 180% Duzce test, the damping ratio was within the 0 and 20% except a jump at the end of the test.

Table 3.6 summarized the test results for ISF. The physical damage correlation with the cyclic behavior of the test frame is presented in Figure 3.63. This figure indicates the damage on column C3 and first story RC joints at the top of the columns C2 and C3 for 50, 100 140% Duzce test. On the other hand, bottom of the column C2 was indicated for 180% Duzce test.

At 50% Duzce test, flexure cracks were observed throughout the column height. In addition, 45 degree cracks were observed at the beam-column joint. The cracks' widths were limited at this Duzce test. Cracks in the concrete of the composite columns developed during each lateral loading excursion that produced tension in the concrete portion of the composite column section. It was observed that there were no hinges occurred at the bottom of the columns. The strain gage measurements indicated that there was no yielding on IPE200 and steel plates on the first story composite beam (see Appendix 2). The base shear capacity did not drop during this test and elastic behavior was observed during this test (Figure 3.55). As a result, this frame was observed to be in the immediate occupancy performance level. This frame can be used after such an earthquake without any repairing.

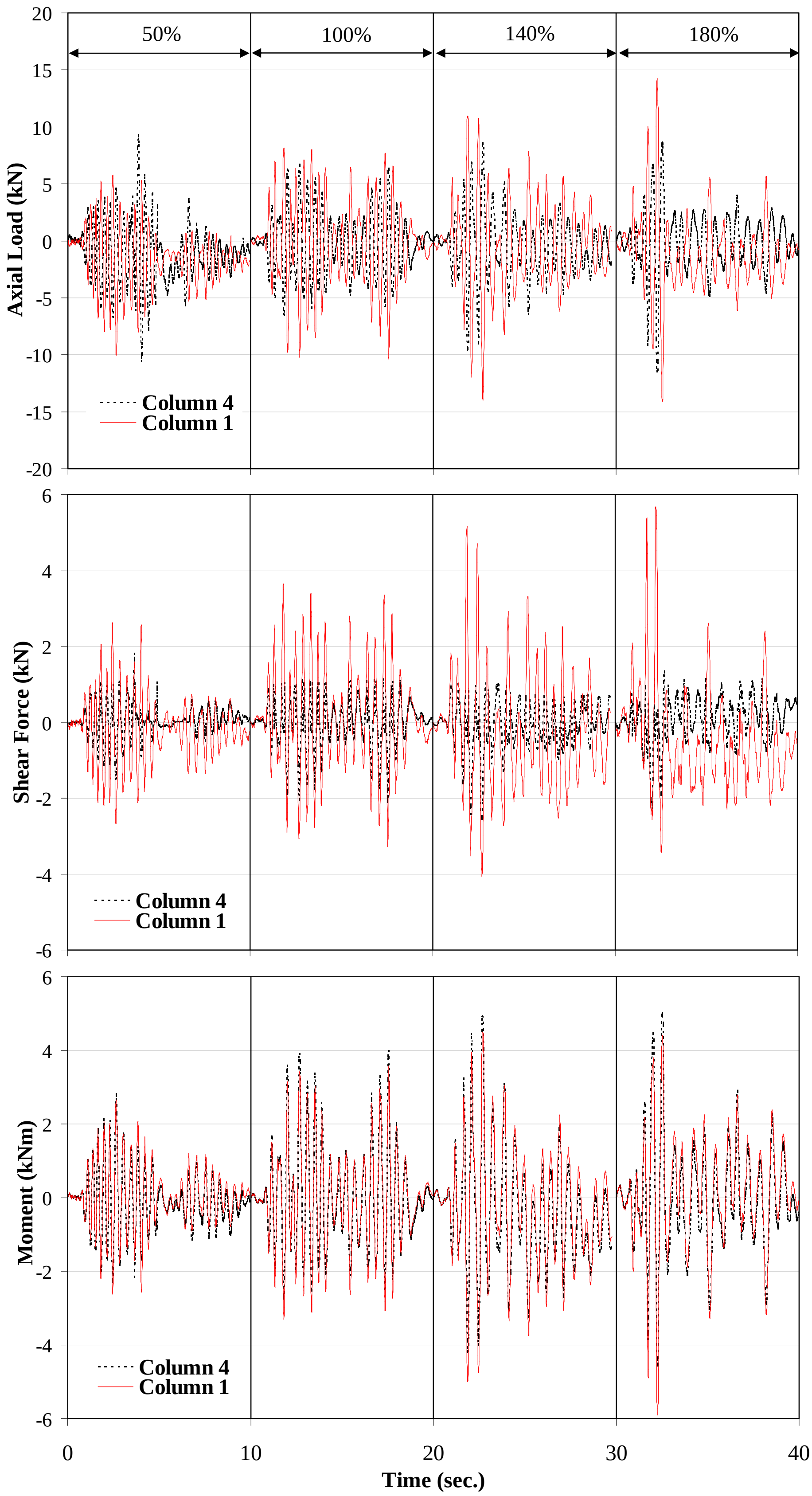

Figure 3.58 Variation at time histories of axial, shear and moment forces for ISF

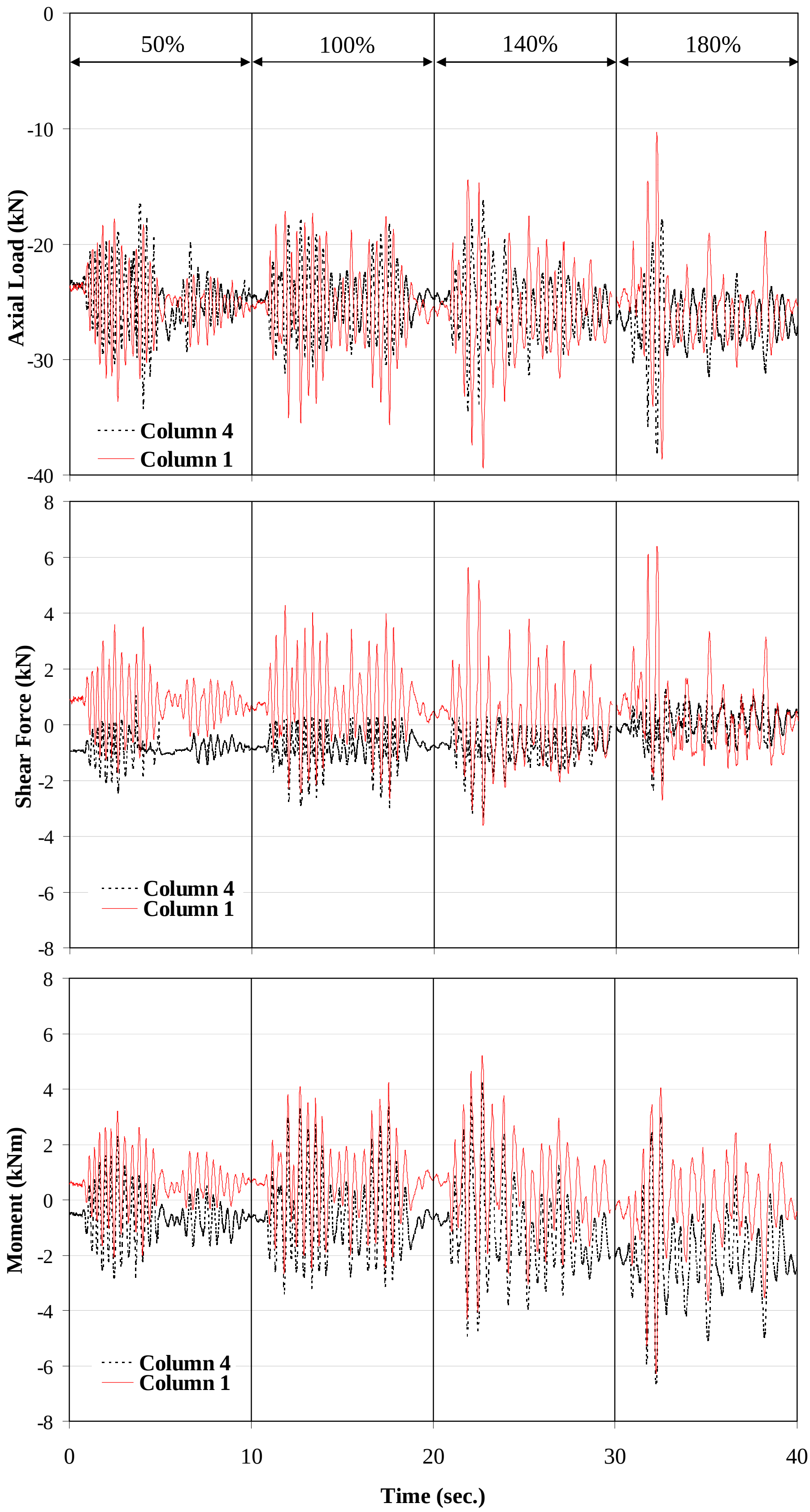

Figure 3.59 Time histories of axial, shear and moment forces for ISF

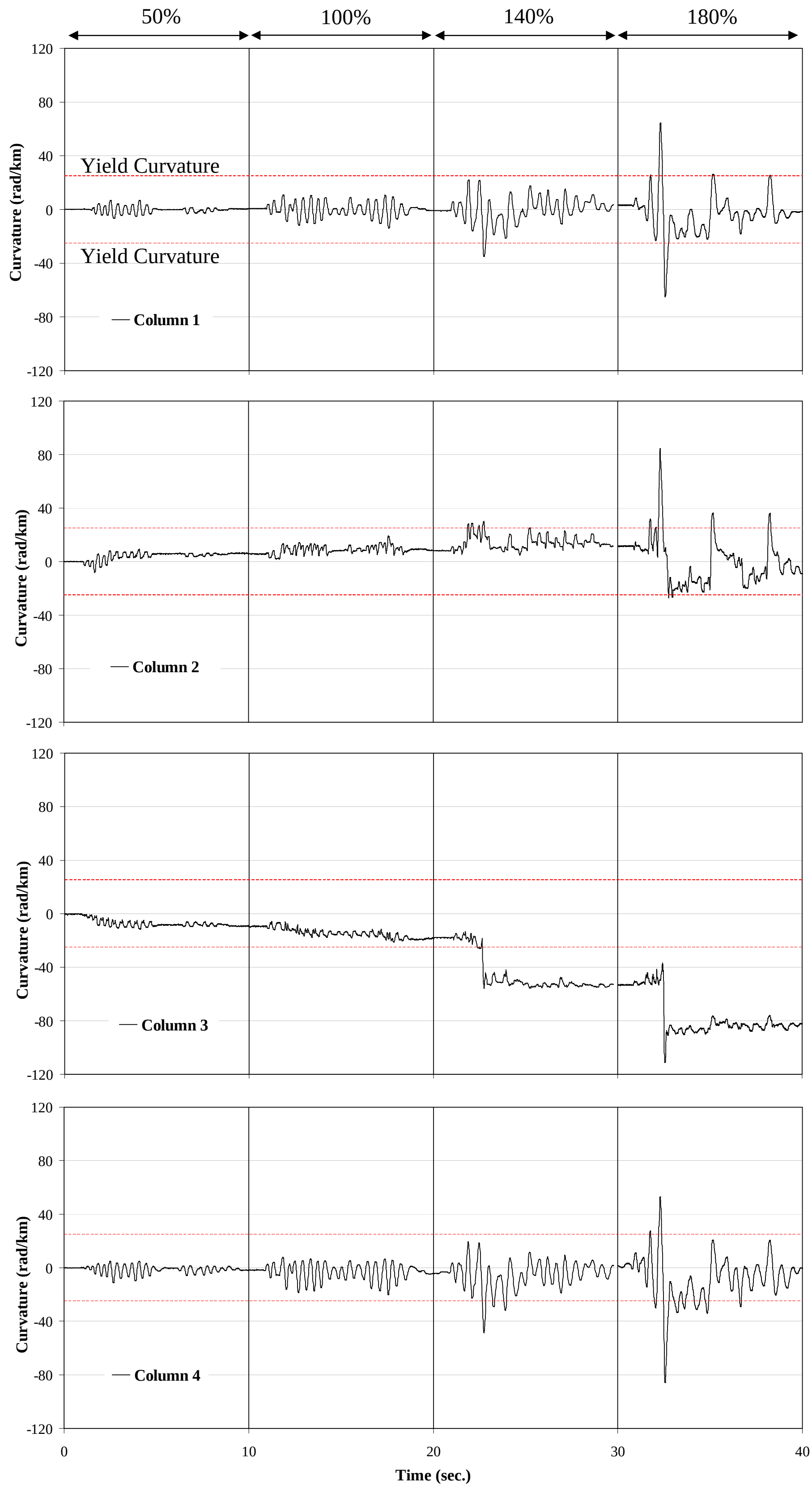

Figure 3.60 Time histories of curvatures at the bottom of the columns for ISF

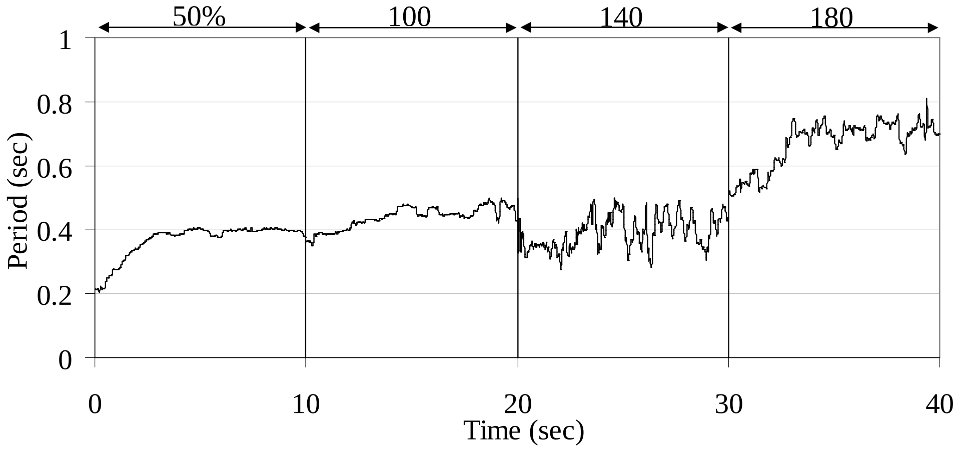

Figure 3.61 Identified period of test specimen for ISF

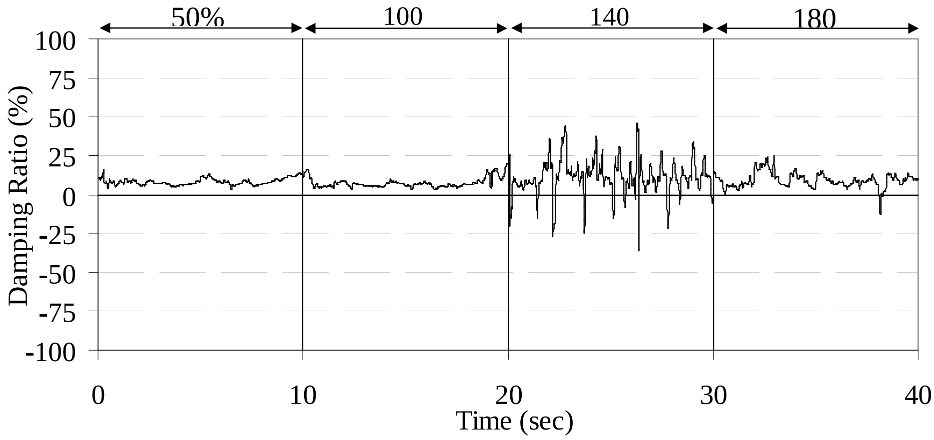

Figure 3.62 Identified damping ratio of test specimen for ISF

Table 3.6 Summary of test results for ISF

Ground Motion	Maximum Displacement Demand (mm)		Maximum Interstory Drift Ratio %		Maximum Story Base Shear Force (kN)		Base Shear Force (kN)	Base Shear Ratio (kN/kN)	Column Plastic Rotation Demands			
									θ_{p1}	θ_{p2}	θ_{p3}	θ_{p4}
	1^{st} Story	2^{nd} Story	1^{st} Story	2^{nd} Story	1^{st} Story	2^{nd} Story			$\mu_{\phi 1}$	$\mu_{\phi 2}$	$\mu_{\phi 3}$	$\mu_{\phi 4}$
50% Düzce	12.6	21.8	0.6	0.7	27.6	49.2	67.6	0.56	0 0	0 0	0 0	0 0
100% Düzce	21.7	39.7	1.1	1.2	34.5	63.2	88.2	0.73	0 0	0 0	0 0	0 0
140% Düzce	40.8	75.6	2	2.3	45.3	84.2	116.6	0.97	0.001 1.4	0.001 1.2	0.004 2.2	0.003 2.0
180% Düzce	57.6	111.9	2.9	3.7	46.5	94.2	123.2	1.03	0.005 2.6	0.008 3.4	0.011 4.5	0.008 3.4

At 100% Duzce test, further cracks developed and spreaded throughout the beam span. On the other hand, further damages were prevented on the beam-column joint by the anchorage rods which were placed to connect the first and second story steel columns and steel plates (Plate 2 and Plate 3 in Figures 3.15 and 3.16) on the top and bottom of the beam. Although there was no yielding at the bottom of the first story columns, the first story composite beam had inelastic behavior. In spite of damage mentioned above, there was no drop in the base shear capacity of the ISF. The maximum IDR was about 1.2 % and an elastic behavior was observed as seen in Figure 3.55 during this test. As a result, this frame was observed to be in the immediate occupancy performance level. This frame can be used after such an earthquake with limited repairing.

At 140% Duzce test, longitudinal bar buckling at the bottom of the column C3 was observed. It progressed between 2^{th} and 3^{rd} seconds of the ground motion. In additional to yielding of steel plate at the bottom and top of the first story composite beam, steel member (IPE200) had inelastic behavior and plastic hinges occurred at the bottom of first story columns. Although such a severe damage occurred, the base shear capacity of ISF did not decrease due to the presence of the steel members. In fact, the lateral strength increased for higher lateral demand. As a result, this frame was observed to be in the life safety performance level. This frame can be used after such an earthquake with repairing.

At 180% Duzce test, spalling of concrete occurred at the bottom of the column C2 between 2^{th} and 3^{rd} second (Figure 3.63). Although there were cracks occurred during previous three tests, no excessive damage was observed at the beam-column joints due to presence of the anchorage rods (ϕ12). Yielding of the steel members (IPE200 and steel plates 2 and 3 in Figure 3.15 to 3.17) were visible during this test as seen in Figure 3.64. Although significant damage (bar buckling, spalling of concrete, cracks on the columns and beam, yielding of the steel members) was observed in the specimen during this test, there was no drop in the base shear capacity. As a result, this frame was observed to be in the collapse prevention performance level. This frame can be used after such an earthquake with proper repairing. The steel column experienced yielding without any weld or connection failure. There was no anchorage rod failure during all tests. The design of composite beam-column joints were successfully during the tests. Although there was not any drop in base shear capacity of the ISF, higher intensity earthquake (220 % Duzce) was not performed due to high IDR which was 3.7% at the 180% Duzce test.

Figure 3.63 Physical damage of the ISF

.

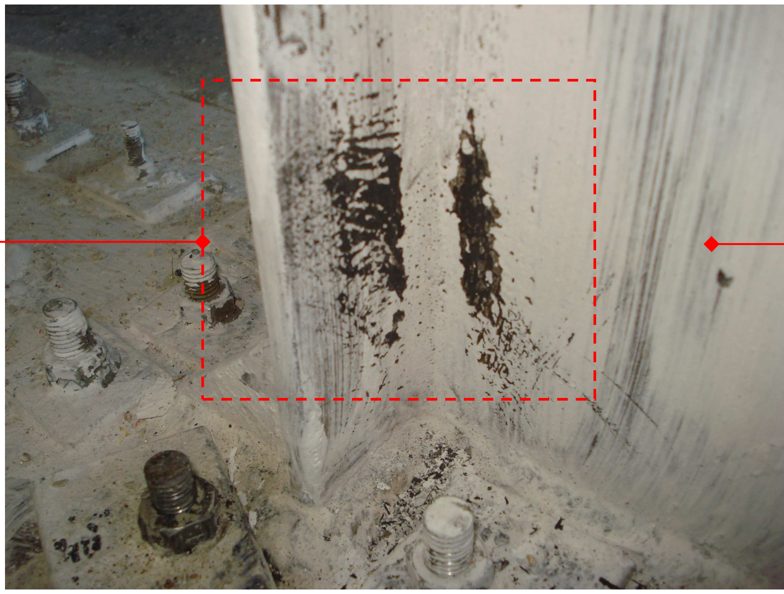

Figure 3.64 Yielding of steel column C3

3.7.4 Discussion on PSD test results

The test results of the reference, chevron braced frame and ISF are compared in this section. Table 3.7 shows the comparison between reference and strengthened frames in terms of base shear, base shear ratio and maximum IDR. As seen in this table, the base shear capacity of the chevron braced frame and ISF were about 3 and 1.8 times that of reference frame, respectively. These results proved that the design target base shear capacities were obtained successfully. The maximum IDR up to end of 140% Duzce test was 4.5, 0.7 and 2.3 % for the reference, chevron braced frame and ISF, respectively. In other words, the chevron braced frames and ISF controlled the IDR 6.4 and 2.3 times more effectively than reference frame, respectively. Figure 3.65 indicates the envelope response obtained from force vs. top displacement behavior of the test frames. These envelopes were plotted for successive tests (50%, 100% and 140% scale) for the reference frame, four tests (50%, 100%, 140% and 180% scale) for the ISF and five tests (50%, 100%, 140%, 180% and 220% scale) for the chevron braced frame. As seen in this figure, there were two separate phenomena for the strengthened techniques. While ISF had a flexible and lower strength but ductile load deformation behavior, chevron braced frame had much stiffer and stronger response with a brittle behavior. The lateral stiffness defined as the ratio between yield strength and top displacement was 4, 8.8 and 2.3 kN/mm for the reference, chevron braced and ISF frames, respectively. The lateral stiffness of the chevron braced frame was two times that of reference frame. On the other hand, lateral stiffness of the reference frame was 1.7 times that of ISF. The high lateral stiffness resulted in lower first mode fundamental period hence the chevron braced frame experienced lower lateral demand imposed by the Duzce ground motion (Figure 3.66). On the other hand, the lower lateral stiffness resulted in higher first mode fundamental period hence the ISF experienced higher lateral demand imposed by the Duzce ground motion. In this case, the maximum IDR should be kept in the desired levels. Furthermore, the flexible behavior of systems such as ISF could be undesirable for the non-structural elements and occupants. On the other hand, chevron braced frame kept down IDR hence it prevents the damage on non-structural components and disturbing the occupants.

Table 3.8 compares the plastic rotation and curvature ductility of the reference frame, chevron braced frame and ISF obtained at the bottom of all columns. As seen here, plastic rotation started to develop at the 50 and 100 Duzce tests for the reference frame. On the other hand, none of the strengthened frames had plastic rotation at these tests. For higher lateral demands, plastic rotation occurred for the chevron brace frame and ISF while that was excessive for the reference frame.

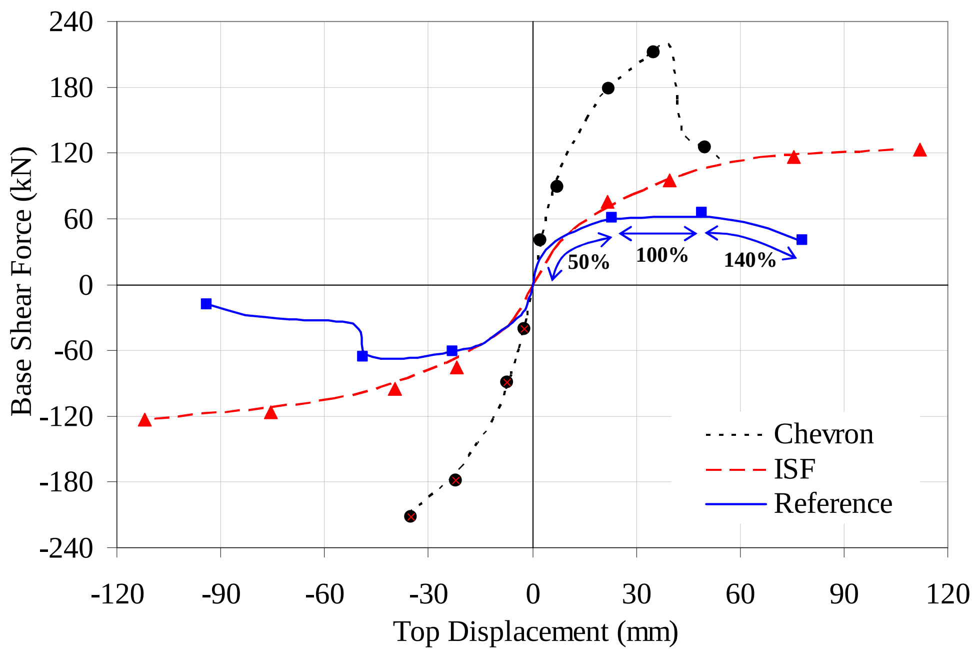

Figure 3.65 Envelope response of the test frames

Table 3.7 Comparison of the all test results in terms of base shear, base shear ratio and IDR

Ground Motion	Base Shear Force (kN)			Base Shear Ratio (kN/kN)			Maximum Inter-story Drift Ratio (%)					
							1. Story			2. Story		
	Reference	Chevron	ISF	Reference	Chevron	ISF	Reference	Chevron	ISF	Reference	Chevron	ISF
50% Duzce	60.4	39.9	67.6	0.50	0.33	0.56	0.7	0.1	0.6	0.6	0.1	0.7
100% Duzce	67.9	89.1	88.2	0.57	0.74	0.73	1.8	0.2	1.1	1.1	0.2	1.2
140% Duzce	54.5	179.0	116.6	0.45	1.49	0.97	4.5	0.7	2.0	1.4	0.6	2.3
180% Duzce	*	206.1	123.2	*	1.72	1.03	*	0.9	2.9	*	1.1	3.7
220% Duzce	*	219.4	*	*	1.83	*	*	1.0	*	*	2.7	*

*: Not tested, Base Shear Ratio: Ratio between base shear force and frame weight

Table 3.9 shows the performance of the test frame resulted from damage observation and measurements during the tests. At the end of the 140% Duzce test, while reference frame was within the CP performance level, the chevron braced frame and ISF were within the IO and LS performance level, respectively. This table indicates that strengthened frames with chevron and ISF were effective methods to upgrade deficient existing RC frames. Table 3.7 and 3.9 explored that LS performance level for the chevron braced frame and ISF was satisfied at the 0.9 and 2 % DR for the first story and it was 1.1 and 2.3 % DR for the second story, respectively. Consequently, the target DRs was found to be 1 and 2 % DR for the former and latter retrofitted techniques, respectively.

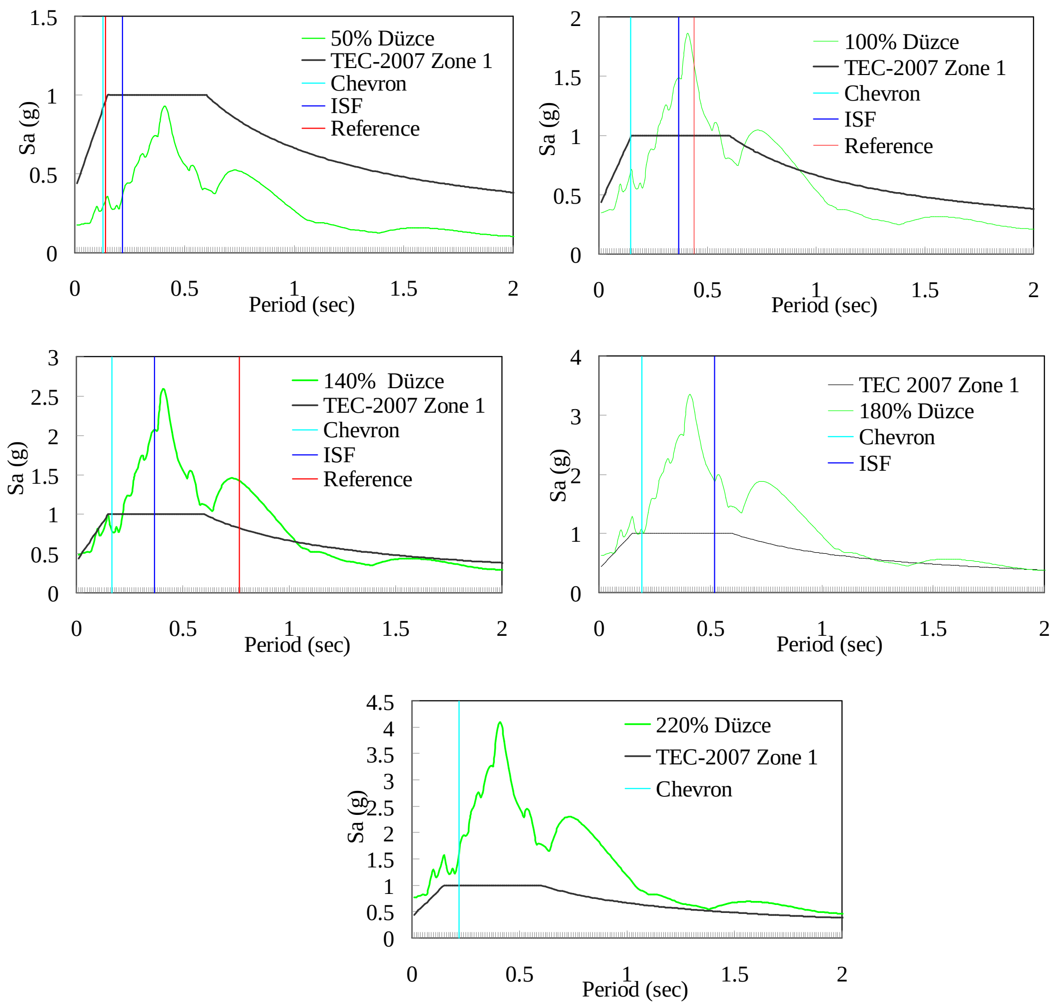

Figure 3.66 Demands of the specimens at the initial period

Table 3.8 Comparison of the all test results in terms plastic rotation and curvature ductility

Ground Motion	Column Plastic Rotation Demands											
	Column C1			Column C2			Column C3			Column C4		
	plastic rotation(θ_p)			plastic rotation(θ_p)			plastic rotation(θ_p)			plastic rotation(θ_p)		
	curvature ductility (μ_ϕ)			curvature ductility (μ_ϕ)			curvature ductility (μ_ϕ)			curvature ductility (μ_ϕ)		
	Reference	Chevron	ISF	Reference	Chevron	ISF	Reference	Chevron	ISF	Reference	Chevron	ISF
50% Düzce	0	0	0	0.003	0	0	0.001	0	0	0	0	0
	0.3	0	0	1.9	0	0	1.5	0	0	0.6	0	0
100% Düzce	0.004	0	0	0.006	0	0	0.008	0	0	0.006	0	0
	2.0	0	0	2.8	0	0	3.5	0	0	2.6	0	0
140% Düzce	0.038	0	0.001	0.055	0.011	0.001	0.025	0	0.004	0.036	0	0.003
	9.4	0	1.4	16.9	4.4	1.2	8.3	0	2.2	11.5	0	2.0
180% Düzce	-	0	0.005	-	0.013	0.008	-	0.005	0.011	-	0	0.008
	-	0	2.6	-	4.9	3.4	-	2.4	4.5	-	0	3.4

Table 3.9 Performance of the test frames

Ground Motion	Performance Level		
	Reference	Chevron	ISF
50 % Duzce	IO	IO	IO
100 % Duzce	LS	IO	IO
140 % Duzce	CP	IO	LS
180 % Duzce	-	LS	CP

IO; immediate occupancy, LS; life safety, CP; collapse prevention

CHAPTER 4

4. NUMERICAL SIMULATIONS

4.1 Introduction

The numerical simulations of the test frames were performed in this chapter. The main objective of numerical simulation was to improve the understanding of the behavior of the test frames and calibrating proper parameters to be used in the case studies. For the cyclic test frames which were one bay one story frames (Chapter 2) a nonlinear static pushover analysis was performed. The performance levels of the members of these frames were determined and labeled on each DR-base shear force plot. The performance levels of the RC frame members were determined from the limit states suggested by the TEC (2007). The pseudo dynamic test frames were also analyzed by using nonlinear time history analysis procedure. The Duzce ground motion which was employed for the tests were utilized in these analyses. Furthermore, an existing deficient 5 story RC building was examined before and after retrofitting in this chapter.

4.2 One Bay-One Story Frames

The nonlinear static pushover analysis was performed by utilizing structural analysis program (SAP2000). The material properties used in the numerical simulations were taken from Chapter 2. Longitudinal bar buckling was modeled by employing the backbone curve of Dhakal and Maekawa (2002) (Figure 4.1). Mander et al. (1988) confined concrete model was used as the concrete model (Figure 4.1).

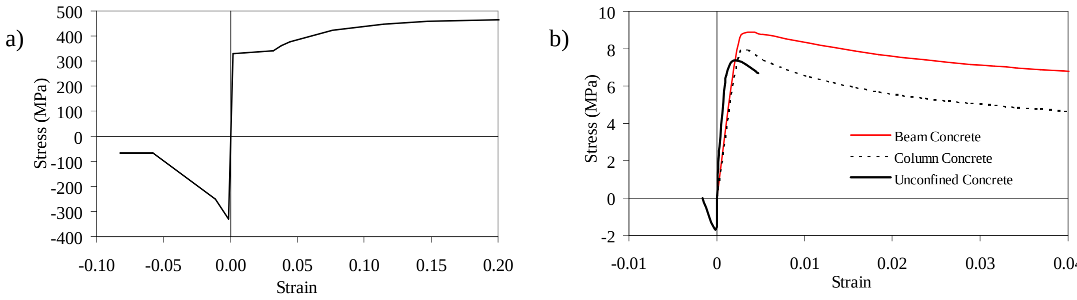

Figure 4.1 Stress-Strain curve a) longitudinal reinforcement, b) confined concrete

First, moment curvature of the RC columns and beams were obtained for the sections defined in Chapter 2. These moment curvature relations were converted into moment-rotation relations to assign plastic hinge properties by utilizing following equations. The yield and plastic rotations can be calculated by using Equation 4.1 and 4.2. In these equations, plastic hinge length was assumed as half of the section height in compliance with TEC (2007).

$$\theta_y = \frac{\phi_y \times L}{6} \tag{4.1}$$

$$\theta_p = (\phi_p - \phi_y) \times L_p \tag{4.2}$$

$$L_p = 0.5h \tag{4.3}$$

Where,

θ_y and θ_p; yield and plastic rotation

ϕ_y and ϕ_p; yield and plastic curvature

L; member length

L_p; plastic hinge length

h; member cross section height

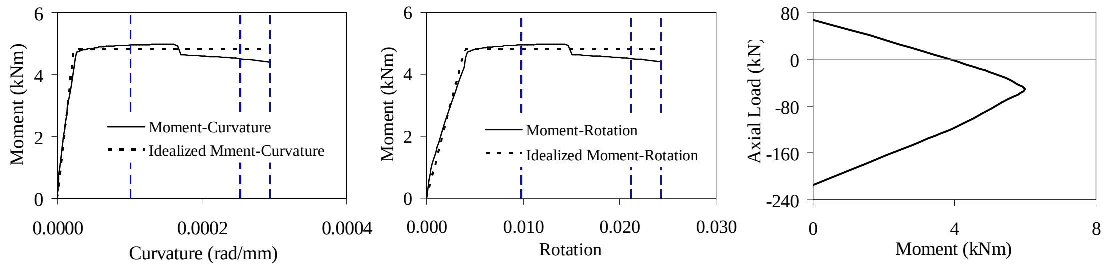

Figure 4.2 a) Moment-Curvature, b) Moment-Rotation and c) Moment-Interaction relation of the column for specimen R_13_10 (N/No=0.13)

As suggested by the TEC (2007), the moment rotation relation can be modeled as elastic perfectly plastic response. Hence, after yielding, no hardening was used to model the moment rotation behavior. The moment interaction relations were used to account the moment capacity change with axial force.

It can be observed that the performance of the RC member depends on the reinforcement and concrete strain (Figure 4.3). The following equations were defined in TEC (2007) for minimum damage (MnD), moderate damage (MdD) and severe damage (SD) performance levels. In this chapter, when the strain limits exceeded the proposed limits below, the name of the abbreviation namely MnD, MdD and SD were used. Beyond the SD performance level, total collapse (TC) was used (Figure 4.3).

MnD performance level;

$$(\varepsilon_{cg})_{MnD} = 0.0035$$

$$(\varepsilon_s)_{MnD} = 0.010$$

MdD performance level;

$$(\varepsilon_{cg})_{MdD} = 0.0035 + 0.01(\rho_s / \rho_{sm}) \leq 0.0135$$

$$(\varepsilon_s)_{MdD} = 0.040$$

SD performance level;

$$(\varepsilon_{cg})_{SD} = 0.004 + 0.014(\rho_s / \rho_{sm}) \leq 0.018$$

$$(\varepsilon_s)_{SD} = 0.060$$

Where,

ε_{cu}; concrete strain at the top fiber

ε_{cg}; concrete strain at the top fiber of the confined concrete

ε_s; Reinforcement bar strain

ρ_s; available volumetric ratio of the stirrup of the member

ρ_{sm}; volumetric ratio of the stirrup of the member calculated by utilizing the TEC (2007)

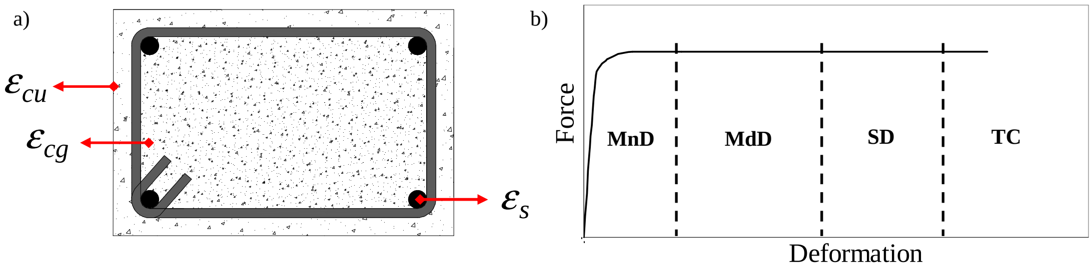

Figure 4.3 a) Strain at the cross section of the RC member, b) performance limits

4.2.1 Numerical Simulations of Reference Frames

The numerical simulations of the reference frames were performed by using two modeling approaches namely distributed (Figure 2.2-b) and lumped plasticity (Figure 4.4) modeling in order to compare the test and numerical simulation results. Figure 4.5-a shows the test and two numerical simulation results. The lumped plasticity model (performed by using Structural Analysis Program (SAP2000)) estimated the lateral strength higher than the test results. Moreover, the difference is lower for the distributed plasticity model (performed by using Opensees simulation platform). The reason of this discrepancy can be due to deviation of clear cover and spatial variability in material strength. A parametric study was performed to examine the effect of longitudinal reinforcement yield strength and clear cover on the response. When the lower bound values for the longitudinal reinforcement strength (220 MPa) and clear cover (12 mm) was utilized, the lateral strength estimation was lower than the test result. On the other hand, the estimated lateral strength was higher than the test results for the upper bound values (Figure 4.5-a). This shows that the test results are somewhat in between the expected range of numerical estimations. Furthermore, it should be mentioned that the distributed plasticity model gives better lateral strength estimation but it is more complex to be used in 3D building simulations. Therefore, the lumped plasticity model was used to simulate the test frames and in the case studies.

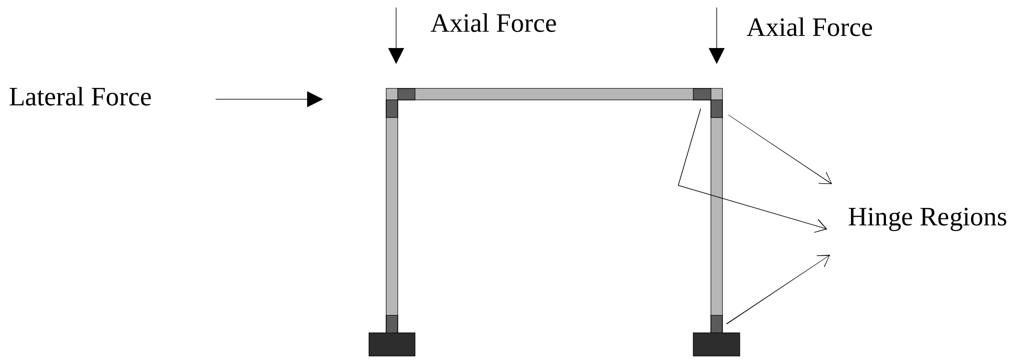

Figure 4.4 Analytical model of the reference frame (Lumped plasticity model)

The results of the nonlinear static pushover analysis are shown in Figure 4.5-b and c for the reference frames R_13_10 and R_25_8.1. This figure indicates the performance levels of the columns. There is colored area of bounded regions for each performance level of the columns. Beginning and ending of this boundary indicates the performance levels when any column enters and all of the columns exceed the labeled performance limits. For example, in Figure 4.5-c, first MnD performance level was exceeded at the bottom of the right column (first line of the colored area for MnD) at about 0.7 % IDR and the last MnD performance level was exceeded at the top of the right column (last line of the colored area for MnD) at 1.1 % IDR. It was observed that the high axial load resulted in lower drift capacity at the SD performance level. The average DR at each performance levels are also summarized in Figure 4.5. The numerical simulation indicated that the average DR of specimen R_13_10 at each performance level was about 1.4 times higher than that of specimen R_25_8.1.

Case	Lower Bond	Upper Bond
Long. Reinf. Strength (Mpa)	220	420
Clear Cover (mm)	12	8

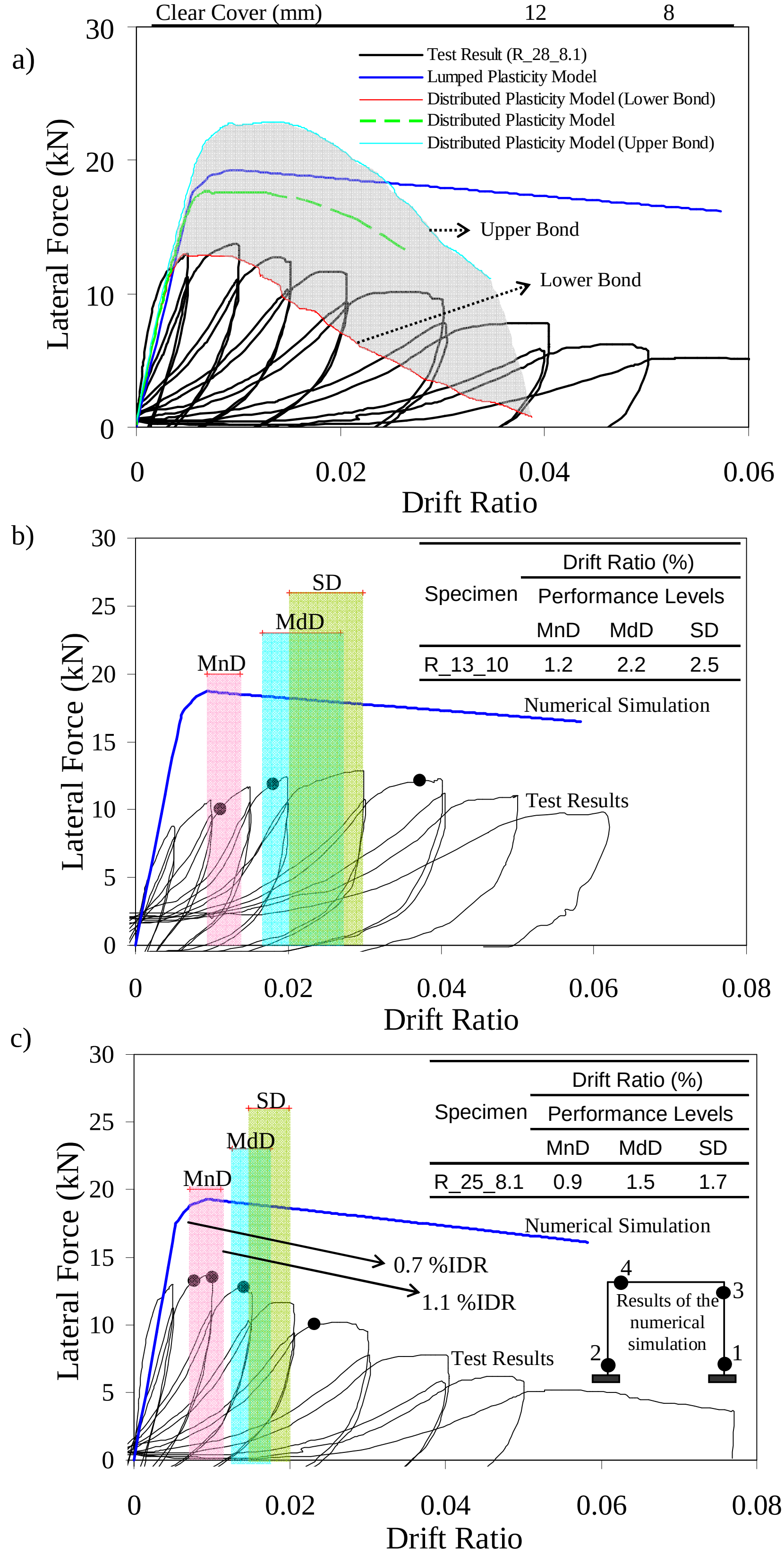

Figure 4.5 Numerical results of the reference frames

4.2.2 Numerical Simulation of the Chevron Brace Strengthening Frames

The numerical simulation techniques of the chevron brace strengthening frames were similar to the reference frame with respect to RC frame modeling approach. The brace force-deformation relation suggested by the ASCE/SEI 41 (2007) document which was utilized to model the braced frame specimens along with proposed American Institute of Steel Construction AISC (2005) equations (Equations 4.4 to 4.7). In Equations 4.8 and 4.9 taken from ASCE/SEI 41 (2007), the values given as axial deformations for each performance levels of the brace compression members are the plastic deformations (Figure 4.6).

$$Fe = \frac{\pi^2 E}{\lambda^2} \tag{4.4}$$

$$\lambda \le 4.71\sqrt{\frac{E}{F_y}} \text{ or } F_e > 0.44 \times F_y \rightarrow F_{cr} = \left[0.658^{\frac{F_y}{F_e}}\right] F_y \tag{4.5}$$

$$\lambda > 4.71\sqrt{\frac{E}{F_y}} \text{ or } F_e < 0.44 \times F_y \rightarrow F_{cr} = [0.877] F_e \tag{4.6}$$

$$\varphi P_c = 0.9 \times F_{cr} \times A_{gb} \tag{4.7}$$

Fe; elastic critical buckling

λ; slenderness ratio

Fcr; critical stress

P_{bc}; compression capacity of the brace member

A_{gb}; brace area

$$\lambda \ge 4.2\sqrt{E/F_y} \rightarrow \mathrm{IO}: 0.25\Delta_c, \mathrm{LS}: 5\Delta_c, \mathrm{CP}: 7\Delta_c \tag{4.8}$$

$$\lambda \le 2.1\sqrt{E/F_y} \rightarrow \mathrm{IO}: 0.25\Delta_c, \mathrm{LS}: 4\Delta_c, \mathrm{CP}: 6\Delta_c \tag{4.9}$$

Where,

E, F_y : Elastic modules and yield strength of the brace members, respectively.

Δ_c : Axial deformation at the brace buckling

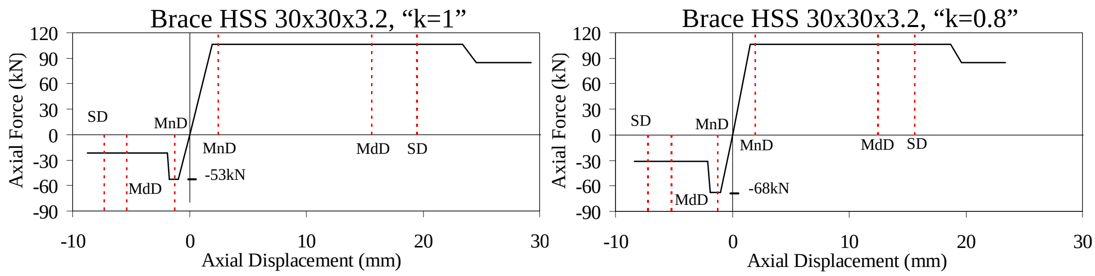

Figure 4.6 Force-Deformation relation of the brace member HSS 30x30x3.2

The buckling load was determined from the AISC (2005) manual. The effective length factor was assumed as one, which defines the pin-pin connection at both brace ends. In addition, Figure 4.6 shows the results for the two different “k=1” and “k=0.8” values (53 and 68 kN, respectively) to show the variation of buckling load with k factor. Besides, this figure also indicates the brace performance levels suggested by the ASCE/SEI 41 (2007) document. The brace length was taken as the actual brace member length (Figure 4.7). Instead of nominal material properties of the brace member, the measured brace yield strength was employed (see Chapter 2). Rigid end zone was defined from RC frame members to gusset plate where at the end of brace weld. At these points, gusset plates rotated freely as expected. The nonlinear static pushover analysis results of the chevron braced frames are indicated in Figure 4.8 and 4.9. In this figure, the boundaries of the performance levels of the columns determined from limits suggested by the TEC (2007) are indicated. In addition, the average values of the performance levels (MnD, MdD and SD) of the columns are indicated as a table on each figure. Furthermore, the brace performance levels determined from the limits suggested by the ASCE/SEI 41 (2007) were also marked as a line on each figures for the compression brace member. Table 4.1 summarized the performance levels of the RC frame (TEC, 2007) and brace members (ASCE/SEI 41, 2007). Figure 4.10 indicates the performance levels of the brace members considering the brace slenderness and IDR of the braced frames.

It was observed that the results of the nonlinear static pushover analysis had lower base shear capacity than test frames. This is because, the brace force deformation relation had significant effect on the base shear of the braced frame. Since the force-deformation capacities of the brace members were determined from the slenderness, the effective length factor “k” should be determined properly. Figure 4.8-b indicates that when the “k” is equal to 0.8 instead of 1, the numerical simulations match better with the measured base shear force.

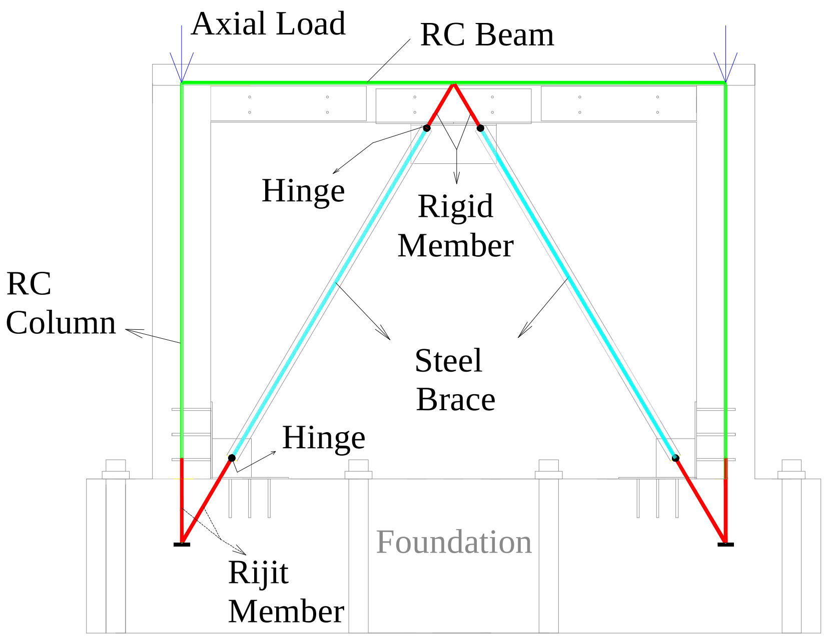

Figure 4.7 Analytical model of the braced frame

It was observed that the brace members have limited effects on the performance levels of the RC columns. Besides, the performance levels of the RC columns depend on the axial load level significantly. All the performance levels of the RC columns were beyond that of compression brace members. This revealed that the post buckling capacity of the brace members can be used for a seismic retrofit design as far as the RC columns are within the acceptable performance levels. Figure 4.10 indicates that reducing the brace slenderness increase the IDR capacity at which the compression brace reaches its performance levels (MnD, MdD and SD). Moreover, results imply that post buckling compression capacity of braces can be relied on at limit states provided that the seismic IDR demands are kept strictly below about 1% DR, which can be critical for seismically deficient axial load bearing RC members (Figure 4.8 and 4.9 and Table 4.1).

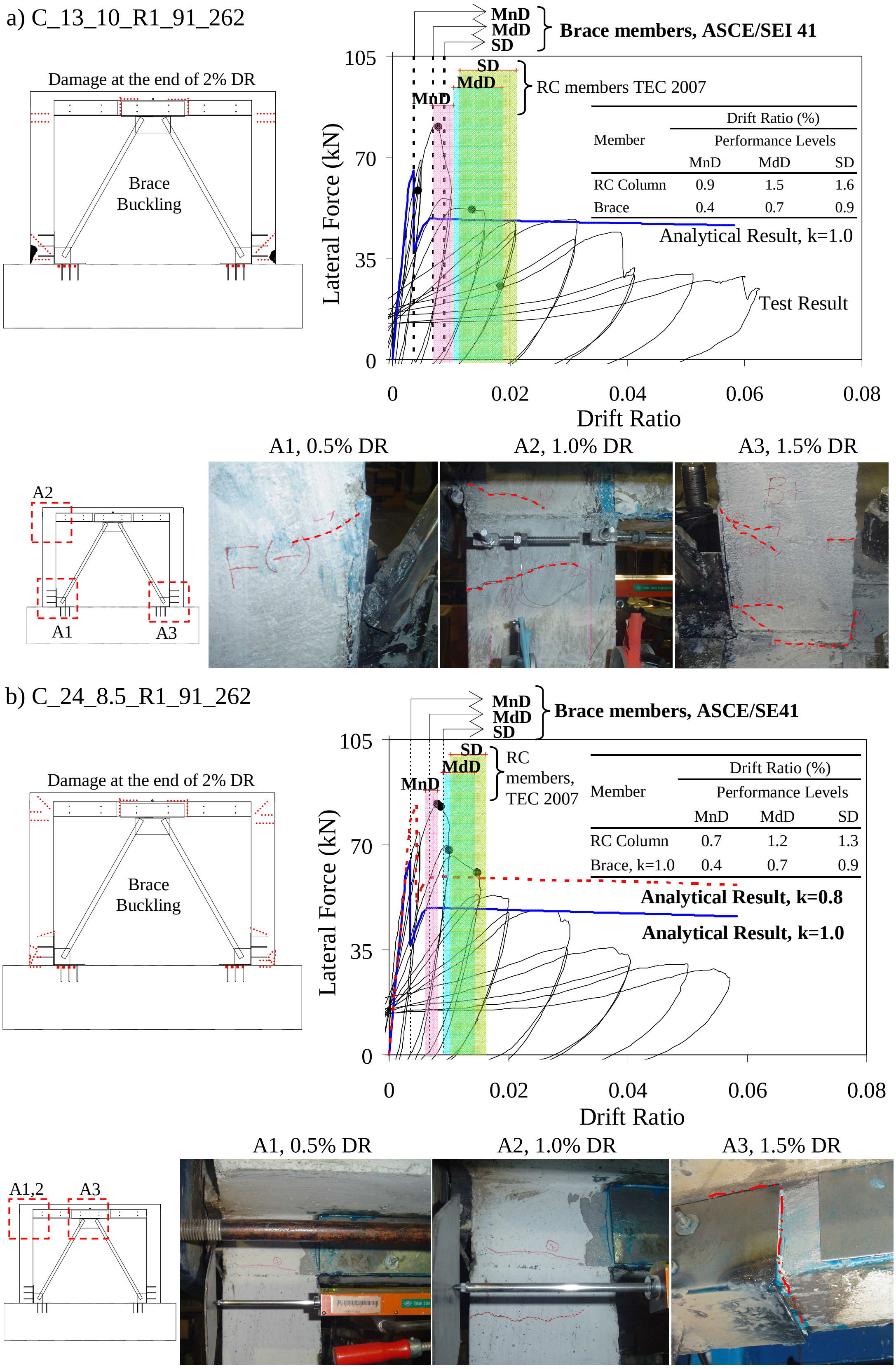

Figure 4.8 Numerical results of the specimens a) C_13_10_R1_91_262 and b) C_24_8.5_R1_91_262

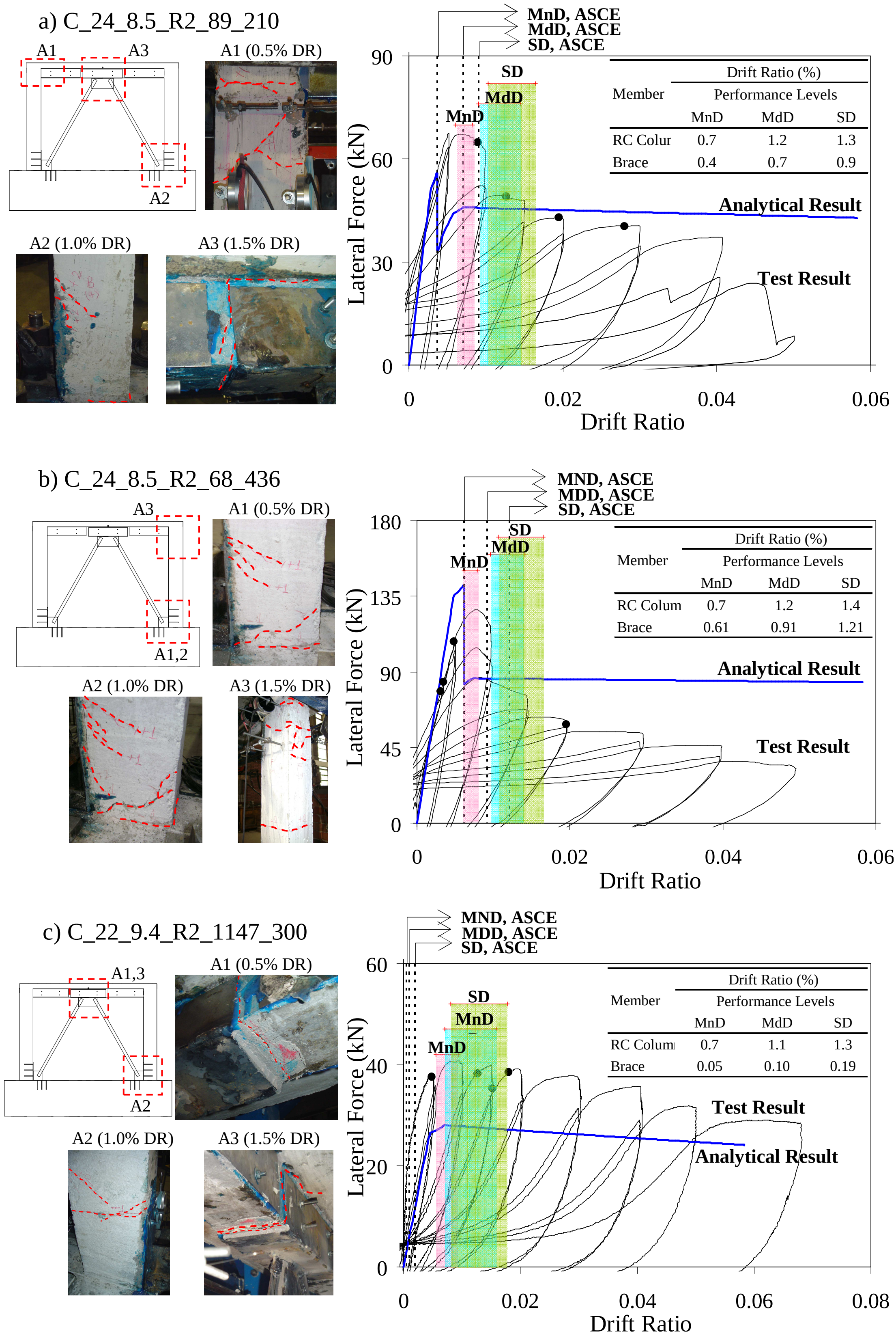

Figure 4.9 Numerical results of the specimens a) C_24_8.5_R2_89_210, b) C_24_8.5_R2_68_436 and c) C_22_9.4_R2_1147_300

Table 4.1 Performance of the reference and chevron braced frame

Specimen	Performance Level								
	RC Column			RC Beam			Brace Member		
	MnD	MdD	SD	MnD	MdD	SD	MnD	MdD	SD
R_13_10	1.16	2.18	2.50	1.28	3.32	4.70	-	-	-
R_25_8.1	0.92	1.51	1.74	1.21	3.22	4.66	-	-	-
C_13_10_R1_91_262	0.86	1.45	1.63	0.93	2.01	2.71	0.36	0.68	0.88
C_24_8.5_R1_91_262	0.71	1.16	1.33	0.95	2.12	2.95	0.36	0.67	0.90
C_24_8.5_R2_89_210	0.71	1.18	1.34	1.03	2.17	2.98	0.37	0.70	0.91
C_24_8.5_R2_68_436	0.70	1.19	1.36	1.06	2.15	2.96	0.61	0.91	1.21
C_22_9.4_R2_1147_300	0.74	1.15	1.29	0.60	2.23	2.23	0.05	0.10	0.19

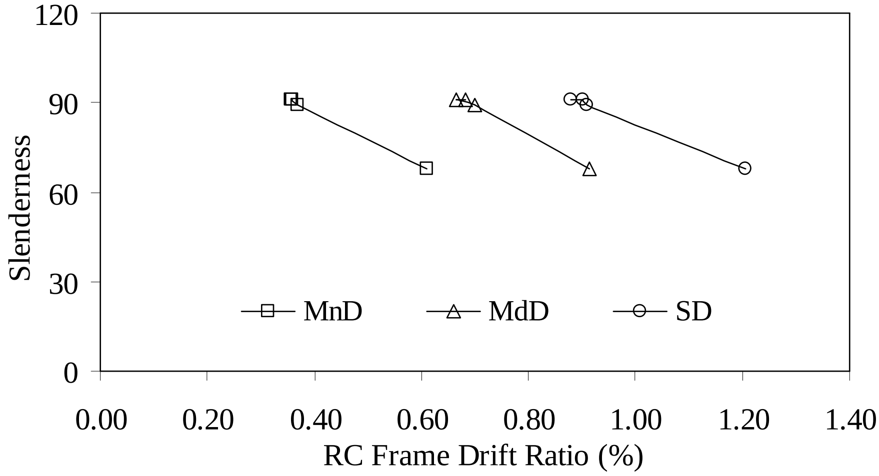

Figure 4.10 Performance relations of the brace members with respect to slenderness vs. drift ratio of the braced frame

4.2.3 Numerical Simulation of the Internal Steel Frame

The ISF strengthened test specimen ISF_28_7.4_III_IS was examined by using lumped plasticity modeling technique among other specimens retrofitted by using ISF (Chapter 2). This is due to the superior cyclic performance obtained from this specimen which employed composite connection details (method III) explained in Chapter 2. It should be kept in mind that there are no specific performance limits suggested for composite members to the best of the authors' knowledge. Hence, the performance levels of the ISF were linked to the strains of the concrete, longitudinal reinforcement and ISF members (I section). These strain limits were similar to the strain limits suggested by the TEC (2007). It was assumed that the strain limits of the ISF members (I- sections) for performance levels were same as that of longitudinal reinforcement.

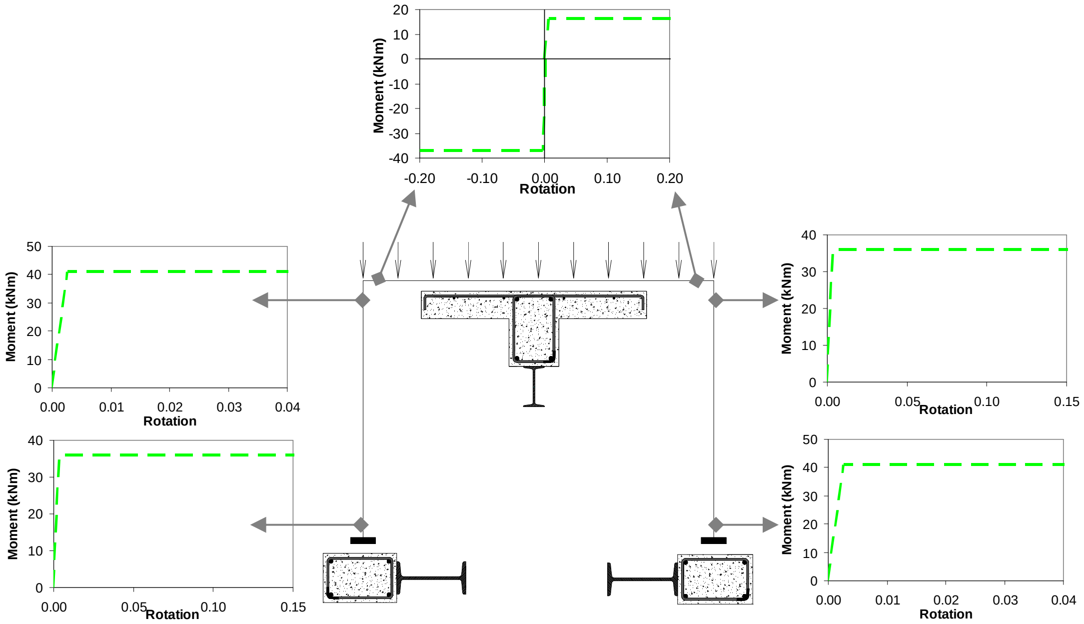

Figure 4.11 Analytical model of the ISF

Figure 4.11 presents the analytical model of the ISF. First, moment rotation relations were developed for sections presented in Chapter 2. The composite column and beam members had unsymmetrical moment curvature relation. When the composite section was under positive bending, the steel member (I-80 for beam and I-140 for column) was under tension and the concrete was under compression. At the negative bending direction, this case was reversed. Hence, two different moment curvature relations were developed for both composite columns and beam. The moment curvature relation was converted into moment rotation relation. The plastic hinge length was assumed as half of the section height (TEC, 2007). P-Δ effect was incorporated into the analytical model. The moment interaction relations of the composite columns were used to account the moment capacity change with axial force.

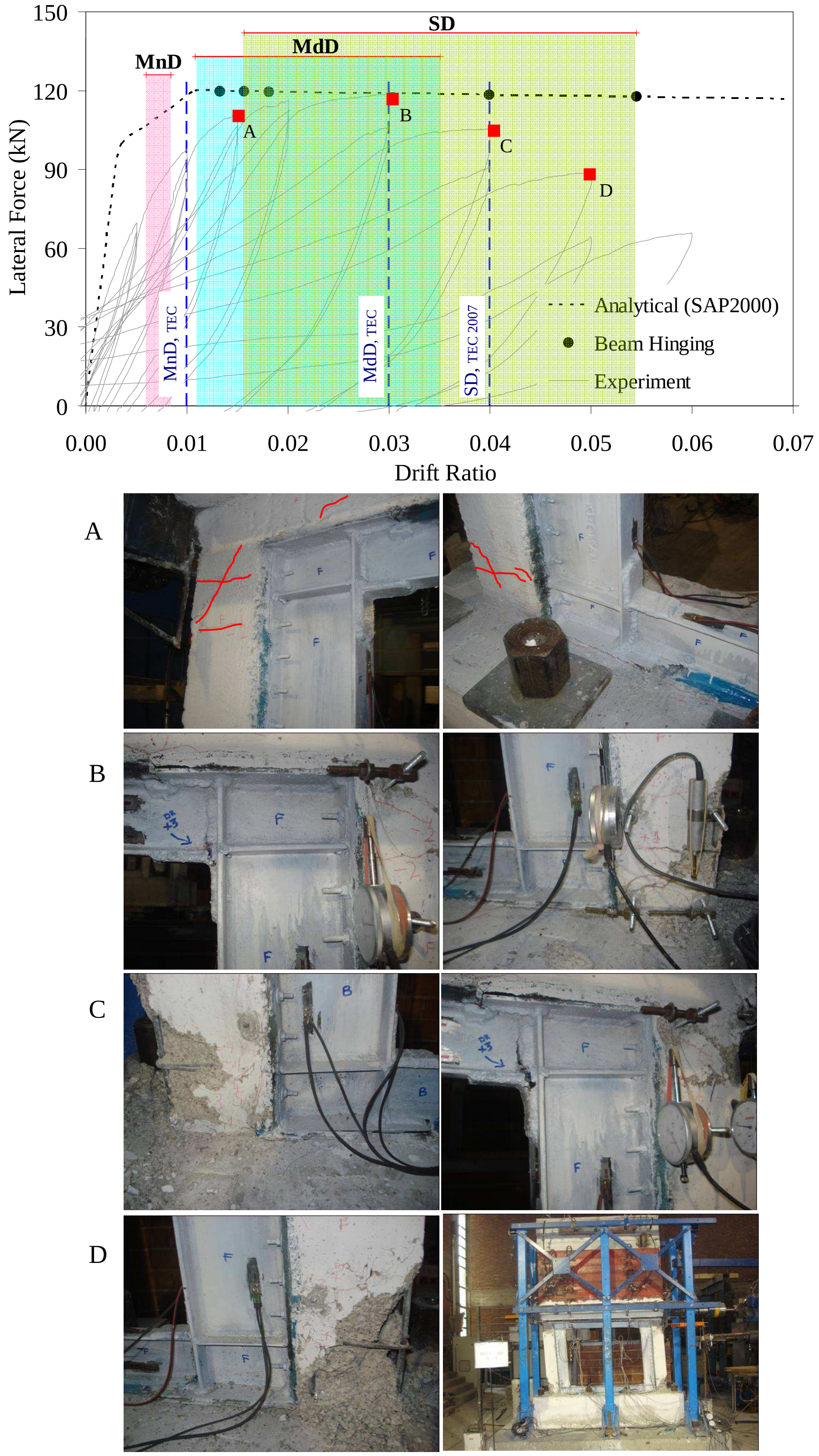

A; Crack iniation, B; Fracture initiation of the steel beam, C; Concrete spalling at the bottom of the column, D; Base hinge mechanism and lateral displacement at 5% DR.

Figure 4.12 Results of the nonlinear static pushover for the ISF

Figure 4.12 presents the static pushover curve of specimen ISF_28_7.4_III_IS. This figure also indicates the damage levels of the columns and beams in terms of the DRs estimated by using the strain limits given in TEC (2007). Each performance levels indicated in Figure 4.12 exceeded the suggested strain limits at the bottom and top of the columns. Furthermore, at the end of each performance levels, the damage observed during the test are also seen in Figure 4.12. The global IDR limits suggested in TEC (2007) are marked on this figure at 1, 3 and 4%. The average DR of the each three performance levels were found as about 0.72, 2.30 and 3.51 %, respectively. As a result of the numerical simulation and observed frame damage, 2% DR was found to be a target design limit for primary design in order to satisfy MnD performance level.

4.3 Numerical Simulation of the Pseudo Dynamic Test Frames

4.3.1 Reference Frame

Nonlinear time history analyses (NTHA) of the reference frame was examined and the details of the results are elsewhere (Akpınar, 2010; Kurt et al., 2011; Akpınar et al., 2011). Although the details are available in these three references, the brief summary about the modeling strategy and results of the reference frame is given in this section. NTHA was performed by utilizing Opensees Simulation Platform (Mazzoni et al., 2009) to observe the ability of estimating the dynamic response of the test frame. Modeling strategy and material models employed for the analysis are summarized in Figure 4.13. Force based fiber frame elements (nonlinearBeamColumn) were used to model RC beam and columns. The material model used for concrete (Concrete01) follows the rules of the confined and unconfined concrete models proposed by Kent and Park (1971) with plastic offset rules proposed by Karsan and Jirsa (1969) (Figure 4.13). The infill walls were modeled as truss members. To simulate the infill wall damage as observed during the test, an element removal algorithm was used. In this algorithm, when the failure strain of the diagonal strut is exceeded in one direction, the struts in both directions are removed from the model (Talaat and Mosalam, 2009). Hence, there were two models namely model with element removal algorithm and model without element removable algorithm (Akpınar, 2010; Kurt et al., 2011; Akpınar et al., 2011). For RC columns second order effects were also taken into account. Linear geometric transformation was used for RC beams due to insignificant effect of geometric nonlinearity on results.

Figure 4.14 shows the results of the NTHA for the reference frame in term of top story displacement vs. time for each scaled Duzce motions. As it is clearly seen in this figure, the model with element removable algorithm predicted the top story displacement demand better than the model without element removable algorithm. Furthermore, the numerical simulation of the reference frame was also capable of tracing force-displacement response of the test frame with a reasonable accuracy (Figure 4.15). The performance evaluation of the reference frame indicated that the observed damage and member performance levels suggested by the TEC (2007) agreed well (Figure 4.16).

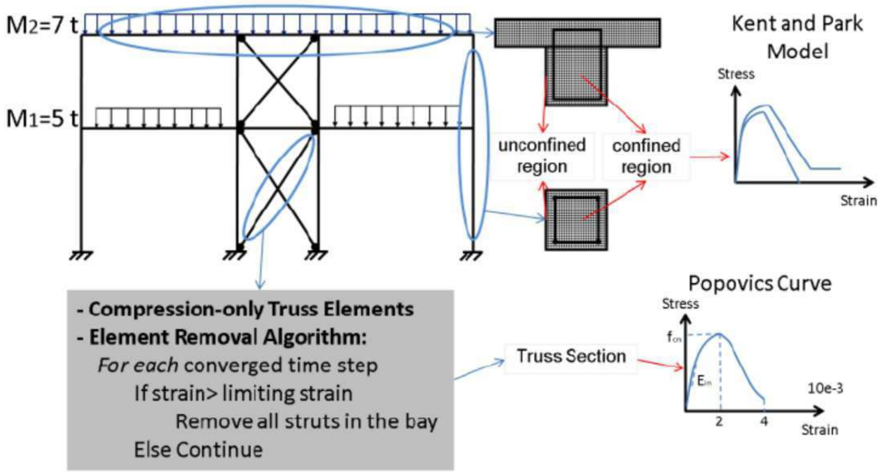

Figure 4.13 Infill wall layout and analytical model of the reference frame (Akpınar, 2010)

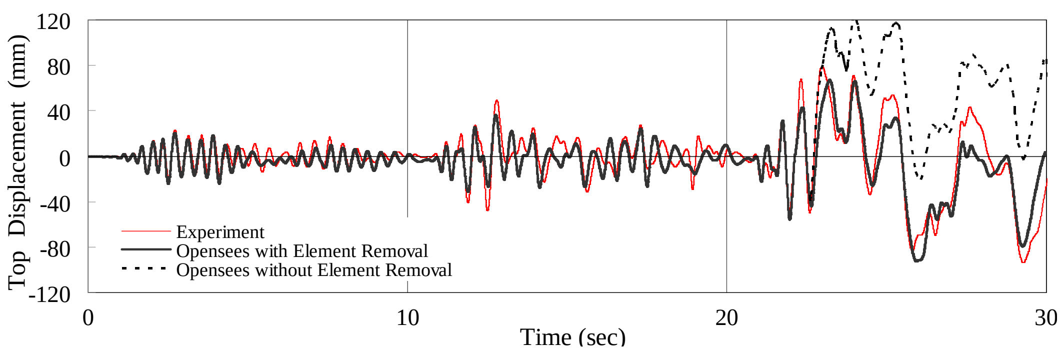

Figure 4.14 Results of the NTHA of the reference frame (Akpınar, 2010)

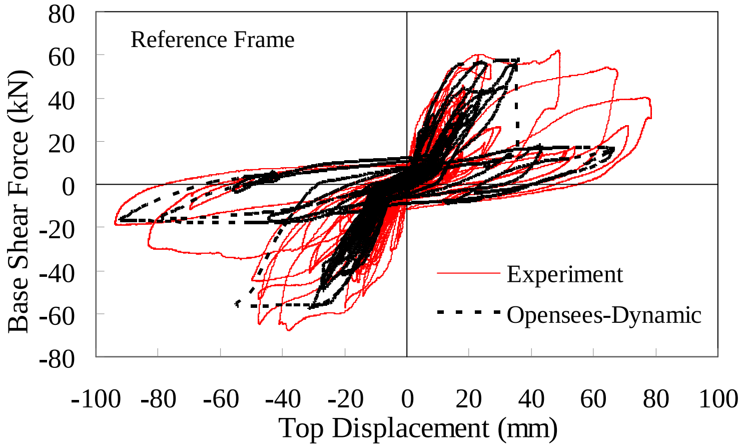

Figure 4.15 Base shear vs. Top displacement of the NTHA of the reference frame (Akpınar, 2010)

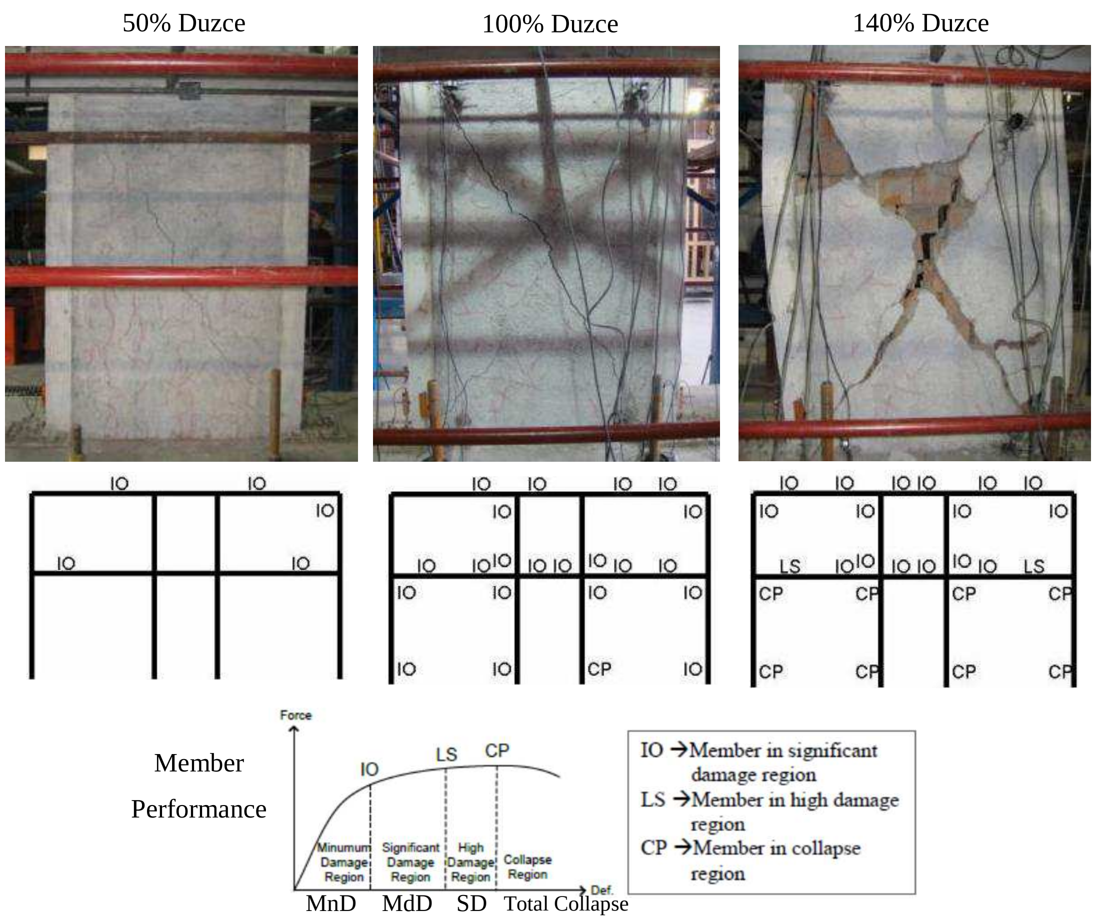

Figure 4.16 Performance evaluation of RC frame members (Akpınar, 2010)

4.3.2 Chevron Braced Frames

NTHA of the braced frames were performed utilizing Opensees Simulation Platform (Mazzoni et al., 2009) to observe the ability of estimating the dynamic response of the chevron braced frame. Modeling strategy and material models employed for the analysis are summarized in Figure 4.17. Force based fiber frame elements (nonlinearBeamColumn) were used to model RC beams and columns. The material model used for concrete (Concrete01) follows the rules of the confined concrete model proposed by Kent and Park (1971) (Figure 4.13-d). For RC columns, second order effects were also taken into account. Linear geometric transformation was used for RC beams due to insignificant effect of geometric nonlinearity. Longitudinal bar buckling was modeled by employing the backbone curve of Dhakal and Maekawa (2002). Force deformation relation of brace members were modeled by the uniaxial rules according to the ASCE/SEI 41 (2007) along with AISC (2005) recommendation for the brace tension and compression capacities (Figure 4.17-b). Although the brace member can be modeled by modeling the exact nonlinear geometry (Uriz at al. 2008), the modeling procedure suggested by the ASCE/SEI 41 (2007) document is more practical for engineering applications especially for a existing RC frame retrofit schemes. Hence, in this thesis this backbone curve for the uniaxial response of the brace was considered for the truss members.

LVDTs placed at brace to column connections indicated that significant uplift (Figure 4.17 and 4.18) at the bottom of the first story brace gusset plates occurred. This uplift was considered in the analysis to simulate the stiffness of the braced frame correctly. Figure 4.18 indicates the calculated brace force from average strain readings and uplift deformations. The brace base uplift movement was taken into account by using elastic springs between column base and brace elements. Spring stiffness values employed for the tests calibrated according to the experimental results are shown in Figure 4.18 for each ground motion. In addition, the numerical model without spring model was also analyzed in order to compare the modeling of uplift. Successive time history analyses were performed similar to the performed experimental sequence. In between each time history analysis appropriate stiffness values for the uplift springs were assigned. A Rayleigh damping of 5 % was used for all nonlinear time history analysis.

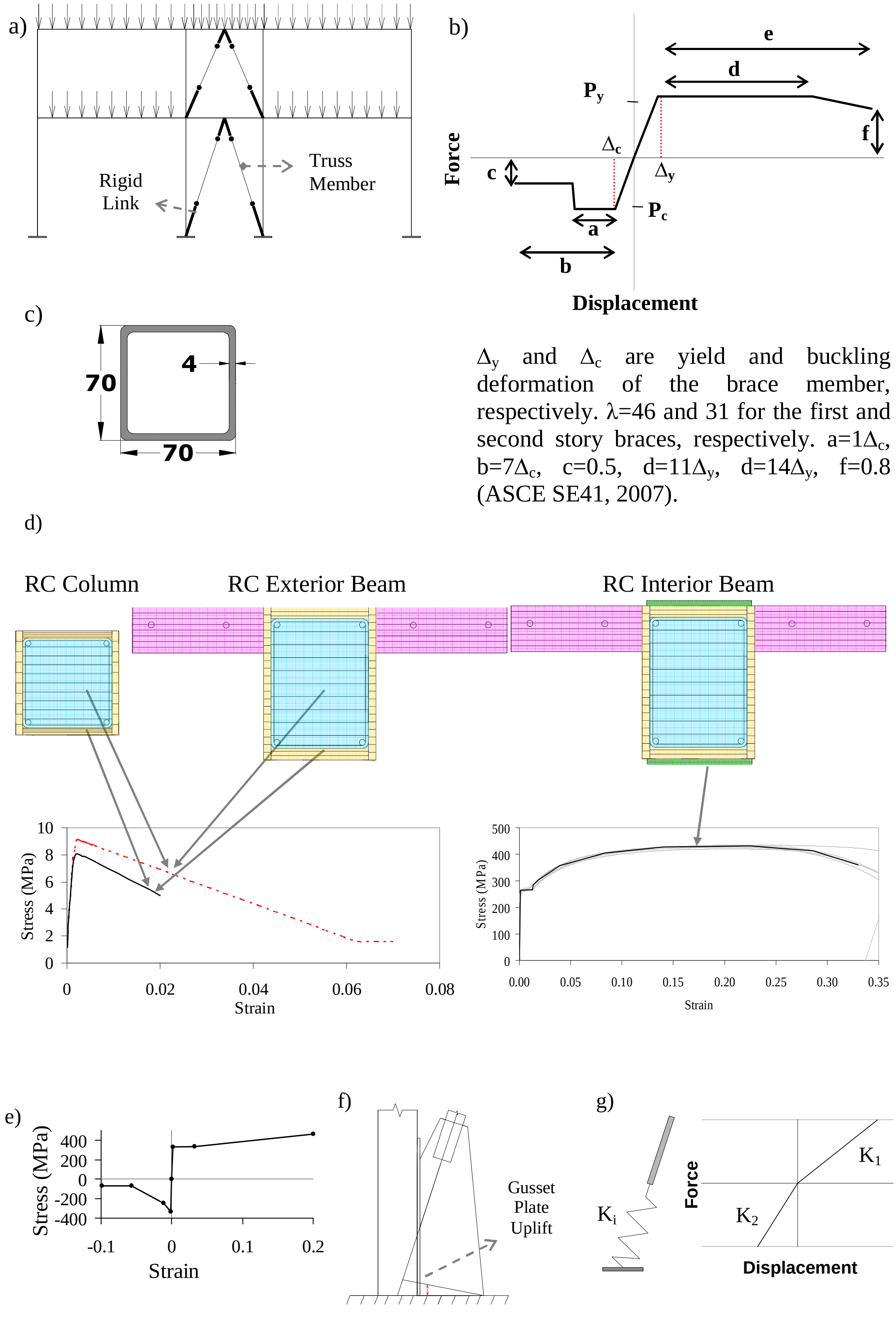

a) Braced frame, b) truss member force deformation relation (ASCE SE-41), c) truss member, d), RC members e) stress-strain relation of column longitudinal reinforcement, f) Gusset plate uplift at the bottom of the interior columns, g) Spring at the bottom of the first story brace member . P_y; Brace yield force, P_c; brace buckling force, K_1; spring constant (tension), K_2 brace constant (compression), unit is mm.

Figure 4.17 Modeling strategy of reference and chevron braced frames

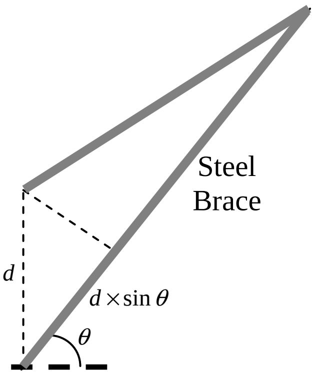

d: uplift of the base plate monitored from the Channels 7 and 8 (C7 and C8 are indicated in Figures A2.11 and A2.14).
Brace deformation (ε) was monitored from the Channels 39-40 and 50-55 (Figures A2.13 and A2.15). The brace force can be calculated by using brace deformation. Furthermore spring constant can be calculated by using the following equation. In this equation, ε: brace deformation, E_s: elastic modulus of the brace, A: brace area, d: uplift

$$K = \frac{\varepsilon \times E_s \times A}{d \times \sin\theta}$$

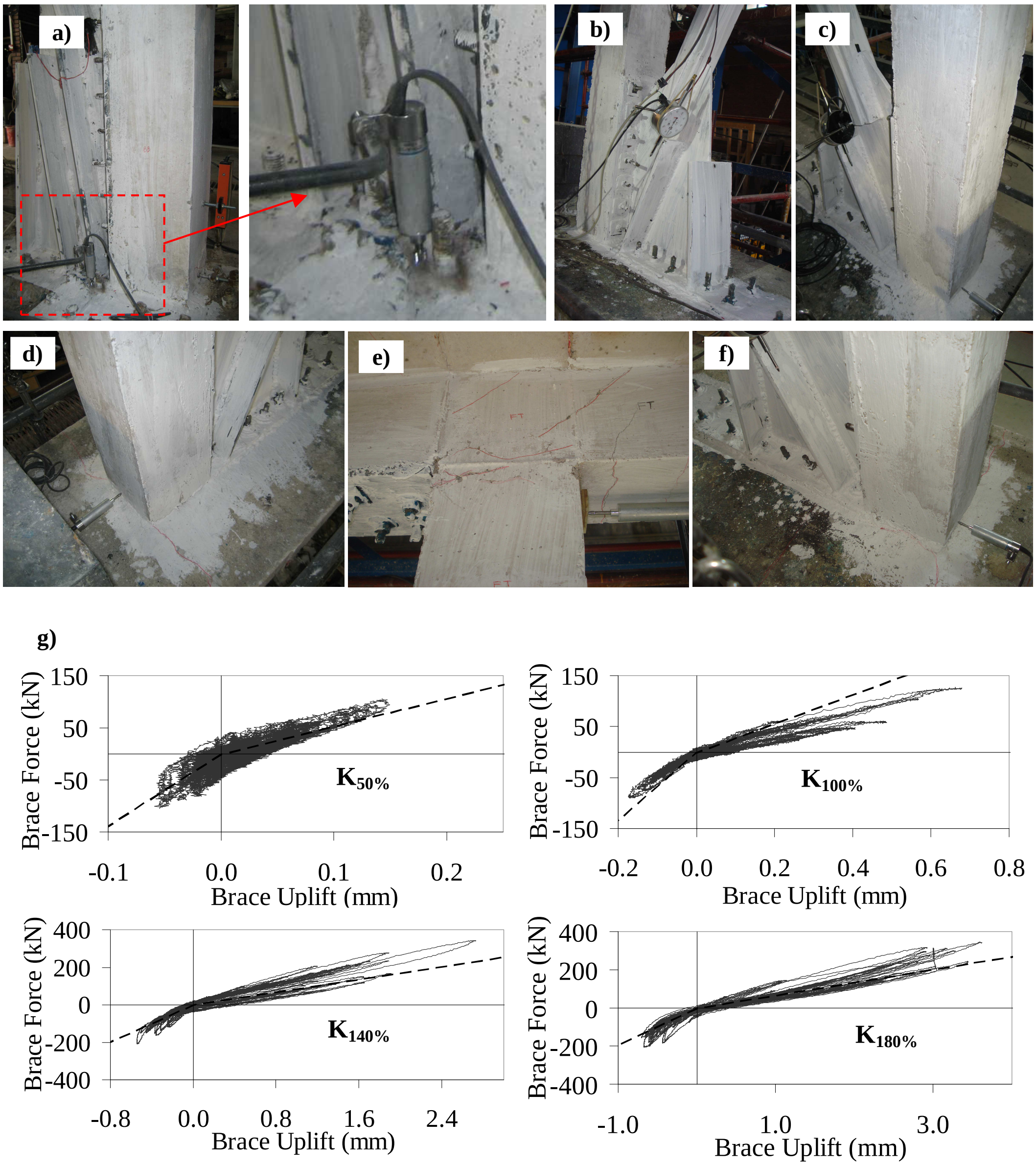

a) LVDT at the bottom of the column to monitor the uplift, 2. story beam-column joint after the test for b) 50%, c) 100%, d)140%, e)180%, f)220 % Düzce test, g) brace force vs. brace uplift.

Figure 4.18 Gusset plate uplift

Figure 4.19 and 4.20 show that simulations were capable of tracing the displacement-time and load-deformation response of the test specimens with reasonable accuracy. Table 4.2 indicates the calculated errors of the maximum base shear and story displacements for the models with and without spring model.

For the 50% Duzce test, the initial stiffness of the numerical simulation results was observed to agree well with that observed in the test. The base shear force of all scaled Duzce test was estimated with an error less than 11%. Likewise, except 180% Duzce test, numerical simulation was able to estimate the story displacement well for braced frames with an error less than 10%. The highest error (28%) was observed during the estimation of the story displacements at 180% Duzce test simulation. The main reason of this error was the brace buckling which was not observed during the test. Since ASCE/SEI 41 (2007) recommendations were employed for brace modeling, such conservative estimates of brace deformations are expected.

Table 4.2 Errors of the NTHA of the braced frame, a) numerical model with spring model, b) numerical model without spring model

Numerical model with spring model

Ground Motion Scale	Braced Frame			Braced Frame			
	Test Max. Base Shear Demand (kN)	Analysis Max. Base Shear (kN)	Error (%)	Story	Test Max. Disp. Demand (mm)	Analysis Max. Disp. (mm)	Error (%)
50%	39.94	39.6	0.8	1	1.7	1.5	7.1
				2	2.5	2.5	2.1
100%	89.13	99.06	11.1	1	4.7	4.4	6.3
				2	7.3	7.5	2.4
140%	178.98	182.24	1.8	1	13.2	13.7	3.8
				2	22.1	19.8	10.4
180%	206.06	204.49	0.7	1	18.2	23.2	27.6
				2	34.9	31.3	10.4

Numerical model without spring model

Ground Motion Scale	Braced Frame			Braced Frame			
	Test Max. Base Shear Demand (kN)	Analysis Max. Base Shear (kN)	Error (%)	Story	Test Max. Disp. Demand (mm)	Analysis Max. Disp. (mm)	Error (%)
50%	39.94	38.9	2.7	1	1.7	1.2	27.0
				2	2.5	2.2	11.0
100%	89.13	67.3	24.5	1	4.7	2.1	55.1
				2	7.3	3.8	47.9
140%	178.98	91.1	49.1	1	13.2	2.9	78.3
				2	22.1	5.5	75.3
180%	206.06	112.1	45.6	1	18.2	3.5	80.6
				2	34.9	7.0	80.0

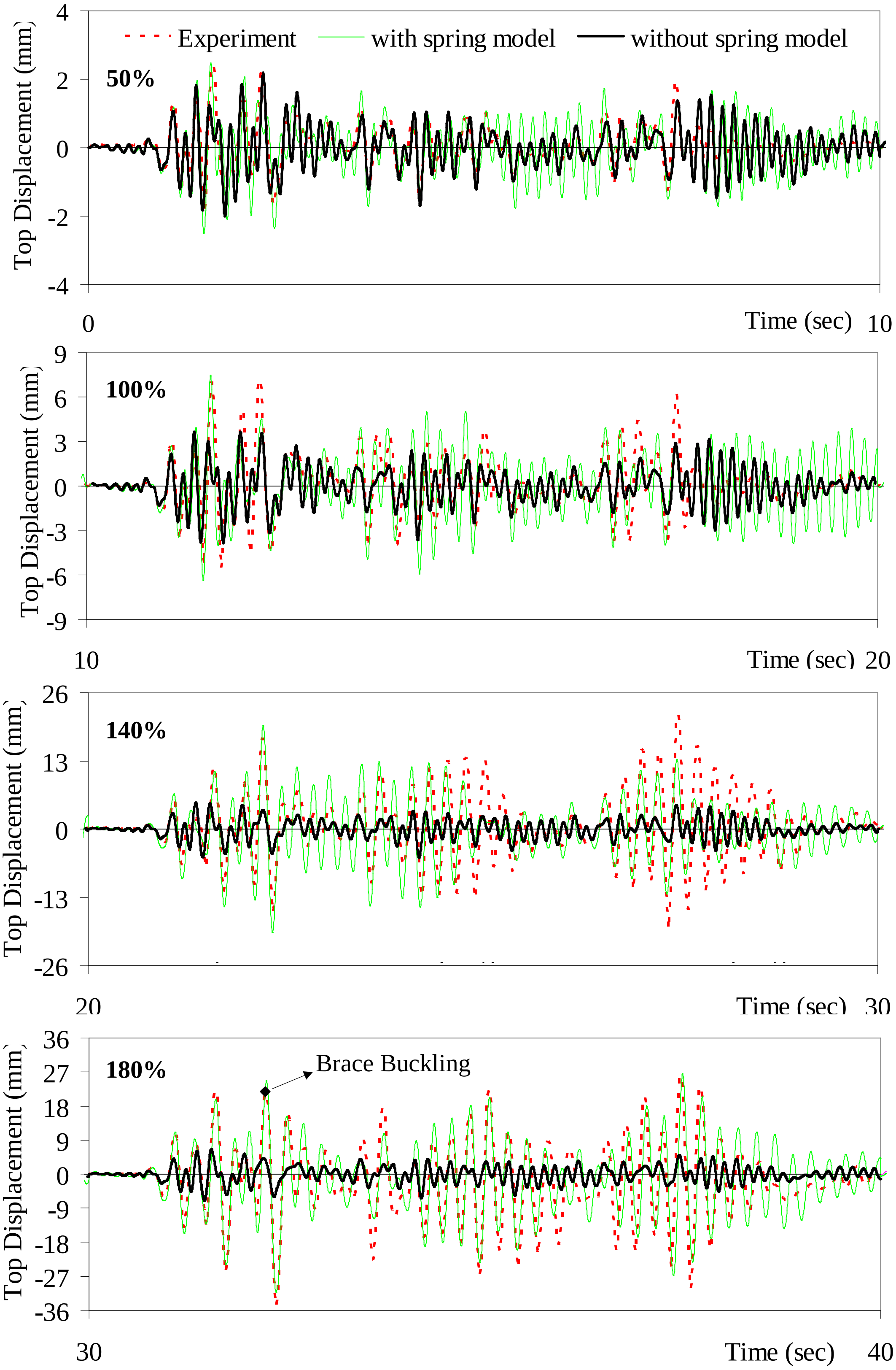

Figure 4.19 Results of the NTHA of the braced frame

Figure 4.21 indicates the stress-strain response of the brace member obtained from the NTHA. As seen in this figure, the brace members were within the MdD performance levels with respect to ASCE/SEI 41 (2007) recommendation. Furthermore, Figure 4.22 indicates the performance of the braced frame. The performance levels of the RC members and brace members were evaluated the strain limits suggested by the TEC (2007) and ASCE/SEI 41 (2007). This figure indicates performance levels of the members when the strain limits exceeded the specified limits suggested by the TEC (2007) and ASCE/SEI 41 (2007). Since the brace members were effective to resist the lateral demands, the damage of the RC frame was limited. On the other hand, since the second story brace members applied additional axial load on first story columns, these columns were within the SD performance limit (strain levels exceeded the specified limit) .

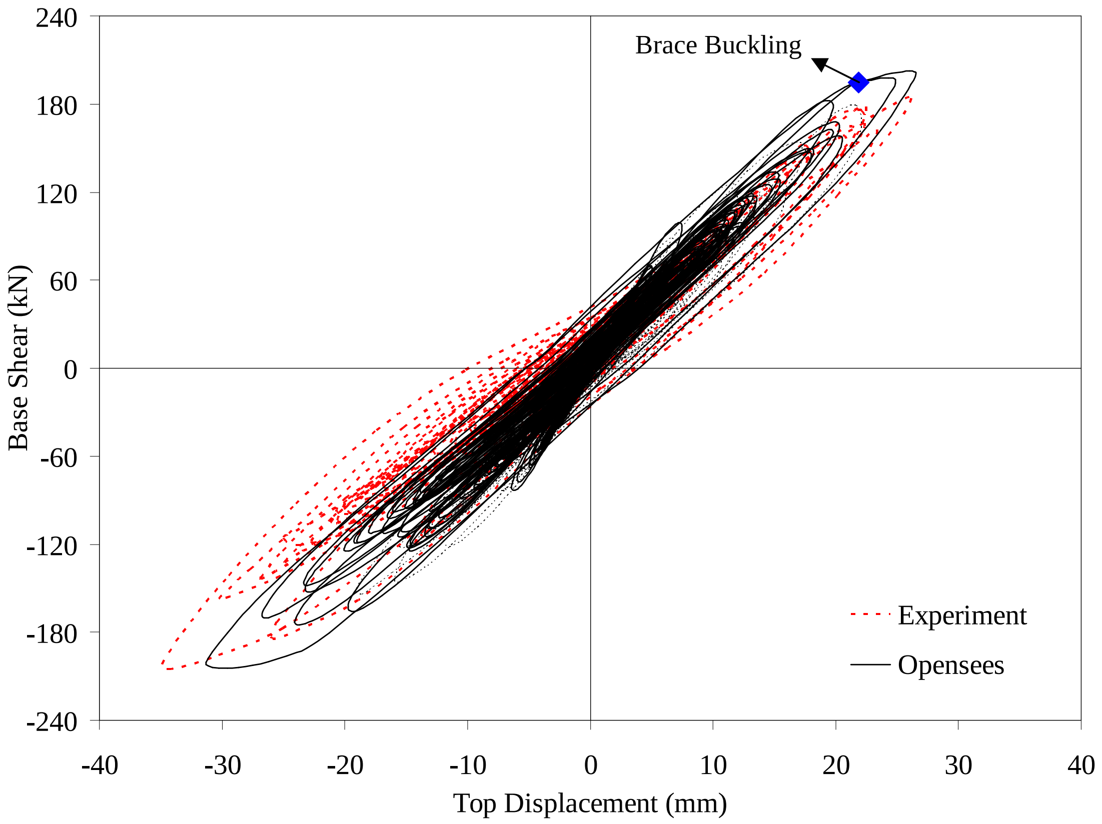

Figure 4.20 Base shear vs. Top displacement of the NTHA of the braced frame

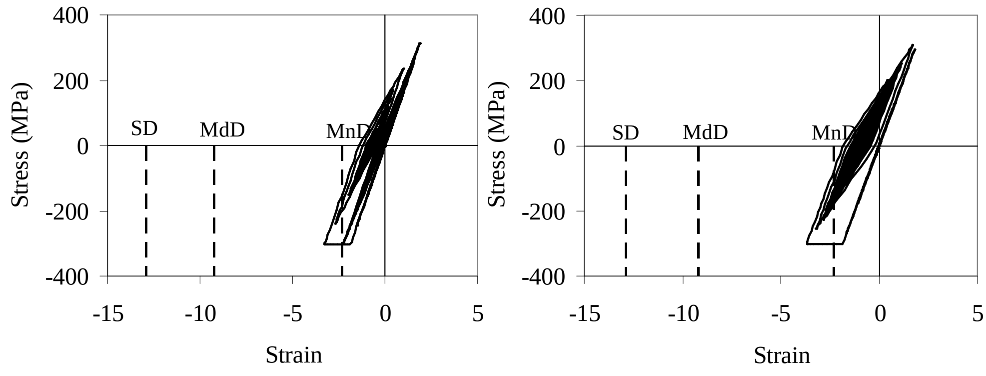

Figure 4.21 Brace stress-strain response of the NTHA

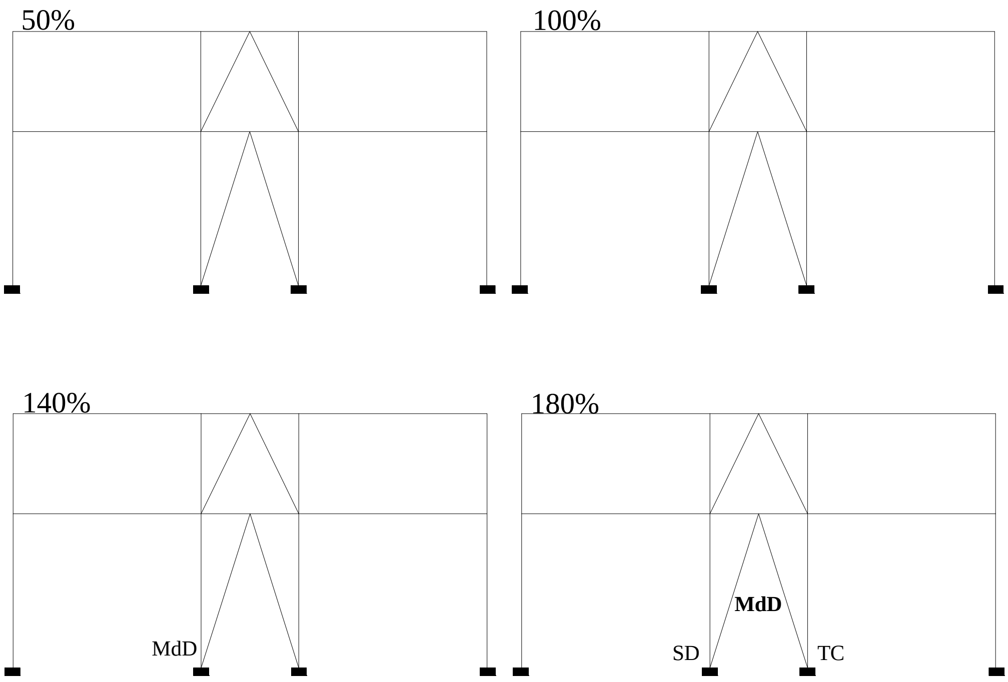

Figure 4.22 Performance levels of the braced frame

4.3.3 Internal Steel Frame

The NTHA of the ISF is presented in this section. The ISF members or the composite columns and beams were modeled from the actual sections presented in the Chapter 3. Figure 4.23 shows the modeling strategy of the ISF retrofitted frame. The composite column and beam members were modeled as a single section with proper numbers of layers. Hence, composite behavior of members was ensured. Force based fiber frame elements were employed to model composite beams and columns. At the bottom of the composite columns, a rotational spring (K_{rot}=1020 kNm/rad) was assigned to match the fundamental period of the test frame in the first model. Such a soft touch was necessary to ensure that dynamic properties of the test frame and simulation agree well prior to the significant inelastic response. Consequently, there were two models namely model with rotational spring and model without rotational spring (fix boundary condition) in this study. The results of the numerical model of the ISF are presented by comparing these two models. The NTHA procedure of the ISF was similar to that of chevron braced frame (section 4.3.2).

Figure 4.24 and 4.25 show that simulations were capable of tracing the displacement-time and load-deformation response of the test specimens with reasonable accuracy. Table 4.3 presents the calculated errors of the maximum base shear and story displacements for the two models. Figure 4.24 and Table 4.3 indicate that the model with rotational spring at the columns base estimated the response of the test frame in terms of lateral strength and displacement better than those predicted by the model without rotational springs.

For the 50% Duzce test, although the top displacement and base shear were estimated with acceptable error which was less than 13%, the estimation of the first story displacement had the highest error which was about 47.5%. This is the highest error for all scales during the numerical simulation of the ISF. The numerical model estimated the base shear and lateral displacement of the test frames with less than error of 25% for the rest of the tests. The base shear force and top displacement were estimated with an error less than 6% for the 180% Duzce test.

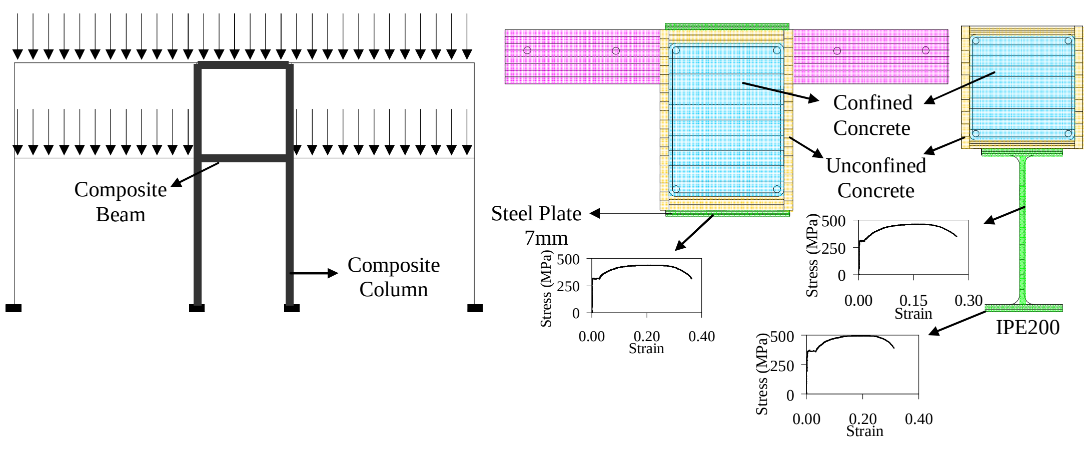

Figure 4.23 Modeling strategy of ISF (composite column and beam)

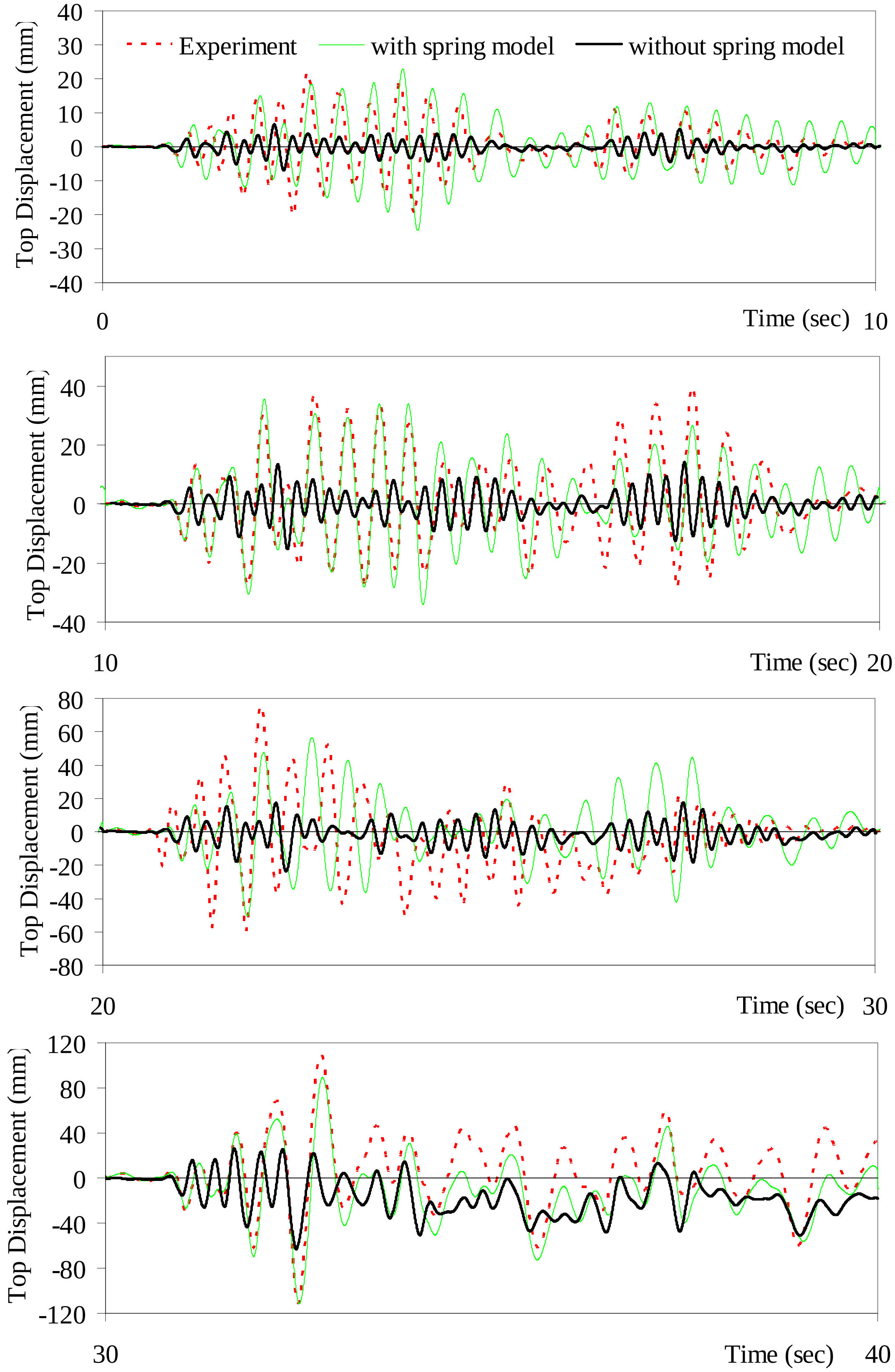

Figure 4.24 Results of the NTHA of the ISF

a) Performance levels of the ISF

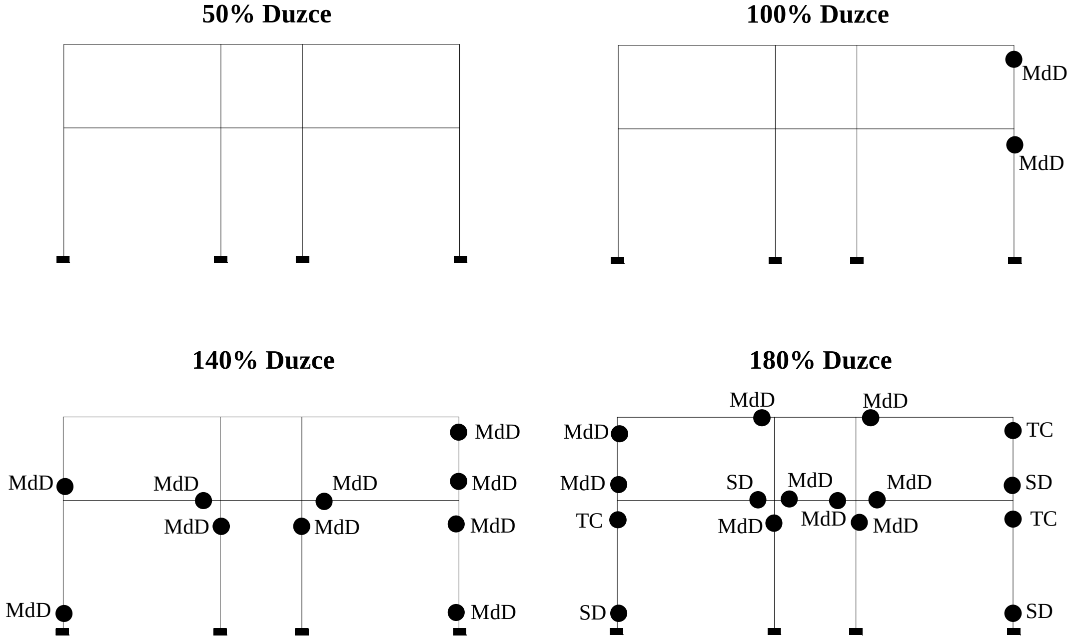

b) Base Shear vs. Top Displacement of the NTHA of the ISF

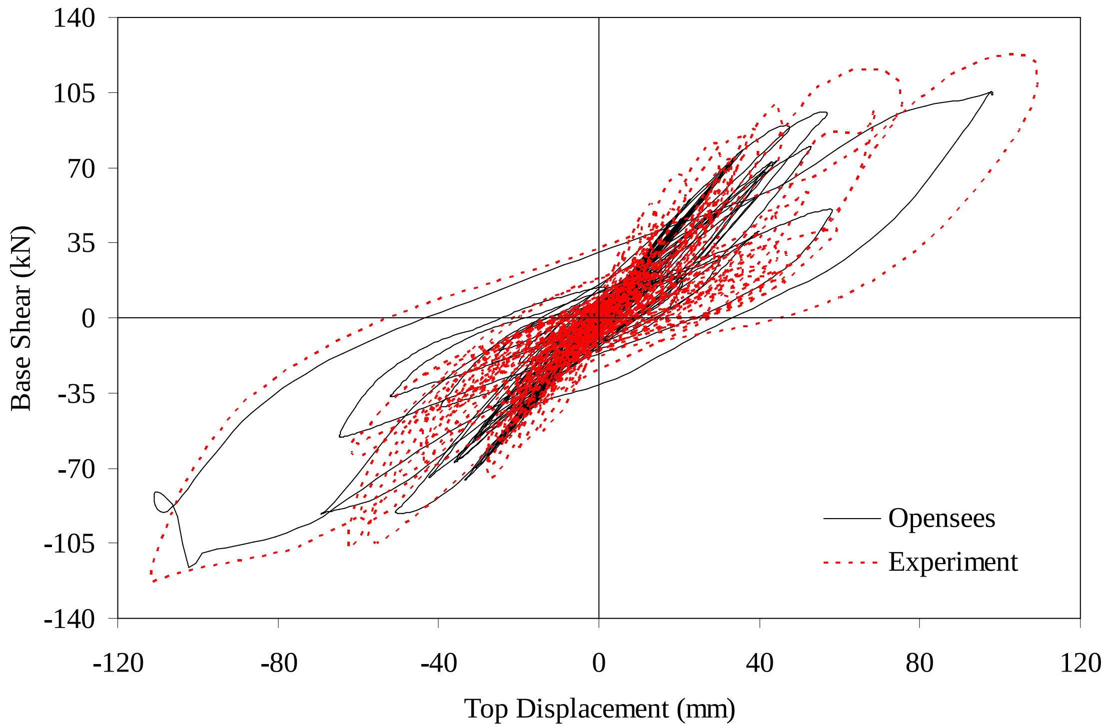

Figure 4.25 a) Performance of the ISF, b) Base shear vs. Top displacement of the NTHA of the ISF

Figure 4.25 indicates the estimated performance of the ISF and force-deformation response of the NTHA of the ISF. The performance levels of the RC members and ISF (IPE200 and steel plates) were evaluated the strain limits suggested by the TEC (2007). This figure indicates performance levels of the members when the strain limits exceeded the specified limits suggested by the TEC (2007). While the exterior columns were found to be within or beyond the SD performance level at the end of the 180% Duzce motion, the interior columns (composite columns) were found to be within the MdD performance level according to the TEC (2007) limits. It can be stated that the strain based seismic evaluation approach of TEC (2007), when applied to a frame with composite section may underestimate the damage state for composite members and overestimate the demand for RC members.

Table 4.3 Errors of the NTHA of the ISF, a) numerical model with rotational spring model, b) numerical model without rotational spring model

a) Model with rotational spring

Ground Motion Scale	ISF						
	Test Max. Base Shear Demand (kN)	Analysis Max. Base Shear (kN)	Error (%)	Story	Test Max. Disp. Demand (mm)	Analysis Max. Disp. (mm)	Error (%)
50%	67.6	58.7	13.1	1	12.6	18.6	47.5
				2	21.8	24.6	12.9
100%	88.2	78.1	11.4	1	21.7	27.0	24.5
				2	39.7	35.6	10.3
140%	116.6	95.9	17.7	1	40.8	41.5	1.7
				2	75.6	56.3	25.5
180%	123.2	116.4	5.5	1	57.6	72.1	25.1
				2	111.9	111.5	0.3

b) Model without rotational spring

Ground Motion Scale	ISF						
	Test Max. Base Shear Demand (kN)	Analysis Max. Base Shear (kN)	Error (%)	Story	Test Max. Disp. Demand (mm)	Analysis Max. Disp. (mm)	Error (%)
50%	67.6	57.2	15.3	1	12.6	4.2	66.4
				2	21.8	6.6	69.9
100%	88.2	118.4	34.2	1	21.7	9.3	57.0
				2	39.7	15.2	61.7
140%	116.6	141.2	21.1	1	40.8	14.6	64.3
				2	75.6	23.6	68.8
180%	123.2	142.7	15.8	1	57.6	35.3	38.8
				2	111.9	63.2	43.5

4.4 Retrofit Example on a Five Story RC Building

The numerical simulations were capable of predicting the behavior of the test frames. Next, a case study retrofit design and analysis conducted to show the effectiveness of both chevron brace and ISF strengthening.

4.4.1 Five Story Existing Deficient RC Building

In this section, the performance based design of existing five story existing deficient RC building located the Istanbul is presented. The building is a reinforced concrete frame structure with rigid shear walls surrounding the basement (Figure 4.26). Within this study, a performance evaluation method based on nonlinear pushover analysis is carried out using the available structural data. The strengthening of the building based on the methodology described previously from the test data is performed. Figure 4.26-a indicates the plan view of the building. Uniaxial compressive strength and modulus of elasticity (calculated from ACI 318, 2008) were used as 8 MPa (close to test frames) and 13435 MPa, respectively. The dimensions of the building in the x and y direction are 8.75 m and 12.23 m, respectively. The columns and beam dimensions are 250x400 and 150x500 mm, respectively. The orientation and also size of the beams and columns are shown in Figure 4.26. The stirrups spacing of the columns and beam are about 220 mm with a clear cover of 20 mm. It is important to mention that the stirrup spacing of columns and beams does not satisfy the current code TEC (2007). Furthermore, the in-situ concrete strength is lower than the code specified minimum. The steel grade of the longitudinal and transverse reinforcement is S220 whose yield strength is 220 MPa.

Nonlinear static pushover analyses by using lumped plasticity model were conducted in order to estimate displacement capacity of the building for the required evaluation techniques. The 3D computer model of the building was generated using from the original drawings of the building (Figure 4.26-d). All the joints on each floor were constrained in order to model the diaphragm effect. Moment–rotation properties derived from sectional analyses with the plastic hinge length (taken equal to half the member depth in the direction of loading as suggested by TEC, 2007) were assigned to the beam and column ends (similar to given moment rotation as seen in Figure 4.11). Axial force-moment yield surfaces obtained from interaction diagrams were used for column plastic hinge regions. Load distributions proportion to story mass and first mode amplitude were used for pushover analysis for x direction. Prior to conducting the pushover analyses, gravity loads and 30% of the live load on the structure were applied. The displacement-controlled pushover analysis was then performed to obtain performance point of the building and plastic deformations (rotations) of the members. After performing the pushover analysis and obtaining the capacity curve (Figure 4.27), the performance points of the building in x direction was calculated using method namely single degree of freedom (SDOF) model employing the Duzce ground motion (DGM) (100% Duzce ground motion in chapter 3). Pushover curve was converted into the acceleration displacement response spectrum (ADRS), Figure 4.27, by using Equation 4.10:

$$S_a = \frac{V_b}{\alpha_1 W} \text{ and } S_d = \frac{\Delta r}{\Gamma_1 \varphi_{r,1}} \tag{4.10}$$

Where,

where W is the total weight of the MDOF structure, Vb is the base shear, Δr is the roof displacement of the MDOF structure, α1 is the modal mass coefficient for the first mode (first fundamental mode), and Γ_1 is the modal participation factor for the first fundamental mode. $\phi r,_1$ is the amplitude of the first fundamental mode at the roof, Sa is spectral acceleration, and Sd is the spectral displacement.

For the SDOF approach, the linearization was performed based on the procedure given in FEMA 353 (2000) (Figure 4.27). The mass of the building is taken as the mass corresponding to the governing x modes and 5% critical damping is assumed. Using the bilinear idealization with elastic unloading a SDOF analysis is conducted using the DGM to obtain the top displacement (performance point).

The performance point according to DGM is shown on the pushover curves in Figure 4.28. It can be observed that the building experiences an overall DR of about 2.4 % in the x direction prior to retrofit. The IDR profiles for x directions obtained from pushover analysis at performance point of DGM are shown in Figure 4.29. It can be observed that highest IDR, which was about 4.7 % in the x direction, occurred in the first story level of the building without any retrofitting.

A member by member evaluation is then performed to determine the damage level of the members. The number of columns and beams at different performance levels are presented in Table 4.3. This evaluation indicated that 100% and 36% of the first story columns and beams of the deficient building were at the total collapse (TC) performance level for x directions, respectively. This result indicates that this deficient building needs to be retrofitted with respect to TEC (2007).

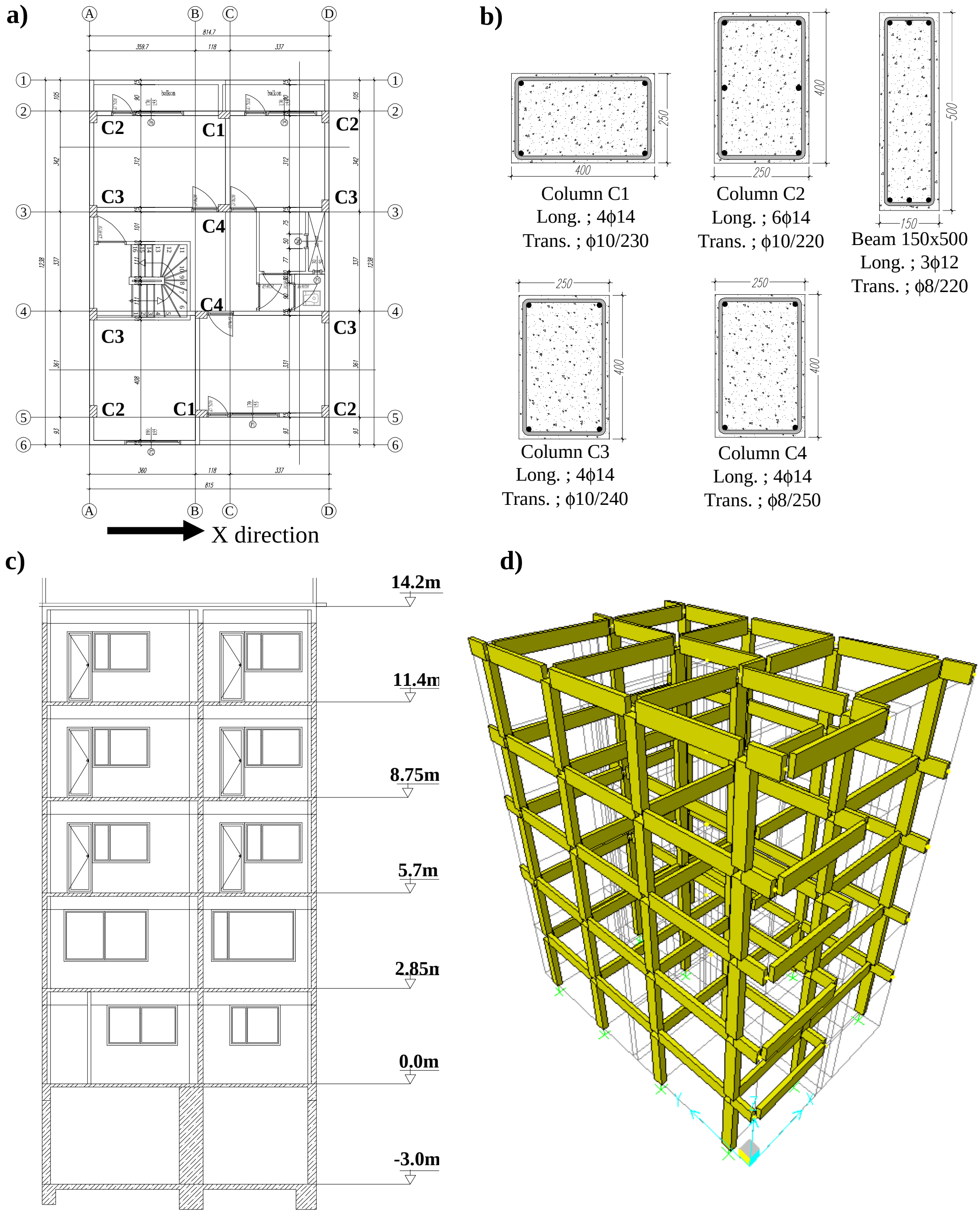

Figure 4.26 Five story building a) plan view, b) column and beam dimensions, c) front view of the building, e) analytical model of the building.

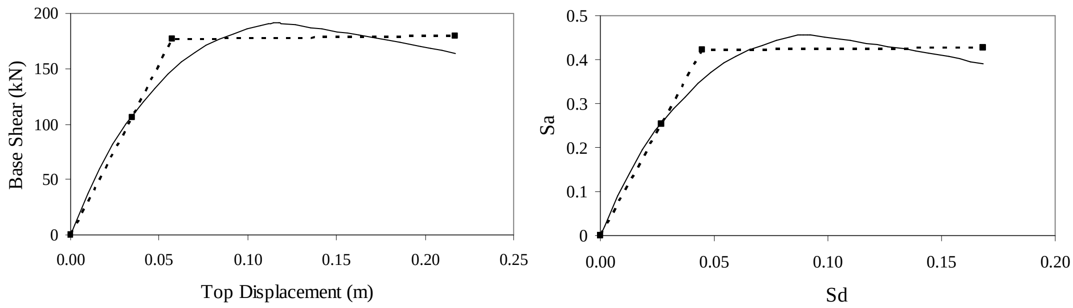

Figure 4.27 a) Pushover curve of the building, b) ADRS of the building.

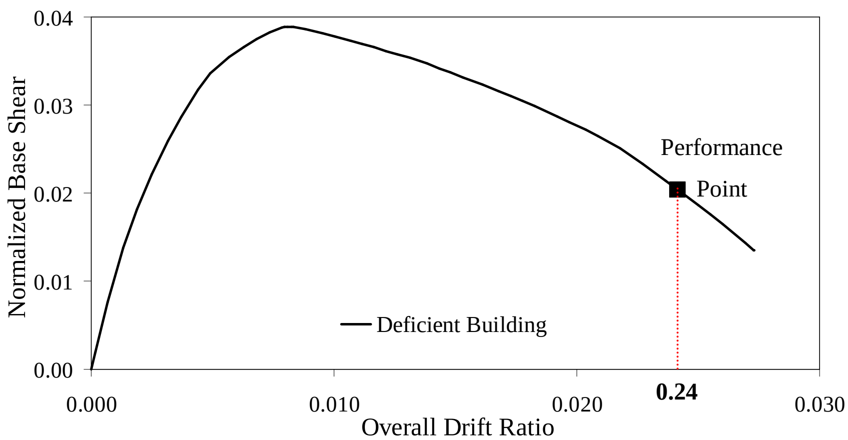

Figure 4.28 Performance point of the deficient Building

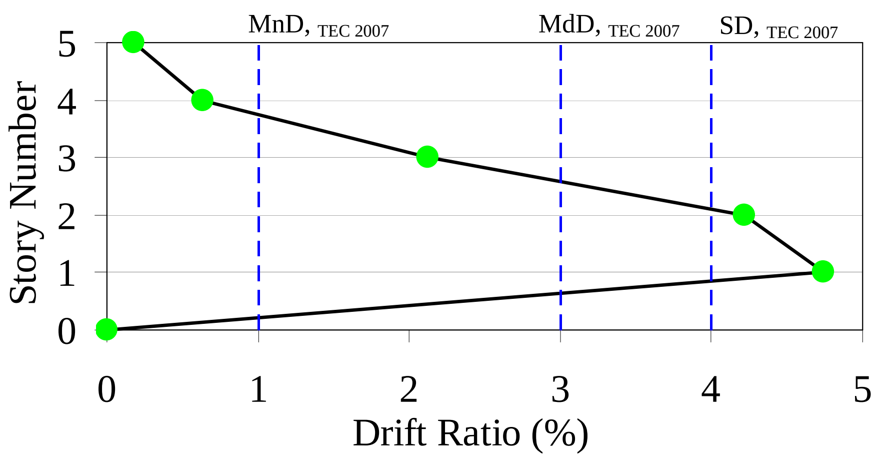

Figure 4.29 ISDR of the deficient building at performance point

Table 4.4 Performance levels of the RC members of the building

Performance Levels	1. story		2. story		3. story		4. story		5. story	
	Column	Beam	Column	Beam	Column	Beam	Column	Beam	Column	Beam
MnD	0	12	1	16	5	17	12	23	12	24
MdD	0	2	4	1	6	7	0	1	0	0
SD	0	0	3	5	1	0	0	0	0	0
Total Collapse	12	8	4	2	0	0	0	0	0	0

4.4.2 Chevron Strengthening of the Five Story RC Building

The strengthened technique was applied to enhance the lateral load resisting capacity of the x direction. Figure 4.30 indicates the strengthened bays of the building. The numbers of braced frame axis is two for each direction. The proposed connection between brace and RC members is indicated in Figure 4.31. 15 mm thick steel plates were utilized at the top and bottom of the beam of the braced frames (Figure 4.31). Three different brace size were employed to retrofit the RC building (Figure 4.30 and 4.32). Figure 4.32 also indicated the braced axis. The yield strength of the both HSS and steel plates were taken as 235 MPa. The force-deformation relations of the brace members were determined with respect to ASCE/SEI 41 (2007) along with AISC (2005). Figure 4.33 indicates the force-deformation relation of the HSS 175x7.1. Table 4.5 indicates the predicted compression capacity of the brace members with their slenderness (λ). These braces had a slenderness of about 40 which is consistent with the brace slenderness used in PsD tests presented in Chapter 3. Since the braces introduced excessive axial load on the columns as observed in the PsD test (chapter 3), first and second story RC columns were strengthened with Fiber Carbon Polymer (FRP) with respect to design guidelines suggested by TEC (2007) (Figure 4.34). Equation 4.11 gives the FRP wrapped concrete strength with respect to TEC (2007). In the primary design, in order to determine the numbers of layers of the FRP, RC column axial load was determined from the additional axial load imposed by the brace members in all stories which were within the post buckling regions (Table 4.5). Hence, 8 layers of FRP were found to be adequate for the desired axial load enhancement of the RC columns. It should be kept in mind that the column strengthening was performed to increase the axial load carrying capacity only. As seen in Figure 4.35 the FRP wrapping increased the compressive strength of the concrete as expected. Figure 4.35 also indicates the moment-interaction and moment curvature relation of the RC columns before and after FRP wrapping. It was observed that

FRP wrapped column had about two times higher axial load capacity than the existing column.

$$f_{cc} = f_{cm}\left(1+2.4\left(f_l / f_{cm}\right)\right) \geq 1.2 f_{cm} \tag{4.11}$$

$$f_l = \frac{1}{2}\kappa_a \rho_f \varepsilon_f E_f \tag{4.12}$$

Where,

f_{cc}: concrete strength wrapped with FRP

f_{cm}: concrete strength of the existing RC building

f_l: lateral confinement provided by the FRP

K_a: shape factor for the RC member

ρ_f: volumetric ratio of the FRP

ε_f: strain limit of the FRP

E_f: elastic modulus of the FRP

The performance point according to DGM is shown on the pushover curves in Figure 4.36. It can be observed that the building retrofitted with chevron brace experiences an overall DR of about 0.6 % in the x direction.

The IDR profiles for x directions obtained from pushover analysis at performance points of DGM are shown in Figure 4.37. It can be observed that highest IDR, which was about 4.7 % in the x direction, occurred in the first story level of the building without any chevron retrofit. Upon retrofit the IDR reduced to about 0.76 % for the x directions. It should be noted that the observed DR is in good agreement with those limits proposed in the TEC (2007). The maximum IDR of the retrofitted building was observed at the second story as indicated in Figure 4.37. In fact, this behavior was also observed for the PsD test members (see Figures 3.40 and 3.53 and Table 3.7).

A member by member evaluation is then performed to determine the damage level of the members. The number of columns and beams at different performance levels are presented in Table 4.6. This evaluation indicated that 100% of the all story columns were at the MnD performance levels. In addition, there were no beams at the SD performance levels. Furthermore, at the performance point of the retrofitted building, there were no brace buckling.

This result shows that the chevron retrofit scheme was successful in controlling drift deformations and reducing the demands in the columns. As a result, the chevron retrofit design presented above was found to be successful in MnD performance level of the building by reducing the deformation demands on the RC columns and controlling the drift deformations.

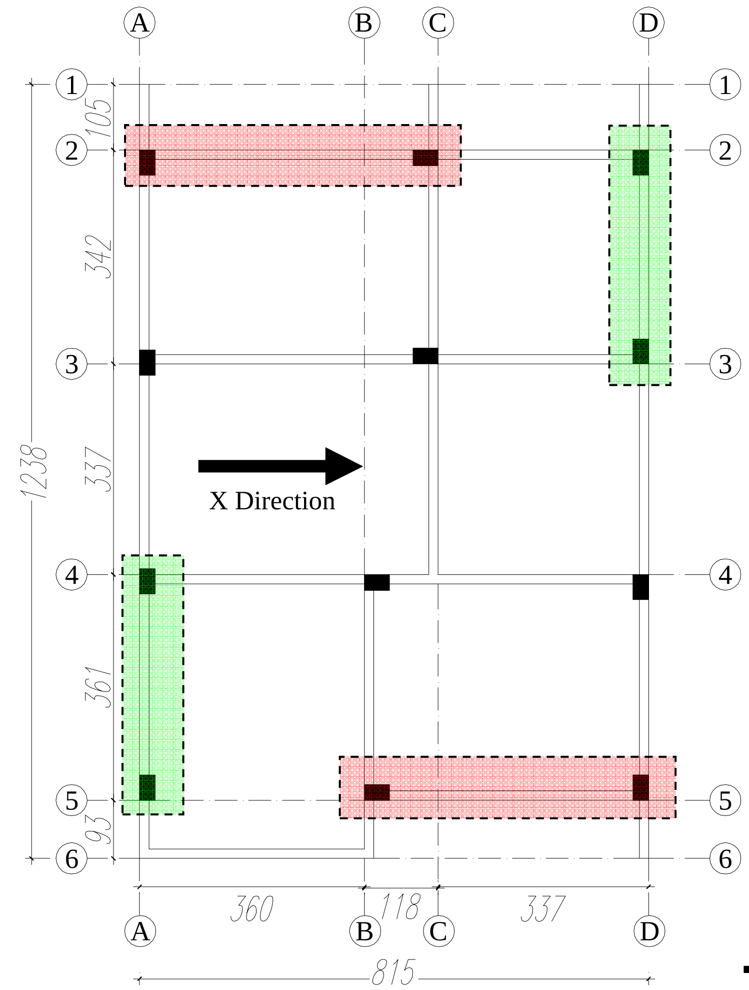

a) Plan View

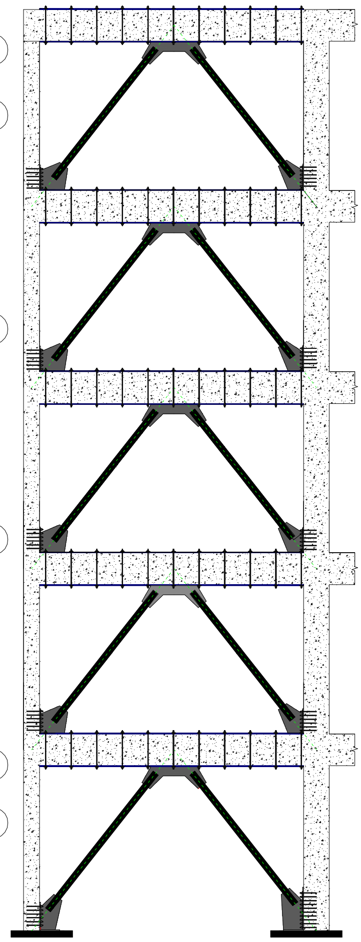

b) Chevron braced frame (axis 2-2)

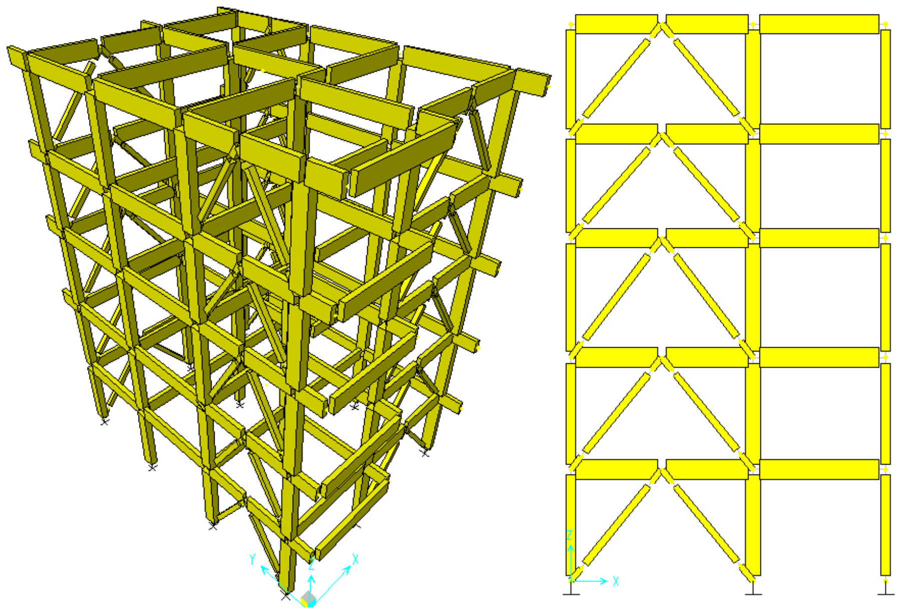

c) Analytical model

Figure 4.30 RC Building view retrofitted with chevron braced a) plan view of the braced axis, b) braced frame axis 2-2, c) 3D view of analytical model

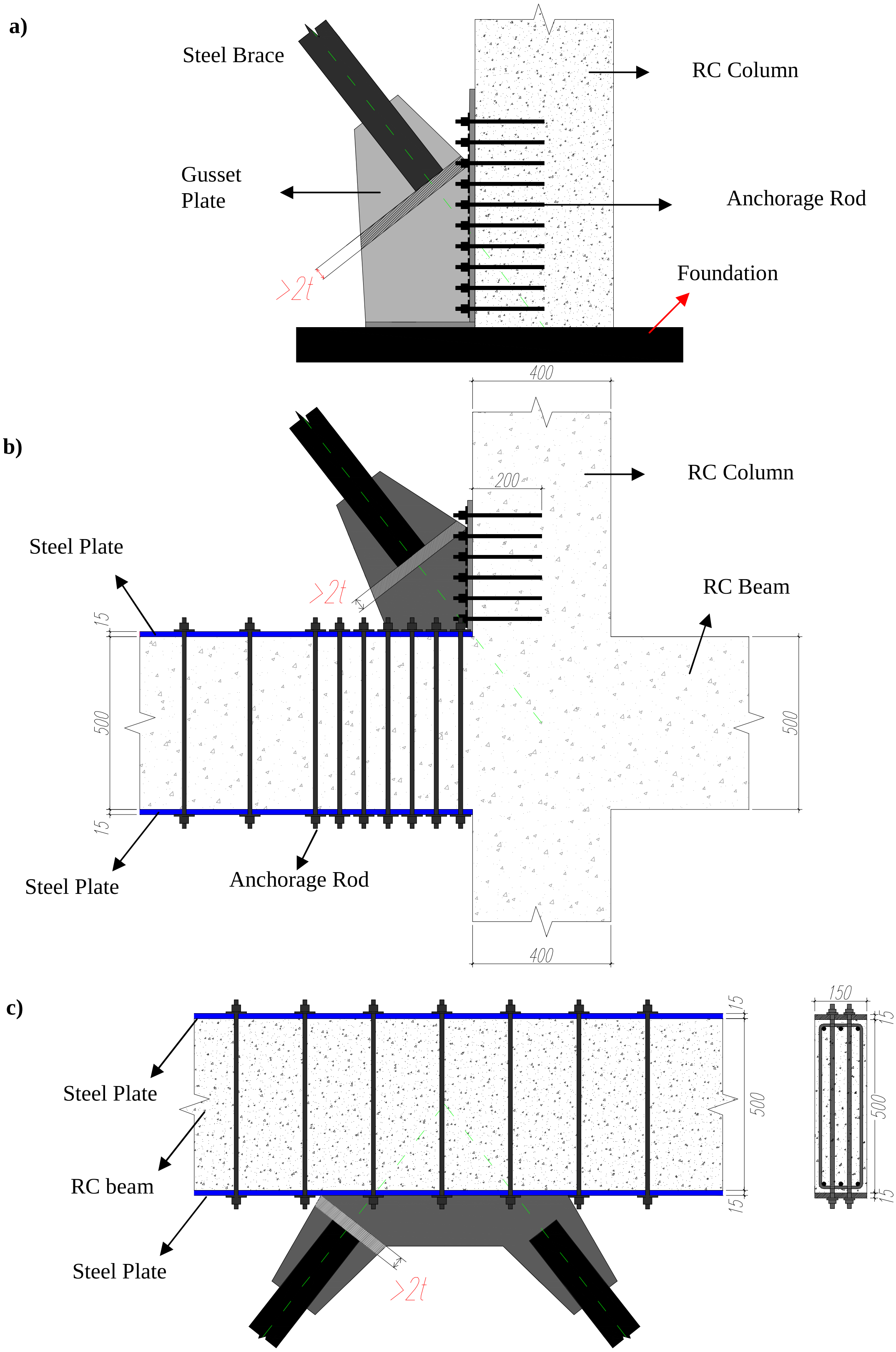

Figure 4.31 Connection details a) at the base, b) at the beam-column joint, c) at the mid span of the beam.

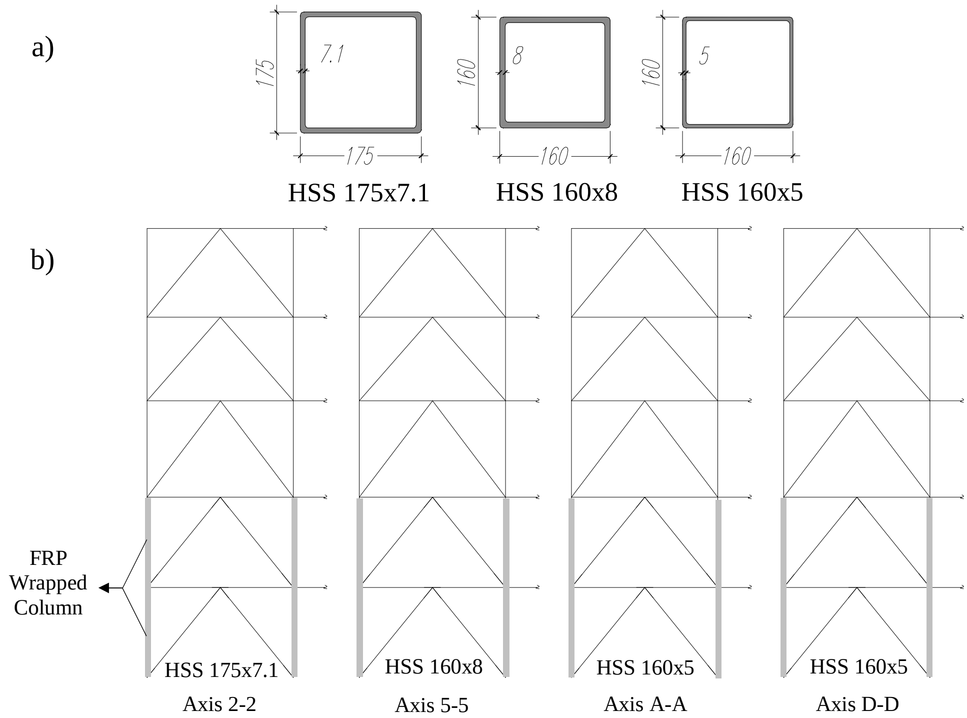

Figure 4.32 a) Brace members, b) Braced frames

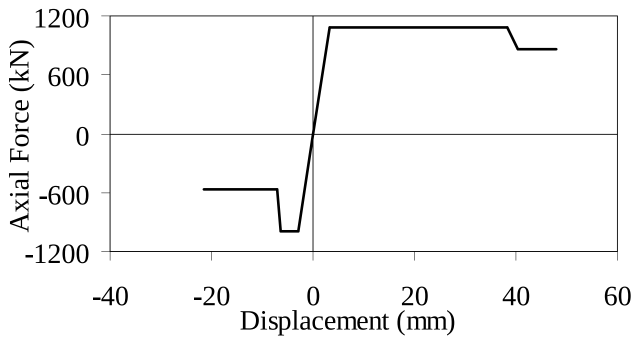

Figure 4.33 Brace member (HSS-175x7.1) axial load-displacement response used for the axis 2-2 (proposed by ASCE/SEI 41, 2007 and AISC, 2005)

Table 4.5 Brace compression capacity

Location	Brace Copmression Capacity (kN)	λ
Axis 2-2 (HSS 175x7.1)	995	41.4
Axis 5-5 (HSS 160x8)	995	43.4
Axis A-A (HSS 160x5)	662	37.2
Axis D-D (HSS 160x5)	664	36.1

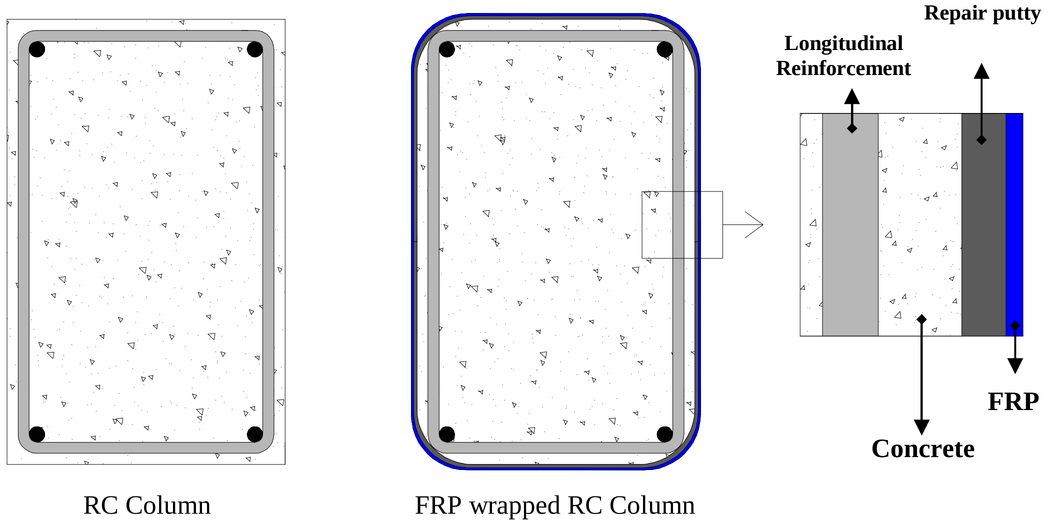

Figure 4.34 FRP strengthened column details

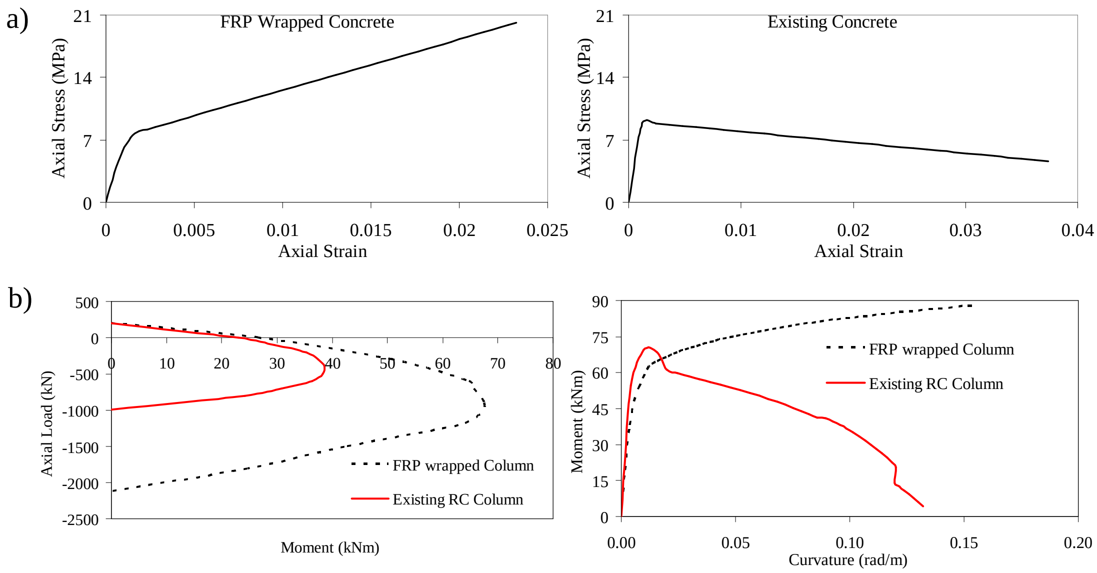

Figure 4.35 a) Concrete compressive strength of existing and FRP wrapped RC column, b) moment-curvature and moment interaction relation of the existing and FRP wrapped RC column

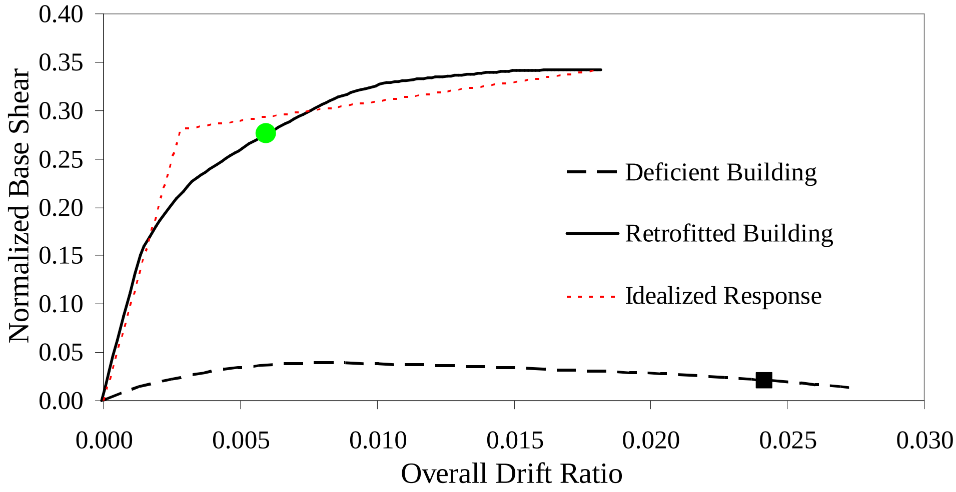

Figure 4.36 Performance point of the building retrofitted with chevron brace

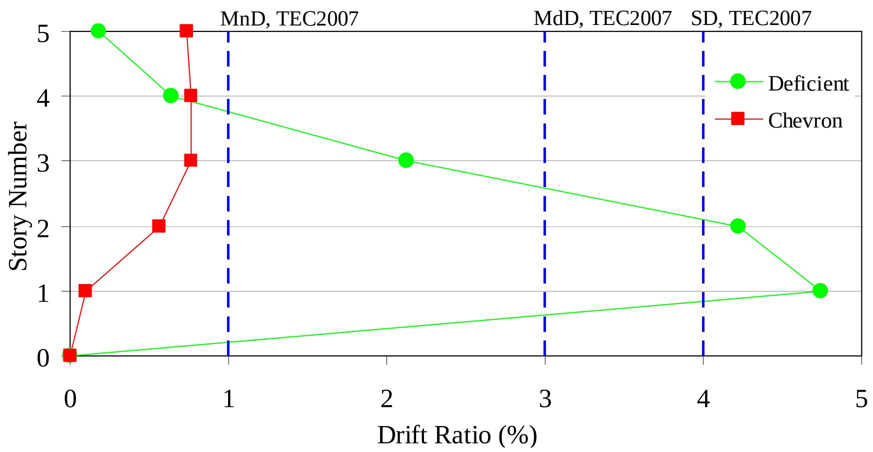

Figure 4.37 IDR of the building retrofitted with chevron braces at performance point

Table 4.6 Performance levels of the RC members of the building retrofitted with chevron braces

RC Member	Performance Levels	1. story		2. story		3. story		4. story		5. story	
		Deficient	Chevron	Deficient	Chevron	Deficient	Chevron	Deficient	Chevron	Deficient	Chevron
Column	MnD	0	12	1	12	5	12	12	12	12	12
	MdD	0	0	4	0	6	0	0	0	0	0
	SD	0	0	3	0	1	0	0	0	0	0
	Total Collapse	12	0	4	0	0	0	0	0	0	0
Beam	MnD	12	21	16	17	17	16	23	17	24	22
	MdD	2	1	1	7	7	8	1	7	0	2
	SD	0	0	5	0	0	0	0	0	0	0
	Total Collapse	8	0	2	0	0	0	0	0	0	0

4.4.3 ISF Strengthening of Five Story RC Building

The strengthened technique was similar to the previously tested frame ISF_28_7.4_III_IS. Figure 4.38 indicates the strengthened bays of the building. There were two strengthened cases namely ISF 1 and ISF 2. The difference between them is; the ISF2 had additional strengthened bays, axis 3-3 and axis 4-4, at the first and second story. The steel members to build composite columns and beams are I-400 and 13 mm-thick-steel plate (Figure 4.38). The proposed connection details are indicated in Figure 4.38. The yield strength of the both steel members was taken as 235 MPa.

The performance point according to DGM is shown on the pushover curves in Figure 4.39. It can be observed that the building retrofitted with ISFs experience an overall DR of about 1.6 and 1.1 % for the ISF1 and ISF2 in the x direction, respectively.

The IDR profiles for x directions obtained from pushover analysis at performance points of DGM are shown in Figure 4.40. Upon retrofit the IDR reduced to about 1.4% for the x directions. It should be noted that the observed DR is in good agreement with those limits proposed in the TEC (2007) (Figure 4.12).

A member by member evaluation is then performed to determine the damage level of the members. The number of columns and beams at different performance levels are presented in Table 4.7. Upon retrofitting, the number of the columns which were in the TC performance level decreased. Although 33% of the first story columns of the building implemented ISF 1 was within the TC performance level, this condition did not satisfy the performance level of the residential building suggested in TEC (2007). Finally, the desired performance level of the deficient building retrofitted with ISF2 was obtained by increasing numbers of retrofitted bays.

This result shows that the ISF retrofit scheme was successful in controlling drift deformations and reducing the demands in the columns. As a results, the ISF retrofit design presented above was found to be successful in MnD performance level of the building by reducing the deformation demands on the RC columns and controlling the drift deformations. In addition, above results clearly indicates that a retrofit technique needs to increase lateral stiffness and strength aside from increasing global ductility capacity (if any member base retrofitting technique is not used) when ductility capacity of the existing columns and beams are insufficient.

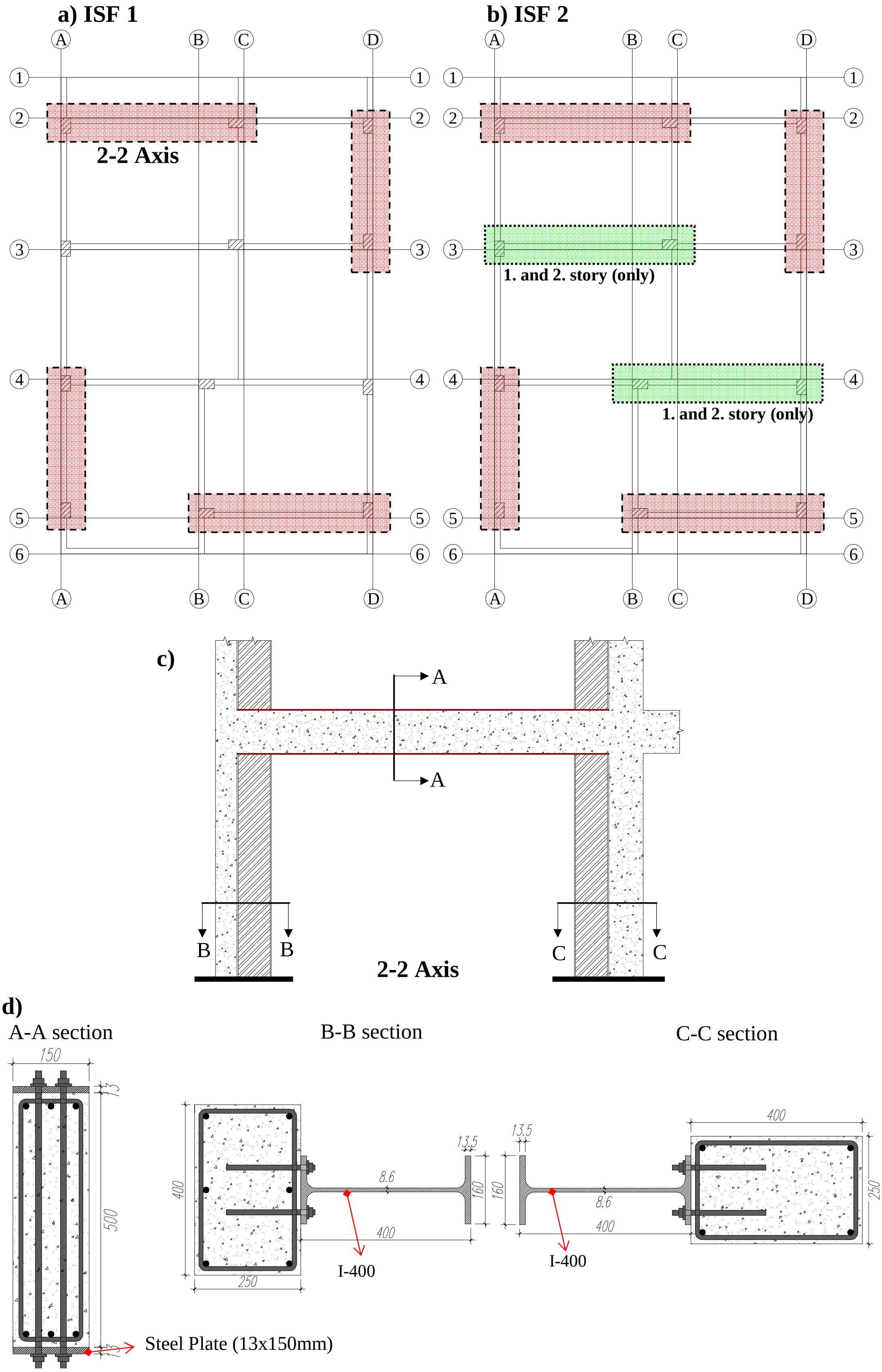

Figure 4.38 a) and b) Strengthened building with ISF1 and ISF2, c) view of the axis 2-2, d) section of the composite members.

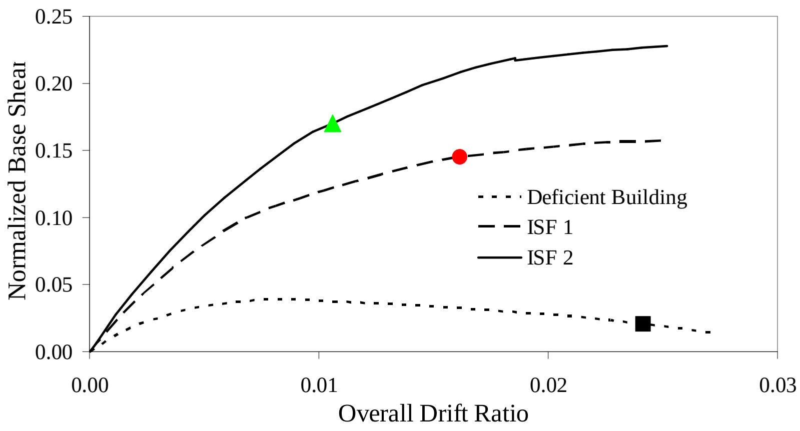

Figure 4.39 Pushover curve of the buildings, building with ISF1 and ISF2.

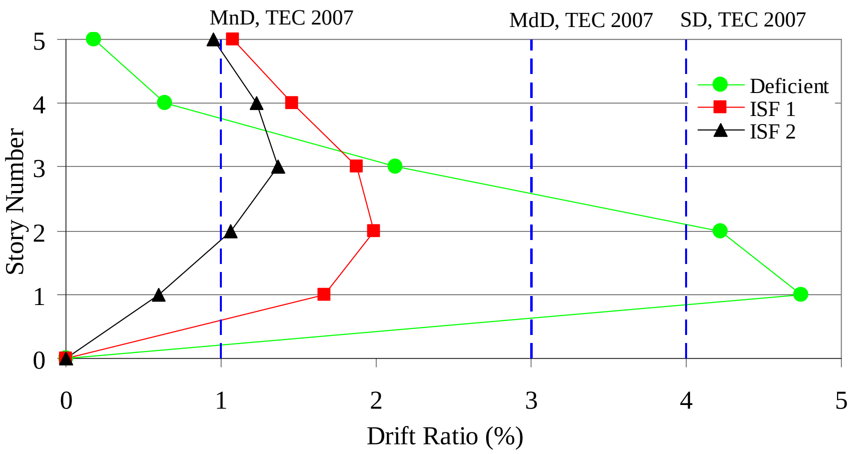

Figure 4.40 IDR of the building retrofitted with ISFs at the performance points.

Table 4.7 Performance levels of the members of the building retrofitted with ISF

Column	1. story			2. story			3. story			4. story			5. story		
Performance Levels	Deficient	ISF 1	ISF 2	Deficient	ISF 1	ISF 2	Deficient	ISF 1	ISF 2	Deficient	ISF 1	ISF 2	Deficient	ISF 1	ISF 2
MnD	0	4	10	1	11	12	5	12	12	12	12	12	12	12	11
MdD	0	3	2	4	0	0	6	0	0	0	0	0	0	0	1
SD	0	1	0	3	0	0	1	0	0	0	0	0	0	0	0
Total Collapse	12	4	0	4	1	0	0	0	0	0	0	0	0	0	0

Beam	1. story			2. story			3. story			4. story			5. story		
Performance Levels	Deficient	ISF 1	ISF 2	Deficient	ISF 1	ISF 2	Deficient	ISF 1	ISF 2	Deficient	ISF 1	ISF 2	Deficient	ISF 1	ISF 2
MnD	12	16	18	16	19	21	17	19	18	23	19	19	24	22	24
MdD	2	5	4	1	4	3	7	5	6	1	5	5	0	2	0
SD	0	1	0	5	1	0	0	0	0	0	0	0	0	0	0
Total Collapse	8	0	0	2	0	0	0	0	0	0	0	0	0	0	0

CHAPTER 5

5. CONCLUSIONS

The strengthening of existing deficient RC structures with structural steel members were examined in the course of this study. A comprehensive experimental program and extensive numerical studies were conducted to better understand the strengthening mechanisms for structural steel retrofit applications of deficient RC frames. Fifteen one bay-one story and two three bay-two story RC frames were tested by using quasi static and pseudo dynamic testing procedures, respectively. The use of chevron braces, internal steel frames, X-braces and column-shear plate applications were investigated. Two potential candidates, namely chevron brace and internal steel frame retrofits, were investigated in detail. Chevron brace retrofitting can be viewed as a stiffening/strengthening retrofit scheme, when applied provides reasonable deformation control with strength increase. However, ductility of such a retrofit scheme is limited due to brace buckling (Chapter 2) and potential damage to the boundary columns exists (Chapter 3). Hence its use can be limited for low to mid rise structures, where the main retrofit objective is deformation control. Internal steel frames, on the other hand, could change the behavior of a non ductile frame to a more ductile one. Hence, it may suit the needs of engineers when deformation capacity need is more pronounced.

Currently, there are no explicit design guidelines for seismic retrofit using structural steel members in TEC (2007). The results of the experimental program and deformation limits for RC members and braces according to TEC (2007) and ASCE/SEI 41 (2007), respectively, were utilized to reveal whether safe retrofit designs can be achieved. The study shows that employing the strain limits suggested by the TEC (2007) for RC and composite members of ISF may be used for ISF retrofit design. Furthermore, for the chevron brace members, force deformation relation suggested by the ASCE/SEI 41 (2007) may be used for the chevron brace retrofit leaving a sufficient margin of safety. A simple design flowchart is presented later in this chapter to lay out the basic principles of incorporating structural steel in RC frame retrofits.

Main Conclusions

The following conclusions were drawn from the measurements and observations of the numerical and experimental studies.

- Seismically deficient RC frames (low concrete strength and insufficient lateral confinement and poor reinforcement details) were successfully upgraded by using Chevron Braces and Internal Steel Frames (ISFs).
- Chevron Brace and ISF can increase the stiffness, strength, and energy dissipation capacity of seismically deficient RC frames significantly.
- Chevron braced frames are effective to control the story drift demands but they are non-ductile systems. On the other hand, the ISFs are flexible and ductile systems but may be less economical for controlling the story drift demands.
- After brace buckling, lateral strength and stiffness of the braced frames decreased significantly. Hence, post-buckling capacity of the brace member governed the performance of the braced frame.
- The post buckling capacity of the brace members can be used for a seismic retrofit design as far as the RC members are within the acceptable performance levels.
- The performance levels of the RC frame and brace members can be evaluated by using the deformation limits suggested by TEC (2007) and ASCE/SEI 41 (2007), respectively. Such an assessment was found to be safe in this study.
- Two ISF applications were examined in the course of the experimental program. It was found that as long as the horizontal shear strength of the RC beam-column joints is sufficient to resist the shear force demand by the ISF, one may pursue ISF installation with minimal anchorage sufficient to avoid out of plane movements. Conversely, if the horizontal shear strength of the RC beam-column joints is smaller than the shear force demanded by the ISF, use of engineered design dowels to ensure composite action is necessary.
- Global drift limits (1% DR for IO, 3% DR for LS and 4% DR for CP) suggested by the TEC (2007) seems to be appropriate to evaluate the seismic performance of the ISF retrofitted buildings.
- Low to mid-rise buildings, i.e. 5 story building in this study, can be retrofitted by using Chevron Brace and ISF retrofitting techniques by utilizing the TEC (2007) and

ASCE/SEI 41 (2007) document. This argument was supported with a case study building presented in Chapter 4.

- X-Brace and Steel Column-Shear Plate applications are not recommended in the way they were employed in this study. Further research is needed to argue the opposite.

A Possible Design Methodology

Based on the knowledge gained from this study, a simple design flow can be established as shown in Figure 5.1 for chevron brace and ISF retrofit design of deficient RC frame buildings.

First, the information about the existing RC building should be prepared as suggested in TEC (2007) or ASCE/SEI 41 (2007). The information from the drawings of the building (location of the columns and beams as well as the foundation), site investigations and laboratory testing for mechanical properties of the materials (concrete and reinforcement bar), should be compiled. The next step is to model the building with proper tools (distributed plasticity or lumped plasticity) such that expected inelastic phenomena are accounted. After conducting the structural analysis for the estimated seismic demands, the damage limit states of RC members, can be checked using either TEC (2007) or ASCE/SEI 41 (2007) guidelines. For chevron braces and ISF composite columns and beams, it is suggested to use of ASCE/SEI 41 (2007) performance limits (Chapter 5, Section 4) and TEC (2007) strain limits (Chapter 7, Section 7.6.9). The section dimensions of the ISF or chevron brace components are iterated until the desired target performance is met. It should be kept in mind that while retrofitting a building, usually a hybrid scheme composed of many retrofit options (use of FRPs, structural walls, chevron braces or ISF) can be combined together depending on the architectural requirements and physical installation constraints. It is believed that the optimal retrofit design may be achieved with such an approach. For a preliminary estimation of the chevron brace member or ISF steel section sizes, limiting the inter story deformations to 1% (Figures 3.50, 3.51, 4.8 and 4.9 and Table 4.1 and Section 3.6.4) and 2% (Figures 3.63 and 4.12 and Tables 3.7 and 3.9, Section 3.6.4) for the chevron brace and ISF retrofit, respectively, is recommended. Final decision of the sizes should certainly be based on the performance level of the retrofitted building (or whether the building is adequate after retrofit or not) dictated by the codes, engineers, owners or based on a consensus of all. It should be reminded that further studies may be needed to further fine tune the damage limit states of composite members in ISF applications.

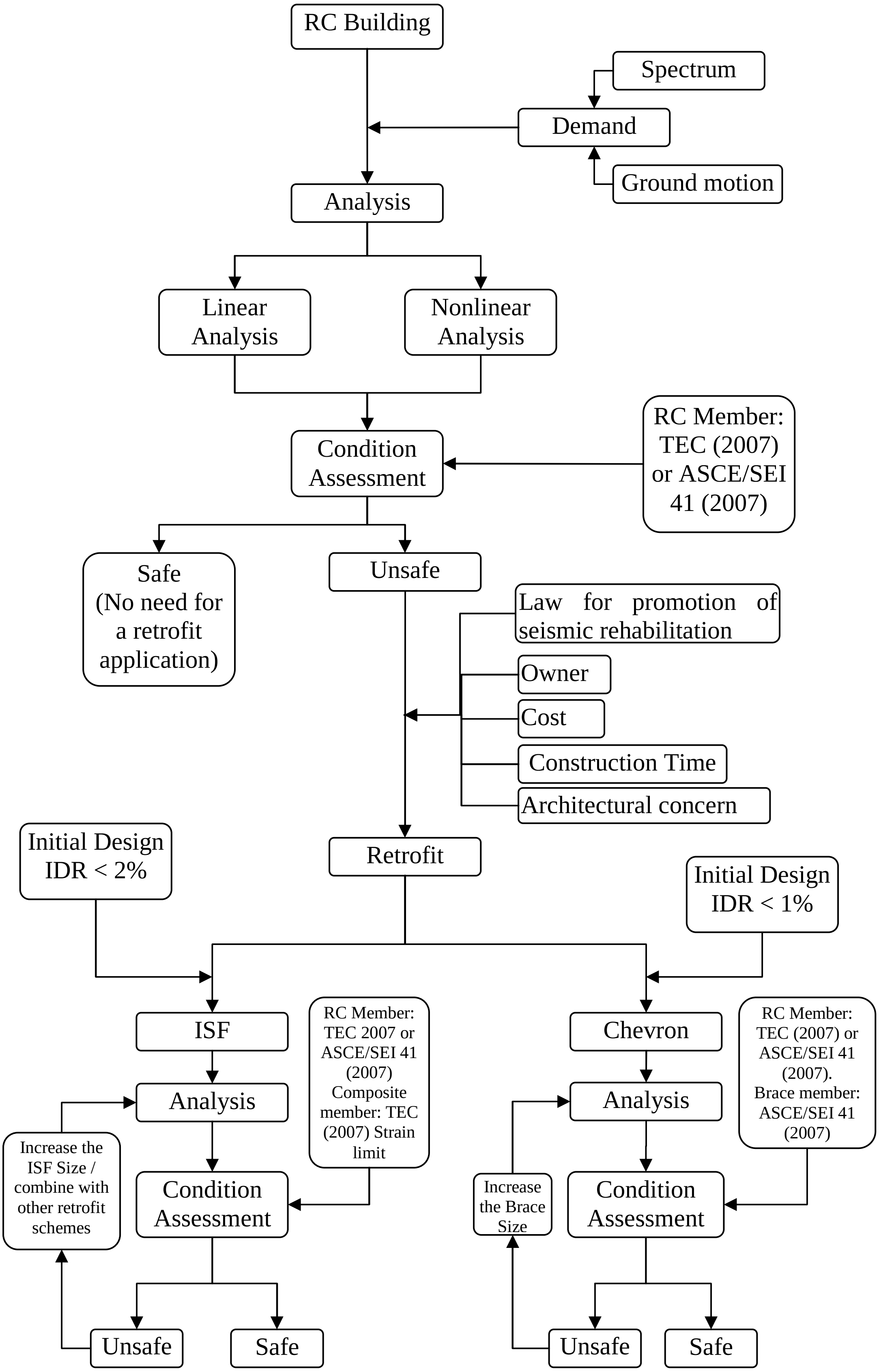

Figure 5.1 Retrofit design flowcharts

Further design recommendations

Based on the designs and the observed performance of the test specimens following recommendations can be given:

1- The use of the Uniform Force Method (LRFD, 1994) is appropriate to estimate the force transferred from the braces to the RC members.
2- The RC beam in the chevron braced span should be strengthened in order to carry the shear force and flexure demands resulting from unbalanced brace force after brace buckling. Instead of the approach followed in Chapter 2 (allowing for shear damage in the RC beam), the philosophy employed in Chapter 3, (the brace size is selected to minimize the unbalanced force and the RC beam is strengthened for sufficient flexure and shear capacity) can be preferred.
3- Gusset plates should be designed by following the equations presented in LRDF (1994) recommendations. The compression capacity of the gusset plate and brace member can be calculated by using AISC (2005). It was found that the use of an effective length factor of 2 was found to be appropriate for the chevron braced retrofitted RC frames. Hence, the stiffeners may be required based on the gusset plate compression capacity. The length of the gusset plate within the Whitmore section (Whitmore, 1952) can be determined from the recommendations of Thornton (1984). For a safe connection, this study recommends the over-strength factor of the HSS sections to be selected between 1.5 and 2.
4- The brace slenderness limits of TS 648 (1980), LRFD (1994) or any other relevant code should be followed when selecting chevron braces.
5- The brace layout through the building height can be arranged to reduce the demands imposed by the brace members to the RC joints.
6- To construct composite beams and columns, the numbers and locations of the anchorage rods can be determined with respect to axial capacity of the steel and RC members. In other words, they is a need to provide sufficient capacity to transfer shear forces from the steel to RC members or vice verse.
7- The size of the weld for the brace and ISF connection can be determined with respect to TS 3357 (1979), LRFD (1994) or any other relevant code.
8- The composite columns and beams at the joints for the ISF retrofit should obey the rule of strong column-weak beam formulation.

REFERENCES

AISC. Steel Construction Manuel (13th Edition) (2005). American Institute of Steel Construction (AISC) Inc., USA.

Akpınar U (2010) Nonlinear Analysis of RC Frames Retrofitted with Structural Steel Elements. MSc. Thesis. Middle East Technical University, Ankara.

Akpınar U, Özçelik R, Binici B (2011). The effect of infill wall on seismic performance of deficient RC structures. COMPDYN 2011 III ECCOMAS Thematic Conference on Computational Methods in Structural Dynamics and Earthquake Engineering Corfu, Greece.

Aktan AE, Bertero VV (1984) Seismic response of r/c frame-wall structures. *Journal of Structural Engineering*, *ASCE* 110(8):1083-1821.

American Society for Testing and Materials (ASTM) (2004) E 8M standard test methods of tension testing of metallic materials (metric). West Conshohocken, United States.

American Society of Civil Engineers (ASCE) (2007). Seismic Rehabilitation of Existing Buildings, Report No.ASCE/SEI 41-06, Reston, Virginia, United States.

American Society of Civil Engineers, Prestandard and Commentary for the Seismic Rehabilitation of Buildings, Report No. FEMA 356. Reston, Virginia, 2000.

Badoux M, Jirsa JO (1990) Steel Bracing of RC Frames for Seismic Retrofitting. *Journal of Structural Engineering*, *ASCE*, 116(1):55-74.

Bartera F, Giacchetti R (2004) Steel Dissipating Braces for Upgrading Existing Building Frames. *Journal of Constructional Steel Research*, *AISC* 60(19):751-769.

Benjamin JR, Williams HA (1958) The behavior of one-story brick shear walls. *Journal of Structural Division, ASCE* 84(ST) 4:1723.

Berman JW, Celik OC, Bruneauc M (2005) Comparing hysteretic behavior of light-gauge steel plate shear walls and braced frames. *Engineering Structures* 27:475-485.

Bertero VV, Aktan AE, Charney FA, Sause R (1984) Earthquake simulation tests and associated studies of a 1=5th-scale model of a 7-storey reinforced concrete test structure. Report No. UCB=EERC-84=05, University of California, Berkeley, CA.

Bertero VV, Aktan AE, Charney FA, Sause R (1984) Earthquake simulation tests and associated studies of a 1/5th-scale model of a 7-story R/C frame-wall test structure. Report No. UCB/EERC-84/05, University of California, Berkeley.

Black GR, Wenger BA, Popov EP. Inelastic Buckling of Steel Struts Under Cyclic Load Reversals. Tech. Rep. UCB/EERC-80/40, EERC, Berkeley, CA, October, 1980.

Broderick BM, Gogginsa JM, Elghazouli AY (2005) Cyclic performance of steel and composite bracing members. *Journal of Constructional Steel Research* 61:493-514.

Building Code Requirements for Structural Concrete and Commentary. American Concrete Institute (ACI 318-08), Farmington Hills, MI, 2008.

Bush TD, Jones EA, Jirsa JO (1991) Behavior of the RC Frames Strengthened Using Structural Steel Bracing. *Journal of Structural Engineering, ASCE* 117(4):1115-1126.

Çağatay IH (2005) Experimental evaluation of buildings damaged in recent earthquakes in Turkey. *Engineering Failure Analysis* 12(3):440-452.

Canbay E, Ersoy U, Tankut T (2004) A three-component Force Transducer for RC Structural Testing. *Engineering Structures* 26(2):257-265.

Dhakal RP, Maekawa K (2002) Modeling for Postyield Buckling of Reinforcement. *Journal of Structural Engineering* 128(9):1139-1147.

Doğangün A (2004) Performance of reinforced concrete buildings during the May 1, 2003 Bingöl Earthquake in Turkey. *Engineering Structures*.26(6):841-856.

Downs RE (1991) Evaluation of two RC buildings retrofit with steel bracing. PhD Thesis. University of Illinois at Urbana-Champaign.

Elkhoraibi T, Mosalam KM (2007) Towards error-free hybrid simulation using mixed variables. *Earthquake Engineering & Structural Dynamics* 36(11):1497-1522.

Ghobarah A, Elfath HA (2001) Rehabilitation of a Reinforced Concrete Frame Using Eccentric Steel Bracing. *Engineering Structures* 23(7):745-755.

Goggins JM, Broderick BM, Elghazouli AY, Lucas AS (2005) Experimental cyclic response of cold-formed hollow steel bracing members. *Engineering Structures* 27:977-989.

Han SW, Kim WT, Foutch DA (2007) Seismic Behavior of HSS Bracing Members according to Width–Thickness Ratio under Symmetric Cyclic Loading. *Journal of Structural Engineering, ASCE*, 133(2):264-273.

Han SW, Kim WT, Foutch DA (2007) Tensile strength equation for HSS bracing members having slotted end connections. *Earthquake Engng Struct. Dyn.* 36:995-1008.

Hassan OF, Goel SC (1991) Modeling of brace members and seismic behavior of concentrically braced steel structures. Research Report UMCE 91-1. Department of Civil Engineering, The University of Michigan College of Engineering.

Higashi Y, Endo T, Okhubo M, Shimizu Y (1980) Experimental study on strengthening reinforced concrete structure by adding shear wall. In: Proceedings of the 7th WCEE, Istanbul, Turkey, 7:173-80.

Higashi Y, Endo T, Shimizu Y (1984) Experimental studies on retrofitting of reinforced concrete building frames. In: Proceedings of the 8th WCEE, 1:477-484.

Johnson SM (2005) Improved Seismic Performance of Special Concentrically Braced Frames. MSc. Thesis. University of Washington.

Kalkan E, Gülkan P (2004) Site-dependent spectra derived from ground motion records in Turkey. *Earthquake Spectra* 20(4):1111-1138.

Karsan ID, Jirsa JO (1969) Behavior of Concrete under Compressive Loading. *Journal of Structural Division, ASCE*, ST12, 95, 2543-2563.

Kawamata S, Ohnuma M (1980) Strengthening effect of eccentric steel braces to existing reinforced concrete frames. In: Proceedings of 7 WCEE, Istanbul, Turkey, 4:513-520.

Kent DC, Park R (1971) Flexural Members with Confined Concrete. Journal *of Structures Division, ASCE* 97(ST7):1969-1990.

Khatib IF, Mahin SA, Pister KS (1988) Seismic Behavior of Concentrically Braced Steel Frames. Report no: UCB/EERC-88/01 Earthquake Engineering Research Center, University of California, Berkeley. California.

Kim J, Choi H (2005) Response modification factors of chevron-braced frames. *Engineering Structures* 27:285-300.

Kotulka BA (2007) Analysis for a Design Guide on Gusset Plates used in Special Concentrically Braced Frames. University of Washington.

Kurt E (2010) Investigation of Strengthening Techniques Using Pseudo-dynamic Testing. MSc. Thesis. Middle East Technical University, Ankara.

Kurt E, Binici B, Kurc O, Canbay E, Akpınar U, Ozcebe G (2011) Seismic Performance of a Reinforced Concrete Test Frame with Infill Walls. *Earthquake Spectra* 27(3):(article in press).

LRFD. Load and Resistance Factor Design. American Institute of Steel Construction, Inc. (1994) USA.

MacRae G, Kimura Y, Roeder C (2004) Effect of Column Stiffness on Braced Frame Seismic Behavior. *Journal of Structural Engineering, ASCE* 130:381-391.

Maheri MR, Hadjipor A (2003) Experimental investigation and design of steel brace connection to RC frame. *Engineering Structures* 25:1707-1714.

Maheri MR, Sahebi A (1997) Use of Steel Bracing in Reinforced Concrete Frames. *Engineering Structures* 19(12):1018-1024.

Mahin SA, Shing PB, Thewalt CR, Hanson RD (1989) Pseudodynamic test method: current status and future directions. *J. Struct. Engng* 115:2113-2128.

Mander JB, Priestley MJN, Park R (1988) Theoretical Stress□Strain Model for Confined. *Concrete. J. Struct. Engrg*. 114(8):1804-1826.

Marino EM, Nakashima M (2006) Seismic performance and new design procedure for chevron-braced frames. *Earthquake Engineering and Structural Dynamics* 35(4):433-452.

Masri AC, Goel SC (1996) Seismic Design and Testing of an RC Slab-Column Frame Strengthened by Steel Bracing. *Earthquake Spectra* 12(4):645-666.

Mazzolani FM (2008) Innovative metal systems for seismic upgrading of RC structures. *Journal of Constructional Steel Research* 64:882-895.

Mazzoni S, McKenna H, Scott MH, Fenves GL (2010) OpenSees Manual, Pacific Earthquake Engineering Research Center, http://opensees.berkeley.edu.

Molina FJ, Pegon P, Verzeletti G (1999) Time-domain identification from seismic pseudodynamic test results on civil engineering specimens. 2nd International Conference on Identification in Engineering Systems, University of Wales, Swansea, March 29-31.

Molina FJ, Verzeletti G, Magonette G, Buchet PH, Géradin M (1999) Bi-Directional pseudodynamic test of a full-size three-storey building. *Earthquake Engineering and Structural Dynamics* 28(12):1541-1566.

Nakashima M, Kato H, Takaoka E (1992) Development of Real-Time Pseudo Dynamic Testing. *Earthquake Engineering and Structural Dynamics* 21:79-92.

Ozcelik R, Binici B (2006) Application of Steel Retrofit Schemes for Deficient Buildings in Turkey. First European Conference on Earthquake Engineering and Seismology, Geneva.

Özkök ME (2010) Seismic Upgrade of Deficient Reinforced Concrete Frames using External Systems. Middle East Technical University, Ankara.

Pincheira JA, Jirsa JO (1995) Seismic Response of RC Frames Retrofitted with Steel Braces or Walls. *Journal of Structural Engineering, ASCE* 121(8):1225-1235.

Popov EP, Takanashi K, Roeder CW (1976) Structural Steel Bracing Systems: Behavior Under Cyclic Loading. Report No. EERC 76-77. Earthquake Engineering Research Center, Berkley, California.

Popovics S (1975) A Review of Stress–Strain Relationships for Concrete. *American Concrete Institute Journal*, 67(3) pp:243–248.

Remennikov AM, Walpole WR (1997) Analytical Prediction of Seismic Behavior for Concentrically-Braced Steel Systems. *Earthquake Engng. Struct. Dyn*. 26:859-874.

Saatcioglu M, Mitchell D, Tinawi R, Gardner RJ, Gillies AG, Ghobarah A, Anderson DL, Lau D (2001) The August 17, 1999, Kocaeli (Turkey) earthquake — damage to structures. *Canadian Journal of Civil Engineering* 28(4):715-737.

Salmon GC, Johnson JE, Malhas FA (2009) Steel Structures, Fifth Edition, Pearson Prentice Hall, NJ, Pp: 804.

SAP2000, version 8.1., SAP2000 integrated finite element analysis and design of structures. Computers and Structures, Inc., Univ. Avenue. Berkeley, CA. 2001

Sezen H, Whittaker AS, Elwood KJ, Mosalam KM (2003) Performance of reinforced concrete buildings during the August 17 1999 Kocaeli, Turkey earthquake, and seismic design and construction practice in Turkey. *Engineering Structures* 25(1):103-114.

Sugano S, Fujimura MA (1980) Seismic srrengthening of existing reinforced concrete buildings. In: Proceedings of 7 WCEE, Istanbul, Turkey, 4:449-56.

Tagawa Y, Aoki H, Huang T, Masuda H (1992) Experimental study of new seismic strengthening method for existing RC structure. In: Proceedings of 10 WCEE, Madrid Spain, 9:5193-5198.

Takanashi K, Udagawa K, Seki M, Okada T, Tanaka H. (1975) Nonlinear earthquake response analysis of structures by a computer-actuator on-line system. *Bull. Earthquake resist. Struct. Res. Center*, Tokyo, Japan.

Talaat K, Mosalam KM (2009) Modeling Progressive Collapse in Reinforced Concrete Buildings Using Direct Element Removal. *Earthquake Engineering & Structural Dynamics*, 38(5):609-634.

Tezcan SS, İpek MA (1995) Reconnaissance report: 1995 Dinar, Turkey, earthquake. *Engineering Structures* 18(12):906-916.

The Ministry of Public Works and Settlement (2007) Turkish Code for Buildings in Seismic Zones (TEC 2007), Ankara, Turkey.

Thornton WA (1984) Bracing Connections for Heavy Construction. *Engineering Journal of AISC*, Vol: 21.

Tremblay R (2002) Inelastic seismic response of steel bracing members. *Journal of Constructional Steel Research* 58:665-701.

Tremblay R, Archambault MH, Filiatrault A (2003) Seismic Response of Concentrically Braced Steel Frames Made with Rectangular Hollow Bracing Members. *Journal of Structural Engineering, ASCE* 129(12):1626-1636.

Tremblay R, Robert N (2001) Seismic performance of low- and medium-rise chevron braced steel frames. *Canadian Journal of Civil Engineering* 27:1192-1206.

TS 3357. Turkish Standards Institute (1979). Building code for the design and execution of welded connections in steel structures Ankara, Turkey.

TS 500. Turkish Standards Institute (1980). Requirements for design and construction of reinforced concrete structures. Necatibey Caddesi, Ankara, Turkey.

TS 5317. Çelik Borular (Dikişli, kare ve dikdörtgen kesitli), Türk Standartları Enstitüsü (1987), Necatibey Caddesi, Bakanlıklar Ankara.

TS 648. Çelik Yapıların Yapım ve Hesap Kuralları. Türk Standartları Enstitüsü (1980), Necatibey Caddesi, Bakanlıklar Ankara.

TS 910. Çelik I profilleri-Sıcak haddelenmiş. Türk Standartları Enstitüsü (1986), Necatibey Caddesi, Bakanlıklar Ankara.

Uriz P, Filippou CF, Mahin SA (2008) Model for Cyclic Inelastic Buckling of Steel Braces. *Journal of Structural Engineering, ASCE* 134(4):619-628.

Vintzileou YL, Zhang GF, Tassios TP (1999) Reinforced concrete scaled columns under cyclic actions. *Soil Dynamics and Earthquake Engineering*18(2):15-167.

Whitmore RE (1952) Experimental Investigation of Stresses in Gusset Plates. Bulletin No.16, Engineering Experiment Station, University of Tennessee.

Yakut A, Gülkan P, Bakır S, Yılmaz MT (2005) Re-examination of damage distribution in Adapazarı: Structural considerations. *Engineering Structures* 27(7):990-1001.

Yamamoto Y. (1993) Strength and ductility of frames strengthened with steel bracing. *Earthquake resistance of reinforced concrete strucstructures, a volume honoring Hiroyuki Aoyama*, pp. 467-76.

Yoo JH, Lehman DE, Roeder CW (2008) Influence of connection design parameters on the seismic performance of braced frames. *Journal of Constructional Steel Research* 64:607-623.

Youssef MA, Ghaffarzadeh H, Nehdi M (2007) Seismic Performance of RC frames with Concentric Internal Steel Bracing. *Engineering Structures* 29(7):1561-1568.

Appendix 1

A1.1 Specimen and Test Setup Details

This section includes the details of the 1/3 scaled one bay-one story RC frames which was mentioned in Chapter 2. The stirrup dimension is indicated in Figure A1.1. A steel plate was welded at the upper end of the column longitudinal reinforcement to prevent anchorage failure of the longitudinal bars.

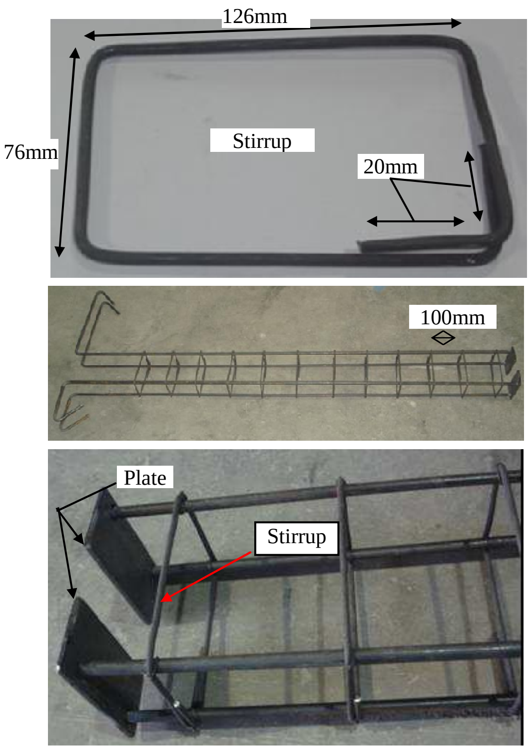

Figure A1.1 Stirrup and column reinforcement details.

Figure A1.2 indicates the beam reinforcement details. The stirrup spacing was 70 mm and there was 4-ϕ4 reinforcement with spacing 100 mm parallel to the main longitudinal reinforcement. In addition, there was ϕ4 reinforcement with spacing 100 mm perpendicular to the longitudinal reinforcement through the beam span.

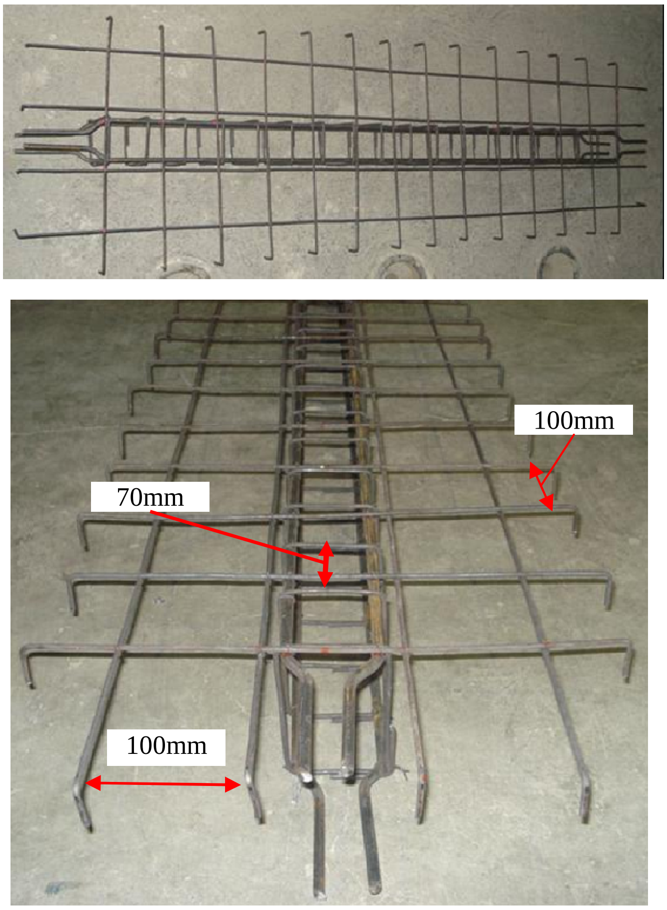

Figure A1.2 Beam reinforcement details.

The concrete was casted into the steel molds placed parallel to the ground as seen in Figure A1.3. Figure A1.4 indicates the RC frame after concrete casting. After curing at this position, the frame erected with proper apparatuses without damaging the RC frame. The test frame after removing the molds and before the placing the setup is indicated in Figure A1.5. Test setup is indicated in Figure A1.6. Figure A1.7 shows the loading apparatus.

In order to determine the mechanical properties of the longitudinal and transverse reinforcement and steel members, a test setup was constructed as seen in Figure A1.8. For each 1/3 scaled one bay-one story RC frame the mechanical properties of the bars were determined as seen in Figure A1. 9.

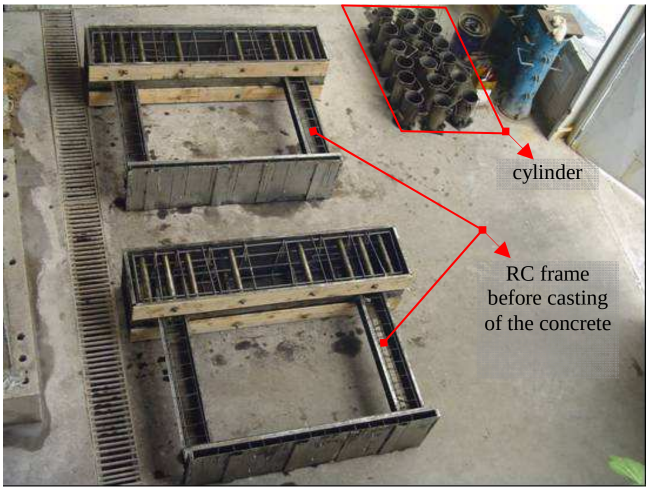

Figure A1.3 Molds before concrete casting

Figure A1.4 RC frame after concrete casting

Figure A1.5 RC frame after removing the molts

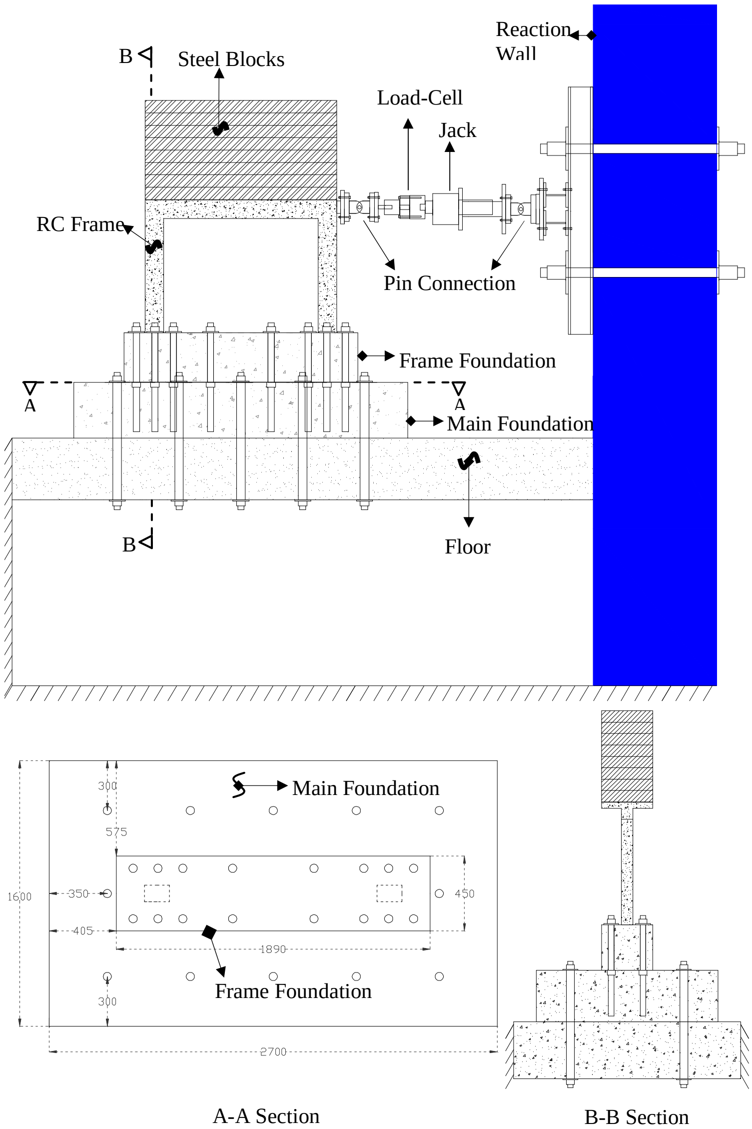

Figure A1.6 Test setup

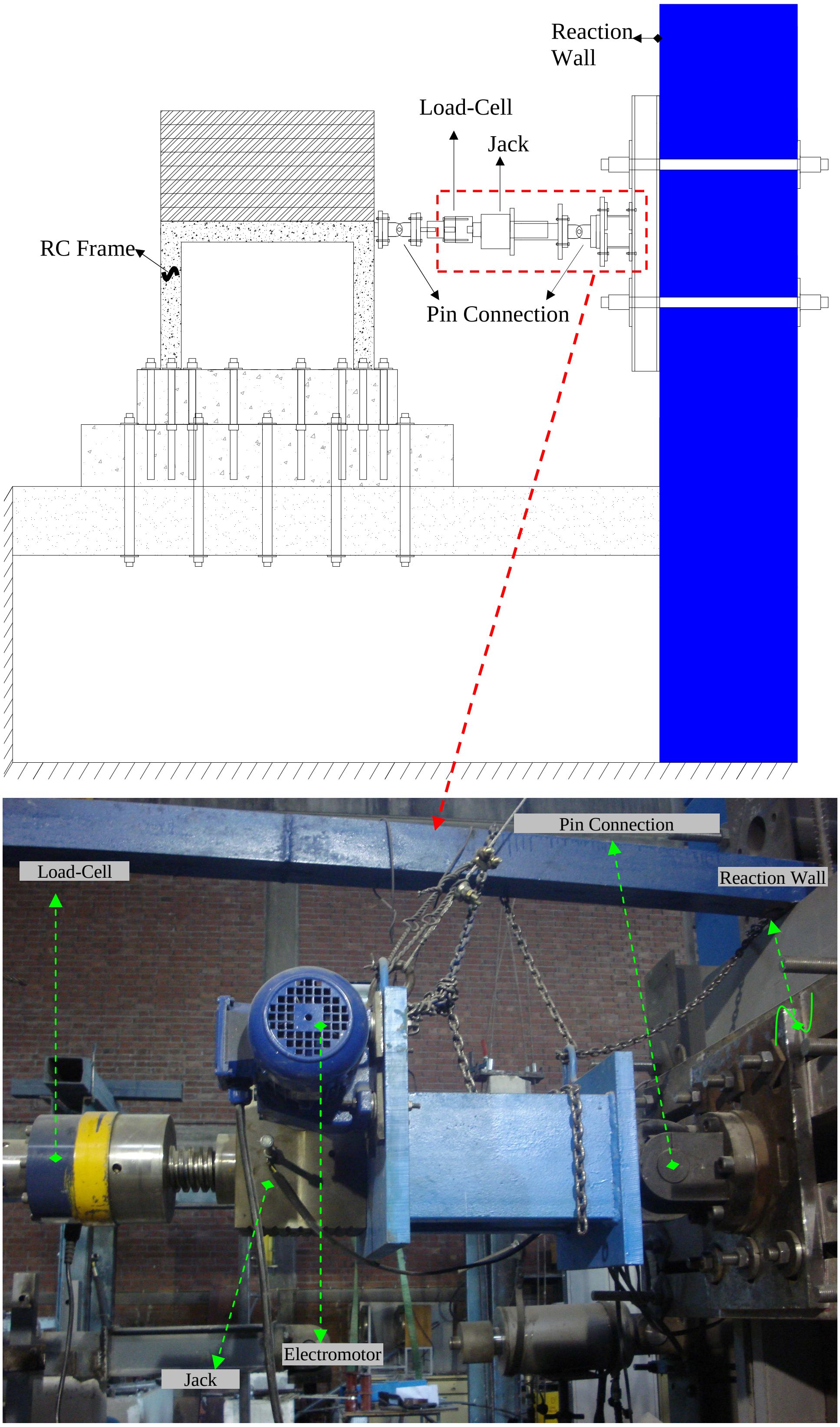

Figure A1.7 Loading apparatus.

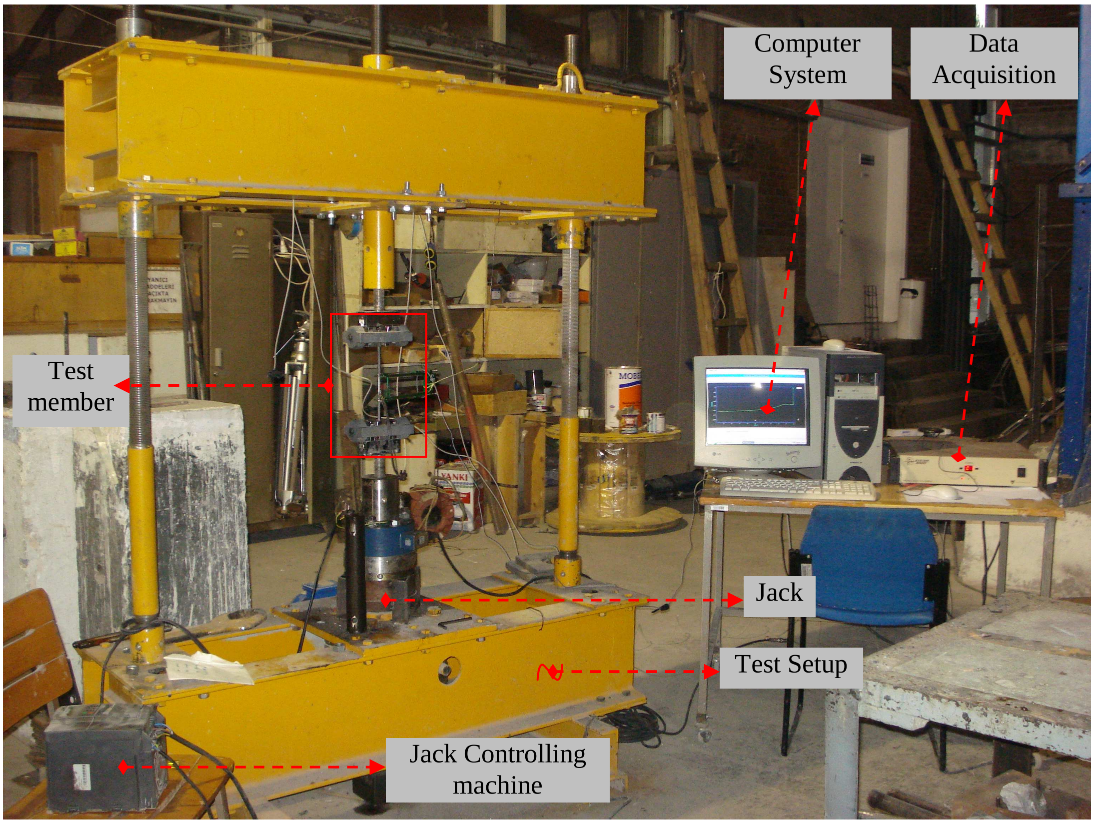

Test Member (ϕ8 reinforcement bar)

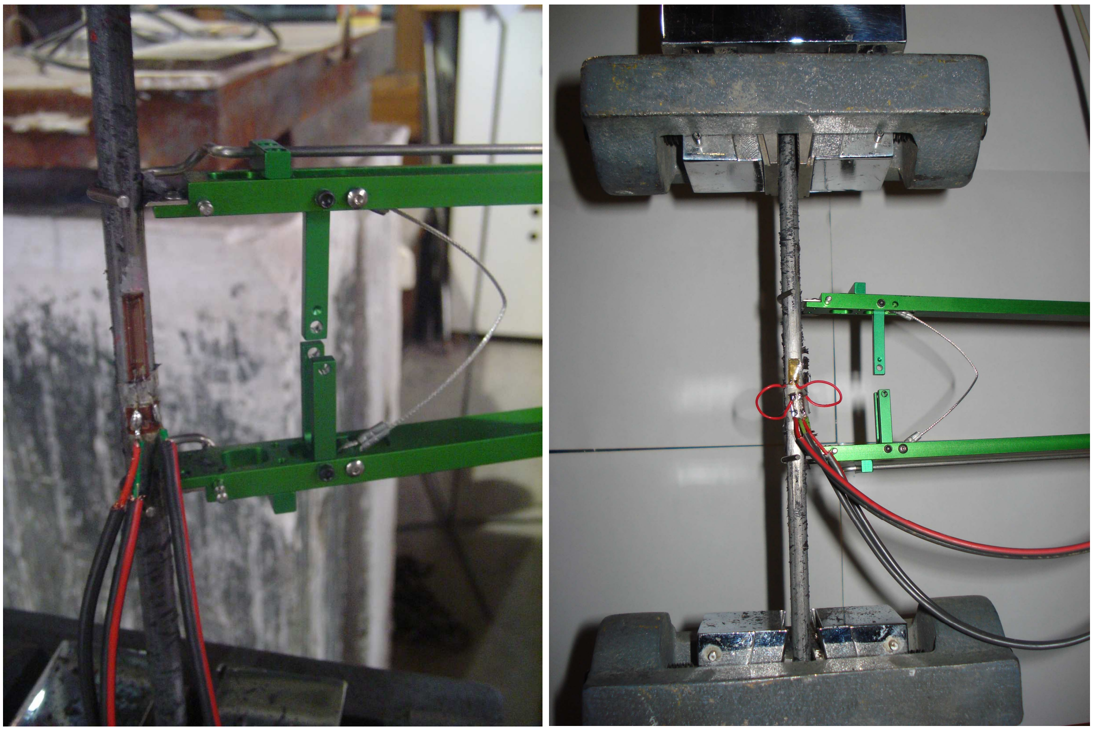

Figure A1.8 Coupon test setup

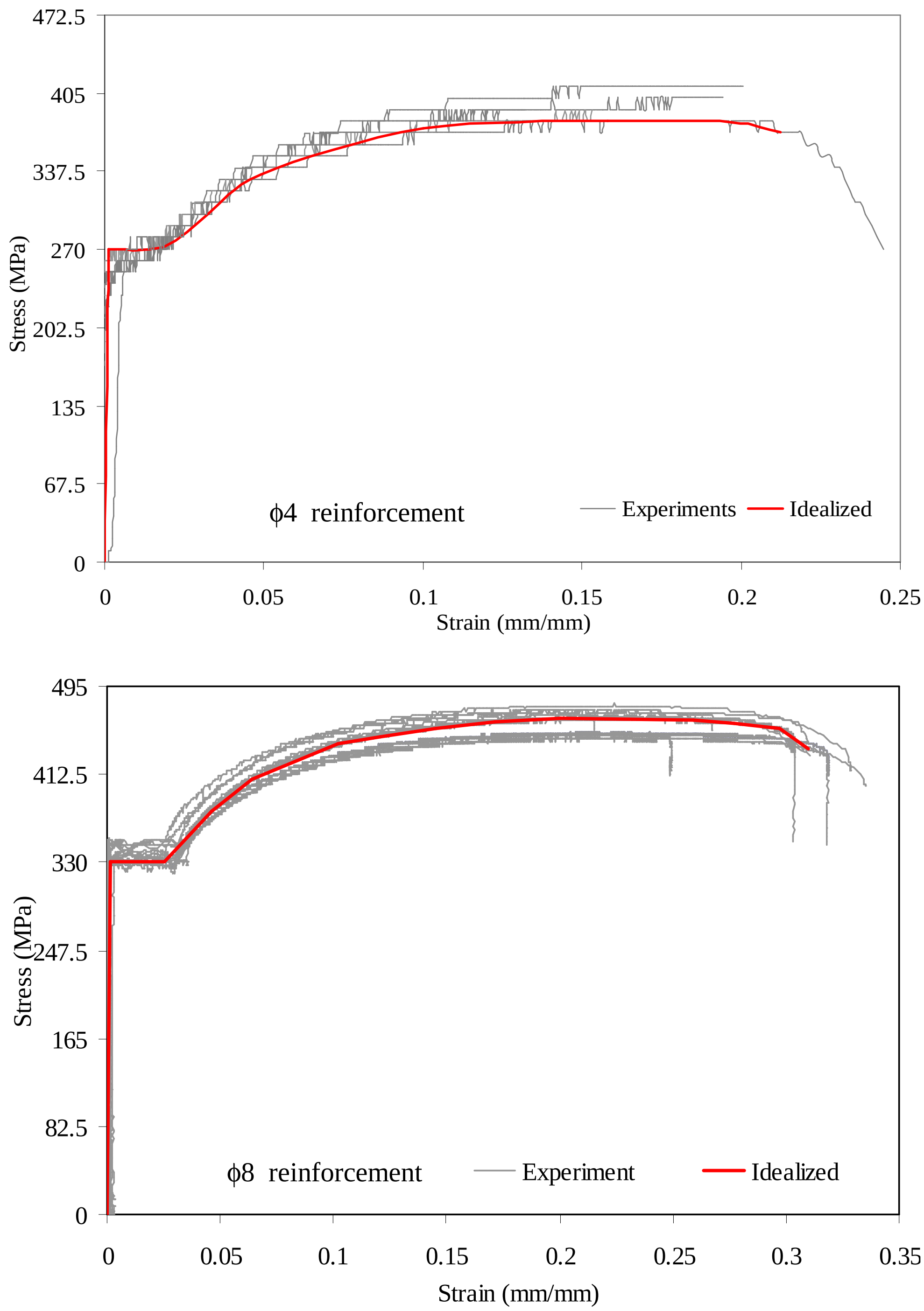

Figure A1.9 Coupon test results for ϕ4 and ϕ8 reinforcements

A1.2 Chevron Brace Design

The brace sections were compact as indicated in Equation A1.1 given in Table B4.1 from AISC (2005). The following equations were performed for design of the HSS 30x30x2.6 brace member. The slenderness, λ, of the brace member was 91 which was lower than the limit suggested by the TS 648 (1980) (the limit is 250).

$$\lambda_p = 1.12\sqrt{E/F_y} \tag{A1.1}$$

$$\lambda_p = 32$$

$$\frac{b}{t} = \frac{30 - 2.6 - 2.6}{2.6} = 9.5 \tag{A1.2}$$

$$\frac{b}{t} < \lambda_p \rightarrow \text{section is compact}$$

Where,

E: Modulus of Elasticity=206182 MPa from TS 648 (1980)

F_y: Nominal yield limit=235 MPa from TS 648 (1980)

b: brace member width from inner face to inner face

t: brace thickness, mm

The weld length was 60 mm between brace and gusset plate. Minimum weld yield strength was 520 MPa.

Check brace-gusset plate weld:

$$\varphi R_w = 0.75 \times (0.6 \times 520) \times (0.707 \times t_w) \times (4 \times 60) \tag{A1.3}$$

$$\varphi R_n = 39.7 \times tw$$

$$P_{bt} = R_y \times A_{gb} \times F_y \tag{A1.4}$$

$$P_{bt} = 1.4 \times 262 \times 235$$

$$P_{bt} = 86198N = 86.2kN$$

$$\varphi R_n \geq P_{bt} \rightarrow t_w = 3mm$$

Where,

R_w: Weld strength

t_w: fillet weld thickness

P_{bt}: Brace tension strength

R_y: over-strength factor

A_{gb}: brace area

Brace wall rupture at weld:

$P_{bt} = 86.2kN$

$$\varphi R_w = 0.75 \times (0.6 \times F_u) \times (A_{nv}) \quad \text{(A1.5)}$$

$\varphi R_w = 0.75 \times (0.6 \times 363) \times (4 \times 60 \times 2.6) = 101.9kN$

$\varphi R_w > P_{bt}$ ...ok

Where,

F_u: tensile strength from TS 648 (1980)

A_{nv}: net area subjected to shear

Compression capacity of the brace member:

The compression capacity of the brace member can be calculated by using the equation suggested by the AISC (2005). The brace length was taken as 993 mm as indicated in Figure A1.10 and the effective length factor, k, was assumed as 1 which is the pin-pin connection case. The nominal yield and ultimate strength of the brace members was taken as 235 and 363 MPa with respect to TS648 (1980), respectively.

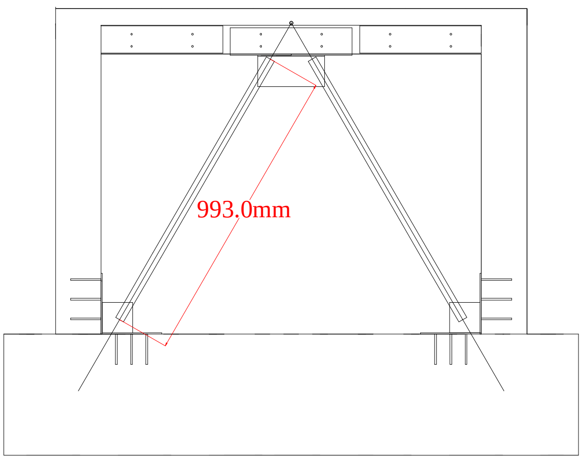

Figure A1.10 Chevron brace length

$k = 1$

$$\varphi P_{bc} = 0.9 \times F_{cr} \times A_{gb} \tag{A1.6}$$

$$\varphi P_{bt} = F_y \times A_{gb} \tag{A1.7}$$

$$Fe = \frac{\pi^2 E}{\lambda^2} \tag{A1.8}$$

$$\lambda \le 4.71\sqrt{\frac{E}{F_y}} \text{ or } F_e > 0.44 \times F_y \rightarrow F_{cr} = \left[0.658^{\frac{F_y}{F_e}}\right] F_y \tag{A1.9}$$

$$\lambda > 4.71\sqrt{\frac{E}{F_y}} \text{ or } F_e < 0.44 \times F_y \rightarrow F_{cr} = [0.877] F_e \tag{A1.10}$$

Where,

F_e: elastic critical buckling

λ: slenderness ratio

F_{cr}: critical stress

P_{bc}: compression capacity of the brace member

E: Modulus of Elasticity=206182 MPa from TS 648 (1980)

F_y: Nominal yield limit=235 MPa from TS 648 (1980)

For brace HSS 30x30x2.6:

$$Fe = \frac{\pi^2 \times 206182}{91^2} = 244 \rightarrow 244 > F_y \tag{A1.11}$$

$$4.71\sqrt{\frac{E}{F_y}} = 4.71\sqrt{\frac{206182}{235}} = 140 \rightarrow \lambda \le 4.71\sqrt{\frac{E}{F_y}}$$

$$F_{cr} = \left[0.658^{\frac{235}{244}}\right] 235 = 157 MPa \tag{A1.12}$$

$$P_{bc} = 157 \times 262 = 41.16 kN$$

RC Beam design for the chevron braced frame:

In order to design of the beam the following two cases were assumed; at the first case, while one brace has tension force, the other has compression force and this case occurred just before the compression brace buckles. This case results in shear and bending forces on gusset plate but no vertical force. The second case was compression brace buckles and tension brace yields. This case causes shear, bending and vertical force on gusset plate. After brace buckling, post buckling capacity of the brace was assumed as 0.4 (FEMA 356, 2000) times compression capacity of the brace. With respect to two extreme case give reasons to forces on gusset plate presented in Figure A1.11, the following equations were needed to be satisfied.

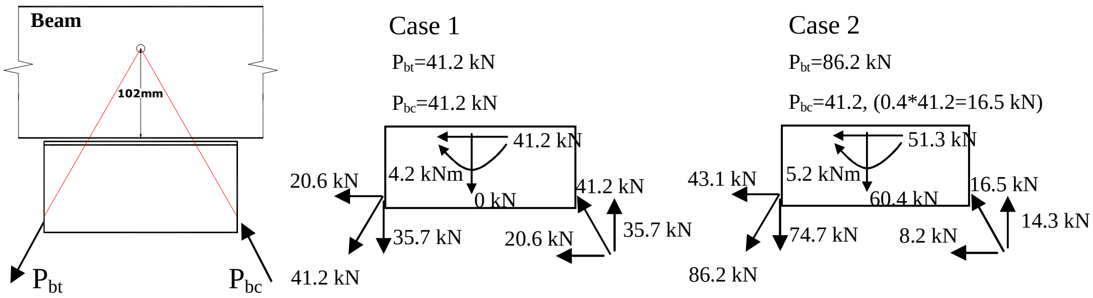

Figure A1.11 Gusset plate at the mid span of the beam (HSS 30x30x2.6)

Case 1

$$S = \frac{1}{6} \times 5 \times 220^2 = 40333 mm^3$$

$$M = 0.102 \times 41.2 = 4.2 kNm$$

$$\sigma_H = \frac{41200}{220 \times 5} = 37.5 MPa$$

$$\sigma_{moment} = \frac{M}{S} = \frac{4.2 \times 10^6}{40333} = 104 MPa$$

$$\sigma_{peak} = \sqrt{104^2 + 37.5^2} = 110.7 MPa \rightarrow \sigma_{peak} < 235 MPa$$

Case 2

$$M = 51.3 \times 0.102 = 5.2 kNm$$

$$\sigma_H = \frac{51300}{1100} = 46.6 MPa$$

$$\sigma_V = \frac{60400}{1100} = 54.9MPa$$

$$\sigma_{moment} = \frac{M}{S} = \frac{5200000}{40333} = 129MPa$$

$$\sigma_{peak} = \sqrt{(129 + 54.9)^2 + 46.6^2} = 189MPa \rightarrow \sigma_{peak} < 235MPa$$

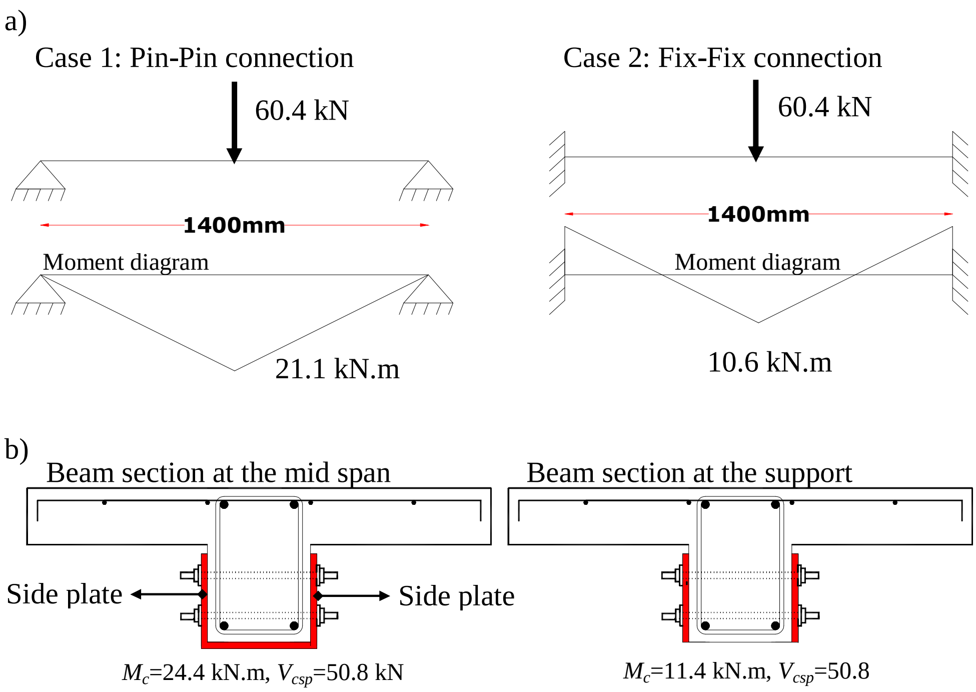

Figure A1.12 a) Force conditions at the beam after brace buckling, b) beam sections with moment capacities

It was found that 5 mm thick gusset plate was adequate for the braced frame design. The next step was to design the side plates of the beam in order to increase the shear capacity. The case 2 imposes the maximum shear forces (30.2 kN) to the RC beam (Figure A1.12-a). Hence, this vertical force should be carried by the beam with side plates. There were two side plates for each side face of the RC beam. The following equation can be used to determine the side plate dimension. Furthermore, the side steel plates were assumed to increase in the moment capacity (Figure A1.12-b). The unbalanced force after brace buckling applies moment force to the beam. This moment can be calculated by assuming two cases: the pin-pin and fix-fix end connections for the beam were assumed for the case 1 and case 2, respectively. As it is seen in Figure A1.12-b the moment demands resulted from the unbalanced force can be carried by the beam installed side plates. The side plates were divided into three parts in order to simulate the installation difficulties in existing RC building. The shear strength of the beam with side plates was calculated by using Equation A1.14.

$$t_{sp} = \frac{30200}{0.6 \times 235 \times (2 \times h_{sp})} = \frac{107}{h_{sp}} \rightarrow t_{sp} h_{sp} = 107 mm^2 \rightarrow t_{sp} = 2 \text{ mm}, \ h_{sp} = 90 \text{ mm} \qquad \text{(A1.13)}$$

$$V_{csp} = 2 \times \lfloor 0.6 \times f_y \times t_{sp} \times h_{sp} \rfloor = 50.8kN \qquad \text{(A1.14)}$$

Where,

t_{sp}: thickness of the side plates

h_{sp}: height of the side plate (maximum 90 mm due to slap)

V_{csp}: Shear strength resulted from side plates (there were two side plates)

The numbers of anchorage rods at the bottom of the column and foundation (Figure 2.8) were determined based on the estimated brace forces. If the horizontal and vertical brace forces are transferred from the brace to column and foundation, respectively the numbers of the anchorage rods can be determined from the equations A1.15 and A1.16.

$$N_{RodXDir} = \frac{F_{ybrace} \times A_{gbrace} \times SF}{F_{yrod} \times A_{rod}} \times \cos\theta \qquad \text{(A1.15)}$$

$$N_{RodYDir} = \frac{F_{ybrace} \times A_{gbrace} \times SF}{F_{yrod} \times A_{rod}} \times \sin\theta \qquad \text{(A1.16)}$$

$$N_{RodXDir} = \frac{235 \times 262 \times 1.4}{15.9 \times 786} \times \cos 60 = 3.45 \rightarrow 4 \text{ anchorage rods at the column}$$

$$N_{RodYDir} = \frac{235 \times 262 \times 1.4}{15.9 \times 786} \times \sin 60 = 5.97 \rightarrow 6 \text{ anchorage rods at the foundation}$$

where,

$N_{rodXDir}$ and $N_{rodYDir}$ are the numbers of the anchorage on the column and foundation, respectively. F_{ybrace} and A_{gbrace} are the nominal yield strength (235MPa) and cross section area of the brace member, respectively. F_{yrod} and A_{rod} are the nominal yield strength and cross section area (assuming 75% of the actual diameter) of the anchorage rod, respectively.

θ is the brace angle with respect to horizontal axis. The required embedment length of the threaded anchors was taken as 20ϕ (ϕ: anchorage rod diameter). SF is the over strength factor.

The base shear capacity estimation (braced frame with HSS 30x30x2.6):

The base shear or lateral strength of the braced frame was calculated by considering the column mechanism, brace yielding and buckling. The lateral strength was determined for two cases; before and after brace buckling. The lateral strength of the braced frame was determined as 60.7 and 56.4 kN for the first and second case, respectively (Figure A1.13). The estimated lateral strength of the braced frame was about 3 times that of reference frame estimated as 17.6 kN as indicated in Figure 2.2.

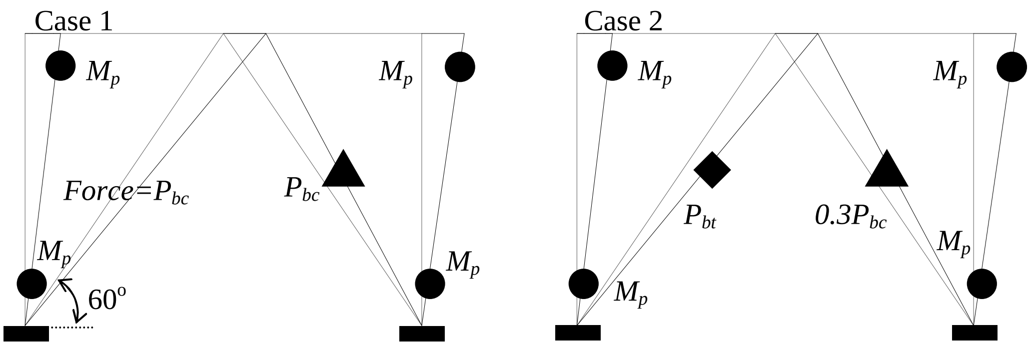

$$P_{bt} = 235 \times 262 = 61.57\,kN$$
$$P_{bc} = 41.2kN$$
$$M_p = 5kNm$$
$$V_{bs} = 4 \times (Mp/1.03) + (P_{bc} + P_{bc})\cos 60 = 60.7kN \rightarrow CaseI$$
$$V_{bs} = 4 \times (Mp/1.03) + (P_{bt} + 0.3P_{bc})\cos 60 = 56.4kN \rightarrow CaseII$$

Figure A1.13 Lateral strength estimation (braced frame with HSS 30x30x2.6)

Block shear rupture in gusset plate:

Equation A1.17 examines the block shear rupture along the shear failure path. The details are available in LRFD (1994).

$$\varphi R_n = \varphi(0.6 \times F_y \times A_{gv} + F_u \times A_{nt}) \text{ OR } \varphi(0.6 \times F_u \times A_{nv} + F_y \times A_{gt}) \quad \text{(A1.17)}$$

$\varphi = 0.75$

$A_{nt} = A_{gt} = 30 \times 5 = 150mm^2$

$A_{nv} = A_{gv} = 2 \times 60 \times 5 = 600mm^2$

$\varphi R_n = 0.75(0.6 \times 235 \times 600 + 363 \times 150)$ OR $0.75(0.6 \times 363 \times 600 + 235 \times 150)$

$\varphi R_n = 104.3kN$ or $124.5\text{kN} \rightarrow \varphi R_n = 104.3kN \rightarrow \varphi R_n > P_{bt} \rightarrow ok$

Where,

A_{gv}: gross area subjected to shear

A_{gt}: gross area subjected to tension

A_{nt}: net area subjected to tension

A_{nv}: net area subjected to shear

The base shear capacity estimation (braced frame with HSS 40x40x3.2):

The lateral strength of the braced frame with HSS 40x40x3x2 brace member was calculated by considering the column mechanism, brace yielding and buckling. The lateral strength was determined for two cases before and after brace buckling as mentioned above and indicated in Figure A1.14. The lateral strength of the braced frame was determined as 101.5 and 83 kN for the first and second case, respectively (Figure A1.14). The estimated lateral strength of the braced frame was about 5 times that of reference frame (17.6 kN in Figure 2.2).

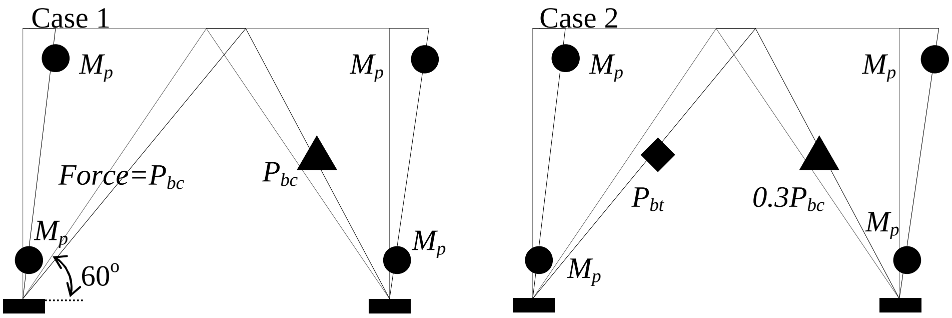

$P_{bt} = 235 \times 436 = 102.5kN$

$P_{bc} = 82.1kN$

$M_p = 5kNm$

$V_{bs} = 4 \times (Mp / 1.03) + (P_{bc} + P_{bc})\cos 60 = 101.5kN \rightarrow CaseI$

$V_{bs} = 4 \times (Mp / 1.03) + (P_{bt} + 0.3P_{bc})\cos 60 = 83kN \rightarrow CaseII$

Figure A1.14 Lateral strength estimation (braced frame with HSS 40x40x3.2)

The base shear capacity estimation (braced frame with Steel Plate 30x5):

The lateral strength of the braced frame with steel plate 30x5 brace member was calculated by considering the column mechanism, brace yielding and buckling. The lateral strength of the braced frame was determined as 56.7 kN for the second case (Figure A1.15). The estimated lateral strength of the braced frame was about 3 times that of reference frame (17.6 kN in Figure 2.2).

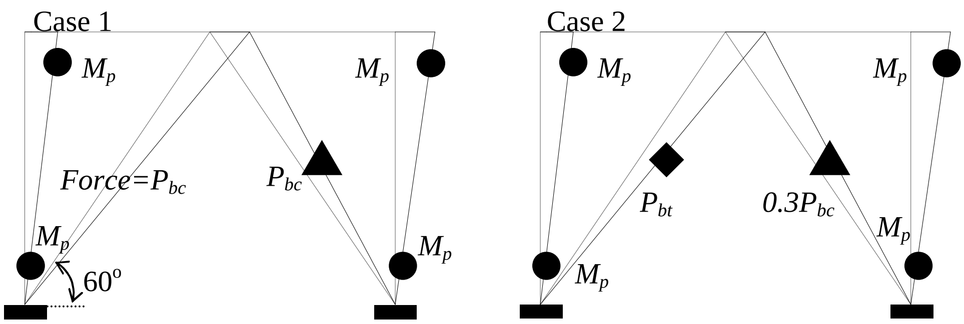

$$P_{bt} = 235 \times 300 = 70.5kN$$
$$P_{bc} \leq 0.1kN$$
$$M_p = 5kNm$$
$$V_{bs} = 4 \times (Mp/1.03) + (P_{bt} + 0.3P_{bc})\cos 60 = 56.7kN \rightarrow CaseII$$

Figure A1.15 Lateral strength estimation (braced frame with Steel Palte 30x5)

Figure A1.16 Pictures of the coupon tests (from left to right HSS70x70x3, HSS 80x80x4, I-80 web, I-80 flange, I-120 web, I-120 flange, I-140 web, I-140 flange, ϕ12)

Figure A1.16 shows the pictures of the coupons tested in order to determine the mechanical propertied of the steel members.

Appendix 2

This section includes the details of the ½ scaled three bay-two story RC frames which was mentioned in Chapter 3.

A2.1 Chevron Brace Design

The brace section was compact as indicated in Equation A2.1 given in Table B4.1 from AISC (2005).

$$\lambda_p = 1.12\sqrt{E/F_y} \quad \text{(A2.1)}$$

$$\lambda_p = 32$$

$$\frac{b}{t} = \frac{70-4-4}{4} = 15.5 \quad \text{(A2.2)}$$

$$\frac{b}{t} < \lambda_p \rightarrow \text{section is compact}$$

Where,

E: Modulus of Elasticity=206182 MPa from TS 648 (1980)

F_y: Nominal yield limit=235 MPa from TS 648 (1980)

b: brace member width from inner face to inner face

t: brace thickness, mm

150 mm weld length was used between brace and gusset plate. Minimum weld yield strength was 520 MPa.

Check brace-gusset plate weld:

$$\varphi R_w = 0.75 \times (0.6 \times 520) \times (0.707 \times t_w) \times (4 \times 150) \quad \text{(A2.3)}$$

$\varphi R_n = 99262 \times tw$

$$P_{bt} = R_y \times A_{gb} \times F_y \tag{A2.4}$$

$P_{bt} = 1.5 \times 1000 \times 235$

$P_{bt} = 353000N = 353kN$

$\varphi R_n \geq P_{bt} \rightarrow t_w = 5mm$

Where,

R_w: Weld strength

t_w: fillet weld thickness

P_{bt}: Brace tension strength

R_y: over-strength factor

A_{gb}: brace area

Brace wall rupture at weld:

$P_{bt} = 353kN$

$$\varphi R_w = 0.75 \times (0.6 \times F_u) \times (A_{nv}) \tag{A2.5}$$

$\varphi R_w = 0.75 \times (0.6 \times 363) \times (4 \times 150 \times 4) = 392040N = 392kN$

$\varphi R_w > P_{bt}$ ...ok

Where,

F_u: tensile strength from TS 648 (1980)

A_{nv}: net area subjected to shear

Gusset plate size and compression check:

The gusset plate dimensions are indicated in Figure A2.1. Brace axial load is resisted by the Whitmore section on the gusset plate (Whitmore, 1952). AISC (2005) defines this section as "Whitmore section, l_w, is determined at the end of the joint by spreading the force from the start of the 30 degree to each side in the connecting element along the line of force" (Figure A2.2). Equation A2.6 gives tension capacity of the gusset plate at the Whitmore section. This capacity should be larger than brace tension capacity (P_{bt}) (Table A2.1).

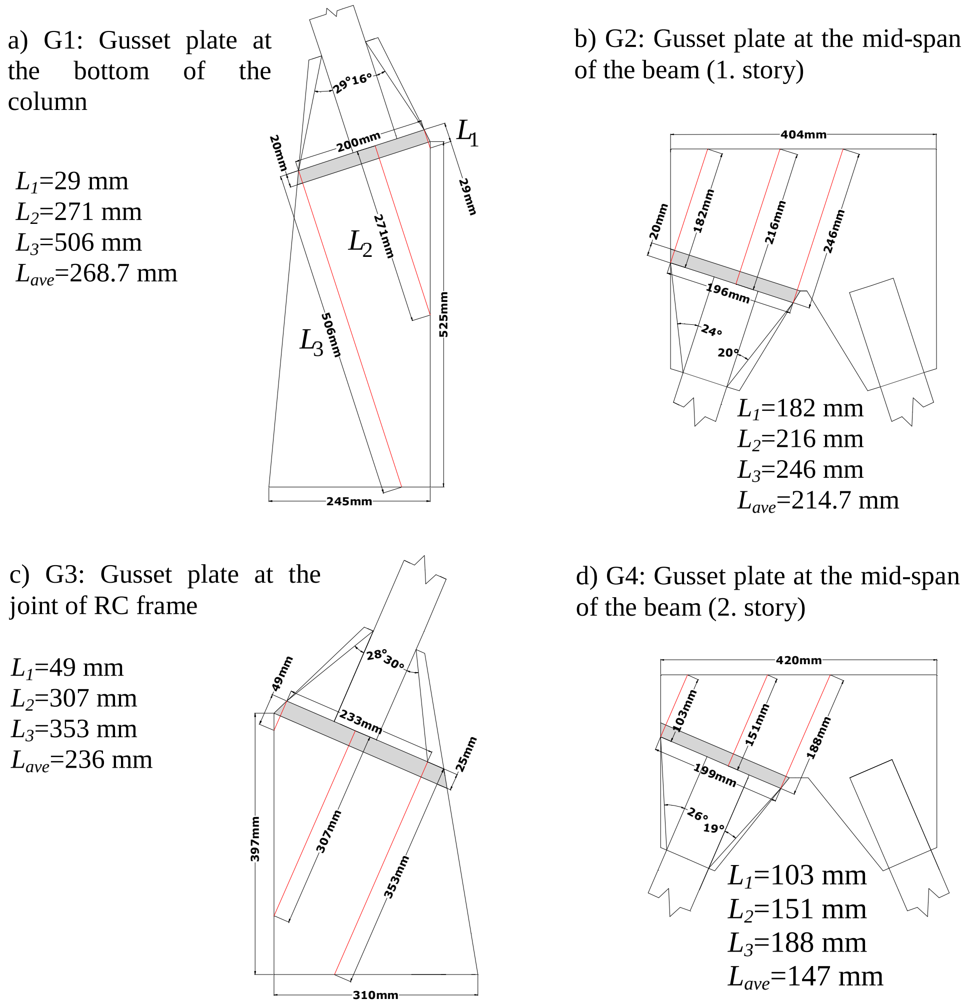

Figure A2.1 Gusset plate dimensions

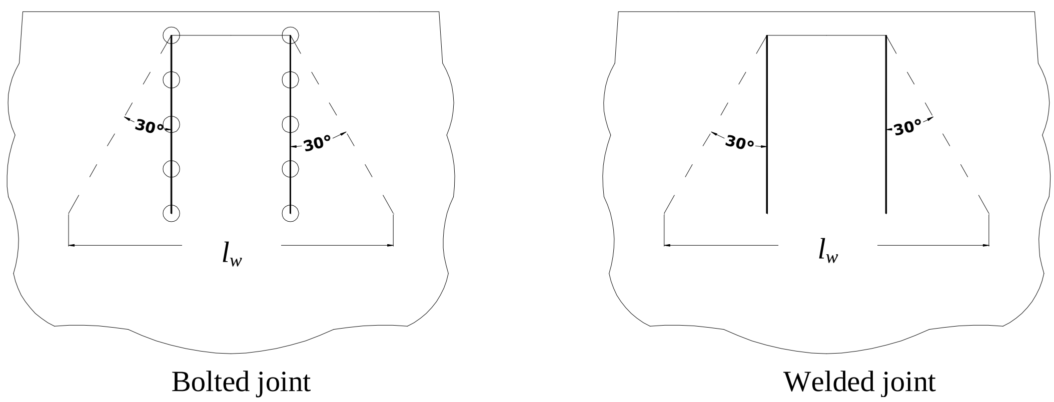

Figure A2.2 Illustration of the width of the Whitmore section (adopted from AISC, 2005)

$$P_{bt} = 353kN$$

$$\varphi P_{gti} = 0.9 \times (F_y) \times (A_{gw}) \tag{A2.6}$$

$$\varphi P_{gt1} = 0.9 \times (235) \times (200 \times 10) = 423kN$$

$$\varphi P_{gt1} > P_{bt} \rightarrow ok.$$

Where,

φP_{gti}: Gusset plate capacity,

A_{gw}: gusset plate area at the Whitmore length

l_w: Whitmore length

i=1; gusset plate at the bottom of the column (Figure A2.1-a), i=2; gusset plate at the mid-span of the beam of the first story (Figure A2.1-b), i=3; gusset plate at the joint of the first story (Figure A2.1-c), i=4; gusset plate at the mid-span of the beam of the second story (Figure A2.1-d).

Table A2.1 Tension check of the gusset plate

Gusset Plate	l_w	φP_{gt} (kN)	P_{bt} (kN)	Validation
P_{gt1}	200	423	353	$\varphi P_{gi} > P_{bt} \rightarrow$ok
P_{gt2}	196	415	353	$\varphi P_{gi} > P_{bt} \rightarrow$ok
P_{gt3}	233	493	353	$\varphi P_{gi} > P_{bt} \rightarrow$ok
P_{gt4}	199	421	353	$\varphi P_{gi} > P_{bt} \rightarrow$ok

Gusset plate compression capacity check:

First of all, the brace compression capacity is needed to be calculated. Two distinct brace lengths (Figure A2.3) were assumed, first is from work point to work point brace length (l_{b1}), other was actual brace length (l_{b2}). Effective length factor, k, was assumed as 1 for brace members. Brace compression capacity can be calculated from equations (Equations A2.7 to A2.12) suggested by the AISC (2005). The calculated axial load capacity of the brace member considering different brace length for each story was summarized in Table A2.2.

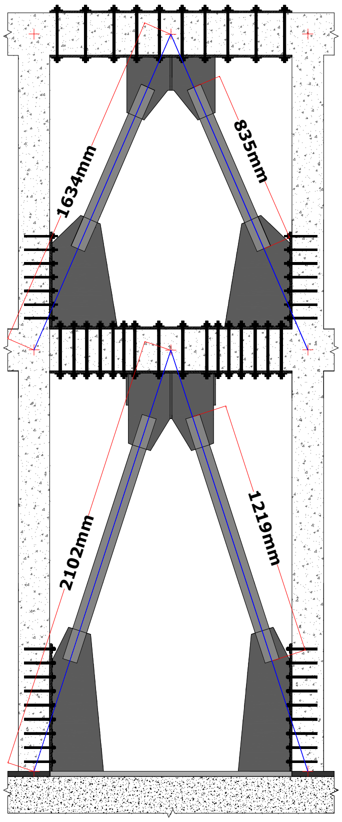

Brace Location	l_{b1} (mm)	l_{b2} (mm)
2. story	1634	835
1. Story	2102	1219

Figure A2.3 Interior span of the braced frame.

$k = 1$

$$\varphi P_c = 0.9 \times F_{cr} \times A_{gb} \tag{A2.7}$$

$$Fe = \frac{\pi^2 E}{\lambda^2} \tag{A2.8}$$

$$\lambda \leq 4.71\sqrt{\frac{E}{F_y}} \text{ or } F_e > 0.44 \times F_y \rightarrow F_{cr} = \left[0.658^{\frac{F_y}{F_e}}\right] F_y \tag{A2.9}$$

$$\lambda > 4.71\sqrt{\frac{E}{F_y}} \text{ or } F_e < 0.44 \times F_y \rightarrow F_{cr} = [0.877] F_e \tag{A2.10}$$

For first story and l_{b1}

$$Fe = \frac{\pi^2 \times 206182}{79.2^2} = 324 \rightarrow 324 > F_y \tag{A2.11}$$

$$4.71\sqrt{\frac{E}{F_y}} = 4.71\sqrt{\frac{206182}{235}} = 140 \rightarrow \lambda \leq 4.71\sqrt{\frac{E}{F_y}}$$

$$F_{cr} = \left[0.658^{\frac{235}{324}}\right]235 = 173.5MPa \qquad \text{(A2.12)}$$

$$P_{bc} = 173.9 \times 1000 = 173.5kN$$

Where,

F_e: elastic critical buckling

λ: slenderness ratio

F_{cr}: critical stress

P_{bc}: compression capacity of the brace member

Table A2.2 Brace compression capacity

Location		λ	P_{bc} (kN)
2. story	l_{b1}	61.6	195.6
	l_{b2}	31.5	224.0
1. story	l_{b1}	79.2	173.5
	l_{b2}	45.9	212.2

Table A2.3 Gusset plate compression capacity

Gusset Plate	gusset heigth (mm)		l_w (mm)	P_{gc} (kN)			P_{bc} (kN)
				k_g=0.5	k_g=1.2	k_g=2	
P_{gc1}	l_2	271	200	1620	281	101	212.2
	l_a	269		1648	286	103	
P_{gc2}	l_2	216	198	2525	438	158	212.2
	l_a	215		2555	444	160	
P_{gc3}	l_2	307	233	1471	255	92	224.0
	l_a	236		2489	432	156	
P_{gc4}	l_2	151	199	452	387	276	224.0
	l_a	147		453	390	283	

The compression capacity of the gusset plate should be larger than that of brace member in order to provide stable brace behavior. Compression capacity of the gusset plate was calculated at the area enclosed by width of Whitmore section and height of this width (Thornton, 1984). There are two definitions about height of the Whitmore section to calculate the gusset plate compression capacity. Firs one is length at the direction of the brace member from brace edge to boundary of the gusset plate (l_2 in Figure A2.1-a). The other is average length (l_a) of the l_1, l_2 and l_3. Effective length factor, k_g, for gusset plate was a research issue. Here, three different k_g, 0.5 (gusset plate is supported on both edge LRFD (1994), 1.2 (gusset plate is supported on one edge LRFD, 1994) and 2 (fix-free connection type) were used and the calculated gusset plate compression capacity by using Equation A2.9 and A2.10 is given in Table A2.3. This table indicates that the compression capacity of the gusset plates is higher than that of brace members for k factor of 2 and 1.2. It was observed from the Chapter 2 that the yield strength of the HSS members were higher than their nominal yield strength used in Equations 2.9 and 2.10. Hence, the gusset plates were strengthened by using stiffener to prevent buckling. The stiffener welded to the gusset plate is exhibited in Figure 3.9 to 11. At the bottom of the column, three stiffener plates for each side were welded to the gusset plate with conservative manner (Figure 3.9). The stiffeners were welded to gusset plate with considering location of anchors used for connection between RC frame and steel members.

Block shear rupture in gusset plate:
Equation A2.13 examines the block shear rupture along the shear failure path. The details are available in LRFD (1994).

$$\varphi R_n = \varphi\left(0.6\times F_y \times A_{gv} + F_u \times A_{nt}\right) \text{ OR } \varphi\left(0.6\times F_u \times A_{nv} + F_y \times A_{gt}\right) \tag{A2.13}$$

$$\varphi = 0.75$$

$$A_{nt} = A_{gt} = 70\times 10 = 700mm^2$$

$$A_{nv} = A_{gv} = 2\times 150\times 10 = 3000mm^2$$

$$\varphi R_n = 0.75\left(0.6\times 235\times 3000 + 363\times 700\right) \text{ OR } 0.75\left(0.6\times 363\times 3000 + 235\times 700\right)$$

$$\varphi R_n = 508kN \text{ or } 613\text{kN} \rightarrow \varphi R_n = 508kN \rightarrow \varphi R_n > P_{bt} \rightarrow ok$$

Where,
A_{gv}: gross area subjected to shear
A_{gt}: gross area subjected to tension
A_{nt}: net area subjected to tension

A_{nv}: net area subjected to shear

The connection between gusset plate and boundary elements was performed in light of the Uniform Force Method. LRFD (1994) defines this method as "The essence of the Uniform Force Method is to select the geometry of the connection so that moments do not exist on the three connection interfaces; i.e., gusset-to-beam, gusset-to-column, and beam-to-column. In the absence of moment, these connections may then be designed for shear and/or tension only, hence the origin of the name Uniform Force Method."

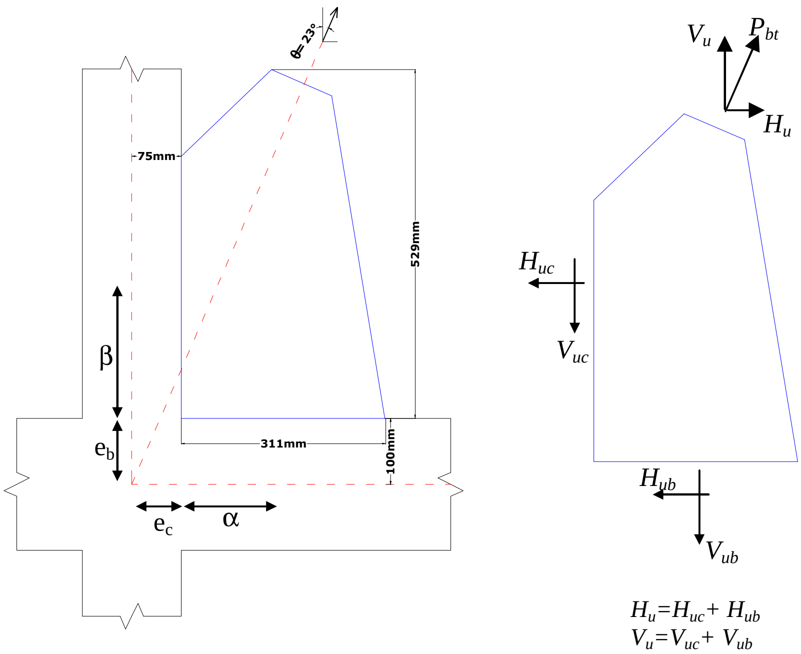

Figure A2.4 Uniform Force Method

$$
\begin{aligned}
V_{uc} &= \frac{\beta}{r} P_{bt} \\
H_{uc} &= \frac{e_c}{r} P_{bt} \\
V_{ub} &= \frac{e_b}{r} P_{bt} \\
H_{ub} &= \frac{\alpha}{r} P_{bt}
\end{aligned}
\qquad \text{(A2.14)}
$$

$$r = \sqrt{(\alpha + e_c)^2 + (\beta + e_b)^2} \tag{A2.15}$$

Assume $\beta = \bar{\beta}$ in order to prevent moment on the gusset to beam connection

$$\alpha = K + \bar{\beta} tan\theta$$

$$K = e_b \, tan\theta - e_c \tag{A2.16}$$

$$M_{ub} = V_{ub}\left(\alpha - \bar{\alpha}\right) \tag{A2.17}$$

Assume $\alpha = \bar{\alpha}$ in order to prevent moment on the gusset to column connection

$$\beta = \frac{\bar{\alpha} - K}{tan\theta} \tag{A2.18}$$

$$M_{uc} = H_{uc}\left(\beta - \bar{\beta}\right) \tag{A2.19}$$

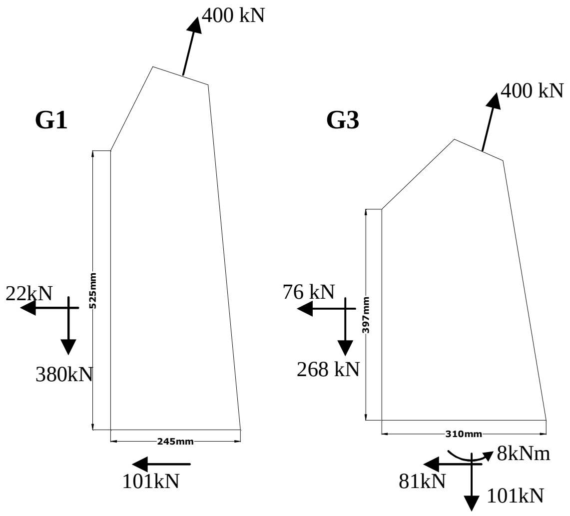

Figure A2.5 Forces on the gusset plate

For gusset G1:

As seen in Figure A2.5 the axial load capacity of the brace member was assumed 400 kN. This is because although the nominal yield strength of the brace member was 235 MPa, the expected yield strength was assumed between 350-400 MPa. Furthermore, it was desired a safe anchorage rod design due to un-predictive material strength of the HSS members. Number of the anchorage was calculated with respect to vertical and horizontal force determined as 380 and 22 kN in Figure A2.5, respectively.

$$\sigma_{Huc} = \frac{22000}{5250} = 4.1MPa$$

$$\sigma_{Vuc} = \frac{380000}{5250} = 72MPa$$

$$\sigma_{ave} = \sqrt{4.1^2 + 72^2} = 73MPa \rightarrow \sigma_{ave} < 235MPa$$

$$\sigma_{Hub} = \frac{101000}{2450} = 41MPa \rightarrow \sigma_{Hub} < 235MPa$$

Use 10 mm diameter anchorage rod (area=$\pi(0.75r)^2$=44.2, r: radius of diameter of the anchorage rod (5 mm)) and the yield strength of this rod was 900 MPa (Figure A2.9 and Table A2.4). To calculate the area of the anchorage rod, the diameter was assumed as 75% of the real anchorage rod diameter. For 18 anchorage rods:

$$\sigma_{Huc} = \frac{22000}{18 \times 44.2} = 27.7MPa$$

$$\sigma_{Vuc} = \frac{380000}{18 \times 44.2} = 477MPa$$

$$\sigma_{ave} = \sqrt{27.7^2 + 477^2} = 478MPa \rightarrow \sigma_{ave} < 900MPa \rightarrow OK$$

Use 5 mm thick weld:

$$\sigma_{weld} = 0.75 \times (0.6 \times 520) \times (0.707 \times 5) = 827MPa \rightarrow \sigma_{weld} > \sigma_{ave} \rightarrow ok$$

For gusset G3:

Figure A2.5 indicates forces acts on the gusset plate. For each edge of the plate the following equations are satisfied. Number of the anchorage was calculated with respect to vertical and horizontal force given as 268 and 76 kN in Figure A2.5, respectively.

$$\sigma_{Huc} = \frac{76000}{3970} = 19MPa$$

$$\sigma_{Vuc} = \frac{268000}{3970} = 67MPa$$

$$\sigma_{ave} = \sqrt{19^2 + 67^2} = 69MPa \rightarrow \sigma_{ave} < 235MPa$$

$$\sigma_{Hub} = \frac{81000}{3100} = 27MPa$$

$$\sigma_{Vub} = \frac{101000}{3100} = 33MPa$$

$$S = \frac{1}{6} \times 10 \times 310^2 = 160000mm^3$$

$$\sigma_{moment} = \frac{M}{S} = \frac{8000000}{160000} = 50MPa$$

$$\sigma_{ave} = \frac{1}{2}\left(\sqrt{(50+33)^2 + 27^2} + \sqrt{(33-50)^2 + 27^2} \right) = 70MPa \rightarrow \sigma_{ave} < 235MPa$$

$$\sigma_{peak} = \sqrt{(33+50)^2 + 27^2} = 92MPa \rightarrow \sigma_{peak} < 235MPa$$

Use 10 mm diameter anchorage rod (area=$\pi(0.75r)^2$ =44.2, r: radius of diameter of the anchorage rod (5 mm)) and the yield strength of this rod was 900 MPa. For 14 anchorage rods:

$$\sigma_{Huc} = \frac{268000}{14 \times 44.2} = 433MPa$$

$$\sigma_{Vuc} = \frac{76000}{14 \times 44.2} = 122.8MPa$$

$$\sigma_{ave} = \sqrt{433^2 + 122.8^2} = 450MPa \rightarrow \sigma_{ave} < 900MPa \rightarrow OK$$

Use 5 mm thick weld:

$$\sigma_{weld} = 0.75 \times (0.6 \times 520) \times (0.707 \times 5) = 827MPa \rightarrow \sigma_{weld} > \sigma_{ave} \rightarrow ok$$

Forces on the gusset plates at the mid-span of the beam are indicated in Figure A2.6. G2 and G4 represent the gusset plates at the first and second story, respectively. For a realistic approach the expected yield strength was assumes as 350 MPa (This was about 1.5x235 MPa where 1.5 was the over-strength factor) for brace member. Along with considering 350 MPa yield strength for brace member and brace length, l_{b2}, (Figure A2.3), the calculated buckling capacity of the braces were 301 kN and 326 kN for the first and second story, respectively. There are two extreme cases for the gusset plate connection as mention Appendix 1. At the first case, while one brace has tension force, the other has compression force and this case occurred just before the compression brace buckles. At the second case, compression brace buckles and tension brace yields. After brace buckling, post buckling capacity of the brace was assumed as 0.5 times compression capacity of the brace (Although the post buckling capacity ratio is suggested as 0.3 in the LRFD (1994), it was calculated as 0.5 from the ASCE/SEI 41 (2007) documentation). With respect to two extreme case give reasons to forces on gusset plate presented in Figure A2.6, the following equations were needed to be satisfied.

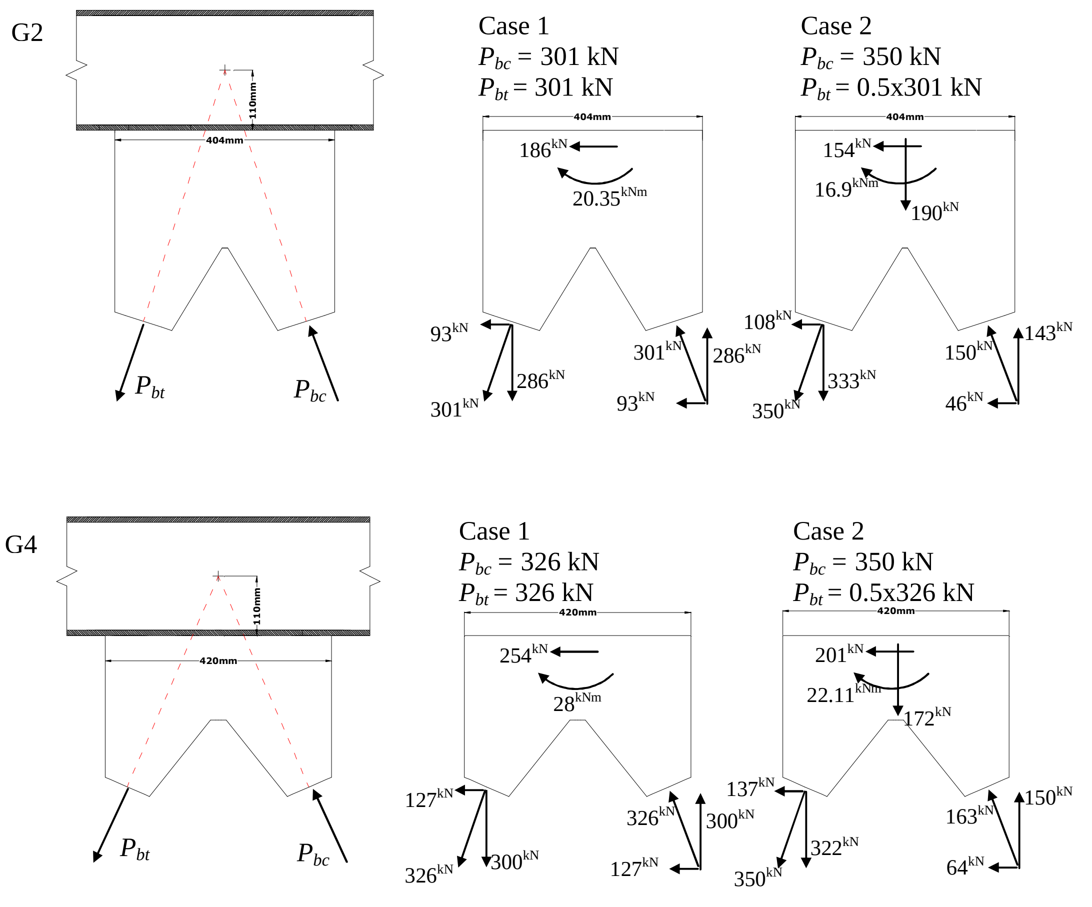

Figure A2.6 Gusset plate at the mid span of the beam, G3; at the first story and G4; at the second story

For gusset plate G2:

Case 1

$$S = \frac{1}{6} \times 10 \times 404^2 = 272000 mm^3$$

$$M = 186 \times 0.11 = 20.35kNm$$

$$\sigma_H = \frac{186000}{4040} = 46MPa$$

$$\sigma_{moment} = \frac{M}{S} = \frac{20350000}{272000} = 74.8MPa$$

$$\sigma_{peak} = \sqrt{46^2 + 74.8^2} = 87.8MPa \rightarrow \sigma_{peak} < 235MPa$$

Case 2

$$M = 154 \times 0.11 = 16.9kNm$$

$$\sigma_H = \frac{154000}{4040} = 38.1MPa$$

$$\sigma_V = \frac{190000}{4040} = 47MPa$$

$$\sigma_{moment} = \frac{M}{S} = \frac{16900000}{272000} = 62MPa$$

$$\sigma_{peak} = \sqrt{(62+47)^2 + 38.1^2} = 1185MPa \rightarrow \sigma_{peak} < 235MPa$$

Use 5mm thick weld,

$$\sigma_{weld} = 0.75 \times (0.6 \times 520) \times (0.707 \times 5) = 827MPa \rightarrow \sigma_{weld} > \sigma_{peak} \rightarrow ok$$

For gusset plate G4:

Case 1

$$S = \frac{1}{6} \times 10 \times 420^2 = 294000mm^3$$

$$M = 254 \times 0.11 = 28kNm$$

$$\sigma_H = \frac{254000}{4200} = 62.9MPa$$

$$\sigma_{moment} = \frac{M}{S} = \frac{28000000}{294000} = 95MPa$$

$$\sigma_{peak} = \sqrt{62.9^2 + 95^2} = 114MPa \rightarrow \sigma_{peak} < 235MPa$$

Case 2

$$M = 201 \times 0.11 = 22.11 kNm$$

$$\sigma_H = \frac{201000}{4200} = 48 MPa$$

$$\sigma_V = \frac{172000}{4200} = 41 MPa$$

$$\sigma_{moment} = \frac{M}{S} = \frac{22110000}{294000} = 75.2 MPa$$

$$\sigma_{peak} = \sqrt{(75.2 + 41)^2 + 48^2} = 98 MPa \rightarrow \sigma_{peak} < 235 MPa$$

Use 5 mm thick weld.

$$\sigma_{weld} = 0.75 \times (0.6 \times 520) \times (0.707 \times 5) = 827 MPa \rightarrow \sigma_{weld} > \sigma_{peak} \rightarrow ok$$

Connection at the beam-column RC joint:

The expected axial load of the brace was 400 kN acts on beam-column RC joint. According to TEC (2007), the joint strength can be calculated from Equation A2.20.

$$V_e = 1.25 \times f_{yk} \times (A_{s1} + A_{s2}) - V_{kol} \tag{A2.20}$$

$$V_{joint} = 0.45 \times b_j \times h \times f_{cd} \tag{A2.21}$$

$$V_e < V_{joint}$$

Where,

b_j: Twice the smaller of the distances measured from the vertical centerline of a beam framing into the beam-column joint in the earthquake direction, to the edges of column

h: Column cross section dimension in the earthquake direction considered

f_{cd}: Design compressive strength of concrete

f_{yk}: Characteristic yield strength of longitudinal reinforcement

A_{s1}: Total area of tension reinforcement placed on one side of the beam-column joint at the top to resist the negative beam moment

A_{s2}: Total area of tension reinforcement placed on the other side of the beam-column joint with respect to As1 at the bottom to resist negative beam moment

V_{kol}: Smaller of the shear forces at above and below the joint

$$V_{joint} = 0.45 \times 150 \times 150 \times 7.5 = 76 kN < P_{bt} = 400 kN$$

In this study, 10x150 mm thick and width plates were employed to enable to connect gusset plate and RC members. Figure A2.7 indicates the beam-column RC joint. The joint dimension, *h*, was handled different from TEC (2007). The hachured area in red was considered the progressed joint dimension. Hence, *h* was introduced 470 mm instead of 150 mm. In addition, there were 10-ϕ12 anchorage rods resisted to shear force in the joint. As a result, the joint strength consisted of enclosed area (red area in Figure A2.7) and shear strength of the anchorage rods. The following equations were employed to provide satisfactory design for the beam-column RC joint.

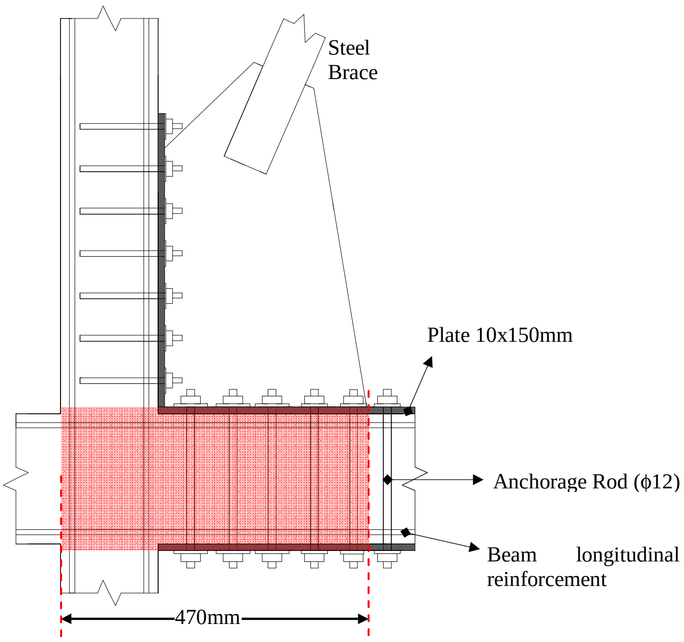

Figure A2.7 RC joint for the chevron braced frame

$$V_e = 1.25 \times \left[f_{yk} \times (A_{s1} + A_{s2}) + f_{yks} \times A_{plate} \right] \quad \text{(A2.22)}$$

$$V_e = 1.25 \times [330 \times (100 + 100) + 235 \times 1500]$$

$$V_e = 523 kN$$

$$V_{joint} = 0.45 \times b_j \times h_a \times f_{cd} + N_{AR} \times V_{AR} \quad \text{(A2.23)}$$

$$V_{joint} = 0.45 \times 150 \times 470 \times 7.5 + 10 \times 40000$$

$V_{jo\,int} = 638kN$

$V_e < V_{jo\,int}$ and $V_{bt} < V_{jo\,int} \rightarrow$ ok

Where,

f_{yks}: Characteristic yield strength of plate

A_{plate}: Plate area

h_a: Updated column cross section dimension in the earthquake direction considered

N_{AR}: number of anchorage rods in the joint bordered by the gusset plate

V_{AR}: Shear strength of the anchorage rods.

Beam design:

The RC beam at the interior span of the braced frame was constructed as compositely. The composite beam member was consisted of steel plates anchored to both bottom and top of the RC beam via anchorage rods. The composite member design is given in Chapter 3. The steel plates top and bottom of the RC beam increased the moment capacity of the RC beam significantly. The moment capacity of the composite beam (with considering nominal material strength) was determined as 74 kNm. Furthermore, the anchorage rods were assumed to carry shear stress (neglecting the contribution of the beam section and stirrups). The shear force carrying capacity of the composite beam can be determined by using equation suggested by the TS 500 (2000) (Equation A2.24). With respect to this equation the beam shear capacity was determined as 342 kN. It can be seen in Figure A2.8 that the composite beam can carry the moment and shear demand after brace buckling safely.

$$V_{shearcapacity} = \frac{A_{sw} \times f_{ywd}}{s} d \qquad \text{(A2.24)}$$

Where,

A_{sw}: Total area of the transverse reinforcement (2 times area of the anchorage rods)

f_{ywd}: yield strength of the transverse reinforcement (yield strength of the anchorage rod, Table A2.5)

s: stirrup spacing (there were 16 layer anchorage rods in 1150 mm beam span hence s is determined as 72 mm (1150/16))

d: beam depth (180 mm for beams)

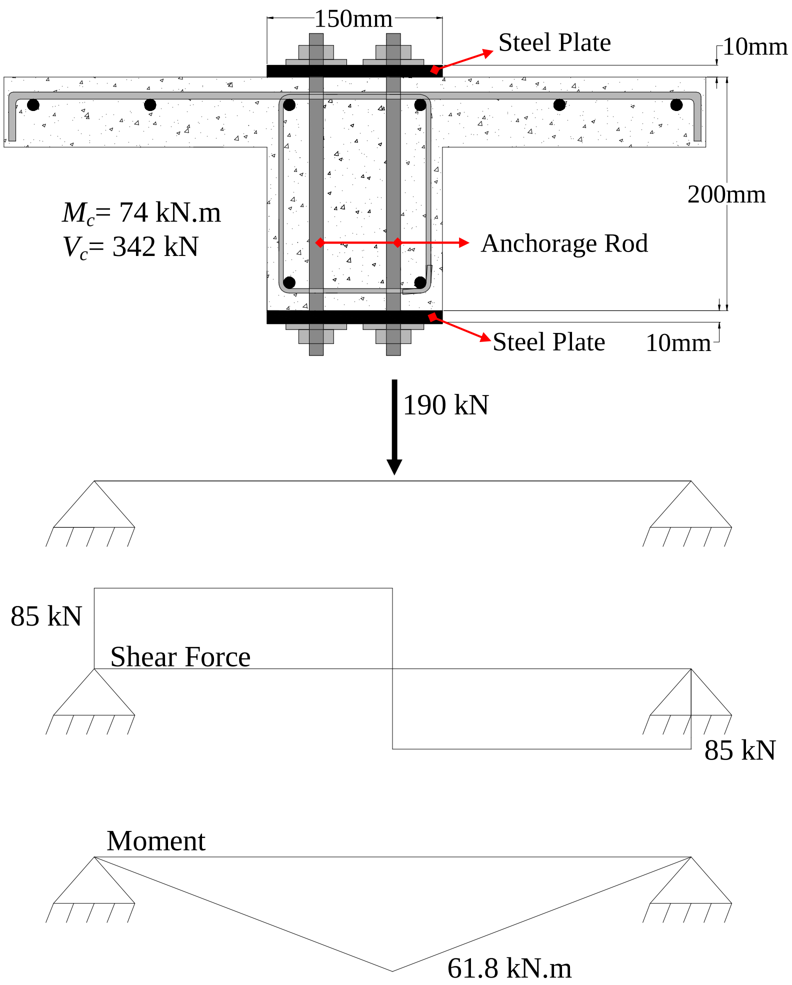

Figure A2.8 a) Force conditions at the beam after brace buckling, b) beam sections with moment capacities

A2.2 ISF Design

Shear stress check at the composite beam and column:

The nominal moment capacity of the composite beam was 53 and 58 kNm with respect to strain at the extreme fiber of the top of the beam. The clear span, from flange to flange of the IPE200, was 750 mm. Maximum shear stress occurred when the beam reaches its plastic moment capacity. The shear demand was assumed to be resisted by the beam section, stirrup and anchorage rods. Equation A2.25 was adopted from the TS 500 (2000) for the composite beam member.

$$V_{shearforce} = 1.4 \times \frac{53+58}{0.75} = 207kN$$

Above, 1.4 was used to include a safety factor.

$$V_{shearcapacity} = \left[\frac{A_{ar} \times f_{ar}}{s_{ar}} d\right]_{ar} + \left[\frac{A_{sw} \times f_{ywd}}{s} d\right]_{stirrupt} + 0.8 \times 0.65 \times f_{ctd} \times b_w \times d \quad \text{(A2.25)}$$

$$207000 = \left[\frac{2 \times 68400}{s_{ar}} 180\right]_{ar} + \left[\frac{25 \times 270}{100} 180\right]_{stirrupt} + 0.8 \times 0.65 \times \left(0.35\sqrt{7.5}\right) \times 150 \times 180$$

$$181392 = \left[\frac{2 \times 68400}{s_{ar}} 180\right]_{ar} \rightarrow s_{ar} \leq \frac{24624000}{181392} \rightarrow s_{ar} \leq 135.8 \rightarrow s_{ar} = 135mm$$

$$V_{shearcapacity} > V_{shearforce} \rightarrow ok$$

Where, f_{ctd}; tension strength of the concrete, A_{ar}; area of the anchorage rod, f_{ar}; yield strength of the anchorage rod, s_{ar}; anchorage rod spacing, A_{sw}; area of the stirrup, f_{ywd}; yield strength of the stirrup, s; stirrup spacing (100 mm), d; beam depth (180 mm for beams), b_w; beam width.

The calculated space of the anchorage rods was 135 mm for composite beam. This spacing can be seen in Figure 3.16. Based on this design strategy the composite beam was desired to perform ductile.

The nominal moment capacity of the composite column was 60 and 72 kNm with respect to strain at the extreme fiber of the top of the beam. The clear span of the composite column was 1900 mm. Maximum shear stress occurred when the column reaches its plastic moment capacity. The web of the IPE200 resisted to this shear demand by using Equation A2.26.

$$V_{shearforce} = 1.4 \frac{72+60}{1.9} = 97.2kN$$

$$V_{shearcapacity} = h_{ipe200} \times t_{ipe200} \times \frac{fy_{ipe200}}{\sqrt{3}} \quad \text{(A2.26)}$$

$$V_{shearcapacity} = 200 \times (0.6 \times 235 \times 5.6) = 158kN$$

$$V_{shearcapacity} > V_{shearforce} \rightarrow ok$$

Where, h_{ipe200}; height of the IPE200, t_{ipe200}; web thickness of the IPE200, fy_{ipe200}; nominal yield strength of the IPE200 and $1/\sqrt{3}$ was assumed as 0.6.

Further design for the ISF

Local buckling (AISC, 2005):

Flange:

$$\frac{b}{t_f} = \frac{50}{8.5} = 5.88 \qquad \text{(A2.27)}$$

$$\lambda p = 0.38\sqrt{\frac{E}{f_y}} = 0.38\sqrt{\frac{200000}{235}} = 11.1 \qquad \text{(A2.28)}$$

$$\lambda p > 5.88 \rightarrow ok$$

Web:

$$\frac{h}{t_w} = \frac{183}{5.6} = 32.7 \qquad \text{(A2.29)}$$

$$\lambda p = 3.76\sqrt{\frac{E}{f_y}} = 3.76\sqrt{\frac{200000}{235}} = 109 \qquad \text{(A2.30)}$$

$$\lambda p > 32.7 \rightarrow ok$$

Lateral torsional buckling:

$$\lambda p = 1.76 \times i_y \times \sqrt{\frac{E}{f_y}} = 1.76 \times 22.4 \times \sqrt{\frac{200000}{235}} = 1150mm \qquad \text{(A2.31)}$$

$$\lambda p < 1830mm \rightarrow \text{inelastic lateral torsional buckling}$$

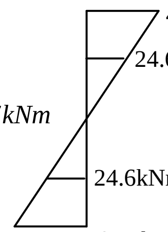

$$Mp = \left(100 \times 8.5 \times 95.75 + \frac{91.5^2}{2} \times 5.6\right) \times 2 \times 235 = 49.27kNm$$

$$S_x = 194000m^3$$

$$J = 7.01 \times 10^4 m^3$$

$$r_{ts} = \frac{bf}{\sqrt{12 \times \left(1 + \frac{1}{6}\frac{h \times t_w}{b_f \times t_f}\right)}} = \frac{100}{\sqrt{12 \times \left(1 + \frac{1}{6}\frac{200 \times 5.6}{100 \times 8.5}\right)}} = 26.13 \qquad \text{(A2.32)}$$

$$r_{ts} = \sqrt{\frac{\frac{1}{12} \times 8.5 \times 100^3 + \frac{1}{12} \times 30.5 \times 5.6^3}{850 + 30.5 \times 5.6}} = 26.13$$

$$c_b = \frac{12.5 \times 49.2}{2.5 \times 49.2 + 3 \times 24.6 + 0 + 3 \times 24.6} = 2.26 \rightarrow c_b = 2 \qquad \text{(A2.33)}$$

$$Lr = 1.95 \times rts \times \frac{E}{0.7 \times Fy}\sqrt{\frac{J \times c}{Sx \times ho}}\sqrt{1 + \sqrt{1 + 6.76\left(\frac{0.7 \times fy}{E} \times \frac{Sx \times ho}{Jc}\right)^2}} \qquad \text{(A2.34)}$$

$$Lr = 1.95 \times 26.35 \times \frac{2E6}{0.7 \times 235}\sqrt{\frac{7.01E4}{194E3 \times 191.5}}\sqrt{1+\sqrt{1+6.76\left(\frac{0.7\times 235}{2E6}\times\frac{194E3\times 191.5}{7.01E4}\right)^2}}$$

$$Lr = 4297mm$$

$$L = 1830mm, Lp = 1150mm, Lr = 4297mm$$
$$Lp < L < Lr \rightarrow \text{inelastic lateral torsional buckling}$$

$$Mn = cb\left(Mp - (Mp - 0.7 \times fy \times Sx)\left(\frac{Lb - Lp}{Lr - Lp}\right)\right) < Mp \qquad \text{(A2.35)}$$

$$Mn = 2\left(49.27E6 - (49.27E6 - 0.7 \times 235 \times 194E3)\left(\frac{1880 - 1150}{4297 - 1150}\right)\right) < Mp$$

$$Mn = 91kNm \leq 49.27kNm \rightarrow ok$$

Material

The mechanical properties of the steel members used in PsD test were given in Table A2.4. The yield strength of the steel members was determined by conducting uniaxial tension tests according to ASTM E8 (2004). Figure A2.9 indicates the stress strain response of the steel members. The yield strength of the anchorage rods, ϕ12, ϕ10 and ϕ8, was assumed as 1075, 900 MPa, respectively and they are shown in Figure A2.9. As expected in the design section, the yield strength of the HSS-70 section was found to be higher yield strength than its nominal strength suggested in TS 648 (1980). The yield strength of the HSS-70 was 350 MPa and the over strength factor was about 1.49 (350/235). In the design the over strength factor was also used as 1.5. As a result, at least 1.5 should be used as an over strength factor for chevron brace retrofitting. Figure A2.10 shows the pictures of the coupon tests.

Table A2.4 Mechanical properties of the steel members used in PsD tests

Steel Members	Yield Strength (Mpa)	Ultimate Strength	Max. Elongation (%)
Brace Member (HSS-70x70x4) [1]	350	382	31
Gusset Plate, t=10 mm [1]	265	429	33
I-200 Flange [2]	310	463	24
I-200 Web [2]	360	495	30
Plate, (t=7 mm) [2]	315	437	28
ϕ12 [1,2,3]	1075	1136	24
ϕ10 [1,2,3]	900	1008	25
ϕ8 [2,3]	900	1008	25

1: Chevron brace frame, 2: ISF, 3: Anchorage rod, the diameter of the threaded anchorage rods was assumed as 0.75 times that of real diameter of the anchorage rod.

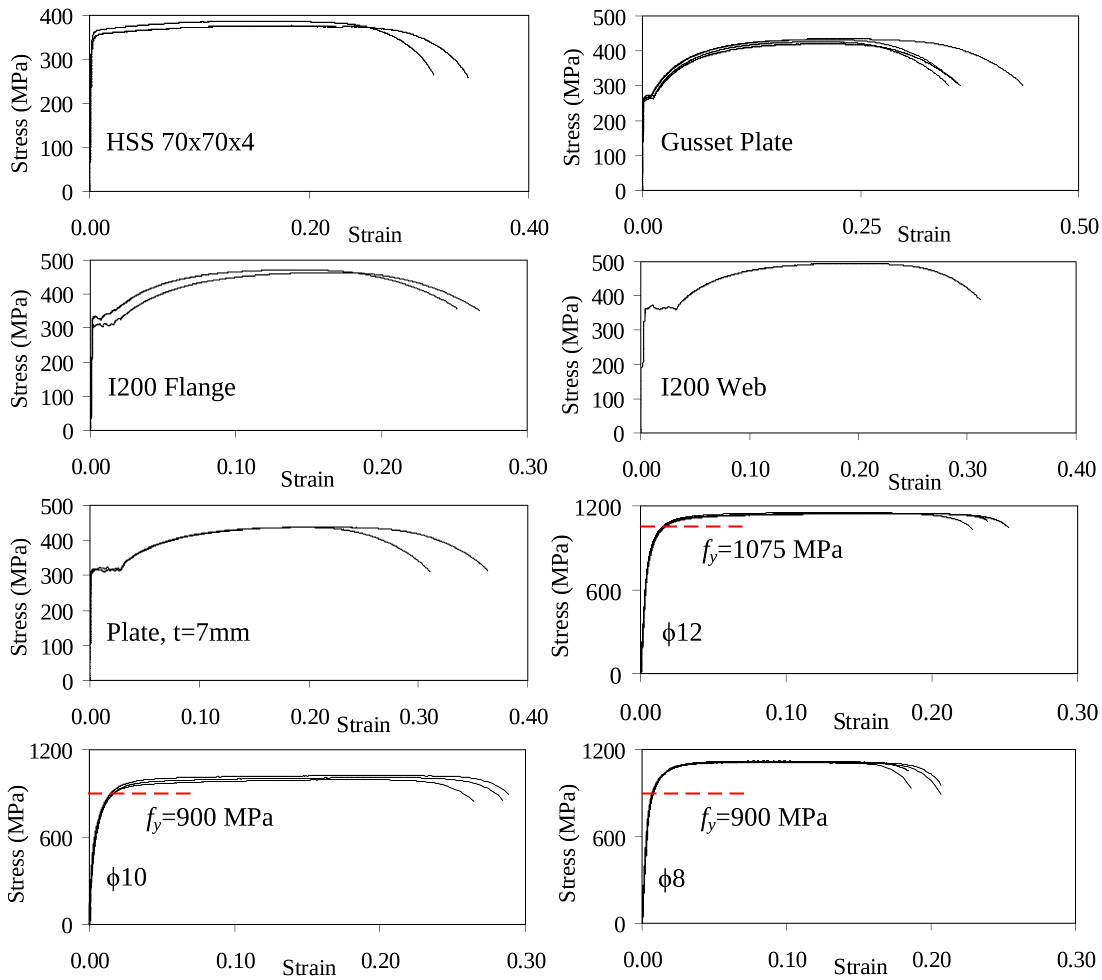

Figure A2. 9 Stress strain response of the steel members used for PsD tests

Figure A2.10 Pictures of the coupon specimens

Measurements of the PsD tests

Figure A2.11 and A2.18 shows the location of the instrumentation of the load-cell, LVDTs and strain gages for the chevron braced frame and ISF, respectively. The channel numbers of the instrumentation with abbreviate of "C" is also shown in these figures. Moreover the time intervals which was 10, 20, 30 and 40 represents the 50, 100, 140 and 180% Duzce test, respectively. Figures A2.12 to A2.23 show the displacements and strains monitored during the tests. Figure A2.12 and A2.19 show that there was no movement at the interior foundation. Figure A2.13 indicates the axial displacements at the first and second story brace members. It can be seen in Figure A2.11-b that whole length which consisted of both sections with plate and without plate was measured. While the brace member with increased area with plates was elastic it may be plastic between the increased brace area. Figure A2.14 shows the uplift of the gusset plate monitored at bottom of the interior columns C2 and C3. This uplift was measured with LVDTs located on the base plate 2 (Figure A2.11 and Figure 3.9). Figure A2.15 shows the brace strains monitored at the first story braces. As seen in Figure A2.11 that there were three strain gages on the mid-length of the brace members. Two of the three strain gages were mutually opposite sides in order to obtain the brace buckling and brace deformations. The brace buckling can be determined when the strain gages starts to measure opposite strains under compression strains as seen in Figure A2.16. Figure A2.17 shows the out off plane displacements monitored by using LVDTs. This figure indicates that using stiffeners on the gusset plates was found to be necessary in order to prevent gusset plate buckling prior to occurrence of brace buckling.

Figure A2.20 shows the uplift of the base plate 1 (Figure A2.18 and Figure 3.16). The steel plates added both top and bottom of the RC beam was monitored by using strain gages (Figure A2.21). Restricted space due to anchorage rods, the gages were bonded on the top surface of the steel plates (Figure A2.18). Figures A2.22 and 23 show the strains monitored for the bottom and top of the composite columns, respectively.

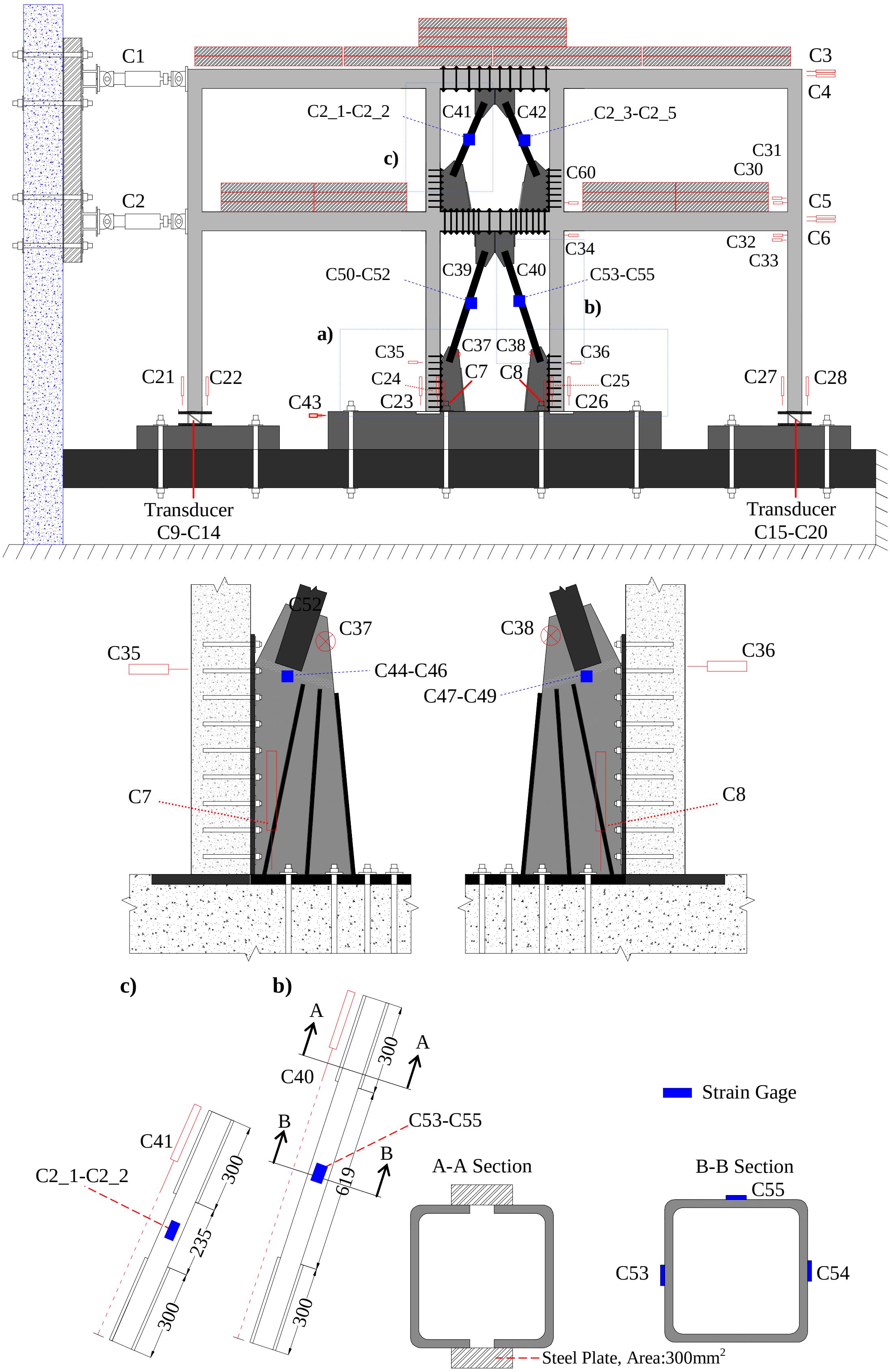

Figure A2.11 Details of the instrumentations for the chevron braced frame

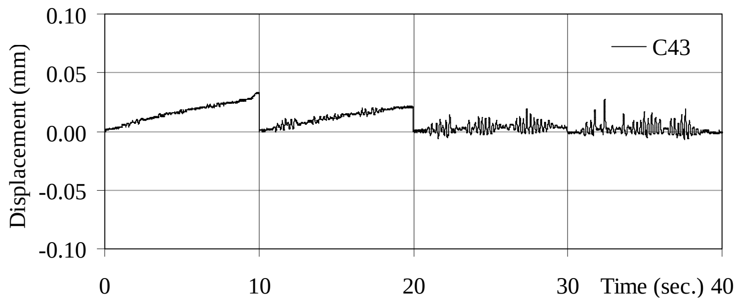

Figure A2.12 Measurement at the foundation for the chevron braced frame

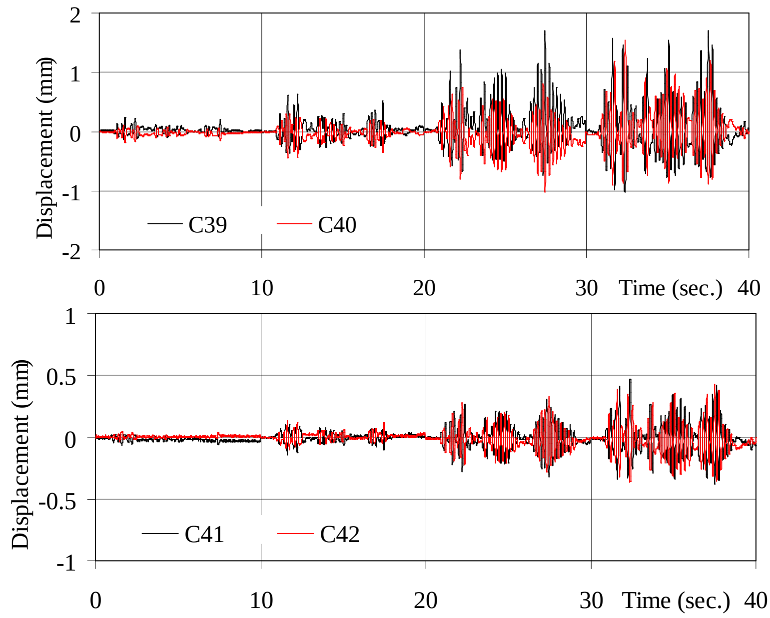

Figure A2.13 Axial displacement monitored at the first and second brace members

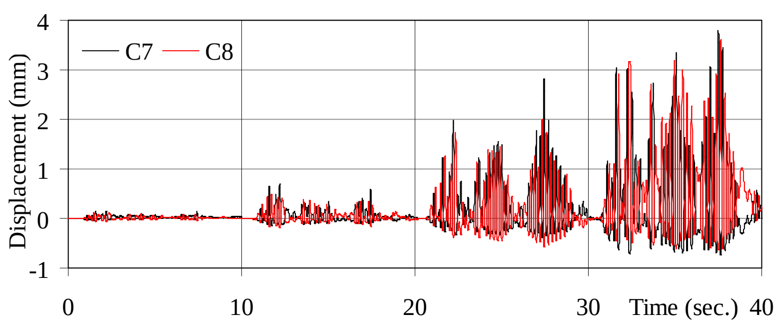

Figure A2.14 Gusset plate uplift

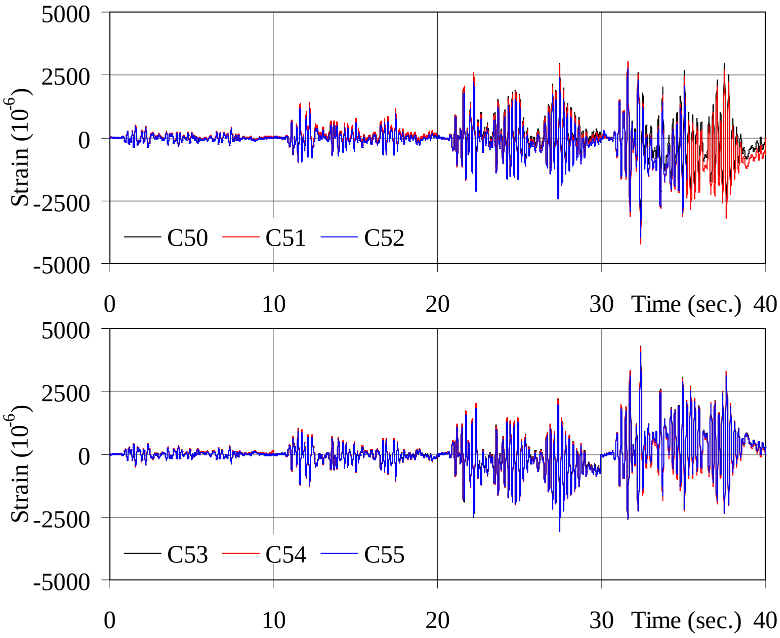

Figure A2.15 Strain gage measurements on the first story brace members

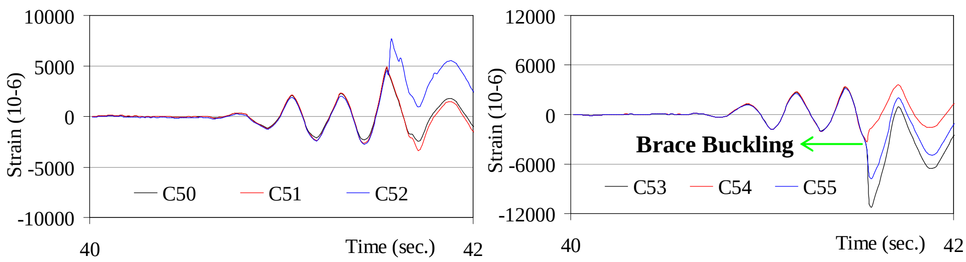

Figure A2.16 Strain gage measurements on the first story brace members for the 220% Duzce test

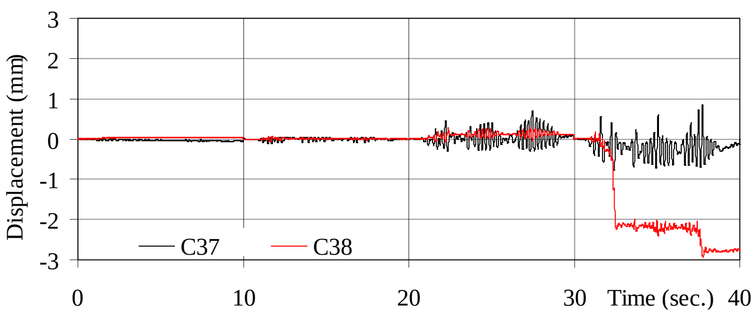

Figure A2.17 Gusset plate out off plane deformation

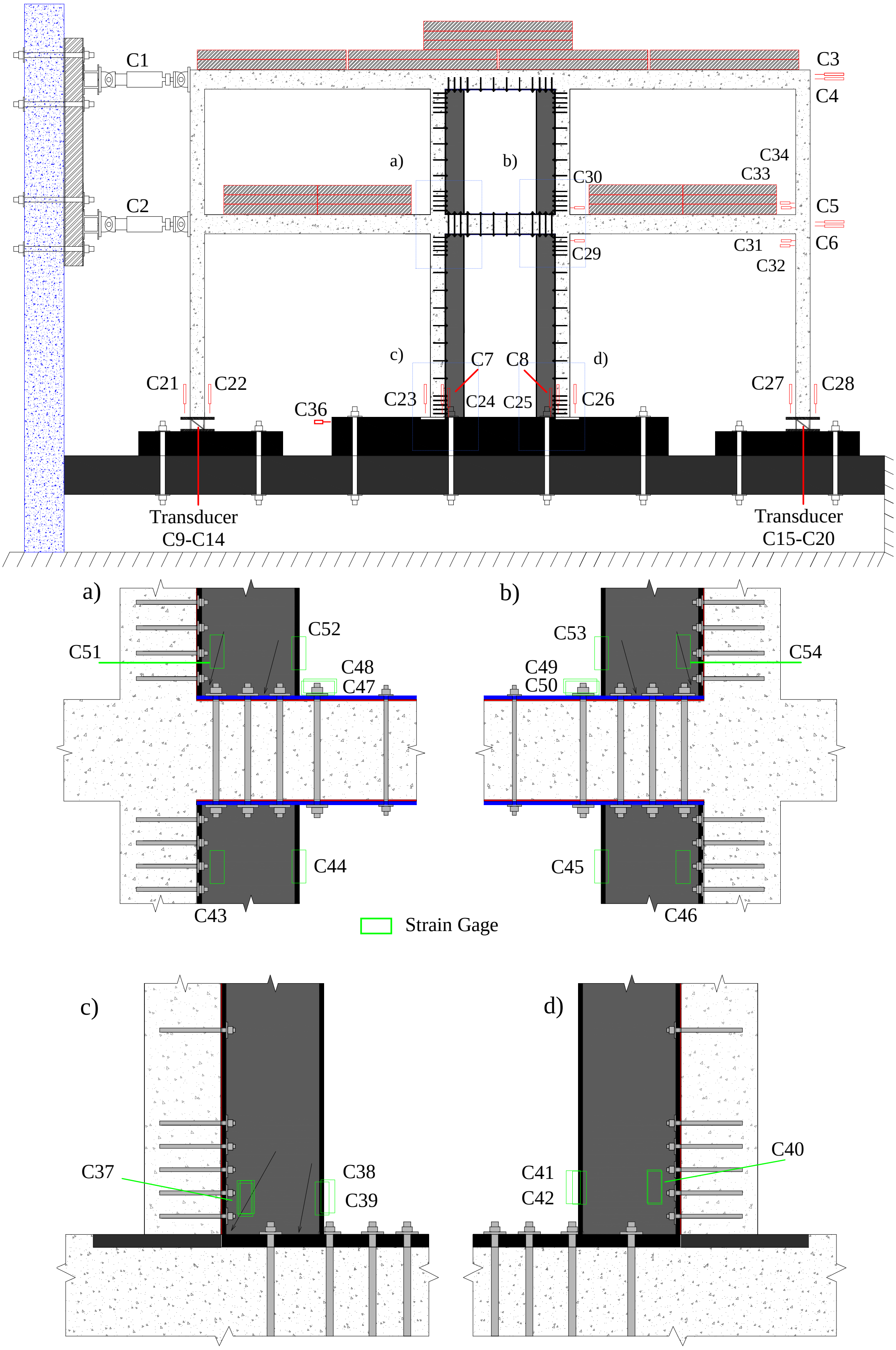

Figure A2.18 Details of the instrumentations for the ISF

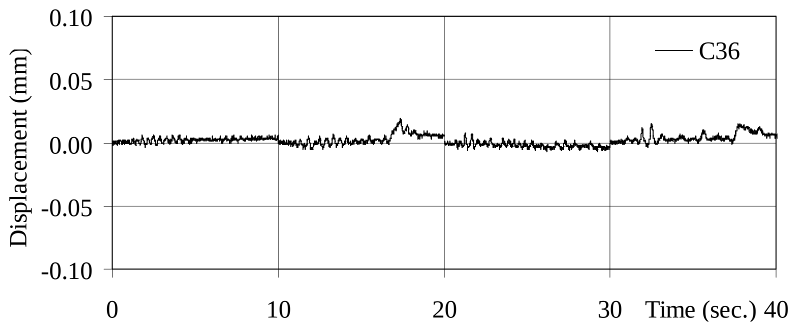

Figure A2.19 Measurement at the foundation for the ISF

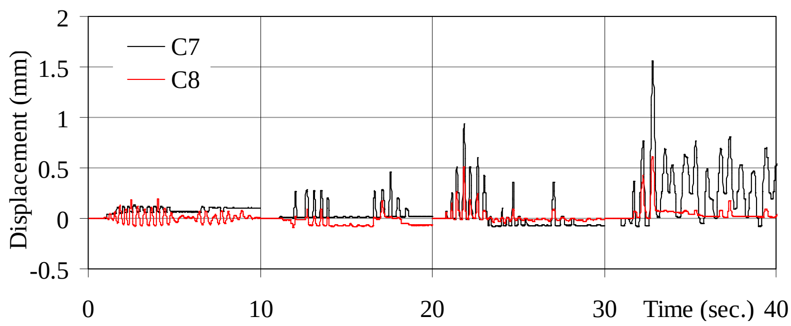

Figure A2.20 Uplift at the base of the composite columns

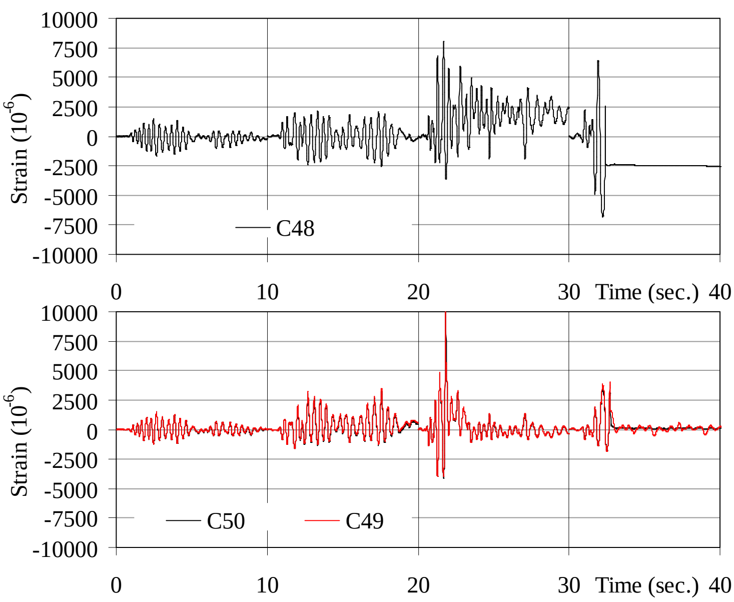

Figure A2.21 Strains on the steel plate of the composite beam

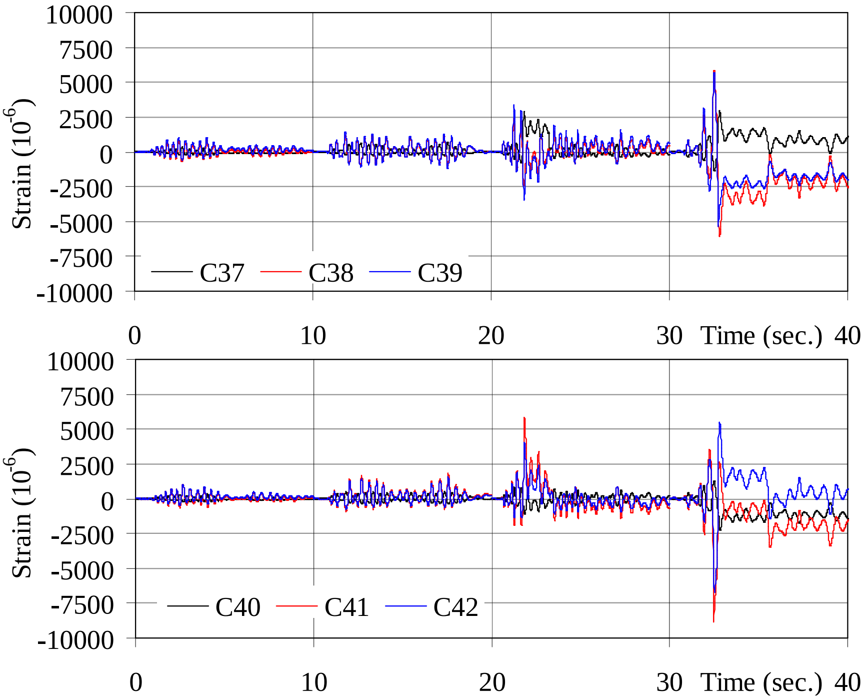

Figure A2.22 Strain measurements at the bottom of the first story composite column (on the I-section)

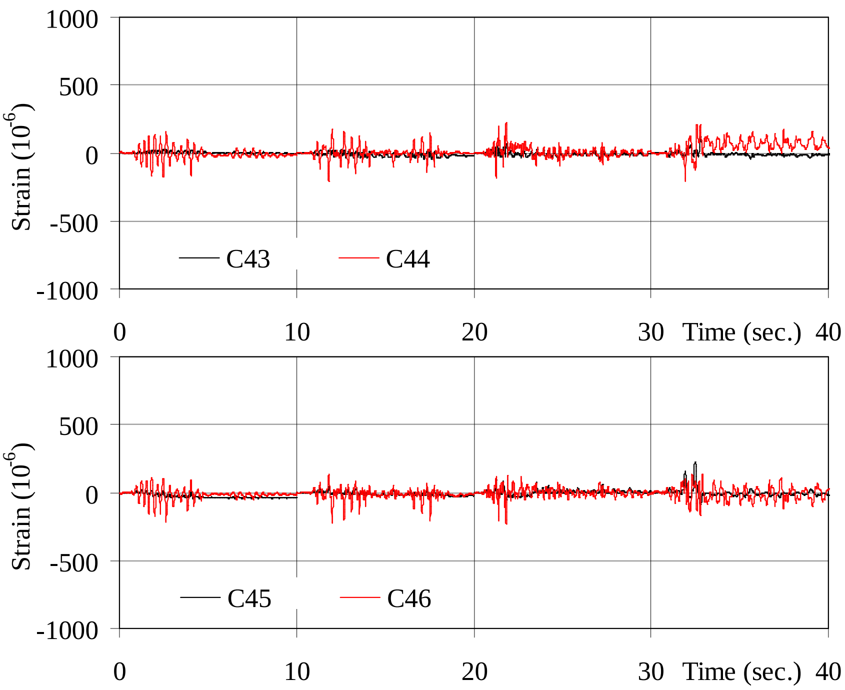

Figure A2.23 Strains at the top of the first story composite column (on the I-section)

VITAE

Ramazan Özçelik was born on July 24, 1980 in Korkuteli-Antalya, Turkey. His mother's & father's name is Necibe and Hüseyin Özçelik. He graduated from Yılmaz Collage in 1994 and entered Department of Civil Engineering of Akdeniz University, Antalya, Turkey. He graduated from Akdeniz University with the degree of Bachelor of Science with a first rank. He joined the Ph.D Program in Civil Engineering Department at the Middle East Technical University in 2003. His current research interests include seismic retrofit of the RC structures and steel structures.

Permanent Address: Güzeloluk Mallesi 1841 sokak No 41 Antalya Türkiye

This dissertation was typed by the author.